Effective Field Theories in the Standard Model and Beyond

Dissertation im Fachbereich Physik - **Matthias König**
9. Oktober 2017

Institut für Physik
Staudingerweg 7, 55128 Mainz, Germany
Johannes-Gutenberg Universität Mainz

Exzellenzcluster PRISMA Präzisionsphysik, fundamentale Wechselwirkungen und Struktur der Materie

PRISMA

JOHANNES GUTENBERG UNIVERSITÄT MAINZ

JG|U

Datum der mündlichen Prüfung: 28. Mai 2018

Declaration of authorship

I hereby certify that this thesis has been composed by myself and is based on my own research, unless stated otherwise. No other than the indicated sources have been used. For projects done in collaboration with others, all calculations presented here have been cross-checked by myself unless explicitly stated otherwise. In the project described in chapter 6, various analyses where carried out by collaborators and they are thus not presented here.

Mainz, Oct 09, 2017

Abstract

Two applications of effective field theories are studied. In the first part we discuss exclusive hadronic decays of the electroweak bosons Z, W and the Higgs in the framework of QCD factorization. The factorization formula is derived using Soft-Collinear Effective Theory and then applied to the decays $Z \to M\gamma$, $W \to M\gamma$, $Z \to MW$, $h \to M\gamma$, $h \to MZ$ and $h \to MW$, where M is a meson. We derive predictions for the radiative decays at next-to-leading order in QCD and resum large logarithms of the form $\alpha_s \log(\mu_0/v)$, where v denotes the electroweak scale and μ_0 is the hadronic scale. We show that power corrections in the expansion parameter are negligible because they are effectively suppressed with at least m_M/v, where m_M is the mass of the final-state meson M. The analysis of the Higgs decays is performed allowing for deviations from the SM couplings of the Higgs to predict the sensitivity of the branching ratios to new-physics effects. Due to a non-trivial interference structure of different decay amplitudes we find a strong sensitivity to new physics in some decay channels.
In the second part we study renormalization group effects on neutrino oscillation parameters in type-I seesaw models. Assuming a flavor-anarchic scenario chosen at a high-scale, we estimate the probability of the observed oscillation parameters to be the results of a random drawing. We show how this probability changes when renormalization group effects are carefully taken into account.

Zusammenfassung

Diese Arbeit diskutiert zwei Anwendungen von effektiven Feldtheorien. Im ersten Beispiel werden die exklusiven, hadronischen Zerfälle von Z-, W und Higgs-bosonen unter Verwendung der QCD-Faktorisierung diskutiert. Die Faktorisierungsformel wird zuerst in der Sprache der "Soft-Collinear Effective Theory" hergeleitet und dann verwendet um Vorhersagen für die Zerfälle $Z \to M\gamma$, $W \to M\gamma$, $Z \to MW$, $h \to M\gamma$, $h \to MZ$ und $h \to MW$ zu erhalten, wobei M für ein Meson steht. Die Zerfallsraten für die radiativen Zerfälle werden auf nächstführender Ordnung in der QCD bestimmt und große Logarithmen der Form $\alpha_s \log(\mu_0/v)$ werden zu allen Ordnungen resummiert, wobei v hier die elektroschwache und μ_0 die hadronische Skala bezeichnet. Es wird gezeigt dass Korrekturen von höherer Ordnung im Entwicklungsparameter der effektiven Theorie vernachlässigbar sind, da sie mindestens durch einen Faktor m_M/v unterdrückt sind, wobei m_M die Masse des Mesons bezeichnet. In der Analyse der Higgs-Zerfälle werden Abweichungen der Higgs-Kopplungen vom jeweiligen Wert im Standardmodell zugelassen um die Sensitivität der Zerfälle auf Effekte neuer Physik zu untersuchen. Die nichtriviale Interferenzstruktur der beitragenden Zerfallsamplituden führt in einigen Fällen zu starken Abhängigkeiten der Zerfallsrate von Effekten neuer Physik.
Der zweite Teil widmet sich einer Renormierungsgruppenanalyse der Neutrinomassenparameter in verschiedenen Typ 1 Seesaw Modellen. Unter der Annahme dass die Parameter rein zufällig und frei von jeglicher Struktur sind ("Flavor Anarchie"), kann die Wahrscheinlichkeit bestimmt werden dass ein zufällig gewählter Satz von Parametern kompatibel mit den experimentell bestimmten Werten ist. In dieser Arbeit wird diskutiert, wie stabil solche Aussagen unter Berücksichtigung von Renormierungsgruppeneffekten sind.

Contents

1. Introduction

The Standard Model of particle physics is the most complete description of the interaction between elementary particles. It is a quantum field theory capable of describing physics across the scales, from extremely low energies like the physics of atoms to extremely high energies, at least up to the electroweak scale that is probed by colliders like the LHC. An important step towards securing its validity has been achieved in 2012, when the ATLAS and CMS experiments announced the discovery of the Higgs boson [1, 2]. The discovered boson, up to this day and in the ways that can be tested experimentally, looks precisely like the particle predicted in the Standard Model (SM), explaining elementary particle masses and restoring scattering unitarity at high energies.

Although the Standard Model is said to be completed, it is clear that it is not a complete and fundamental description of physics. One problem is the question of what balances the electroweak scale against the Planck scale. It arises from the renormalization group evolution of the Higgs boson mass, which receives non-multiplicative corrections proportional to the masses of the particles it couples to. The Higgs mass is thus driven up to the scale of the heaviest particle in the theory. The heaviest particle in the SM, the top quark, is of a similar mass as the Higgs boson, so it might seem natural as long as we assume the SM to be valid up to an arbitrarily high scale. However, any new physics (NP) mediated at a scale Λ will lead to huge corrections to the Higgs mass of $\mathcal{O}(\Lambda)$, spoiling its naturalness. This is the famous *hierarchy problem*.

Electroweak symmetry breaking explains in an economic way how the SM particles (excluding neutrinos) acquire masses without breaking gauge invariance. The Higgs mechanism is however merely a parameterization of electroweak symmetry breaking and does not explain why the symmetry is broken in the first place. Similarly, the couplings of the Higgs boson to quarks determine both their mass hierarchies as well as the CKM mixing parameters. They enter the SM Lagrangian as a priori arbitrary numbers and it is an interesting question whether they can be predicted by a more fundamental theory. In the lepton sector the problem is more involved since the origin of the non-vanishing neutrino masses is unclear to this day.

These examples are of course only an excerpt of the full list of open questions. The origin of dark matter and dark energy, the unification of quantum field theory with general relativity and the strong CP problem are just some examples of intriguing questions that the physics community is facing. Proposed extensions to the SM

and completely new theories solve subsets of these problems at various different energy scales, some of them much higher than the ones typically associated with the SM. In order to understand how we can probe these theories, a systematic way to treat scale hierarchies is needed. The tools of the trade for this application are collected under the term *effective field theory* (EFT). Effective field theories provide a framework to cure the problem of logarithms of the large scale ratios, which can spoil convergence of the perturbation series by overpowering the suppression of the expansion parameter. These *large logarithms* play a role even well within the SM. For example, weak decays of hadrons are mediated by physics at the electroweak scale, but the typical momentum transfers are of the order of the hadronic scale. Therefore, predictions in perturbation theory are plagued by logarithms of the ratio of these two scales. Likewise, the problem can also arise in situations where the relevant particles are light and highly energetic.

While the solutions to both of the above examples are achieved by the use of an effective field theory, the term has to be understood as a collective one: Many different types of effective theories exist, and the nature of the problem determines the concrete implementation one has to use or construct. In this work, we will cover two specific examples. In the conventional effective field theory, scales are separated by the mass of the particles involved in a reaction. We will use this framework to determine the probability of the neutrino oscillation parameters being the result of a draw from a random distribution. The majority of this work however is devoted to the study of exclusive hadronic decays of electroweak bosons. In these decays, the relevant scales are given by the mass of the heavy decaying bosons and the hadronic scale. Using Soft-Collinear Effective Theory (SCET), we can separate these scales and derive the QCD factorization formula, which will allow us to deal with the non-perturbative effects of hadronization. The results are theoretically clean and provide interesting tests of both the QCD factorization approach as well as couplings of the Higgs boson to other fields in the SM.

This work is structured as follows. In chapter 2, we will discuss the concept of effective fields theories by looking at the classic example of the weak effective Lagrangian. We will proceed to introduce the necessary ingredients of SCET in chapter 3. In chapter 4, the QCD factorization formula is derived and applied to the decays $Z \to M\gamma$, $W \to M\gamma$ and $Z \to MW$, where M denotes any meson including the light pseudoscalars $\eta^{(\prime)}$, which are special due to their flavor-singlet admixtures. The framework is then generalized to exclusive decays of the Higgs boson, where we allow for anomalous couplings of the Higgs boson to quarks and gauge bosons and predict the sensitivity to NP effects in chapter 5. Chapter 6 contains a renormalization group analysis of neutrino oscillation parameters to determine the plausibility of a flavor-anarchic scenario. Finally, in chapter 7 we will summarize our results and conclude. Lengthy details of the calculations and numerical input parameters along with their determinations are relegated to several appendices.

2. Effective Field Theories

In this chapter, we will introduce the notion of effective field theories. A vast amount of literature on the subject is available and we will closely follow the examples commonly employed. For more complete overviews, see for example refs. [3–7].

2.1. Naive Dimensional Analysis

The idea behind effective theories is a central one in physics. The core concept of making predictions based on mathematical formulations relies on our ability to identify relevant properties of the problem, focusing our attention to them and discarding the subdominant effects. This means abridging a more complete theory for the sake of computational feasibility. For example, when asked to compute the impact velocity of an apple falling from a tree, one would typically not include effects from general relativity, even though we know that it is the most complete theory of gravity. In fact, one would not even work with the full Newtonian picture but instead just assume the gravitational force to be constant along the trajectory of the apple. The reasoning behind this comes from naive dimensional analysis: The Earth's radius is large compared to the height of an apple tree.

In a quantum field theory, these arguments apply as well: Processes at an energy scale m will only very weakly depend on physics living at scales $M \gg m$. Consequently, we can introduce the small ratio $\lambda = m/M$ and expand in it whenever it is possible. As a classical example, consider the weak decay $d \to u\, e\, \bar{\nu}_e$, mediated by a W boson. The amplitude is given by

$$\mathcal{A}_{d\to ue\bar{\nu}_e} = \frac{ig^2}{2} \left[\bar{u}(p_u)\, \gamma^\mu P_L\, u(p_d)\right] \Pi_{\mu\nu}(p_d - p_u) \left[\bar{u}(p_e)\, \gamma^\nu P_L\, v(p_\nu)\right] , \tag{2.1}$$

where g is the weak coupling, p_i denotes the momentum of the particle j and $\Pi_{\mu\nu}$ is the propagator of the W boson in unitary gauge:

$$\Pi_{\mu\nu}(k) = \frac{1}{k^2 - m_W^2} \left(g_{\mu\nu} - \frac{k_\mu k_\nu}{m_W^2} \right) . \tag{2.2}$$

In β-decay, the momentum transfer k^2 will typically be much smaller than m_W^2, and thus we can expand $\Pi_{\mu\nu}$ in $\lambda = k^2/m_W^2$, leaving us with

$$\Pi_{\mu\nu}(k) \to -\frac{g_{\mu\nu}}{m_W^2} \left[1 + \mathcal{O}(\lambda)\right] . \tag{2.3}$$

Furthermore, the W cannot appear as an external particle because the energy scales associated with the theory are too small to produce it on-shell. We can therefore write down an *effective Lagrangian*, in which the W does not appear anymore, but interactions between the remaining fields are modified such that the phenomenology of processes with intermediate W bosons - including the decay $d \to u\, e\, \bar{\nu}_e$ - remains unchanged. In our example, this amounts to adding new interaction operators between the four fermion fields d, u, e and ν_e. If we adopt the expansion in eq. (2.3), the relevant operator for our process would be:

$$\frac{\mathcal{C}(\mu)}{\Lambda^2} \left(\bar{u}_L \gamma^\mu d_L\right) \left(\bar{e}_L \gamma_\mu \nu_L\right) . \tag{2.4}$$

This *effective operator* comes with a yet undetermined coupling $\mathcal{C}(\mu)$, customarily called the *Wilson coefficient*, which depends on the renormalization scale μ. The operator has a mass dimension of $4 \cdot 3/2 = 6$ and thus its coupling has to be divided by two powers of the mass scale Λ. This scale is associated with the energy at which the effective theory breaks down. In our example we have $\Lambda = m_W$, indicating the scale above which our approximation $k^2/m_W^2 \ll 1$ is no longer justified. Of course, heavy and yet unknown particles could contribute in the same way and lead to terms where Λ is larger. This opens the possibility to study new physics effects in a model-independent way and is the reason why Λ is very often referred to as the *new-physics scale*.

At the scale m_W itself, both theories must be equivalent descriptions of physics. To ensure this, we can compute the same process in both the full theory and the effective theory. After performing the same expansion in both results (in our case expanding the result in k^2/m_W^2), the results have to be equal. This procedure, called *matching*, fixes the Wilson coefficients of the theory at the matching scale, in our case $\mathcal{C}(m_W)$. Note how we went from a theory in which the W mediates the interaction between the quarks and leptons to a theory where the quarks and leptons interact locally in one space-time point, as represented in Fig. 2.1. Very simply put, the approximation $k^2 \ll m_W^2$ means that the momentum of the W is so small, it effectively does not propagate.

2.2. The Local Operator Product Expansion

Let us be more systematic. The effective operator (2.4) is only one of many terms that have to be added to the effective Lagrangian, since the W mediates more processes than just the one considered above. In fact, even for $d \to u\, e \bar{\nu}_e$ more operators must exist, since the one we wrote down in eq. (2.4) only corresponded to the leading term of the expansion in λ. To capture the full phenomenology of the intermediate W boson, we would have to add an infinite series of operators, each of higher order in

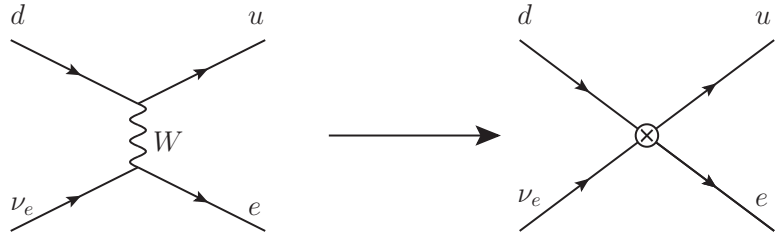

Fig. 2.1.: Diagrammatic representation of integrating out the W boson: The intermediate propagator is shrunk to a local interaction in the limit of $k^2 \ll m_W^2$. Computing both diagrams and demanding the amplitude to be equal fixes the Wilson coefficient of the effective operator in the diagram on the right.

our power-counting and thus suppressed by more powers of Λ. The next term in the Lagrangian would have two more powers of m_W in the denominator and thus would be of the form $\mathcal{C}_8(\mu)\mathcal{O}_8(\mu)/\Lambda^4$. Here $\mathcal{O}_8$ is an operator including the field content of the effective theory and the subscript denotes the mass dimension of the operator. It can include more fields or derivative operators. It is not hard to imagine that at this order in our power-counting, lots of operators can be written down. Luckily, naive dimensional analysis tells us that they are suppressed by two more powers of Λ, compared to the operators with mass dimension 6. This is one of the central aspects of effective theories: Higher-dimensional operators are power-suppressed by the expansion parameter and thus contribute less to our predictions. Therefore, after choosing a level of accuracy, we can construct the effective Lagrangian by writing down all operators composed from the field content of our effective theory that are consistent with the power-counting and the symmetries of the theory. This is called *operator product expansion* (OPE).

In expanding the propagator in the small ratio k^2/m_W^2, we have replaced a non-local interaction with a series of local ones: In the full theory, the W is created from a fermion current at a space-time point x and then propagates to a space-time point $x+\eta$, where it is annihilated by another fermion current. The expansion in λ corresponds to an expansion around $\eta = 0$, meaning that the effective operators are functions of only one point in space-time. The coefficients then encode the details of the short-range interactions at length scales of order η.

In full generality, the effective Lagrangian we obtain from an OPE can be written as

$$\mathcal{L}_{\text{eff}} = \sum_d \frac{1}{\Lambda^{d-4}} \sum_{i=1}^{n_d} \mathcal{C}_d^i(\mu)\mathcal{O}_d^i(\mu)\,, \tag{2.5}$$

where n_d is the number of operators contributing at dimension d. The operators

$\mathcal{O}_d^i(\mu)$ describe the long range interactions mediated by the light fields, whereas the Wilson coefficients $\mathcal{C}_d^i(\mu)$ contain the physics at short distance scales. In this way, the effective field theory isolates the physics at different scales from each other, with the renormalization scale μ serving as a handle on where the section is made. As a result, it is possible to treat each scale separately. This is what makes effective field theories such a powerful tool when dealing with multi-scale problems, as we will see below.

Some comments are in order: First and foremost, it is important to keep in mind that the effective Lagrangian constructed here is merely one example: By integrating out heavy degrees of freedom and expanding around small momenta, we arrived at a theory made of local operators. This is not case in many other examples of effective theories, where effective operators can be non-local under certain circumstances. We will explore one example in chapter 3.

In our example the degrees of freedom of the effective Lagrangian and the full Lagrangian were identical up to the removed W boson: All the light fermions remained untouched. This is not generically true. For example in chiral perturbation theory - the effective theory of mesons - the degrees of freedom in the effective theory are completely different from those in the full theory: In the low-energy Lagrangian, the quarks and gluons are replaced by mesons and baryons.

2.3. Renormalization

In the last section, we saw that an effective Lagrangian separates high-energy and low-energy physics. Which scale exactly we choose as a crossover scale is an unphysical question: Predictions made by the effective theory cannot depend on this choice. From this requirement, a set of equations can be derived, allowing us to continuously vary this scale. With this, we can compute high- and low-energy ingredients each at a scale where they are well-behaved and then connect them by translating each to one single scale. This section will discuss all these parts in more detail, starting with what is meant by "well-behaved".

2.3.1. Radiative Corrections and Large Logarithms

When computing loop-corrections, integrals of the form

$$\int \frac{d^4k}{(2\pi)^4} I(k, \ldots) \tag{2.6}$$

have to be carried out. While the integrand $I(k, ...)$ follows from a theory that we tested to be valid at specific energy scales, the integral extrapolates it to arbitrary regions in phase space and it is not surprising that they diverge in extreme regions.

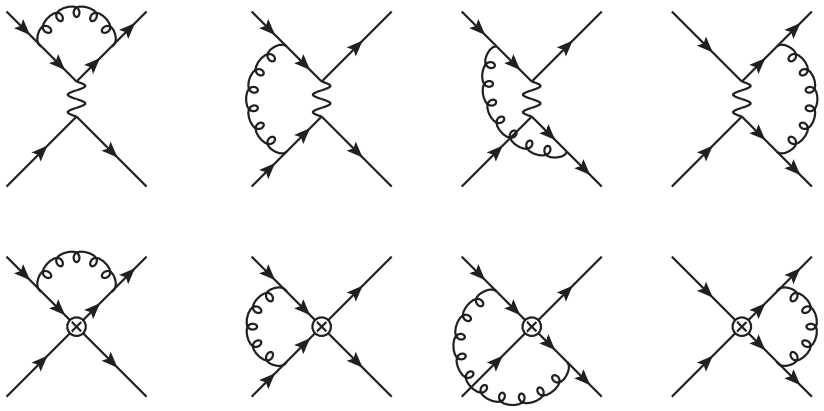

Fig. 2.2.: Examples of one-loop QCD corrections to four-fermion processes like $b \to u\bar{c}s$ in the full theory (top) and their EFT counterparts (bottom).

The plan to remedy this problem is to first find a way of regularizing the integrals. In *dimensional regularization*, divergent integrals are regularized by carrying them out in $d = 4 - 2\epsilon$ spacetime dimensions and expanding the result around $\epsilon = 0$. The divergences of the integrals then manifest themselves as poles in $1/\epsilon^k$.

As an example, let us consider the process $b \to u\bar{c}s$. Just like the beta decay $d \to ue\bar{\nu}_e$, it is mediated in the SM by the W boson. In nature, this quark transition leads to the hadronic decay $\bar{B}^0 \to \pi^+ D_s^-$. Since the typical energy scale of this process is of order $\mathcal{O}(\text{GeV})$, we can again construct an EFT without the W boson and the new-physics scale $\Lambda = m_W$. The dimension six effective operators of interest are

$$\begin{aligned} \mathcal{O}_1 &= (\bar{s}^j \gamma^\mu P_L c^j)(\bar{u}^i \gamma_\mu P_L b^i)\,, \\ \mathcal{O}_2 &= (\bar{s}^i \gamma^\mu P_L c^j)(\bar{u}^j \gamma_\mu P_L b^i)\,, \end{aligned} \tag{2.7}$$

where i, j are color indices. Note that the color structure in the operator $\mathcal{O}_2$ can only arise at the loop level (when the SM is assumed to be the full theory), meaning that the Wilson coefficient starts at order $\mathcal{O}(\alpha_s)$, whereas a contribution from $\mathcal{O}_1$ exists at tree-level. The Wilson coefficients again follow from a matching computation, as illustrated in Fig. 2.2. They are given by [7, 8]:

$$\begin{aligned} \mathcal{C}_1(\mu) &= \frac{g^2}{2} V_{cs}^* V_{ub} \left\{ 1 - \frac{\alpha_s(\mu)}{4\pi} \left(\frac{1}{\epsilon} + \log \frac{\mu^2}{m_W^2} + \frac{11}{6} \right) \right\}, \\ \mathcal{C}_2(\mu) &= \frac{3g^2}{2} V_{cs}^* V_{ub} \left\{ \frac{\alpha_s(\mu)}{4\pi} \left(\frac{1}{\epsilon} + \log \frac{\mu^2}{m_W^2} + \frac{11}{6} \right) \right\}, \end{aligned} \tag{2.8}$$

where V_{ij} are the CKM matrix elements. The striking features of this result are the poles in $1/\epsilon$. While the one-loop amplitude in both full and effective theories

will have divergences, not all of them survive the matching procedure: Infrared (IR) divergences arising from massless loops will be identical in both theories since they have the same low-energy limit. Similarly, both theories will produce ultraviolet (UV) divergences at large energy scales $\Lambda \gg m_W$. However, the effective theory breaks down at scales $\Lambda \gtrsim m_W$ and produces additional UV divergences at this scale, whereas the full theory is still valid and produces finite results. These residual divergences do not cancel in the matching procedure and give rise to the $1/\epsilon$-poles in eq. (2.8). They are subtracted by introducing counterterms for $\mathcal{O}_1$ and $\mathcal{O}_2$.

As a remnant from our regularization procedure, the result depends on the renormalization scale μ. Perturbation theory demands that the coefficient of α_s does not become too large, otherwise the perturbation series cannot converge. Our example $b \to u\bar{c}s$ is a partonic contribution to the decay $\bar{B}^0 \to \pi^+ D_s^-$ and thus the proper scale choice would be $\mu \sim \Lambda_{\text{QCD}}$, with Λ_{QCD} denoting the hadronic scale[1]. In cases like this, the logarithm can become large enough to overcome the power-suppression from the coupling constant. Therefore in our expansion in α_s, the combination $\alpha_s \log\left(\mu^2/m_W^2\right)$ should count as $\mathcal{O}(1)$, as should any arbitrary power of this expression. What was the leading term in the perturbative expansion c_0, is now only one of infinitely many terms in this new power-counting scheme, where the large logarithms should be included to all orders:

$$c_0 \to c_0 \left\{ 1 + \sum_{k=1}^{\infty} b_k \left(\alpha_s \log \frac{\mu^2}{m_W^2} \right)^k \right\} . \tag{2.9}$$

Our task now is to determine the series coefficients b_k. As it turns out, it is possible to do this to all orders, meaning that we can resum the series completely. We will do so by employing the renormalization group equations for the Wilson coefficients $\mathcal{C}_1(\mu)$ and $\mathcal{C}_2(\mu)$.

2.3.2. The Renormalization Group

We have seen that divergent corrections come with potentially large logarithms of the renormalization scale μ. Of course, the scale μ is a remnant of our regularization procedure and physical observables must not depend on it. An observable computed from the effective theory, can be written in the form

$$\mathcal{A} \sim \mathcal{C}_k(\mu) \langle O_k(\mu) \rangle , \tag{2.10}$$

[1] The quantity Λ_{QCD} commonly represents the energy scale at which the renormalization group drives the strong coupling constant α_s into a non-perturbative regime, associated with the dynamics of hadronic bound states. The numerical value thus depends on the interpretation of this definition. Typical choices in the context of perturbation theory are $\mathcal{O}(1\text{ GeV})$.

where the sum over repeated indices is implicit. Now, we require scale independence:

$$\begin{aligned} \mu\frac{d}{d\mu}\left\{\mathcal{C}_k(\mu)\left\langle O_k(\mu)\right\rangle\right\} &\stackrel{!}{=} 0 \\ \Rightarrow \qquad \left(\mu\frac{d}{d\mu}\mathcal{C}_k(\mu)\right)\left\langle\mathcal{O}_k(\mu)\right\rangle + \mathcal{C}_k(\mu)\left(\mu\frac{d}{d\mu}\left\langle\mathcal{O}_k(\mu)\right\rangle\right) &= 0\,. \end{aligned} \tag{2.11}$$

The second term can be rewritten: If all allowed operators are included in the effective Lagrangian, the operator basis is complete and thus the derivative of $\langle\mathcal{O}_k\rangle$ can be written as a linear combination of all effective matrix elements $\langle\mathcal{O}_j\rangle$. We define

$$\mu\frac{d}{d\mu}\left\langle\mathcal{O}_k(\mu)\right\rangle = -\gamma_{kj}(\mu)\left\langle\mathcal{O}_j(\mu)\right\rangle\,, \tag{2.12}$$

and arrive at

$$\begin{aligned} \left(\mu\frac{d\,\mathcal{C}_j(\mu)}{d\mu} - \mathcal{C}_k(\mu)\gamma_{kj}(\mu)\right)\left\langle\mathcal{O}_j(\mu)\right\rangle &= 0 \\ \Rightarrow \qquad \mu\frac{d}{d\mu}\vec{\mathcal{C}}(\mu) - \gamma^T(\mu)\cdot\vec{\mathcal{C}}(\mu) &= 0\,. \end{aligned} \tag{2.13}$$

The γ_{ij} are the components of the $N\times N$ matrix called *anomalous dimension matrix*, where N is given by the number of effective operators in the EFT. Note that it is in general not diagonal, which leads to operator mixing when we solve the above equation. To solve the equation, we first recall that we only looked at QCD-corrections and thus the scale dependence of the anomalous dimension γ is only through the running of α_s. Consequently, we replace

$$\mu\frac{d}{d\mu} = \mu\frac{d\alpha_s(\mu)}{d\mu}\frac{d}{d\alpha_s(\mu)} = \beta_{\alpha_s}\frac{d}{d\alpha_s(\mu)}\,, \tag{2.14}$$

and obtain the renormalization group equation

$$\frac{d\vec{\mathcal{C}}}{d\alpha_s} = \frac{1}{\beta_{\alpha_s}}\left(\gamma^T\cdot\vec{\mathcal{C}}\right)\,, \tag{2.15}$$

where β_{α_s} is the β-function of QCD. It is instructive to solve this equation for a one-loop example, where $\gamma = \alpha_s\gamma_0/(4\pi)$ and $\beta = -\alpha_s^2\beta_0/(2\pi)$, with

$$\beta_0 = 11 - \frac{2}{3}n_F\,, \tag{2.16}$$

and n_F the number of quark flavors in the theory. The solution can be obtained by diagonalizing γ such that $\gamma^T_{\text{diag}} = V^{-1}\gamma^T V$. With this, the solution is:

$$\begin{aligned} \vec{\mathcal{C}}(\mu) &= U(\mu,\mu_r)\vec{\mathcal{C}}(\mu_r)\,, \\ U(\mu,\mu_r) &= V\,\text{diag}\left(\vec{u}(\mu,\mu_r)\right)\,V^{-1}\,, \\ u_i(\mu,\mu_r) &= \left[\frac{\alpha_s(\mu_r)}{\alpha_s(\mu)}\right]^{(\gamma_{0,\text{diag}})_{ii}/(2\beta_0)}\,. \end{aligned} \tag{2.17}$$

With this equation, we know how the Wilson coefficients change as functions of the renormalization scale μ. The renormalization scale can be thought of as the scale at which we split the theory into high and low energy part. When we lower the renormalization scale by $\delta\mu$, dynamics that previously counted as low energy physics are shuffled into the high energy regime. Even if there is no field in the Lagrangian with a mass between $\mu - \delta\mu$ and μ to remove from the Lagrangian, we are still removing high frequency modes of the light fields, hence the continuous running of the Wilson coefficients. Note that the number n_F in the QCD beta function changes when the scale is lowered beneath the mass of a quark, since it is integrated out from the theory.

2.3.3. Resummation of Large Logarithms

With the solution (2.17) in place, the problem with the large logarithms in the Wilson coefficients is essentially solved. Recall that the logarithms were of the form $\alpha_s \log(\mu^2/m_W^2)$ and that we wanted to know the Wilson coefficients at a scale $\mu \gtrsim \mathcal{O}(\Lambda_{\text{QCD}})$, where they would become large. However, we can now translate the Wilson coefficients between different scales. In our example, evaluating the Wilson coefficients at their natural scale $\mu = m_W$ yields an expression that trivially contains any power of $\alpha_s \log(\mu^2/m_W^2)$. We can then use the RG equations to evolve them down to the low scale and get a result that should still be correct to all powers of $\alpha_s \log(\mu^2/m_W^2)$, since the RG evolution employs scale independence of physical observables.

To see explicitly that the RG evolution resums the large logarithms, let us go to a simple example and assume there is only one operator in the operator basis. With this, the equations (2.17) simplify to:

$$\mathcal{C}(\mu) = \left(\frac{\alpha_s(\mu_r)}{\alpha_s(\mu)}\right)^{\frac{\gamma_0}{2\beta_0}} \mathcal{C}(\mu_r)\,. \tag{2.18}$$

We can now express $\alpha_s(\mu)$ through $\alpha_s(\mu_r)$ by the means of the β-function of QCD,

$$\alpha_s(\mu) = \frac{\alpha_s(\mu_r)}{1 + \frac{\beta_0}{4\pi}\alpha_s(\mu_r)\log(\mu^2/\mu_r^2)}\,, \tag{2.19}$$

and insert this into the prefactor of the Wilson coefficient on the right-hand side of eq. (2.18). The result can be cast into the form of eq. (2.9) and we obtain the series coefficients

$$b_k = \left(-\frac{\beta_0}{4\pi}\right)^k \frac{\Gamma\left(k - \frac{\gamma_0}{2\beta_0}\right)}{\Gamma(k+1)\,\Gamma\left(-\frac{\gamma_0}{2\beta_0}\right)}\,. \tag{2.20}$$

We have seen that the renormalization group resums the logarithms to all orders in α_s. This shows, why scale separation is desirable: If we can split up a multi-scale problem into independent pieces that each depend on a single scale, we can evaluate each of them at their natural scale where they are free from large logarithms. The renormalization group evolution then resums the large logarithms and we can use it to evolve each piece of the problem to one single scale.

2.4. Applications of Effective Field Theories

The formalism of effective field theories is used far and wide in particle physics. There are several ways in which the EFT approach is useful, and we will briefly review some of most important ones. Of course, an exhaustive discussion is impossible due to the vast popularity of the framework.

Naturally, all applications have a common denominator: They are motivated by some scale hierarchy being present. In flavor physics, for example, processes are typically mediated by the electroweak forces, giving rise to flavor-changing interactions. One then studies certain hadronic observables, like radiative decays of mesons or neutral-meson mixing. At the parton-level, these processes are governed by amplitudes in which quarks undergo a transition into different flavors. Within the SM, these transitions happen under the exchange of a W boson, beyond the SM they can be mediated by new particles. With the typical momentum transfer scales of such processes being in the vicinity of Λ_{QCD}, the flavor-changing amplitudes are best matched onto an effective operator basis, as the W (and hypothetical new physics) are heavy and the interaction is described by a local OPE. The example discussed in the previous section is exactly such a case. The matching is then performed at the high scale of at least the W boson mass and large QCD logarithms are resummed via the renormalization group, just as discussed above. A vast compilation of flavor physics observables and the relevant effective operator bases is found in ref. [8].

Effective field theories are also commonly employed to deal with non-perturbative phenomena in QCD. The chiral Lagrangian, for example, describes the interactions of QCD bound states by expanding a non-linear sigma model of chiral symmetry breaking in the small momenta of the Goldstone bosons [9]. At low momentum transfer, chiral perturbation theory (χPT) is a tool to address the dynamics of QCD. The inner workings of the framework are complicated and well beyond the scope of this work. The interested reader is referred to the literature (see refs. [10, 11] for reviews) and references therein.

When dealing with mesons containing heavy quark flavors, an additional scale becomes relevant, given by the mass of the heavy quark. Effective theories, specifically tailored to these cases, exist: In the case of heavy quarkonia, the appropriate theory is Non-Relativistic QCD (NRQCD), where one expands around the limit of

the two heavy quarks being at rest in the meson rest frame. Many properties of heavy quarkonia can then be determined perturbatively, since the strong coupling at the relevant scale $\alpha_s(m_Q)$ is reasonably small [12, 13].

Mesons containing one light and one heavy quark flavor can be addressed in Heavy-Quark Effective Theory (HQET). Here the velocity of the heavy quark is promoted to a conserved quantum number, since the non-perturbative physics live at much lower scale. As a result, the theory contains new symmetries (spin and flavor of the heavy quark), allowing one to parameterize the properties of heavy-light mesons in an expansion in $1/m_Q$ and infer them from other mesons to a certain extend. An example of this the mass splitting between the D and D^* mesons, which can be related to the mass splitting of B and B^*: Spin symmetry tells us that the mass difference should be scale as

$$m_{B^*} - m_B = \frac{\Lambda_{\text{QCD}}^2}{m_b}\lambda + \mathcal{O}(m_b^{-2})\,, \tag{2.21}$$

with an $\mathcal{O}(1)$ parameter λ. The observed difference of 44 MeV is consistent with this estimate. Furthermore, the mass-squared difference between the mesons should be identical up to power corrections due to flavor symmetry:

$$m_{B^*}^2 - m_B^2 = m_{D^*}^2 - m_D^2 + \mathcal{O}(m_Q^{-1})\,. \tag{2.22}$$

This prediction is accurate at the level of 1%. The construction of the actual effective theory is not of relevance to this work and the reader is again forwarded to the literature [14, 15].

Another important situation is the one where the physics at high energies is not just governed by heavy particles, but also (or exclusively) by energetic light particles. Examples in flavor physics are decays of heavy mesons into light degrees of freedom, like exclusive B decays $B \to \pi\pi$ or $B \to \phi K_S$ or inclusive decays like $B \to X_s\gamma$. In these cases, one integrates out hard modes, meaning particles that are far off-shell with propagators $\propto 1/(k^2 - m^2)$, where $k^2 \gg m^2$. The resulting Soft-Collinear Effective Theory (SCET) contains modes of fields that are approximately light-like or off-shell with small squared momenta and is expanded in the ratio of energy scales. Beyond flavor physics, it is also applied to jet physics. We will need SCET to derive the QCD factorization formula. A brief overview of the theory is offered in the following chapter.

Let us close this chapter with a popular application of a conventional EFT: Model independent searches of new physics (NP). We know, for a number of reasons, that the SM cannot be a complete description of physics. The number of extensions to the SM on the market trying to mitigate its various shortcomings is overwhelming and speaks for both the lack of concrete NP evidence and the creativity[2] of the beyond-the-SM (BSM) community. In view of the experimental situation, more analyses

[2] Although a pessimist might argue "despair" instead.

focus on parameterizing NP effects through a general effective Lagrangian under the assumption that new particles are heavy and can be integrated out. The operator basis most commonly used is called the "Warsaw basis" [16] and it contains all local operators built from the SM field content up to dimension six compatible with the symmetries of the SM. The clear benefit of this approach is the model-independence. Results obtained in this way can be translated into concrete NP models by performing simple matching computations, as long as they new particles are heavy enough. On the other hand, several subtleties tarnish the picture. First, one should note that the Warsaw basis contains 59 operators, not counting different flavor combinations. Depending on the process in consideration, amplitudes can depend on lots of different Wilson coefficients. Not only can this render the computation a tedious task but it can (and generically will) lead to encumbering results: Only rarely will a calculated process depend on a single Wilson coefficient. When one tries to obtain bounds on the Wilson coefficients, they will usually not be of the form $\mathcal{C}_i < \dots$. Instead, bounds are placed on complicated combinations of different coefficients. In an attempt to make these expressions less cluttered, certain coefficients are then usually removed or equated to each other under more or less well-motivated assumptions, which curtail the model-independence of the analysis and can be overlooked or simply forgotten when the results are reused later on. Another subtlety we want to mention is the truncation of the power series: Consider an amplitude, computed with a dimension-six Lagrangian, given as a power series in $1/\Lambda$

$$i\mathcal{M} = \mathcal{C}_4 \langle \mathcal{O}_4 \rangle + \frac{\mathcal{C}_6}{\Lambda^2} \langle \mathcal{O}_6 \rangle + \mathcal{O}(\Lambda^{-4}) \,, \tag{2.23}$$

where $\mathcal{C}_n \mathcal{O}_n$ is abstract for all dimension-n operators and their couplings contributing to the amplitude. When squaring the matrix element, the mathematically rigorous treatment would be to also truncate the squared matrix element at $\mathcal{O}(\Lambda^{-4})$,

$$|M|^2 = \mathcal{C}_4^2 \, |\langle O_4 \rangle|^2 + \frac{\mathcal{C}_4 \mathcal{C}_6}{\Lambda^2} (\langle O_4 \rangle^\dagger \, \langle O_6 \rangle + \text{h.c.}) \,. \tag{2.24}$$

and neglect the term $\sim |\langle \mathcal{O}_6 \rangle|^2$ since it is of the same order as the interference between $\mathcal{O}_4$ and operators of higher dimensions, that we have not considered. However, no consensus exists on the matter. One might argue that we do know at least the contribution $\sim |\langle \mathcal{O}_6 \rangle|^2$ could just as well keep it. An example is found in recent dijet-analyses done by ATLAS and CMS [17, 18]. Note how this practice would be completely ill-defined in regular perturbation theory, where keeping the $\mathcal{O}(\alpha^2)$-term of $|1 + \alpha \, c_1|^2$ could give rise to incurable IR-divergences. Treating the $|\langle \mathcal{O}_6 \rangle|^2$ term as an estimate for the uncertainty from higher-dimension operators would yield considerably weaker bounds on Wilson coefficients and NP-scales, when EFT predictions are compared against experimental data [19]. The EFT approach also does

not capture NP effects from light new particles, like the typical QCD-axion. Additionally, even if the new field content is heavy, problems can arise when there is a more complex sector of new fields in a similar mass range: Assuming a newly found scalar resonance decaying to photons S, as LHC data suggested in late 2016, it is tempting to write the effective Lagrangian

$$\mathcal{L}_{\text{eff}} \supset \frac{\mathcal{C}_{\gamma\gamma}}{\Lambda} S F_{\mu\nu} F^{\mu\nu} + \frac{\tilde{\mathcal{C}}_{\gamma\gamma}}{\Lambda} S F_{\mu\nu} \tilde{F}^{\mu\nu} \,, \tag{2.25}$$

as a model-independent parameterization. When the decay is however mediated through heavy particles with masses similar to the one of the resonance, the framework breaks down since the leading operators of higher dimension come with factors of $m_S/m_X \sim 1$, spoiling the convergence of the power series: Higher power operators could, for example, involve derivatives (like $(\partial^2 S) F \cdot F$, for instance) and technically have higher mass dimension. But since the momenta in the process are typically large, the higher mass dimension does not necessarily yield a suppression [20]. The framework of Soft-Collinear Effective Theory, introduced in the next chapter, can be used to address this issue.

3. Soft-Collinear Effective Theory

This chapter features a brief overview of the basic aspects of the Soft-Collinear Effective Theory (SCET). By no means is it meant to capture all details and subtleties of the theory, but rather to introduce the necessary ingredients for the later chapters of this work. Many variants of the theory exist, tailored to mitigate specific shortcomings of the basic framework. For our purposes, the latter is sufficient and we will skip over most of the subtleties. For a more detailed review, see for example ref. [21] and references therein.

3.1. Strategy of Regions

In the treatment of the local OPE, we highlighted the benefit of scale separation: Heavy fields could be integrated out and their propagator collapsed to local interactions between the low-energy field content. In this way, we separated short-distance and long-distance physics into Wilson coefficients and operator matrix elements. This implies that all physics at the high scale is mediated by heavy particle exchanges which are removed from the theory. However, it is easy to imagine examples where this approach misses out important parts of the high energy interactions: Consider the decay of a heavy particle with mass M into a light final state, mediated by loop-diagrams like the ones shown in Fig. 3.1. If we assign momenta k and q to the final state particles, the relevant loop integral is of the form

$$I = \int \frac{d^d l}{(2\pi)^d} \frac{1}{l^2 - m^2} \frac{1}{(l+k)^2 - m^2} \frac{1}{(l-q)^2 - m^2} \,, \tag{3.1}$$

where m is the mass of the particle in the loop. In general, a second integral can contribute with an additional l^2 in the numerator of the integrand. For simplicity, we

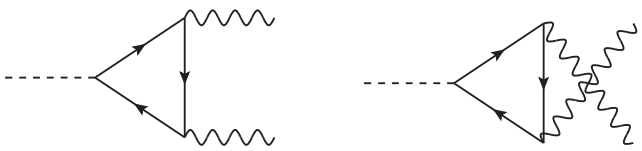

Fig. 3.1.: Examples of loop diagrams generating the decay of a heavy particle (dashed line) into two light particles (wavy lines).

neglect this case and focus only on the above integral. Assuming m is large compared to the mass M of the decaying particle, we can shrink the loop down to an effective interaction and in this way separate the high scale (the mass of the loop particle) from the low scale (the mass of the decaying particle). This is the approach we would apply following the last chapter. If we assume the opposite scale hierarchy $M \gg m$, there is no particle to integrate out from the theory according to our procedure from the last chapter. However, there are regions where the integral I describes physics at the high scale and should be matched onto Wilson coefficients [22]. We will now identify these regions by looking at the different possible values of l^2 and how they influence the propagators of the virtual particles.

The first and most intuitive region is the one where every component of the loop momentum is of the order of the high energy scale and $l^2 \sim M^2$. In this *hard region* the internal masses m are tiny power corrections, suppressed by a factor of $\lambda^2 = m^2/M^2$ with respect to l^2 and can thus be dropped. Neglecting the masses of the particles in the final state, we find:

$$\begin{aligned} I_h &= \mu^{2\epsilon} \int \frac{d^d l}{(2\pi)^d} \frac{1}{l^2} \frac{1}{(l+k)^2} \frac{1}{(l-q)^2} \\ &= \frac{i}{32\pi^2 M^2} \left\{ \frac{1}{\epsilon^2} - \frac{\pi^2}{6} + \left(\frac{1}{\epsilon} + \log \frac{\mu^2}{M^2} + i\pi \right)^2 \right\} . \end{aligned} \tag{3.2}$$

The loop integral converges for $\epsilon < 0$ and the $1/\epsilon$ pole is thus the manifestation of an infrared divergence. Note also that the full integral in eq. (3.1) is finite in the limit $\epsilon \to 0$. Clearly, the expansion in small m and the loop integration do not commute. Therefore, assuming $l^2 \ll m^2$ is a priori not justified since the integration area includes regions where $l^2 \lesssim m^2$, which we will now identify.

In order to make the discussion more systematic, we introduce light-cone coordinates. Any vector k^μ can be decomposed into light-like components $k_\pm$ and a residual vector $k_\perp$. To this end, one chooses light-like reference vectors n^μ and $\bar{n}^\mu$ obeying the identities

$$n^2 = \bar{n}^2 = 0 \,, \qquad\qquad n \cdot \bar{n} \neq 0 \,. \tag{3.3}$$

A common choice for these vectors is $n = (1, 0, 0, 1)$ and $\bar{n} = (1, 0, 0, -1)$. Using these reference vectors, we can decompose any vector into its components proportional to n^μ and $\bar{n}^\mu$ and a residual component. The general form of this decomposition for a vector k^μ is

$$k^\mu = \frac{\bar{n} \cdot k}{n \cdot \bar{n}} n^\mu + \frac{n \cdot k}{n \cdot \bar{n}} \bar{n}^\mu + k_\perp^\mu \equiv k_+ n^\mu + k_- \bar{n}^\mu + k_\perp^\mu \,, \tag{3.4}$$

and it is independent on the concrete choice of n^μ and $\bar{n}^\mu$. In our example, we can go to the rest frame of the decaying particle, where the final-state momenta can be

chosen as $k^\mu = n^\mu M/2$ and $q^\mu = \bar{n}^\mu M/2$. If we now glance back at eq. (3.1), we can identify other relevant regions: When l^μ is approximately light-like and collinear to k, its light-cone components scale as $l = (l_+, l_-, l_\perp) \sim M(1, \lambda^2, \lambda)$, which is called *collinear scaling*[1]. Oppositely, if l^μ is collinear to q^μ, it obeys *anti-collinear scaling* with $l \sim M(\lambda^2, 1, \lambda)$. In both these regions $l^2 \simeq 0$ and we can no longer ignore the mass terms in all three propagators.

If we now look at eq. (3.1) and consider the region where l^μ is collinear, the leading-power expression is[2]

$$I_c = -\int \frac{d^d l}{(2\pi)^d} \frac{1}{l^2 - m^2} \frac{1}{(l+k)^2 - m^2} \frac{1}{2\, l \cdot q}\,, \tag{3.5}$$

whereas in the anti-collinear region, it is

$$I_{\bar{c}} = \int \frac{d^d l}{(2\pi)^d} \frac{1}{l^2 - m^2} \frac{1}{2\, l \cdot k} \frac{1}{(l-q)^2 - m^2}\,. \tag{3.6}$$

If we compare these integrals to eq. (3.2), it is now clear that the infrared divergences in the hard regions come from areas in the integration where l^μ becomes (anti-)collinear. In return, we should expect the functions I_c and $I_{\bar{c}}$ to exhibit UV divergences in regions where l^μ rather obeys hard scaling $l \sim M(1,1,1)$.

The (anti-)collinear integrals are ill-defined by themselves. This manifests itself in unregulated divergences when we try to evaluate them. We can however introduce a new analytic regulator to make the divergences explicit by replacing

$$\begin{aligned} I_c &\to -\mu^{2\epsilon} \int \frac{d^d l}{(2\pi)^d} \frac{1}{l^2 - m^2} \frac{\nu^{2\alpha}}{((l+k)^2 - m^2)^{1+\alpha}} \frac{1}{2\, l \cdot q}\,, \\ I_{\bar{c}} &\to \mu^{2\epsilon} \int \frac{d^d l}{(2\pi)^d} \frac{1}{l^2 - m^2} \frac{\nu^{2\alpha}}{(2\, l \cdot k)^{1+\alpha}} \frac{1}{(l-q)^2 - m^2}\,, \end{aligned} \tag{3.7}$$

where α is the analytic regulator and ν the associated renormalization scale [23]. Evaluating the integrals yields:

$$\begin{aligned} I_c &= -\frac{i}{16\pi^2 M^2} \left(\frac{1}{\epsilon} + \log\frac{\mu^2}{m^2}\right)\left(\frac{1}{\alpha} + \log\frac{\nu^2}{M^2}\right)\,, \\ I_{\bar{c}} &= -\frac{i}{32\pi^2 M^2} \left\{ \frac{1}{\epsilon^2} - \frac{\pi^2}{6} + \left(\frac{1}{\epsilon} + \log\frac{\mu^2}{m^2}\right)^2 \right. \\ &\qquad \left. -2\left(\frac{1}{\epsilon} + \log\frac{\mu^2}{m^2}\right)\left(\frac{1}{\alpha} + \log\frac{\nu^2}{m^2} - i\pi\right)\right\}\,. \end{aligned} \tag{3.8}$$

[1] The scalar quantity $l_\perp$ here denotes the norm of the vector $l_\perp^\mu$ that we defined in eq. (3.4)

[2] Note that the integrals in all regions are of the same order in λ. The factors of λ^{-4} from the propagators in the (anti-)collinear regions are canceled by the integral measures since they count as λ^d.

It is important to take the limit of $\alpha \to 0$ before taking $\epsilon \to 0$, because the full integral is only independent of the regulator α for non-zero values of ϵ. The poles for $\alpha \to 0$ cancel in the sum of the collinear and anti-collinear integrals, but an additional logarithm of the scale ratio λ remains. This is called *collinear anomaly* [23]. If we now add the hard region, we obtain a finite result:

$$I_h + I_c + I_{\bar{c}} = \frac{i}{32\pi^2 M^2} \left(\log \frac{m^2}{M^2} - i\pi \right)^2 . \tag{3.9}$$

This is precisely the result that we would have found if we had evaluated the integral in eq. (3.1) before expanding in λ. In general one can imagine contributions from additional regions. A common example is the soft region, where the loop momentum scales as $l \sim M(\lambda^2, \lambda^2, \lambda^2)$. In our particular example this region happens to not contribute at leading power.

In summary, we have identified regions where individual or all propagators in a given one-loop diagram are far off-shell. In cases, where not all loop momenta were hard, the residual momenta are in turn either (anti-)collinear or soft. These regions yield important contributions to the result since the (anti-)collinear or soft propagators are strongly enhanced when the masses are small. We can therefore construct the effective theory by splitting up fields into the relevant modes and integrating out the hard modes. In this way, the resulting effective theory also accounts for light particles with very high momenta to be part of the high-scale interactions. This is in contrast to the conventional EFT approach, where we split up the field content by mass. Consequently, the effective theory will separate scales more reliably, allowing us to resum logarithms like the one found in eq. (3.9).

Before we move on, it should be noted that depending on the application, other modes might be relevant degrees of freedom to construct an effective theory. Examples are ultra-soft, collinear-soft ("coft") [24], or ultra-collinear [25].

3.2. Construction of the Effective Theory

We now construct the effective theory by building a Lagrangian from the degrees of freedom we identified above. For simplicity, the basic notions are first explained for a simple scalar theory before we generalize it to QCD. We begin with the Lagrangian

$$\mathcal{L}(\phi) = \frac{1}{2}(\partial_\mu \phi)(\partial^\mu \phi) - \frac{1}{2} m^2 \phi^2 - g\phi^3 , \tag{3.10}$$

and split each field into the (anti-)collinear modes and the soft mode:

$$\phi \to \phi_c + \phi_{\bar{c}} + \phi_s . \tag{3.11}$$

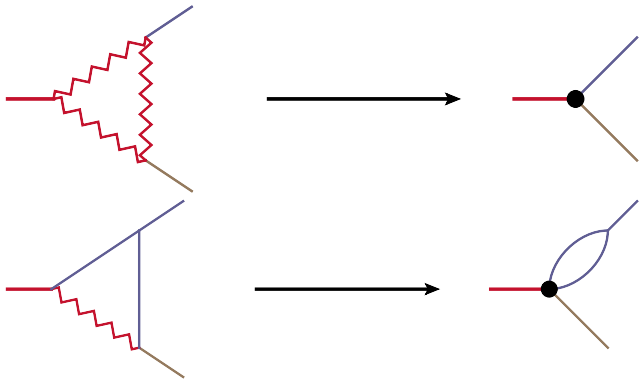

Fig. 3.2.: Examples of effective interactions obtained from removing hard modes (red, zig-zagged lines).

Up to the interaction term that couples different modes to each other, our Lagrangian now splits up into three copies of itself with each one containing only one of the modes, $\mathcal{L}(\phi) = \mathcal{L}(\phi_c) + \mathcal{L}(\phi_{\bar{c}}) + \mathcal{L}(\phi_s) + \mathcal{L}_{\text{int}}$. Special care is needed when writing down interaction terms. First, interactions are restricted by the fact that collinear fields can only have collinear momenta and soft fields can only have soft momenta. Therefore, because a collinear field cannot decay into a collinear and an anti-collinear field by momentum conservation, a term of the form $\phi_c^2\phi_{\bar{c}}$ cannot be part of our Lagrangian. The three-point interaction in the effective Lagrangian is then of the form [21]:

$$\phi^3(x) \to \phi_c^3(x) + \phi_{\bar{c}}^3(x) + \phi_s^3(x) + 3\phi_c^2(x)\phi_s(x_+) + 3\phi_{\bar{c}}(x)\phi_s(x_-)\,. \tag{3.12}$$

The fact that the soft fields in the soft-collinear interactions only depend on specific light-cone components of the coordinate is a consequence of expanding the operator around the small momentum of the soft mode, and is called *multiple expansion* [26].

Next we need to include effective interactions obtained from removing hard modes from the theory, as depicted in Fig. 3.2: In our example, the hard region of the full theory gives rise to a tree-level decay of the heavy particle to a collinear and an anti-collinear mode in the effective theory. The collinear regions are loop diagrams in the effective theory involving an effective operator obtained by removing one intermediate hard mode. First and foremost however, we need to establish our power-counting. We already anticipated that the expansion parameter is the scale ratio $\lambda = m/M$. Since the relevance of a mode is determined by how its propagator scales with λ, each effective degree of freedom can be assigned a scaling by looking at its two-point correlator and counting the powers of λ appearing in the expression.

For a collinear particle, we find:

$$\begin{aligned}\langle 0|\, T\{\phi_c(x)\phi_c(0)\}\,|0\rangle &\sim \int d^4p\, e^{-i\,p\cdot x}\,\frac{i}{p^2}\\ &\sim \lambda^4\cdot\lambda^0\cdot\lambda^{-2}=\lambda^2\,.\end{aligned} \tag{3.13}$$

Here we used that a collinear momentum scales as $p^2\sim\lambda^2$ and the measure scales as the momentum $d^4p\sim(p^2)^2$. We conclude that $\phi_c^2\sim\lambda^2$ and thus a collinear field scales as one power of λ. Since a soft momentum as we defined it earlier squares to an expression of $\mathcal{O}(\lambda^4)$, the soft scalar field counts as λ^2 and is of subleading power. The power counting of an operator is done by looking at the action of each term, $\int d^4x\,\mathcal{O}(x)$. The scaling of $\mathcal{O}(x)$ is deduced from the fields appearing in it whereas the scaling of the measure can be derived from the sum of the momenta in the operator and noting that each component of x scales inversely to the corresponding component of the momentum.

In the example of a heavy particle, here denoted by Ψ, decaying into two light particles, denoted ϕ, the tree-level contribution must be generated by an effective operator of the form

$$\mathcal{O}_{\text{eff}}^{\text{tree}}=\Psi(x)\,\phi_c(x)\,X\,\phi_{\bar{c}}(x)\,, \tag{3.14}$$

where X is a placeholder for any allowed structure compatible with the symmetries of the theory. At leading power, X could simply be identity. However, a derivative of the anti-collinear field along the direction of its large momentum component does not yield a power-suppression. Thus, the operator

$$\Psi(x)\,\phi_c(x)\frac{(n\cdot\partial)}{n\cdot\bar{n}}\phi_{\bar{c}}(x) \tag{3.15}$$

is of the same order as the one where $X=1$: both count as λ^2. In fact, an infinite tower of operators contributes at this order in λ and it can be written as a single operator with a continuous parameter using the identity

$$\phi_{\bar{c}}(x+tn)=\sum_{i=0}^{\infty}\frac{t^i}{i!}(n\cdot\partial)^i\phi_{\bar{c}}(x)\,. \tag{3.16}$$

We can use this to write down the effective operator

$$\mathcal{O}_{\text{eff}}^{\text{tree}}=\Psi(x)\,\phi_c(x+s\bar{n})\,\phi_{\bar{c}}(x+tn)\,. \tag{3.17}$$

This operator is non-local along the light-like directions of the large momentum components, a typical feature of SCET. The operator generating the second graph in Fig. 3.2 can now be written along the same lines:

$$\mathcal{O}_{\text{eff}}^{\text{loop}}=\Psi(x)\,\phi_c(x+s\bar{n})\,\phi_c(x+t\bar{n})\,\phi_{\bar{c}}(s+rn)\,. \tag{3.18}$$

Note that this operator counts as λ^3, one λ for each ϕ field. The usual form of the effective Lagrangian, a sum over all effective operators and their Wilson coefficients, has now turned into a convolution over the continuous parameters r, s and t:

$$\begin{aligned}\mathcal{L}_{\text{eff}} = &\iint ds\, dt\, \mathcal{C}_{\text{eff}}^{\text{tree}}(s,t,\mu)\, \mathcal{O}_{\text{eff}}^{\text{tree}}(s,t) \\ &+ \iiint dr\, ds\, dt\, \mathcal{C}_{\text{eff}}^{\text{loop}}(r,s,t,\mu)\, \mathcal{O}_{\text{eff}}^{\text{loop}}(r,s,t) + \dots\end{aligned} \tag{3.19}$$

Here we have written an explicit dependence on the renormalization scale, introduced by quantum corrections. In momentum space, the non-locality transforms into a dependence of the Wilson coefficients on the high energy scales. This is seen by expressing C, ϕ_c and $\phi_{\bar{c}}$ through their Fourier-transformed counterparts $\tilde{C}$, $\tilde{\phi}_c$ and $\tilde{\phi}_{\bar{c}}$ and performing the integrals over s and t:

$$\begin{aligned}&\iint ds\, dt\, C(s,t,\mu)\phi_c(x+s\bar{n})\phi_{\bar{c}}(x+tn) \\ =&\int \frac{d^4k}{(2\pi)^4}\int \frac{d^4q}{(2\pi)^4}\iint ds\, dt\, C(s,t,\mu)e^{-ik\cdot(x+s\bar{n})}e^{-iq\cdot(x+tn)}\tilde{\phi}_c(k)\,\tilde{\phi}_{\bar{c}}(q) \\ =&\int \frac{d^4k}{(2\pi)^4}\int \frac{d^4q}{(2\pi)^4}\tilde{\mathcal{C}}(\bar{n}\cdot k, n\cdot q,\mu)e^{-i(k+q)\cdot x}\tilde{\phi}_c(k)\tilde{\phi}_{\bar{c}}(q)\,.\end{aligned} \tag{3.20}$$

Scale separation is apparent now: The Wilson coefficients depend on the high energy scale that we have integrated out. In contrast to the local OPE, these dependences are not introduced by heavy particles but by light (virtual) particles carrying large energies. This is especially important in processes, where the energy scale is large but no heavy particles are present. An example of such a process would be $e^+e^- \to q\bar{q}$ at a high energy lepton collider, with q being a light quark flavor. QCD corrections would yield logarithms of the form $\alpha_s \log(m_q^2/s)$. These logarithms could not be resummed using a conventional EFT since the high scale is not given by a heavy particle mass but rather high momentum transfer.

3.3. Fermions and Gauge Fields

Let us now go to a more realistic picture that includes fermions and gauge fields, more specifically: QCD. Again, we start by separating the fields into their modes. This time however, things become more complicated since fermion fields and gauge fields have multiple components and they scale differently in SCET power counting.

We start with fermions and split them up in the familiar way:

$$\psi \to \psi_c + \psi_{\bar{c}} + \psi_s\,. \tag{3.21}$$

By defining projectors $P_+ = \not{n}\not{\bar{n}}/(n\cdot\bar{n})$ and $P_- = \not{\bar{n}}\not{n}/(n\cdot\bar{n})$, the (anti-)collinear fermions can be further split into:

$$\begin{aligned} \xi_c &= P_+\psi_c\,, & \eta_c &= P_-\psi_c\,, \\ \xi_{\bar{c}} &= P_-\psi_{\bar{c}}\,, & \eta_{\bar{c}} &= P_+\psi_{\bar{c}}\,. \end{aligned} \tag{3.22}$$

The reason we do this is because the fields ξ and η have different scaling:

$$\begin{aligned} \langle 0|\, T\{\xi_c(x)\bar{\xi}_c(0)\}\,|0\rangle &= \frac{\not{n}\not{\bar{n}}}{n\cdot\bar{n}}\,\langle 0|\, T\{\psi_c(x)\bar{\psi}_c(0)\}\,|0\rangle\,\frac{\not{\bar{n}}\not{n}}{n\cdot\bar{n}} \\ &\sim \int d^4k \frac{\not{n}\not{\bar{n}}\,\not{k}\,\not{\bar{n}}\not{n}}{k^2} \\ &\sim \lambda^4\cdot\lambda^0\cdot\lambda^{-2} = \lambda^2\,. \end{aligned} \tag{3.23}$$

For the η component, the numerator has two additional powers of λ because only the subleading component $n\cdot k\sim\lambda^2$ survives the projectors. For the soft field, every momentum component scales as λ^2. Thus, we obtain the scalings

$$\xi\sim\lambda\,, \qquad \eta\sim\lambda^2\,, \qquad \psi_s\sim\lambda^3\,. \tag{3.24}$$

For the gluon fields we write

$$\langle 0|\, T\{A^\mu(x)A^\nu(0)\,|0\rangle \sim \int\frac{d^4k}{(2\pi)^4}\frac{1}{k^2}\left\{-g^{\mu\nu}+\xi\frac{k^\mu k^\nu}{k^2}\right\}, \tag{3.25}$$

showing that a gluon field counts as its momentum $A^\mu\sim k^\mu$, leading to

$$\bar{n}\cdot A_c\sim\lambda^0\,, \qquad n\cdot A_c\sim\lambda^2\,, \qquad A_\perp\sim\lambda\,, \qquad A_s^\mu\sim\lambda^2\,. \tag{3.26}$$

We can now construct the SCET Lagrangian of QCD. Since the η components of the fermions are power-suppressed, they can be integrated out from the theory. To this end, we write down the collinear quark Lagrangian:

$$\begin{aligned} \mathcal{L}_c &= \bar{\psi}_c i\not{D}\psi_c \\ &= \bar{\xi}_c\frac{\not{\bar{n}}}{2}(n\cdot iD)\xi_c + \bar{\xi}_c(iD_\perp)\eta_c + \bar{\eta}_c(iD_\perp)\xi_c + \bar{\eta}_c\frac{\not{n}}{2}(\bar{n}\cdot iD)\eta_c\,. \end{aligned} \tag{3.27}$$

By deriving the equations of motion from this Lagrangian and solving for η_c, we can remove the power-suppressed component of the quark from the theory. This yields the identities [21, 26]

$$\eta_c = -\frac{\not{\bar{n}}}{2\bar{n}\cdot iD}(i\not{D}_\perp)\xi_c\,, \qquad \bar{\eta}_c = -\bar{\xi}_c i\overleftarrow{\not{D}}_\perp\frac{\not{\bar{n}}}{2\bar{n}\cdot i\overleftarrow{D}}\,, \tag{3.28}$$

leading to the effective collinear Lagrangian

$$\mathcal{L}_c = \bar{\xi}_c \frac{\bar{n}\!\!\!/}{2}(n \cdot iD)\xi_c + \bar{\xi}_c i\not{D}_\perp \frac{1}{\bar{n} \cdot iD} i\not{D}_\perp \frac{\bar{n}\!\!\!/}{2}\xi_c \,, \tag{3.29}$$

containing the gauge-kinetic terms for the leading collinear quark field. The equivalent Lagrangian for the anti-collinear fermions are found from the obvious replacements $c \to \bar{c}$ and $n \leftrightarrow \bar{n}$. The kinetic terms for collinear gluons are simply given by

$$\mathcal{L}_c^{g,\text{kin}} = -\frac{1}{4} F^a_{c,\mu\nu} F_c^{a,\mu\nu} \,, \tag{3.30}$$

where $F_c^{a,\mu\nu}$ is the field strength tensor of the collinear gluons $A_c^{a,\mu}$.

As noted in the previous section, interactions between the soft and collinear sectors are more involved since we need to perform the multipole expansion, as discussed in ref. [26] (see also the chapter 4 in the review [21]). Since soft modes are not relevant for this work, we will skip the discussion here.

3.4. Wilson Lines

When constructing effective operators in SCET, we typically find non-local operators by the means of identity (3.16), since derivatives along the large momentum component are not power-suppressed. However, these operators are not allowed in a realistic model, since expressions of the form

$$\bar{\psi}_c(x + s\bar{n})\psi_c(x) \tag{3.31}$$

are in general not gauge-invariant by themselves. In order to restore gauge invariance, we have to introduce *Wilson lines*, defined for collinear fields by

$$[x + s\bar{n}, x] \equiv \hat{P} \exp\left[ig \int_0^s dt\, \bar{n} \cdot A_c(x + t\bar{n})\right] . \tag{3.32}$$

Here $\hat{P}$ is the path ordering operator. A collinear fermion field, transforming under the gauge symmetry according to $\psi_c(x) \to V_c(x)\psi_c(x)$, can now be dressed with a Wilson line, which itself transforms as

$$[x + s\bar{n}, x] \;\to\; V_c(x + s\bar{n})\,[x + s\bar{n}, x]\,V_c^\dagger(x) \,. \tag{3.33}$$

Inserting now a Wilson line between the fields in eq. (3.31) yields

$$\bar{\psi}_c(x + s\bar{n})[x + s\bar{n}, x]\psi_c(x) \,, \tag{3.34}$$

which is gauge invariant.

The transformation property (3.33) can now be used to define *gauge covariant building blocks* by using Wilson lines extending to infinity:

$$W_c(x) \equiv [x, -\infty\,\bar{n}] = \hat{P} \exp\left[ig \int_{-\infty}^{0} ds\, \bar{n} \cdot A_c(x + s\bar{n})\right] . \tag{3.35}$$

Assuming gauge functions vanishing at infinity, the object $W_c(x)$ transforms as

$$W_c(x) \to V_c(x) W_c(x) , \tag{3.36}$$

and the objects

$$\chi_c(x) \equiv W_c^\dagger(x)\xi_c(x) \qquad\qquad \bar{\chi}_c(x) = \bar{\xi}_c(x) W_c(x) \tag{3.37}$$

are gauge invariant by themselves. Similarly, we can define the building blocks for collinear gluons and their perpendicular components

$$\mathcal{A}_c^\mu \equiv W_c^\dagger(x)\,(iD_c^\mu W(x)) \qquad\qquad \mathcal{A}_{c\perp}^\mu \equiv W_{c\perp}^\dagger(x)\,(iD_{c\perp}^\mu W(x)) , \tag{3.38}$$

Together with these, one defines the covariant derivative

$$i\mathcal{D}_\mu = i\partial_\mu + \mathcal{A}_\mu , \tag{3.39}$$

dressed with appropriate indices c and $\perp$. The objects defined in (3.37) and (3.38) can now be used to construct effective operators non-local along the direction of large momentum. An example of such a construction is the QCD factorization formula, which will be centrally important in the next chapter.

3.5. Concluding Remarks

When constructing the SCET Lagrangian, we have to do so with a particular kinematic situation in mind, since the relevant effective degrees of freedom are field modes collinear and anti-collinear to the large momenta in the process. Depending on the process at hand, other modes can become important. In this way, the application of SCET to a problem can require a significant amount of preparatory work, where the relevant degrees of freedom need to be identified and the appropriate Lagrangian needs to be constructed. The trade off is that SCET properly treats multi-scale problems, allowing one to resum logarithms that could not be resummed otherwise. Just as in a conventional EFT, this is possible because the physics associated to the different scales factorize into functions depending on a single scale. In the simplest example where a heavy particle decays to two massless particles and soft interactions are suppressed, these functions are called the *hard functions*, encoding short distance physics, and the *jet functions*, which describe the physics

associated with the collinear and anti-collinear legs of the process. Renormalizing and scale-evolving them to a common scale then resums the large logarithms.

The emergence of factorization theorems from the effective theory are not always as apparent as in the case of eq. (3.20). As an example, when multiple collinear sectors are present in the theory, soft and ultra-soft particle exchanges between the sectors can spoil the naive factorization. In this case, one needs to perform a field redefinition of the collinear fields, called *decoupling transformation* to absorb the soft exchanges into a *soft function* and restore factorization [27–32].

As we have seen, SCET is the appropriate effective theory for processes where the relevant degrees of freedom are light and highly energetic. The theory was developed for inclusive radiative decays of the B meson, in which the hard scale is set by the heavy decaying meson [33]. Ever since then, the theory has seen application to numerous similar decays, both inclusive and exclusive. Examples are the above-mentioned inclusive $B \to X_s\gamma$ decays[3], inclusive $B \to X_u l\nu$ probing the CKM matrix element $|V_{ub}|$ [43], and exclusive B decays like various $B \to D$ decays [44, 45] and B decays into pions and kaons [46–48]. In all of these cases, the scale separation between the hard scale and the hadronic scale is not large enough to work at leading power and thus, power corrections need to be taken into account. In contrast to that, SCET is also a popular choice for collider physics applications, where light particles are produced with typically very large momenta. This includes computations of cross sections as well as describing the dynamics of individual jets in the final state. The list of studies using SCET here is long and growing steadily. See the last chapter of ref. [21] for a very long compilation of relevant literature on the subject. Further applications are exclusive hadronic decays of electroweak bosons like W, Z and the Higgs, where the hard scale is set by the heavy mass of the decaying bosons. We will discuss these at length in the next two chapters.

[3] In addition to the analysis [33], the decay has been studied in great deal including power corrections [27–29, 31, 32], perturbative corrections [34–40] and non-perturbative treatment of the soft function [41, 42].

4. Exclusive Hadronic Decays of Electroweak Bosons

In the next two chapters, we will discuss exclusive hadronic decays of Z, W and Higgs bosons. These are decays where the final state contains individual hadrons. To compute processes of this class, we need a way of dealing with the non-perturbative dynamics of hadron formation. The reason why we can still make predictions for the decays in question is the hierarchy between the momentum-transfer scale in the process and the hadronization scale. If the scale separation is large enough, we can expand in the scale ratio and obtain the QCD factorization formula, resulting in the hadronization being parameterized by a process-universal function that can be separated from the process-specific hard-scattering function.

We will explain the framework in the next section and then apply it to hadronic decays of Z and W bosons. The decay channels discussed are $Z \to M\gamma$, $W \to M\gamma$, as well as $Z \to MW$. In the following chapter, we will extend our analysis to exclusive decays of the Higgs boson, using the tools developed in this chapter. The results presented in these two chapters are published in refs. [49–54].

4.1. The QCD Factorization Approach

The QCD factorization (QCDF) approach [55–59] is applicable to exclusive processes with a large energy release to the hadrons in the final state. Amplitudes are given as convolutions of partonic hard scattering kernels with hadronic matrix elements, called light-cone distribution amplitudes (LCDAs). The result is given as an expansion in the scale ratio between the large energy release into the final state and the typical energy scale of hadronization: $\lambda \sim \Lambda_{\mathrm{QCD}}/E$. The intuitive picture as to why the result splits into these independent parts is a consequence of the large scale separation: While the hard-scattering (physics at high momentum transfer) happens at very short time and distance scales, hadronization takes a longer time. Through this, the physics of hadronization does not see the details of how the partons where created, because it sets in at a time where the partonic scattering has already happened. In this way, the formalism is very similar to deep-inelastic scattering, where the non-perturbative effects in the initial state hadron are described by the parton distribution functions (PDFs).

Originally developed in light-cone perturbation theory, the QCDF formalism can be rephrased in the language of SCET, where the decay amplitude will factorize into partonic scattering and a hadronic quantity. We will see that the partonic scattering amplitude will become the Wilson coefficient of an effective non-local SCET operator that, sandwiched between the QCD vacuum and the hadronic final state, becomes the LCDA. In this way, the problem factorizes into a hard function (the Wilson coefficient), living at the high scale, and the hadronic function, living at the low scale. By evaluating the two parts each at their natural scale and RG-evolving them to one common scale, large logarithms of the form $\alpha_s \log \Lambda_{\text{QCD}}/v$ are resummed to all orders.

Typical applications of QCDF in the past were exclusive decays of heavy mesons in regions where the partonic momentum transfer allows for a perturbative treatment [60–63]. In these applications, the high scale is of the order of the mass of the heavy meson, meaning $\sim \mathcal{O}(5\text{ GeV})$. Due to this, these examples are plagued by the fact that the expansion parameter λ is not very small and that power corrections become non-negligible and hard to distinguish from hadronic uncertainties. We will see that the latter is also a consequence of the relatively small value for the high scale.

In our case, the decays of heavy electroweak gauge bosons and the Higgs, the high scale is very large compared to Λ_{QCD}, as it is set by the mass of the decaying boson. This has two benefits: Power corrections will parametrically be suppressed by powers of m_M/v where m_M is the mass of the final state meson and v stands for any weak-scale mass. Even in the worst possible case, this parameter would be $m_B/m_W \sim 0.05$. The second benefit comes from renormalization group effects, which render hadronic uncertainties small as we evolve the LCDAs to the high scale. As a result, our predictions are theoretically relatively clean. The downside is that the decays rates are very small and are experimentally challenging. Still, with the large number of W, Z and Higgs bosons produced at LHC and possible next-generation particle colliders in the future, measuring exclusive hadronic W, Z and Higgs decays can yield important information on both the validity of the QCDF approach as well as possible new physics.

4.1.1. The Factorization Formula

We will start by deriving a factorization formula for the decay $Z \to M\gamma$ and furthermore assume that the meson M does not transform as a singlet under the flavor symmetry $SU(N_f)$. Later on, we will generalize to the flavor-singlet case and consider decays of the Higgs boson as well.

We assign the momenta k and q to the final state meson and the photon respectively. In the rest frame of the decaying Z boson, the quarks inside the meson move along the direction of the meson momentum k, with small perturbations of $\mathcal{O}(\Lambda_{\text{QCD}})$ due to the dynamics of the binding force. The meson momentum obeys collinear

scaling $k \sim m_Z(1, \lambda^2, \lambda)$, with the power-counting parameter $\lambda \sim \Lambda_{\rm QCD}/m_Z$. In the language of SCET, we need to find operators made from collinear partons with correct quantum numbers to excite the meson from the QCD vacuum. SCET tells us that operators with more fields are power-suppressed, so the leading contribution comes from operators with two collinear partons. With the help of our gauge covariant building blocks defined in eq. (3.37), we can write down the decay amplitude for $Z \to M\gamma$:

$$\mathcal{A} = \sum_i \int dt\, \mathcal{C}_i(t,\mu)\, \langle M(k)|\, \bar\chi_c(t\bar n) \frac{\bar{n}\!\!\!/}{2} \Gamma_i\, \chi_c(0)\, |0\rangle + \text{subleading power}\,. \tag{4.1}$$

Here $\Gamma_i \in \{1, \gamma^5, \gamma_\perp^\mu\}$ are the possible spin structures with appropriate quantum numbers to create the meson M. The Wilson coefficients can be determined in a matching computation from perturbation theory and are specific to each decay. They describe the hard scattering at the factorization scale μ. We can use the definition of the building blocks (3.37) to rewrite the field operators in the matrix elements into the quark fields and a Wilson line:

$$\langle M(k)|\, \bar\chi_c(t\bar n)\, \frac{\bar{n}\!\!\!/}{2}\, \Gamma_i\, \chi_c(0)\, |0\rangle = \langle M(k)|\, \bar q(t\bar n)\, \frac{\bar{n}\!\!\!/}{2}\, \Gamma_i\, [t\bar n, 0]\, q(0)\, |0\rangle\ . \tag{4.2}$$

These matrix elements define the LCDAs of pseudoscalar and vector mesons. For the pseudoscalars we have

$$\langle P(k)|\, \bar q(t\bar n) \frac{\bar{n}\!\!\!/}{2}\, \gamma^5\, [t\bar n, 0]\, q(0)\, |0\rangle = -i f_P \bar n\cdot k \int_0^1 dx e^{i(xk)\cdot(t\bar n)} \phi_P(x,\mu)\,, \tag{4.3}$$

whereas for the longitudinal and transverse polarizations of the vector mesons it is

$$\begin{aligned} \langle V_\parallel(k)|\, \bar q(t\bar n) \frac{\bar{n}\!\!\!/}{2} [t\bar n, 0] q(0)\, |0\rangle &= -i f_V \bar n\cdot k \int_0^1 dx e^{i(xk)\cdot(t\bar n)} \phi_V(x,\mu)\,, \\ \langle V_\perp(k)|\, \bar q(t\bar n) \frac{\bar{n}\!\!\!/}{2} \gamma_\perp^\mu [t\bar n, 0] q(0)\, |0\rangle &= -i f_V^\perp(\mu) \bar n\cdot k\, \varepsilon_V^{\perp *\mu} \int_0^1 dx e^{i(xk)\cdot(t\bar n)} \phi_V^\perp(x,\mu)\,. \end{aligned} \tag{4.4}$$

Here E is the energy of the meson, $\varepsilon_V^\perp$ is the polarization vector of the transverse vector meson and $\phi_M(x,\mu)$ are the LCDAs and f_M are the meson decay constants. Their definition is recovered in the local limit $t \to 0$ after using the normalization of the LCDAs $\int_0^1 \phi(x) dx = 1$. Explicitly we have:

$$\begin{aligned} \langle P(k)|\bar q_1 \gamma^\mu \gamma^5 q_2|0\rangle &= -i f_P k^\mu\,, \\ \langle V(k)|\bar q_1 \gamma^\mu q_2|0\rangle &= -i f_V m_V \varepsilon_V^{*\mu}\,, \\ \langle V_\perp(k)|\bar q_1 i\sigma^{\mu\nu} q_2|0\rangle &= i f_V^\perp(\mu)(k^\mu \varepsilon^{*\nu} - k^\nu \varepsilon^{*\mu})\,. \end{aligned} \tag{4.5}$$

For mesons being superpositions of multiple flavor states $|M\rangle = \sum_q c_q^M |\bar{q}q\rangle$ it is useful to introduce flavor-specific decay constants f_M^q which are defined analogously to the above equations but with respect to one flavor-specific current $j^{(q)} = \bar{q}\,\Gamma\,q$. The scale-dependence of the transverse decay constant can be understood by the fact that it is associated with a non-conserved QCD current[1]. It is now clear that the LCDAs are simply the generalization of the decay constants to the non-local case. The variable $x \in [0,1]$ is called momentum fraction variable and the LCDA at leading order can thus be interpreted as the probability amplitude to find a quark with the momentum xk^μ and the anti-quark with the momentum $\bar{x}k^\mu = (1-x)k^\mu$ in the meson.

We can further simplify the factorization formula by introducing the Fourier transform of the Wilson coefficient

$$\int dt\, \mathcal{C}_i(t,\mu)\, e^{i(xk)\cdot(t\bar{n})} = H_i(x,\mu)\,, \tag{4.6}$$

which is the hard function in momentum space. Inserting this into eq. (4.1) along with the definition of the LCDAs and using that for each meson only a single spin structure contributes, we obtain

$$\mathcal{A} = -if_M\, E \int_0^1 dx\, H_M(x,\mu)\, \phi_M(x,\mu) + \text{power corrections}\,. \tag{4.7}$$

To compute the hard function systematically, one defines the so-called light-cone projectors [63, 64]. These are applied to the partonic amplitudes with the partons assigned momenta $k_1^\mu = xk^\mu + k_\perp^\mu$ and $k_2^\mu = \bar{x}k^\mu - k_\perp^\mu$. The partonic amplitudes are then replaced by:

$$\bar{u}(k_1) A(q,k_1,k_2)\, v(k_2) \to \int_0^1 dx\, \mathrm{Tr}\left[M_M(k,x,\mu)\, A(q,k_1,k_2)\right]_{k_\perp \to 0}\,. \tag{4.8}$$

Here $M_M(k,x,\mu)$ is the light-cone projector for the meson M. The leading-power expressions for pseudoscalar, longitudinal vector and transverse vector mesons are:

$$\begin{aligned} M_P(k,x,\mu) &= i\frac{f_P}{4}\not{k}\gamma_5\, \phi_P(x,\mu)\,, \\ M_V^{\parallel}(k,x,\mu) &= -i\frac{f_V}{4}\not{k}\, \phi_V(x,\mu)\,, \\ M_V^{\perp}(k,x,\mu) &= i\frac{f_V^\perp(\mu)}{4}\not{k}\not{\epsilon}_V^{\perp *}\, \phi_V^\perp(x,\mu)\,. \end{aligned} \tag{4.9}$$

Corrections arising at subleading power in the expansion in Λ_{QCD}/E are discussed in Appendix A.

[1] When generalizing the factorization formula to the case of flavor singlet mesons, we will see that the pseudoscalar decay constant is also scale-dependent since the axial anomaly spoils the conservation of the axial vector current.

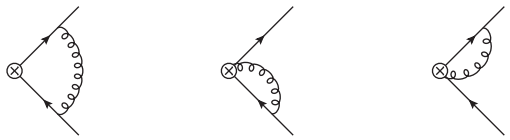

Fig. 4.1.: Examples of one-loop QCD corrections to the LCDAs. In the second and third graph, the gluon is emitted from the Wilson line between the fields in the bi-local current.

4.1.2. Renormalization of the Light-Cone Distribution Amplitudes

Since we are dealing with a huge scale hierarchy, we have to worry about large logarithms arising from radiative corrections at order $\mathcal{O}(\alpha_s)$. The light-cone distributions are defined as matrix elements of currents between the QCD vacuum and the hadronic final state. The resummation of large logarithms is carried out by the renormalization of these currents. Diagrammatically, this is performed by evaluating one-loop diagrams like the ones shown in Fig. 4.1. The renormalization of the LCDAs is multiplicative in the sense of a convolution over the momentum-fraction variable:

$$\phi_M^{\text{bare}}(x) = \left[Z_\phi^{-1}(\mu) \otimes (f_M(\mu)\phi_M(\mu))\right](x) = \int_0^1 dy\, Z_\phi^{-1}(x,y,\mu)\; (f_M(\mu)\,\phi_M(y,\mu)) \tag{4.10}$$

The renormalization kernel Z_ϕ at one-loop order in QCD is [55, 59]:

$$Z_\phi(x,y,\mu) = \delta(x-y) + \frac{\alpha_s(\mu)\,C_F}{4\pi\epsilon} V_0(x,y) + \mathcal{O}(\alpha_s^2)\,, \tag{4.11}$$

where $V_0(x,y)$ is the one-loop Brodsky-Lepage kernel, explicitly given by:

$$\begin{aligned} V_0(x,y) =& \delta(x-y) - \frac{2}{y\,\bar{y}}\left[x\,\bar{y}\,\frac{\theta(y-x)}{y-x} + y\,\bar{x}\,\frac{\theta(x-y)}{x-y}\right]_+ \\ & - 2c_\Gamma\left[\frac{x}{y}\,\theta(y-x) + \frac{\bar{x}}{\bar{y}}\,\theta(x-y)\right], \end{aligned} \tag{4.12}$$

with $c_\Gamma = 1$ for pseudoscalar and longitudinal vector mesons and $c_\Gamma = 0$ for transverse vector mesons. The expression $[...]_+$ denotes the symmetric plus distribution, defined as:

$$[f(x,y)]_+ = f(x,y) - \delta(x-y)\int_0^1 dw\, f(w,y)\,. \tag{4.13}$$

The renormalization group equation for the LCDAs follows straightforwardly from our derivation in section 2.3.2, by demanding that the product $\mathcal{C}(\mu)\,\langle\mathcal{O}(\mu)\rangle$ has to be

independent of the renormalization scale μ. In the present case, the matrix element $\langle \mathcal{O}(\mu) \rangle$ is a product of the LCDA ϕ_M and the meson decay constant f_M, which - in the case of a transverse vector meson - is renormalized and thus scale dependent. The renormalization group equation for the LCDA is

$$\mu \frac{d}{d\mu} \phi_M(x,\mu) = -\int_0^1 dy\, V(x,y,\mu)\, \phi_M(y,\mu)\,. \tag{4.14}$$

This integro-differential equation can be cast into an infinite set of simple differential equations. To this end, the LCDAs are expanded in the basis of Gegenbauer polynomials according to [55, 59]

$$\phi_M(x,\mu) = 6x\,(1-x) \left[1 + \sum_{n=1}^{\infty} a_n^M(\mu) C_n^{(3/2)}(2x-1) \right], \tag{4.15}$$

where $C_n^{(m)}(w)$ are the Gegenbauer polynomials and the coefficients $a_n^M(\mu)$ are called Gegenbauer moments. They contain the scale dependence of the LCDA. Combining eqs. (4.14) and (4.15), the RG equation for the LCDA can then be turned into a set of RG equations for the Gegenbauer moments:

$$\mu \frac{d}{d\mu} a_n^M(\mu) = -\gamma_{nm} \frac{\alpha_s(\mu)}{4\pi} a_m^M(\mu)\,. \tag{4.16}$$

At one-loop order in QCD, the anomalous dimension is a diagonal matrix with the diagonal entries:

$$\gamma_n = 2C_F \left(4H_{n+1} - \frac{2}{(n+1)(n+2)} - 3 \right), \qquad \text{and} \quad H_n = \sum_{k=1}^{n} \frac{1}{k}\,. \tag{4.17}$$

This is in fact the reason why the LCDAs are expanded in Gegenbauer polynomials in the first place: They are the eigenfunctions of the Brodsky-Lepage kernel.

Note that for every n, the anomalous dimensions are positive, $\gamma_n > 0$. Glancing at the leading-order solution

$$a_n^M(\mu) = \left(\frac{\alpha_s(\mu)}{\alpha_s(\mu_0)} \right)^{\frac{\gamma_n}{2\beta_0}} a_n^M(\mu_0) \tag{4.18}$$

and noting that for $\mu > \mu_0$ the ratio of strong couplings is always smaller than 1, it can be seen that the Gegenbauer moments decrease when evolved to a high scale. In the limit $\mu \to \infty$, all moments vanish and the LCDA takes the form

$$\phi_M(x, \mu \to \infty) = 6x(1-x)\,, \tag{4.19}$$

for any meson. This means that the influence of the Gegenbauer moments on the final result weakens with higher renormalization scales. In Fig. 4.2, some examples

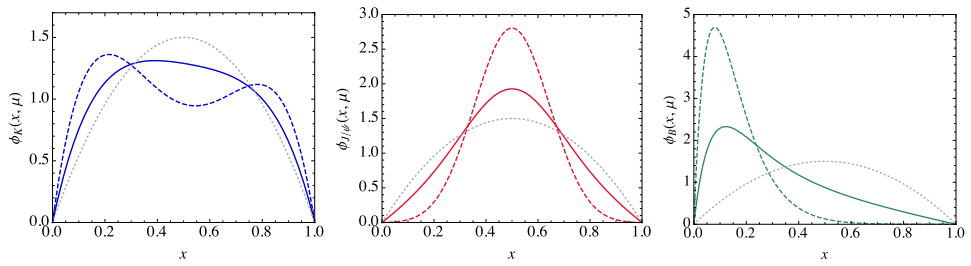

Fig. 4.2.: LCDAs of the kaon (left), J/ψ (middle), and the B meson (right) at the hadronic scale $\mu_0 = 1\,\text{GeV}$ (dashed colored lines) and the high scale $\mu = m_Z$ (solid colored lines). The gray dotted line denotes the asymptotic LCDA in the limit $\mu \to \infty$.

are shown for the LCDAs of the kaon, the J/ψ and the B, evolved from a hadronic reference scale $\mu_0 = 1\,\text{GeV}$ up to the scale $\mu = m_Z$. One can see that the scale-evolved LCDAs is considerably closer to the shown asymptotic form, rendering the dependence of the result on the moments a_n small. Since these Gegenbauer moments are usually not very well-known, this also means that the uncertainties associated with them are weaker than in typical applications of the QCDF approach.

The solution (4.18) resums the leading large logarithms $\alpha_s \log(\mu_0/m_Z)$. The RG resummation of the next-to-leading logarithms requires the two-loop renormalization of the LCDA, which is more complicated [65–70]. The anomalous dimension matrix for this case is no longer diagonal but lower triangular, meaning that Gegenbauer moments of order m mix under renormalization with moments of order $0 < k \leq m$. Considering the large uncertainties in the moments a_n^M we neglect these effects.

When computing radiative corrections in dimensional regularization, additional subtleties arise from the γ^5 matrices in the loops, which anti-commute with the Dirac matrices γ^μ only in $d = 4$ dimensions. As discussed in Appendix B, the axial current $j^{\mu 5} = \bar{\psi}\gamma^\mu\gamma^5\psi$ receives a finite renormalization to preserve the chiral Ward identities

$$j^{\mu 5} = Z_{\text{HV}}(\mu)\, j^{\mu 5}_{(0)} = \left(1 - \frac{\alpha_s(\mu) C_F}{\pi} + \mathcal{O}(\alpha_s^2)\right) j^{\mu 5}_{(0)}\,. \tag{4.20}$$

In the hadronic decays of the Higgs boson, the pseudoscalar current $j^5 = \bar{q}\gamma^5 q$ is relevant for the Yukawa couplings of the quarks. This current receives a finite renormalization [71]

$$Z^P_{\text{HV}} = 1 - 2\frac{\alpha_s(\mu) C_F}{\pi} + \mathcal{O}(\alpha_s^2)\,. \tag{4.21}$$

Similarly, a finite renormalization is needed for the non-local axial current that

defines the LCDA of a pseudoscalar meson according to eq. (4.3):

$$\phi_{P,\mathrm{HV}}(x,\mu) = \int_0^1 dy\, Z^{-1}_{\mathrm{HV}}(x,y,\mu)\, \phi_P(y,\mu)\,. \tag{4.22}$$

The renormalization kernel is [72]:

$$Z^{-1}_{\mathrm{HV}}(x,y,\mu) = \delta(x-y) + \frac{2\alpha_s(\mu)C_F}{\pi}\left[\frac{x}{y}\theta(y-x) + \frac{\bar{x}}{\bar{y}}\theta(x-y)\right] + \mathcal{O}(\alpha_s^2)\,. \tag{4.23}$$

This achieves the finite renormalization of $\phi_P(x,\mu)$, as is seen by integrating $\phi_{P,\mathrm{HV}}(x,\mu)$ over x, yielding

$$\begin{aligned}\int_0^1 dx\, \phi_{P,\mathrm{HV}}(x,\mu) &= \int_0^1 dy \left(\int_0^1 dx\, Z^{-1}_{\mathrm{HV}}(x,y,\mu)\right) \phi_P(y,\mu) \\ &= \left(1 + \frac{\alpha_s(\mu)C_F}{\pi}\right)\int_0^1 dy\, \phi_P(y,\mu) \\ &= Z^{-1}_{\mathrm{HV}}(\mu)\,,\end{aligned} \tag{4.24}$$

where $Z_{\mathrm{HV}}(\mu)$ in the last line is precisely the renormalization constant in eq. (4.20).

According to eq. (4.10), the matrix elements of the currents we are renormalizing with diagrams like the ones shown in Fig. 4.1 define the products of the LCDAs and the meson decay constants. In the case of transverse vector mesons, the decay constants are scale-dependent as well, since the QCD tensor current $j_T^{\mu\nu} = \bar{q}\, i\sigma^{\mu\nu} q$ is not conserved. The scaling behavior of the transverse decay constants is governed by the RG equation

$$\mu\frac{d}{d\mu} f_V^{\perp}(\mu) = -\gamma^T(\mu) f_V^{\perp}(\mu)\,, \qquad \text{with} \qquad \gamma^T = \sum_{k=0}^{\infty} \gamma_k^T \left(\frac{\alpha_s(\mu)}{4\pi}\right)^k. \tag{4.25}$$

The one- and two-loop contributions to the anomalous dimension are [73]

$$\gamma_0^T = 2\,C_F\,, \qquad \text{and} \qquad \gamma_1^T = -19\,C_F^2 + \frac{257}{9} C_F\, C_A - \frac{52}{9} C_F\, T_F n_f\,. \tag{4.26}$$

Using the ingredients in this section, we can resum the logarithms $\alpha_s \log(\mu_0/m_Z)$ arising from the one-loop corrections to the hard scattering kernels.

4.1.3. Accessing the Meson LCDAs

In order to make actual predictions, we need values for the Gegenbauer moments a_n^M. They are non-perturbative quantities, and therefore there is no way to predict them from first principles in an analytic computation. Determining them numerically using lattice gauge theory is challenging because in these frameworks one uses a

euclidean spacetime, making light-cone kinematics hard to access. Nevertheless, estimates for the first few Gegenbauer moments exist for light mesons from the lattice and light-cone QCD sum rules and have been extracted from data [74–76]. The compiled list of results along with the corresponding references they were taken from is found in Appendix C.

For mesons containing heavy quarks $Q = c, b$, the relatively high quark mass m_Q introduces another relevant scale to the hierarchy $v > m_Q > \Lambda_{\rm QCD}$. Using effective theories, estimates on the LCDA shapes can be obtained.

For heavy quarkonia $M \sim (\bar{Q}Q)$, we can make several assumptions on the LCDA shape. In the limit of $m_Q \to \infty$, the LCDA should simply be $\delta(x - 1/2)$, as both quarks are at rest in the meson rest frame and carry exactly half of the meson momentum. Corrections to this distribution can be estimated from non-relativistic QCD (NRQCD), where one systematically expands in the small velocity of the heavy quarks $v \sim \alpha_s(m_Q v)$ [12, 13]. Reference [77] quotes the relation between the LCDA and the second moment of v:

$$\int_0^1 dx \frac{\phi_M(x,\mu_0)}{x} = \int_0^1 dx \frac{\phi_M(x,\mu_0)}{\bar{x}} = 2\left[1 + \frac{\langle v^2\rangle_M}{3} + \mathcal{O}(v^4)\right]. \tag{4.27}$$

As a plausible model LCDA for a heavy quarkonium, we choose a Gaussian function

$$\phi_M(x,\mu_0) = N_\sigma \frac{4x\bar{x}}{\sqrt{2\pi}\sigma} \exp\left[-\frac{(x-\frac{1}{2})^2}{2\sigma^2}\right], \tag{4.28}$$

with N_σ such that $\int_0^1 dx\, \phi_M(x,\mu_0) = 1$ and $\mu_0 = 1\,\text{GeV}$, with $\sigma^2 = \langle v^2\rangle_M/12$. For the transverse vector mesons, the relevant NRQCD relation, including one-loop QCD corrections, is [78, 79]:

$$4\sigma_V^2(\mu) = \int_0^1 dx\,(2x-1)^2 \phi_V^\perp(x,\mu) = \frac{\langle v^2\rangle_V}{3} + \frac{\alpha_s(\mu) C_F}{4\pi}\left(\frac{28}{9} - \frac{2}{3}\log\frac{m_Q^2}{\mu^2}\right) \tag{4.29}$$

For the second moments $\langle v^2\rangle_M$ we use the estimates

$$\langle v^2\rangle_{J/\psi} \sim 0.30 \pm 0.15\,, \qquad \langle v^2\rangle_{\Upsilon(1S)} \sim 0.10 \pm 0.05\,. \tag{4.30}$$

The Gegenbauer moments of the model functions $\phi_{J/\psi}$ and $\phi_{\Upsilon(1S)}$ can be extracted by inverting the expansion (4.15), giving

$$a_n^M(\mu) = \frac{2(2n+3)}{3(n+1)(n+2)} \int_0^1 dx\, C_n^{(3/2)}(2x-1)\,\phi_M(x,\mu)\,. \tag{4.31}$$

For our numerical analysis, we keep the first 20 Gegenbauer moments obtained in this way.

For heavy-light mesons $M \sim (\bar{Q}q)$, a similar approach is chosen. First, the LCDA in this case should peak at a small value $x \sim \Lambda_{\text{QCD}}/m_M$ with x being the momentum fraction of the light quark. The proper effective theory in this case is HQET. Using HQET, one can define [61]

$$\int_0^1 dx \frac{\phi_M(x,\mu_0)}{x} \equiv \frac{m_M}{\lambda_M(\mu_0)} + \text{power corrections}\,, \tag{4.32}$$

where the hadronic parameter $\lambda_M(\mu_0) \sim \Lambda_{\text{QCD}}$ does not depend on m_Q and is poorly known. For the B meson, an estimate from QCD sum rules exists: $\lambda_B(1\,\text{GeV}) = (460 \pm 110)\,\text{MeV}$ [80]. Since the parameter is independent of the heavy quark-mass m_Q, we use this for both B and D mesons. For B_s and D_s, we use $\lambda_{M_s} - \lambda_M \sim 90\,\text{MeV}$ [81] and conservatively estimate the error to be $\Delta\lambda_{M_s} = \pm 150\,\text{MeV}$. Similarly to the heavy meson case in eq. (4.28), we use as a model LCDA [82]:

$$\phi_M(x,\mu_0) = N_\sigma \frac{x\bar{x}}{\sigma^2} \exp\left(-\frac{x}{\sigma}\right) \qquad \text{with} \qquad \sigma = \frac{\lambda_M(\mu_0)}{m_M}\,. \tag{4.33}$$

Again, N_σ is a constant factor ensuring the proper normalization of the LCDA. For mesons where the light quark is the antiquark $M \sim (\bar{q}Q)$, one replaces $x \leftrightarrow \bar{x}$.

4.1.4. The Case of Flavor-Singlet Mesons

In section 4.1.1 we wrote down the QCD factorization formula under the assumption that the final state meson M does not contain a flavor-singlet component. In the naive constituent quark model, a meson state written as

$$|M\rangle = \sum_i^{n_f} c_{q_i}^M \, |q_i\bar{q}_i\rangle \;, \tag{4.34}$$

is a flavor-singlet if all flavor coefficients are equal $c_{q_i}^M = 1/\sqrt{n_f}$. In this case, the meson can be formed not only from two collinear quarks but two collinear gluons as well. Note that the flavor coefficients c_q^M for nonsinglet mesons obey $\sum_i c_{q_i}^M = 0$ and thus the gluon contribution cancels out, as gluons couple to each flavor equally. The additional two-gluon contribution to the factorization formula makes the situation more complicated for two reasons. First, the hadronic matrix elements defining the two-gluon LCDA and the two-quark LCDA mix under renormalization, leading to the fact that the flavor-singlet component of a meson behaves differently under scale variation compared to the nonsinglet component. Furthermore, at high scales the c and b quarks become dynamical fields, changing the number of active flavors n_f and with that the definition of a flavor singlet in eq. (4.34).

In order to establish the factorization formula, we use again the gauge-covariant building blocks defined in (3.38) and (3.38) and write down the bilocal two-gluon

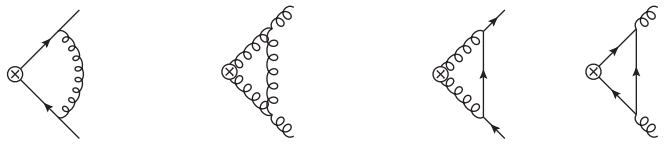

Fig. 4.3.: Examples of one-loop QCD corrections to the LCDAs. The first two graphs are simple $\mathcal{O}(\alpha_s)$ corrections to the quark and gluon LCDAs whereas the last two graphs are examples of corrections mixing the two LCDAs.

current

$$\frac{1}{g_s^2}\langle P(k)|\,\mathrm{Tr}\left[\mathcal{A}^\mu_{c\perp}(t\bar n)\epsilon^\perp_{\mu\nu}\mathcal{A}^\nu_{c\perp}(0)\right]|0\rangle = T_F f_P^{uds}(\mu)\int_0^1 dx\,\frac{e^{i(xk)\cdot(t\bar n)}}{x\;\bar x}\phi_P^g(x,\mu)\,, \quad (4.35)$$

with $\epsilon^\perp_{\mu\nu} = \epsilon_{\mu\nu\rho\sigma}\,\bar n^\rho n^\sigma/(n\cdot\bar n)$ and the trace acting in color space. We have furthermore defined the decay constant f_P^{uds} as a sum of the light-flavor decay constants:

$$f_P^{uds}(\mu) = f_P^u(\mu) + f_P^d(\mu) + f_P^s(\mu)\,. \quad (4.36)$$

The gluon LCDA ϕ_P^g is odd under the transformation $x \leftrightarrow \bar x$ and thus the normalization to f_P^{uds} is arbitrary, but will prove convenient later on. Note that the axial anomaly spoils the conservation of the axial vector current and thus the decay constants are renormalized at two-loop order [83]. With the identity [84]

$$\mathcal{A}^\mu_c(x) = g_s\int_{-\infty}^0 ds\,\bar n_\alpha\left[W_c^\dagger\,G_c^{\alpha\mu}\,W_c\right](x+s\bar n) \quad (4.37)$$

the right-hand side of eq. (4.35) can be written as [85–88]:

$$\langle P(k)|\bar n_\alpha\bar n_\beta G^\alpha{}_{\mu,A}(t\bar n)[t\bar n,0]_{AB}\,\tilde G_B^{\beta\mu}(0)|0\rangle = (\bar n\cdot k)^2 f_P^{uds}(\mu)\int_0^1 dx e^{i(xk)\cdot(t\bar n)}\,. \quad (4.38)$$

Proceeding for the gluon contribution as we did for the quarks in section 4.1.1, we obtain the factorization formula

$$iA_{Z\to P\gamma} = -i\int_0^1 dx\,\left[\sum_q H_q(x,\mu)f_P^q(\mu)\phi_P^q(x,\mu) + f_P^{uds}(\mu)\,H_g(x,\mu)\phi_P^g(x,\mu)\right], \quad (4.39)$$

The flavor-singlet quark and gluon LCDAs are renormalized beginning at $\mathcal{O}(\alpha_s)$ by diagrams as the ones shown in Fig. 4.3. Note that the last two diagrams generate a mixing the quark and gluon LCDAs. To account for this effect, we define a vector

$$\overrightarrow{f\phi}_P(x) = \begin{pmatrix}\sum_q f_P^q\phi_P^q\\ f_P^{uds}\phi_P^g(x)\end{pmatrix}, \quad (4.40)$$

and relate bare and renormalized functions via

$$\overrightarrow{f\phi}_P^{\text{bare}}(x) = \int_0^1 dy\, Z_{f\phi}^{-1}(x,y,\mu)\, \overrightarrow{f\phi}_P(y,\mu)\,, \tag{4.41}$$

where $Z_{f\phi}$ is a matrix of renormalization kernels:

$$Z_{f\phi}(x,y,\mu) = \delta(x-y) + \frac{\alpha_s(\mu)}{4\pi\epsilon}\begin{pmatrix} V_{qq}(x,y) & V_{qg}(x,y) \\ V_{gq}(x,y) & V_{gg}(x,y)\end{pmatrix} + \mathcal{O}(\alpha_s^2)\,. \tag{4.42}$$

Here $V_{qq}(x,y)$ is simply the Brodsky-Lepage kernel as defined in eq. (4.12). The kernel function $V_{gg}(x,y)$ is its analog for the two-gluon case. The off-diagonal kernels parameterize the mixing between the two LCDAs. The explicit expressions have been derived in ref. [89–92] and are relegated to Appendix E. The eigenfunctions of the kernel function V_{gg} are again Gegenbauer polynomials $C_n^{(k)}(\omega)$ and hence the gluon LCDA is customarily written in its Gegenbauer expansion

$$\phi_P^g(x,\mu) = 30x^2\bar{x}^2 \sum_{n=2,4,\ldots} b_n^P(\mu)\, C_{n-1}^{(5/2)}(2x-1)\,, \tag{4.43}$$

where b_n^P are the Gegenbauer moments and only the polynomials odd under the exchange $x \leftrightarrow \bar{x}$ are kept because the gluon LCDA is normalized to zero. The renormalization group equation of the object $\overrightarrow{f\phi}_P$ can be written as

$$\mu\frac{d}{d\mu}\overrightarrow{f\phi}_P(x,\mu) = -\int_0^1 dy\, \Gamma(x,y,\mu)\, \overrightarrow{f\phi}_P(y,\mu)\,, \tag{4.44}$$

with the anomalous dimension matrix

$$\Gamma(x,y,\mu) = 2\alpha_s\frac{\partial}{\partial\alpha_s}Z_{f\phi}^{[1]}(x,y,\mu) = \frac{\alpha_s(\mu)}{2\pi}\begin{pmatrix} V_{qq}(x,y) & V_{qg}(x,y) \\ V_{gq}(x,y) & V_{gg}(x,y)\end{pmatrix} + \mathcal{O}(\alpha_s^2)\,. \tag{4.45}$$

Inserting the Gegenbauer expansion for the LCDAs, the RG equation (4.44) yields the generalization of eq. (4.16) to the flavor-singlet case:

$$\left[\mu\frac{d}{d\mu} + \frac{\alpha_s(\mu)}{4\pi}\begin{pmatrix}\gamma_n^{qq} & \gamma_n^{qg} \\ \gamma_n^{gq} & \gamma_n^{gg}\end{pmatrix} + \mathcal{O}(\alpha_s^2)\right]\begin{pmatrix}\sum_q f_P^q(\mu)\, a_n^{P,q}(\mu) \\ f_P^{uds}(\mu)\, b_n^P(\mu)\end{pmatrix}. \tag{4.46}$$

The explicit expressions of the γ_n^{ij} are given in Appendix E.

In practice, we need to account for the fact that physical mesons are not purely singlet or nonsinglet, but mixed states (see Appendix C for details on the parameterization). Therefore, for a physical pseudoscalar meson P containing a flavor-singlet admixture, the amplitudes need to be split up into singlet and nonsinglet contributions, where the LCDAs scale evolve differently, as we have just seen. As mentioned above already, with higher factorization scales, the b and c quarks become dynamical, reshuffling the singlet and nonsinglet combinations. Therefore, the RG running is slightly more complicated than in the non-singlet case. We will discuss it in detail after having derived the full decay amplitudes.

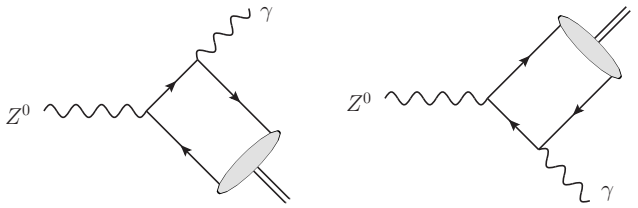

Fig. 4.4.: The tree-level contribution to $Z \to M\gamma$.

4.2. Radiative Z-Boson Decays

We have now gathered the ingredients to compute the decay rates $Z \to M\gamma$, $W \to M\gamma$ and $Z \to WM$. Let us start by analyzing the structure of the contributions to the decay amplitude of $Z \to M\gamma$. The tree-level contribution is depicted in Fig. 4.4. We assign momenta $k_1^\mu = xk^\mu$ to the collinear quark and $k_2^\mu = \bar{x}k^\mu$ to the collinear antiquark, neglecting the small transverse momentum components $k_\perp^\mu$. The intermediate quark propagator is always hard, since it carries both a collinear momentum (from the final state meson) and an anti-collinear momentum (from the photon). In the language of SCET, the intermediate quark can be integrated out and the process is mediated by a tree-level effective operator.

When evaluated, the two partonic graphs yield

$$i\mathcal{A}_{Z\to q\bar{q}\gamma} = \frac{eg\,Q_q}{c_W m_Z^2}\,\bar{u}(xk)\left\{\left[\frac{\not\epsilon_Z(x\not k+\not q)\not\epsilon_\gamma^*}{x} - \frac{\not\epsilon_\gamma^*(\bar{x}\not k+\not q)\not\epsilon_Z}{\bar{x}}\right](v_q - a_q\gamma_5)\right\} v(\bar{x}k)\,. \tag{4.47}$$

Note that the spin chains contain three Dirac matrices in the partonic amplitude. The replacement rule (4.8) tells us to drop the spinors, multiply the amplitude with the light-cone projectors (4.9) and take the trace over the Dirac matrices. Since traces with an odd number of Dirac matrices vanish, only pseudoscalar and longitudinal vector mesons can be produced at leading power. By including the quark mass in the intermediate propagator, contributions to the partonic spin chain are introduced with an even number of Dirac matrices, allowing for projections onto the transverse vector meson. Since we would be trading a large momentum for a small mass, this contribution is of subleading power. Another way of obtaining non-zero traces is by using light-cone projectors of higher twist (see Appendix A), which have different numbers of Dirac matrices, as well. These corrections however also come with small parameters and are thus power-suppressed.

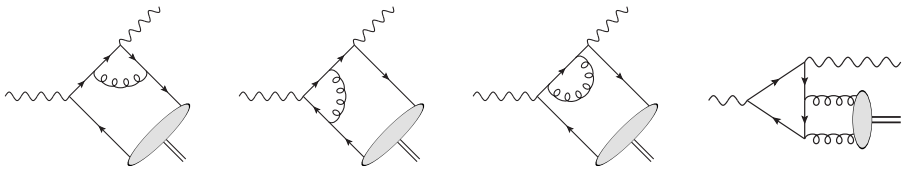

Fig. 4.5.: One-loop corrections to the decay amplitudes $Z \to M\gamma$. In the fourth graph the meson is formed from gluons and contributes only for mesons with flavor-singlet components.

4.2.1. Computation of the Hard Scattering Kernels

After applying the light-cone projectors, the amplitude for $Z \to M\gamma$ can be written in a form factor decomposition:

$$i\mathcal{A} = \pm\frac{eg}{2c_W}\left[i\epsilon_{\mu\nu\alpha\beta}\frac{k^\mu q^\nu \varepsilon_Z^\alpha \varepsilon_\gamma^{*\beta}}{k\cdot q}F_1^M - \left(\varepsilon_Z^\perp \cdot \varepsilon_\gamma^{*\perp}\right)F_2^M\right], \tag{4.48}$$

where the positive sign holds for pseudoscalar mesons and the negative sign for longitudinal vector mesons. The product $\varepsilon_Z^\perp \cdot \varepsilon_\gamma^{*\perp}$ expresses the fact that both the photon and the Z boson are transversely polarized. It is given by the more explicit expression

$$\varepsilon_Z^\perp \cdot \varepsilon_\gamma^{*\perp} = \varepsilon_Z \cdot \varepsilon_\gamma^* - \frac{q\cdot\varepsilon_Z\, k\cdot\varepsilon_\gamma^*}{k\cdot q}\,. \tag{4.49}$$

For neutral mesons that are eigenstates of charge-conjugation, the form factor F_2^M vanishes [93]. The case of $F_2^M \neq 0$ is here only relevant for mesons that are flavor-nondiagonal. The corresponding diagrams arise in the SM through one-loop electroweak corrections, which are tiny. Beyond the SM, they can be generated through effective operators. These couplings would however generate neutral meson mixing through tree-level Z-boson exchange and are thus heavily constrained by experimental data, as we will revisit in section 4.6.2. At next-to-leading order in QCD, the amplitude receives two kinds of corrections, displayed in Fig. 4.5. First, simple QCD corrections to the tree-level diagrams exist. Second, box graphs generating $Zgg\gamma$ at the parton level contribute for flavor-singlet mesons.

Evaluating the quark diagrams, we find for the form factors

$$\begin{aligned} F_1^M &= \left(\sum_q f_M^q \mathcal{Q}_M^q\right)\left[I_+^M(m_Z) + \bar{I}_+^M(m_Z)\right], \\ F_2^M &= \left(\sum_q f_M^q \mathcal{Q}_M'^q\right)\left[I_-^M(m_Z) - \bar{I}_-^M(m_Z)\right], \end{aligned} \tag{4.50}$$

where we defined the effective couplings

$$\mathcal{Q}_P^q = Q_q v_q \,, \qquad\qquad \mathcal{Q}_V^q = Q_q a_q \,. \tag{4.51}$$

Their primed counterparts $\mathcal{Q}'_M$ are obtained by exchanging $v_q \leftrightarrow a_q$. The integrals $I_\pm^M$ are convolutions of the hard scattering kernels with the LCDAs,

$$\begin{aligned} I_\pm^M(m_V) &= \int_0^1 dx\, H_\pm(x, m_V, \mu)\, \phi_M(x,\mu)\,, \\ \bar{I}_\pm^M(m_V) &= \int_0^1 dx\, H_\pm(\bar{x}, m_V, \mu)\, \phi_M(x,\mu)\,, \end{aligned} \tag{4.52}$$

where

$$H_\pm(x, m_V, \mu) = \frac{1}{x}\left[1 + \frac{\alpha_s(\mu) C_F}{4\pi} h_\pm(x, m_V, \mu) + \mathcal{O}(\alpha_s^2)\right], \tag{4.53}$$

and

$$h_\pm(x, m_V, \mu) = (2\log x + 3)\left(\log\frac{m_V^2}{\mu^2} - i\pi\right) + \log^2 x - 9 + (\pm 1 - 2)\frac{x\log x}{\bar{x}}\,. \tag{4.54}$$

The convolutions (4.52) can be written as sums over the Gegenbauer moments weighted by a closed-form coefficient $C_n^{(\pm)}$ by using a technique explained in Appendix F. The results we find are:

$$I_\pm^M(m_V) = 3\sum_{n=0}^{\infty} (-1)^n C_n^{(\pm)}(m_V,\mu)\, a_n^M(\mu)\,, \tag{4.55}$$

$$\bar{I}_\pm^M(m_V) = 3\sum_{n=0}^{\infty} C_n^{(\pm)}(m_V,\mu)\, a_n^M(\mu)\,, \tag{4.56}$$

with

$$C_n^{(\pm)}(m_V,\mu) = 1 + \frac{\alpha_s(\mu) C_F}{4\pi} c_n^{(\pm)}\left(\frac{m_V}{\mu}\right) + \mathcal{O}(\alpha_s^2)\,, \tag{4.57}$$

and

$$\begin{aligned} c_n^{(\pm)}\left(\frac{m_V}{\mu}\right) = &\left[\frac{2}{(n+1)(n+2)} - 4H_{n+1} + 3\right]\left(\log\frac{m_V^2}{\mu^2} - i\pi\right) \\ &+ 4H_{n+1}^2 - \frac{4(H_{n+1} - 1) \pm 1}{(n+1)(n+2)} + \frac{2}{(n+1)^2(n+2)^2} - 9\,. \end{aligned} \tag{4.58}$$

The partonic $Z \to gg\gamma$ diagrams like the fourth diagram in Fig. 4.5 give an additional contribution to F_1^P:

$$\delta F_1^P = \mathcal{Q}_S^{(n_f)} f_P^{uds}(\mu) \int_0^1 dx\, H_g(x,\mu)\phi_P^g(x,\mu)\,, \tag{4.59}$$

with $\mathcal{Q}_S^{(n_f)} = \sum_q Q_q v_q / n_f$. The hard scattering kernel at the high scale (for $n_f = 5$) is

$$H_g(x,\mu) = \frac{\alpha_s(\mu) T_F}{4\pi}\left[5\, h_g(x,\mu) + \frac{Q_t v_t}{\mathcal{Q}_S^{(5)}} h_g^{(t)}(x) - (x \to \bar{x})\right] + \mathcal{O}(\alpha_s^2)\,, \tag{4.60}$$

and

$$\begin{aligned} h_g(x,\mu) &= -\frac{8\log x}{\bar{x}^2}\left[\left(\log\frac{m_Z^2}{\mu^2}) - i\pi\right) + \frac{\log x}{2} + \frac{1}{x} - 3\right], \\ h_g^{(t)}(x) &= \left(\frac{2r_t^3}{315} + \frac{r_t^4}{504}\right)(\bar{x} - x) + \mathcal{O}(r_t^5)\,, \qquad r_t = \frac{m_Z^2}{m_t^2}\,. \end{aligned} \tag{4.61}$$

The function $h_g^{(t)}(x)$ is the contribution from the massive top quark in the loop and is numerically insignificant. The functions h_g and $h_g^{(t)}$ can be compared to literature results for $\gamma\gamma^* \to \eta^{(\prime)}$ [87, 88], we find complete agreement. Using the technique explained in Appendix F, we can write the form factor as a sum over the gluon LCDA Gegenbauer moments b_n^P:

$$\delta F_1^P = 6\mathcal{Q}_S^{(5)} f_P^{uds}(\mu) \sum_n D_n(\mu) b_n^P(\mu)\,, \tag{4.62}$$

with

$$D_n\left(m_V,\mu\right) = \frac{\alpha_s(\mu) T_F}{4\pi}\left[5 d_n\left(\frac{m_V}{\mu}\right) + \frac{Q_t v_t}{\mathcal{Q}_S^{(5)}} d_n^{(t)}\right] + \mathcal{O}(\alpha_s^2)\,, \tag{4.63}$$

and

$$\begin{aligned} d_n\left(\frac{m_V}{\mu}\right) &= \frac{20n(n+3)}{3(n+1)(n+2)}\left[\left(\log\frac{m_V^2}{\mu^2} - i\pi\right) - 2H_{n+1} - 1 + \frac{1}{(n+1)(n+2)}\right], \\ d_n^{(t)} &= -\left(\frac{2r_t^3}{1323} + \frac{5r_t^4}{10584}\right)\delta_{n2} + \mathcal{O}(r_t^5)\,. \end{aligned} \tag{4.64}$$

Note that the loop corrections from diagrams like the ones shown in Fig 4.5 are in general divergent, leading to the $\log\mu$ terms in the hard scattering functions at $\mathcal{O}(\alpha_s)$. The $1/\epsilon$ poles originally accompanying these logarithms are removed by the

n_f	$\mathcal{Q}_S^{(n_f)}$	Up-type quarks	Down-type quarks
5	$\frac{7}{60} - \frac{11}{45}\sin^2\theta_W \approx 0.0601$	$c_{u,c}^{(5)} = \frac{3}{5}$	$c_{d,s,b}^{(5)} = -\frac{2}{5}$
4	$\frac{1}{8} - \frac{5}{18}\sin^2\theta_W \approx 0.0608$	$c_{u,c}^{(4)} = \frac{1}{2}$	$c_{d,s}^{(4)} = -\frac{1}{2}$
3	$\frac{1}{9} - \frac{2}{9}\sin^2\theta_W \approx 0.0597$	$c_{u}^{(3)} = \frac{2}{3}$	$c_{d,s}^{(3)} = -\frac{1}{3}$

Tab. 4.1.: Flavor-number dependent coefficients entering the factorization formula.

renormalizations (4.10) and (4.41). The cancellation of the poles is demonstrated explicitly in Appendix D.

Since the physical η and η' mesons are not pure flavor-singlets, the full form factors F_1^P for $P = \eta^{(\prime)}$ consist of both flavor-singlet and nonsinglet pieces. The full factorization formula at the high scale in this case is

$$\begin{aligned} F_1^P =& 6\mathcal{Q}_S^{(5)} \left[\sum_n C_n^S(\mu) \sum_q f_P^q a_n^{P,q} + \sum_n D_n(\mu) f_P^{uds}(\mu) b_n^P(\mu) \right] \\ &+ 6(Q_u v_u - Q_d v_d) \sum_n C_n(\mu) \sum_q c_q^{(5)} f_P^q(\mu) a_n^{P,q}(\mu)\,, \end{aligned} \tag{4.65}$$

where the first line governs the flavor-singlet component of the pseudoscalar meson P and the second line the nonsinglet one. The coefficients $\mathcal{Q}_S^{(n_f)}$ and $c_q^{(n_f)}$ are compiled in Tab. 4.1.

Radiative decays of the Z boson into a transversely polarized meson are of subleading power, as follows directly from counting the number of gamma matrices in the partonic amplitude and the light-cone projectors. The two ways of obtaining a non-vanishing result for the amplitude are either including the quark mass in the hard propagator $x\not{k} + \not{q} \to x\not{k} + \not{q} + m$ or employing subleading-power projectors. In the first case, corrections suppressed by a factor of m_q/m_Z are introduced. Less trivial are the corrections from higher-power projectors, which are discussed in detail in Appendix A. When effects from the quark masses are neglected, the decay amplitude can be decomposed into form factors according to

$$i\mathcal{A}(Z \to V_\perp \gamma) = -\frac{eg}{2c_W}\frac{m_V}{m_Z}\left(i\epsilon_{\mu\nu\alpha\beta}\frac{k^\mu q^\nu \varepsilon_V^{*\alpha}\varepsilon_\gamma^{*\beta}}{k\cdot q} F_1^\perp - \varepsilon_V^{\perp *}\cdot\varepsilon_\gamma^{\perp *} F_2^\perp \right). \tag{4.66}$$

Since both the vector meson and the photon are transversely polarized, the Z boson must be longitudinally polarized, allowing us to write its polarization vector as $\varepsilon_Z^\mu = (q-k)^\mu/m_Z$. From the twist-3 projectors we get the suppression factor m_V/m_Z, which shows explicitly how strongly these modes are suppressed. Using

the relations given in Appendix A, the form factors are:

$$\begin{aligned} F_1^\perp &= -2\sum_q f_V^q Q_q a_q \int_0^1 dx \left(\frac{\log x}{\bar{x}} + \frac{\log \bar{x}}{x}\right) \phi_V(x,\mu)\,, \\ F_2^\perp &= -2\sum_q f_V^q Q_q v_q \int_0^1 dx \left(\frac{\log x}{\bar{x}} - \frac{\log \bar{x}}{x}\right) \phi_V(x,\mu)\,. \end{aligned} \tag{4.67}$$

We use the technique from Appendix F to rewrite the form factors into sums:

$$\begin{aligned} F_1^\perp &= 6\sum_q f_V^q Q_q v_q \left[1 + \sum_{n=1}^{\infty} \frac{a_{2n}^V(\mu)}{(n+1)(2n+1)}\right]\,, \\ F_2^\perp &= 6\sum_q f_V^q Q_q v_q \left[1 + \sum_{n=0}^{\infty} \frac{a_{2n+1}^V(\mu)}{(n+1)(2n+3)}\right]\,. \end{aligned} \tag{4.68}$$

Note that neutral meson LCDAs are symmetric under the exchange $x \leftrightarrow \bar{x}$. This means that the moments a_n for odd n - and with that $F_2^\perp$ - vanish. When squaring the amplitude and comparing it to the leading contribution $Z \to V_\parallel \gamma$, we find that

$$\frac{\Gamma(Z \to V_\perp \gamma)}{\Gamma(Z \to V_\parallel \gamma)} \approx \frac{m_V^2}{m_Z^2}\,, \tag{4.69}$$

meaning that power corrections are suppressed by four orders of magnitude, making them fully negligible for any practical purpose.

4.2.2. Resummation of Large Logarithms

To resum the large logarithms $\alpha_s \log(\mu_0^2/m_Z^2)$ we now apply the evolution equations (4.16) and (4.46). First, note that these equations, in the language of section 2.3.2, are renormalizations of the operator matrix elements:

$$\mu \frac{d}{d\mu} \langle \mathcal{O}(\mu) \rangle = -\gamma(\mu) \langle \mathcal{O}(\mu) \rangle\,. \tag{4.70}$$

For our case it is more practical to perform the running of the Wilson coefficients instead of the matrix elements. Their evolution equation is of course identical up to a relative sign, as is explicitly seen by multiplying both sides of the above equation with the Wilson coefficients and using $d/d\mu\,(\mathcal{C}\langle O\rangle) = 0$:

$$\mu \frac{d}{d\mu} \mathcal{C}(\mu) = \gamma(\mu)\, \mathcal{C}(\mu)\,. \tag{4.71}$$

For the flavor-nonsinglet contributions this is a simple equation and will just rescale the hard scattering coefficients $C_n^{(\pm)}(m_Z)$:

$$C_n^{(\pm)}(\mu_0) = U_n(\mu_0, \mu_1) C_n^{(\pm)}(\mu_1)\,, \tag{4.72}$$

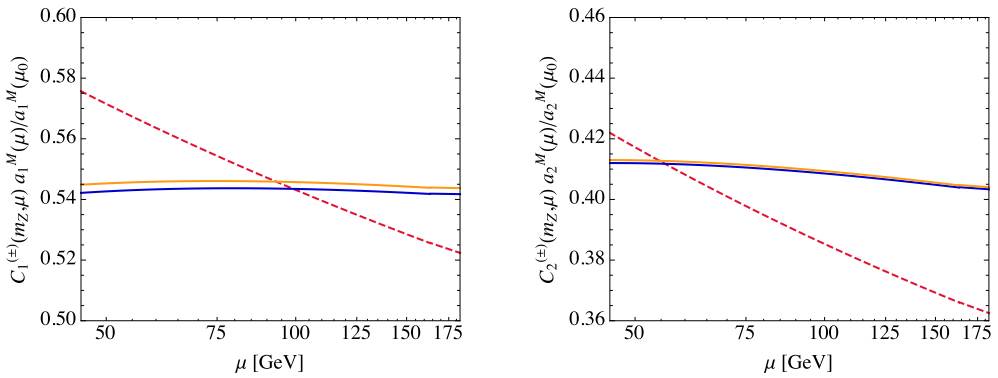

Fig. 4.6.: Scale dependence of the combinations $C_n^{(\pm)}(m_Z,\mu)\,a_n^M(\mu)/a_n^M(\mu_0)$ for the first two Gegenbauer moments ($n=1,2$). The red dashed lines show the results at leading-order, where $C_n^{(\pm)}(m_Z,\mu)=1$. The blue and yellow lines show the results at next-to-leading order obtained when the one-loop expressions in (4.57) are used.

with the evolution factors $U_n(\mu_1,\mu_2)$ given in Appendix E. The form factors expressed through the Gegenbauer moments at different scales are

$$\begin{aligned}\operatorname{Re} F_1^M &= \mathcal{Q}_M\left[0.94+1.05\,a_2^M(m_Z)+1.15\,a_4^M(m_Z)+1.22\,a_6^M(m_Z)+\dots\right]\\ &= \mathcal{Q}_M\left[0.94+0.41\,a_2^M(\mu_0)+0.29\,a_4^M(\mu_0)+0.23\,a_6^M(\mu_0)+\dots\right],\end{aligned} \tag{4.73}$$

where $\mu_0=1$ GeV. This equation clearly reflects the fact that the LCDAs approach their asymptotic form at high scales, meaning that the dependence of the form factor on the Gegenbauer moments a_n for $n>0$ is decreased after RG running. By virtue of the renormalization group, the combinations $C_n^{(\pm)}(\mu)a_n^M(\mu)$ are scale-dependent up to $\mathcal{O}(\alpha_s^2)$, as can be appreciated in Fig. 4.6: When the one-loop corrections are used, the scale dependence is only very weak, suggesting corrections of $\mathcal{O}(\alpha_s^2)$ to be small.

For the flavor-singlet case we need to carefully match singlet and nonsinglet form factors at each quark scale. The running of the singlet hard-scattering coefficients C_n^S and D_n is obtained in the same manner as the nonsinglet running, only this time starting from the matrix evolution equation (4.46) and transforming it into an evolution equation for C_n^S and D_n. The solution is of the form

$$\begin{pmatrix}C_n^S(\mu_1)\\ D_n(\mu_1)\end{pmatrix} = \boldsymbol{U}_n^S(\mu_1,\mu_2)\begin{pmatrix}C_n^S(\mu_2)\\ D_n(\mu_2)\end{pmatrix}, \tag{4.74}$$

where the explicit expression for $\boldsymbol{U}_n^S$ is again given in Appendix E. At the scale of the b-quark mass, the b-quark decouples. The sum in the first line of eq. (4.65)

now only runs over the quarks $q \in u, d, s, c$. In the four-flavor theory, the singlet contribution is matched onto the proper admixture of singlet and nonsinglet and evolved to the c-quark mass, where the procedure is repeated until we arrive at the hadronic scale $\mu_0 \sim 1$ GeV. At the scale $\mu_b \sim m_b$, the relevant matching conditions are

$$\begin{aligned} C_n^S(\mu_b)\big|_{n_f=4} &= \frac{\mathcal{Q}_S^{(5)}}{\mathcal{Q}_S^{(4)}}\, C_n^S(\mu_b)\big|_{n_f=5} + \left(1 - \frac{\mathcal{Q}_S^{(5)}}{\mathcal{Q}_S^{(4)}}\right) C_n(\mu_b)\big|_{n_f=5}\,, \\ D_n(\mu_b)\big|_{n_f=4} &= \frac{\mathcal{Q}_S^{(5)}}{\mathcal{Q}_S^{(4)}}\, D_n(\mu_b)\big|_{n_f=5}\,, \qquad C_n(\mu_b)\big|_{n_f=4} = C_n(\mu_b)\big|_{n_f=5}\,, \\ C_n^b(\mu_b) &= C_n(\mu_b)\big|_{n_f=5} + \frac{\mathcal{Q}_S^{(5)}}{Q_b v_b}\left[C_n^S(\mu_b) - C_n(\mu_b)\right]\big|_{n_f=5}\,. \end{aligned} \tag{4.75}$$

Similarly, at the threshold scale $\mu_c \sim m_c$ we find

$$\begin{aligned} C_n^S(\mu_c)\big|_{n_f=3} &= \frac{\mathcal{Q}_S^{(4)}}{\mathcal{Q}_S^{(3)}}\, C_n^S(\mu_c)\big|_{n_f=4} + \left(1 - \frac{\mathcal{Q}_S^{(4)}}{\mathcal{Q}_S^{(3)}}\right) C_n(\mu_c)\big|_{n_f=4}\,, \\ D_n(\mu_c)\big|_{n_f=3} &= \frac{\mathcal{Q}_S^{(4)}}{\mathcal{Q}_S^{(3)}}\, D_n(\mu_c)\big|_{n_f=4}\,, \qquad C_n(\mu_c)\big|_{n_f=3} = C_n(\mu_c)\big|_{n_f=4}\,, \\ C_n^c(\mu_c) &= C_n(\mu_c)\big|_{n_f=4} + \frac{\mathcal{Q}_S^{(4)}}{Q_c v_c}\left[C_n^S(\mu_c) - C_n(\mu_c)\right]\big|_{n_f=4}\,. \end{aligned} \tag{4.76}$$

Finally, this leads to the factorization formula at the low scale:

$$\begin{aligned} F_1^P = 6\mathcal{Q}_S^{(3)} &\left[\sum_n C_n^S(\mu_0) \sum_{q=u,d,s} f_P^q(\mu_0)\, a_n^{P,q}(\mu_0) + \sum_n D_n(\mu_0)\, f_P^{uds}(\mu_0)\, b_n^P(\mu_0)\right] \\ &+ 6\left(Q_u v_u - Q_d v_d\right) \sum_n C_n(\mu_0) \sum_{q=u,d,s} c_q^{(3)} f_P^q(\mu_0)\, a_n^{P,q}(\mu_0) \\ &+ 6Q_b v_b \sum_n C_n^b(\mu_b)\, f_P^b(\mu_b)\, a_n^{P,b}(\mu_b) + 6Q_c v_c \sum_n C_n^c(\mu_c)\, f_P^c(\mu_c)\, a_n^{P,c}(\mu_c)\,. \end{aligned} \tag{4.77}$$

The numerical values for the hard scattering coefficients entering here are given in Tab. 4.2 for the first 6 moments in the Gegenbauer expansion. It should be noted that C_n and D_n are of similar size except for $n = 0$, despite the fact that the C_n starts at tree-level whereas D_n starts at one loop. Furthermore, the singlet coefficients C_n^S and the nonsinglet coefficients C_n are numerically almost equal, meaning that the mixing between quark and gluon LCDAs is a small effect.

At two-loop order, the renormalization running becomes more involved since the Gegenbauer polynomials are only the eigenfunctions of the one-loop renormalization

n	0	2	4	6
$C_n^S(\mu_0)$	0.937	$0.413 + 0.063i$	$0.291 + 0.061i$	$0.233 + 0.055i$
$C_n(\mu_0)$	0.937	$0.409 + 0.064i$	$0.290 + 0.061i$	$0.232 + 0.055i$
$C_n^b(\mu_b)$	0.937	$0.658 + 0.101i$	$0.579 + 0.121i$	$0.535 + 0.127i$
$C_n^c(\mu_c)$	0.937	$0.464 + 0.071i$	$0.346 + 0.072i$	$0.287 + 0.068i$
$D_n(\mu_0)$	0	$0.430 + 0.024i$	$0.265 + 0.043i$	$0.192 + 0.040i$

Tab. 4.2.: Short-distance coefficients entering the factorization formula (4.77) evaluated at the low scale $\mu_0 = 1$ GeV. We use $\mu_Z = m_Z$, as well as $\mu_b = m_b = 4.163$ GeV and $\mu_c = m_c = 1.279$ GeV for the heavy-flavor thresholds.

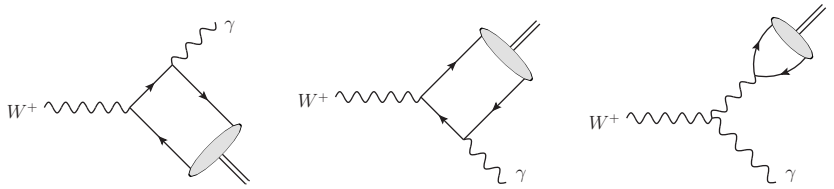

Fig. 4.7.: The tree-level contribution to $W^+ \to M^+\gamma$. The third diagram involves the local hadronic matrix element that defines the meson decay constant. The computation of the first two graphs is in complete analogy to the computation of $Z \to M\gamma$ in the last section.

kernels and thus moments of different rank mix starting at two-loop. The two-loop kernels have been derived in refs. [94, 95] and have been compiled in ref. [88]. Instead of performing a detailed study of the two-loop running here, we assume a global factor κ_{NLO}, estimated from the two-loop running of the flavor-singlet decay constant [83]:

$$\kappa_{\text{NLO}} = 1 + \frac{30}{23}\frac{\alpha_s(\mu_Z)}{\pi} - \frac{198}{575}\frac{\alpha_s(\mu_b)}{\pi} - \frac{22}{75}\frac{\alpha_s(\mu_c)}{\pi} - \frac{2}{3}\frac{\alpha_s(\mu_0)}{\pi} \approx 0.89\,. \tag{4.78}$$

and apply this to all our form factors for the mesons containing flavor-singlets $P = \eta^{(\prime)}$ in our phenomenological analysis.

4.3. Radiative W-Boson Decays

Let us now proceed to radiative decays of the W boson. The tree-level diagrams contributing to this decay are depicted in Fig. 4.7. These decays are similar in nature to the Z decays. However, an additional diagram involving the triple gauge vertex exists, where the W first radiates off a photon and then converts into the charged final state meson. Graphs of this type are computed using the definition of

the decay constants (4.5), which leads to the Feynman rule

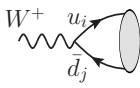

$$= \frac{g f_M}{\sqrt{2}} V_{ij} \begin{cases} k^\mu\,; & M^+ = P^+\,, \\ m_V \varepsilon^{*\mu}\,; & M^+ = V_\parallel^+\,, \end{cases} \tag{4.79}$$

where V_{ij} is the relevant CKM matrix element. The decay constant is per definition exact to all orders in QCD and thus no higher-order corrections exist to this graph in QCD. The amplitude of what we will call the indirect contribution is then:

$$\begin{aligned} i\mathcal{A}_{\text{ind}}(W^+ \to P^+\gamma) &= \frac{egf_P}{2\sqrt{2}} V_{ij}\, \varepsilon_W \cdot \varepsilon_\gamma^*\,, \\ i\mathcal{A}_{\text{ind}}(W^+ \to V^+\gamma) &= -\frac{egf_V}{2\sqrt{2}} V_{ij} \frac{2m_V}{m_W^2 - m_V^2} \Big((q \cdot \varepsilon_V^*)(\varepsilon_W \cdot \varepsilon_\gamma^*) - (q \cdot \varepsilon_W)(\varepsilon_\gamma^* \cdot \varepsilon_V^*) \Big)\,. \end{aligned} \tag{4.80}$$

Here the second amplitude can be further simplified by discriminating between transverse and longitudinal vector mesons in the final state. The polarization vector of the longitudinal vector meson can be constructed from

$$\varepsilon_V^{\parallel\mu} = \alpha\, k^\mu + \beta\, q^\mu \quad \text{with} \quad \left(\varepsilon_V^\parallel\right)^2 = -1 \quad \text{and} \quad k \cdot \varepsilon_V^\parallel = 0\,. \tag{4.81}$$

From these equations α and β can be determined to give

$$\varepsilon_V^{\parallel\mu} = \frac{1}{m_V} \left(k^\mu - \frac{2m_V^2}{m_W^2 - m_V^2} q^\mu \right)\,. \tag{4.82}$$

The same decomposition can be done for the W when it is longitudinally polarized, as it is the case for a transverse vector meson in the final state. We can then write

$$i\mathcal{A}_{\text{ind}}(W^+ \to V^+\gamma) = -\frac{egf_V}{2\sqrt{2}} V_{ij} \begin{cases} \varepsilon_W \cdot \varepsilon_\gamma^* + \mathcal{O}\left(\frac{m_V^2}{m_W^2}\right)\,; & V = V_\parallel\,, \\ \frac{m_V}{m_W} \varepsilon_\gamma^{\perp *} \cdot \varepsilon_V^{\perp *}\,; & V = V_\perp\,. \end{cases} \tag{4.83}$$

The computation of the direct amplitude, corresponding to the first two graphs in Fig 4.7, is completely analogous to the computation of $Z \to M\gamma$ and the results are obtained by replacing

$$v_q,\, a_q \to \frac{c_W}{2\sqrt{2}} V_{ij}\,. \tag{4.84}$$

We can write the amplitude in our familiar form factor decomposition:

$$i\mathcal{A} = \pm \frac{egf_M}{4\sqrt{2}} V_{ij} \left(i\epsilon_{\mu\nu\alpha\beta} \frac{k^\mu q^\nu \varepsilon_W^\alpha \varepsilon_\gamma^{*\beta}}{k \cdot q} F_1^M - \varepsilon_W^\perp \cdot \varepsilon_\gamma^{\perp *} F_2^M \right)\,, \tag{4.85}$$

where the upper sign holds in case $M = P$ and the lower sign for $M = V_\parallel$. The form factors are

$$\begin{aligned} F_1^M &= \sum_{n=0}^{\infty} \left[C_{2n}^{(+)}(m_W,\mu) a_{2n}^M(\mu) - 3\delta_Q\, C_{2n+1}^{(+)}(m_W,\mu) a_{2n+1}^M(\mu) \right] , \\ F_2^M &= \sum_{n=0}^{\infty} \left[3\delta_Q\, C_{2n}^{(-)}(m_W,\mu) a_{2n}^M(\mu) - C_{2n+1}^{(-)}(m_W,\mu) a_{2n+1}^M(\mu) \right] - 2\delta_Q \,, \end{aligned} \tag{4.86}$$

The constant term in F_2^M independent of the LCDA shape parameters originates from the indirect contribution. The quantity $\delta_Q = Q_u - Q_d$ changes sign when decays $W^- \to M^-\gamma$ are considered. Furthermore, for these opposite sign decays the replacement $V_{ij} \to V_{ij}^*$ has to be made. Note also that odd Gegenbauer moments change sign under $M^+ \to M^-$. From the form factors we can read off that F_1^M then stays invariant whereas F_2^M changes its overall sign. The square of the amplitude, and with that the decay rate, will be the same for both signs $W^\pm \to M^\pm\gamma$.

The resummation of large logarithms proceeds exactly the same as for $Z \to M\gamma$. In analogy to eq. (4.73), the form factors are:

$$\begin{aligned} \operatorname{Re} F_1^M &= 0.94 - 2.98\, a_1^M(m_W) + 1.05\, a_2^M(m_W) - 3.31\, a_3^M(m_W) \mp \dots \\ &= 0.94 - 1.65\, a_1^M(\mu_0) + 0.42\, a_2^M(\mu_0) - 1.03\, a_3^M(\mu_0) \mp \dots \,, \\ \operatorname{Re} F_2^M &= 0.85 - 1.00\, a_1^M(m_W) + 3.16\, a_2^M(m_W) - 1.11\, a_3^M(m_W) \mp \dots \\ &= 0.85 - 0.55\, a_1^M(\mu_0) + 1.25\, a_2^M(\mu_0) - 0.34\, a_3^M(\mu_0) \mp \dots \,. \end{aligned} \tag{4.87}$$

Like in the previous section, after RG evolution the dependence on the shape parameters decreases.

Decays into transverse vector mesons are power-suppressed. The amplitude in form factor decomposition is

$$i\mathcal{A}(W_\parallel^+ \to V_\perp^+\gamma) = -\frac{egf_V}{4\sqrt{2}} V_{ij} \frac{m_V}{m_W} \left(i\epsilon_{\mu\nu\alpha\beta} \frac{k^\mu q^\nu \varepsilon_V^{*\alpha} \varepsilon_\gamma^{*\beta}}{k\cdot q} F_1^\perp - \varepsilon_V^{\perp *} \cdot \varepsilon_\gamma^{\perp *}\, F_2^\perp \right) , \tag{4.88}$$

with the transverse form factors

$$\begin{aligned} F_1^\perp &= -2 \int_0^1 dx \left(\frac{Q_u \log x}{\bar{x}} + \frac{Q_d \log(\bar{x})}{x} \right) \phi_V(x,\mu) \,, \\ F_2^\perp &= -4\,(Q_u - Q_d) - 2 \int_0^1 dx \left(\frac{Q_u \log x}{\bar{x}} - \frac{Q_d \log(\bar{x})}{x} \right) \phi_V(x,\mu) \,, \end{aligned} \tag{4.89}$$

where we have again ignored the quark masses. In the Gegenbauer expansion the

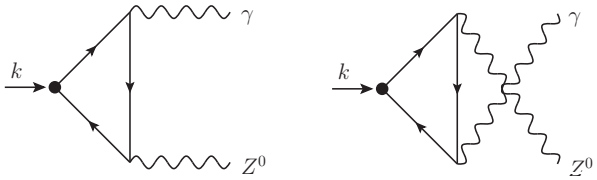

Fig. 4.8.: One-loop triangle graphs giving rise to the axial anomaly. The dot represents the axial-vector current $j_q^{\mu 5}$.

form factors become:

$$\begin{aligned} F_1^{\perp} &= 1 + \sum_{n=1}^{\infty} \frac{a_{2n}^V(\mu)}{(n+1)(2n+1)} - \sum_{n=0}^{\infty} \frac{3a_{2n+1}^V(\mu)}{(n+1)(2n+3)}\,, \\ F_2^{\perp} &= -1 + \sum_{n=1}^{\infty} \frac{3a_{2n}^V(\mu)}{(n+1)(2n+1)} - \sum_{n=0}^{\infty} \frac{a_{2n+1}^V(\mu)}{(n+1)(2n+3)}\,. \end{aligned} \tag{4.90}$$

The rates are power-suppressed by m_V^2/m_W^2 with respect to the longitudinal mesons and are thus negligible.

4.4. Absence of an Axial-Anomaly Contribution

It has been suggested in the past, that the decays $Z \to P\gamma$ and $W \to P\gamma$ could receive potentially large enhancements from an analog of the axial anomaly, as it is the case for the decay $\pi^0 \to \gamma\gamma$ [96–98]. In this section we show that this enhancement does not exist.

To do so, we first evaluate the triangle diagrams in Fig. 4.8, where the black dot represents the axial-vector current $j_q^{\mu 5} = \bar{q}\gamma^\mu\gamma^5 q$. Taking the divergence corresponds to contracting the amplitude with $-ik_\mu$. The amplitude only gives a non-vanishing result if one uses a consistent treatment of the γ^5 matrix, like the HV scheme (see App. B). In the limit $m_q \to 0$, one finds:

$$\partial_\mu\, j_q^{\mu 5} = -\frac{\alpha N_c}{2\pi} \frac{Q_q v_q}{s_W c_W}\, F^{\mu\nu} \epsilon_{\mu\nu\alpha\beta}\, Z^{\alpha\beta}\,. \tag{4.91}$$

Analogous terms exist for two photons (which is the famous ABJ-anomaly [99, 100]) and other gauge bosons, that we did not write down since they are irrelevant to this discussion. Similarly, for charged currents $j_{ij}^{\mu 5} = \bar{d}_j\gamma^\mu\gamma^5 u_i$ we find:

$$\partial_\mu\, j_{ij}^{\mu 5} = -\frac{N_c\,\alpha}{4\pi} \frac{V_{ij}}{3\sqrt{2}\sin\theta_W}\, \epsilon_{\mu\nu\alpha\beta}\, F^{\mu\nu} W^{+\alpha\beta}\,, \tag{4.92}$$

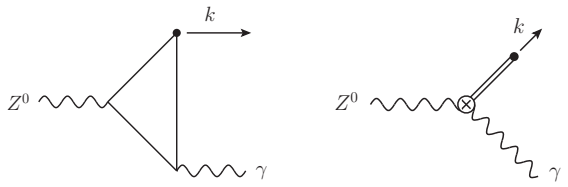

Fig. 4.9.: Left: One-loop diagram contributing to the amplitude $\mathcal{M}^{\mu\alpha\beta}$ describing the decay of a Z boson into a photon and an axial current A_q^μ. Right: A hypothetical anomaly-mediated contribution to the $Z^0 \to P\gamma$ decay amplitude. The crossed circle represents the decay amplitude in (4.93); the double line shows the meson propagator.

where again we dropped terms irrelevant to our discussion. x In order to show that no anomaly-enhancement exists for $Z \to P\gamma$, we parameterize the hypothetical contribution by:

$$i\mathcal{A}(Z \to P\gamma) = i\lambda\epsilon_{\mu\nu\alpha\beta}k^\mu q^\nu \varepsilon_Z^\alpha \varepsilon_\gamma^\beta \,. \tag{4.93}$$

Similarly, we parametrize the amplitude of an initial-state Z boson to the current $j_q^{\mu 5}$ and a photon as:

$$i\mathcal{M}^\mu(k,q) = i\mathcal{M}^{\mu\alpha\beta}(k,q)\varepsilon_Z^\alpha \varepsilon_\gamma^{*\beta} \,. \tag{4.94}$$

This amplitude is obtained from the left diagram in Fig. 4.9. Next, we insert a complete set of hadron states, interpolated by the axial-vector current and sum over the quarks flavors q. We see from the second diagram in Fig. 4.9 that $i\mathcal{M}^{\mu\alpha\beta}$ in the limit of $m_P \to 0$ contains

$$i\mathcal{M}^{\mu\alpha\beta}(k,q) \ni \sum_q c_q^P \,(-if_P k^\mu)\, \frac{i}{k^2 - m_P^2} i\lambda\, \epsilon_{\rho\sigma\alpha\beta}\, k^\rho q^\sigma \to i\sum_q c_q^P\, \frac{f_P\lambda}{k^2}\, k^\mu \epsilon_{\rho\sigma\alpha\beta}\, k^\rho q^\sigma . \tag{4.95}$$

If such an anomalous contribution would be generated by the left digram in Fig. 4.9, it would need to have a pole in $1/k^2$ to match onto the above amplitude. When evaluating the triangle graph (and its mirrored counterpart), we find that the relevant tensor structure is proportional to

$$\frac{\Gamma(1+\epsilon)\,\Gamma^2(1-\epsilon)}{\Gamma(2-2\epsilon)}\, \frac{\mu^{2\epsilon}}{(p^2-k^2)^2} \left[p^2\, \frac{(-p^2)^{-\epsilon} - (-k^2)^{-\epsilon}}{\epsilon} + \frac{(-k^2)^{1-\epsilon} - (-p^2)^{1-\epsilon}}{1-\epsilon} \right], \tag{4.96}$$

with $p^2 = m_Z^2$ and $k^2 = m_P^2$. Clearly, this reproduces the amplitude for the $\pi^0 \to \gamma\gamma$ decay, where $p^2 = 0$. In our case, however, the amplitude is rather proportional to

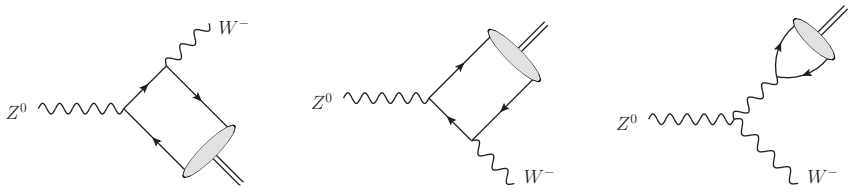

Fig. 4.10.: Tree level diagrams governing the $Z \to M^+W^-$ decays. As was the case for the radiative W boson decays, we find both direct (first two graphs) and indirect (third graph) contributions, where the latter involves the local matrix element defining the decay constant of the meson M^+.

$1/m_Z^2$ and hence does not match onto eq. (4.95). Therefore, no enhancement from the anomaly exists for $Z \to P\gamma$.

4.5. Weak Radiative Z-Boson Decays

The last class of decays we discuss here are the channels $Z \to M^+W^-$. Kinematics dictate that the final state meson must not be heavier than $m_Z - m_W \sim 10.8$ GeV. Furthermore, the QCD factorization approach is only valid if the meson momentum is considerably larger than its mass. This is the case if

$$\frac{\lambda(m_Z^2, m_W^2, m_M^2)}{2m_Z^2} \gg m_M\,, \quad \text{where} \quad \lambda(x,y,z) = \sqrt{(x-y-z)^2 - 4yz}\,. \tag{4.97}$$

This condition is satisfied for meson masses $m_M \ll (m_Z^2 - m_W^2)/(2m_Z) \approx 10.2$ GeV, and the factorization approach can therefore be used for light mesons, but not for heavy B mesons. Note also that in this case the expansion parameter is $\lambda = (\Lambda_{\rm QCD} m_Z)/(m_Z^2 - m_W^2)$ rather than $\Lambda_{\rm QCD}/m_Z$. This leads to a much lower factorization scale then in the previous sections, giving an opportunity to study the QCDF approach at an intermediate scale - higher than in the case of exclusive B meson decays but considerably lower than for the $Z/W \to M\gamma$.

The diagrams contributing to the decay amplitude are shown in Fig. 4.10. The occurring topologies are similar to the $W^+ \to M^+\gamma$ channels: There exist direct contributions where the ingoing Z decays to the constituent quarks of the meson, computable using QCD factorization and the indirect contribution involving the trilinear ZZW gauge vertex. The computation proceeds analogously to the W

decays and we find for the indirect amplitude:

$$\begin{aligned} i\mathcal{A}_{\text{ind}}(Z \to P^+W^-) &= -\frac{g^2 \cos\theta_W f_P}{2\sqrt{2}}\, V_{ij}\, \frac{m_Z^2 - m_W^2}{m_W^2}\, \varepsilon_Z \cdot \varepsilon_W^*\,, \\ i\mathcal{A}_{\text{ind}}(Z \to V^+W^-) &= \frac{g^2 \cos\theta_W f_V}{2\sqrt{2}}\, V_{ij}\, \frac{2m_V}{m_W^2 - m_V^2} \\ &\quad \times \Big(q \cdot \varepsilon_V^*\, \varepsilon_Z \cdot \varepsilon_W^* - k \cdot \varepsilon_W^*\, \varepsilon_Z \cdot \varepsilon_V^* + k \cdot \varepsilon_Z\, \varepsilon_W^* \cdot \varepsilon_V^* \Big)\,. \end{aligned} \tag{4.98}$$

This result can again be simplified by considering the different polarization states of the meson separately. The longitudinal polarization vector can be written as

$$\varepsilon_V^{\parallel\mu} = \frac{1}{m_V} \frac{m_Z^2 - m_W^2 - m_V^2}{\lambda(m_Z^2, m_W^2, m_V^2)} \left(k^\mu - \frac{2m_V^2}{m_Z^2 - m_W^2 - m_V^2} q^\mu \right)\,, \tag{4.99}$$

and thus the indirect amplitude for $Z \to V_\parallel^+ W^-$ is:

$$i\mathcal{A}_{\text{ind}} = \frac{g^2 \cos\theta_W f_V}{2\sqrt{2}}\, V_{ij}\, \frac{m_Z^2 - m_W^2}{m_W^2}\, \varepsilon_Z \cdot \varepsilon_W^* \left[1 + \mathcal{O}\left(\frac{m_V^2 m_Z^2}{\left(m_Z^2 - m_W^2\right)^2} \right) \right]. \tag{4.100}$$

By decomposing the different polarization vectors for W and Z, we can study the amplitudes for $Z_\parallel \to V_\perp^+ W_\perp^-$ and $Z_\perp \to V_\perp^+ W_\parallel^-$ and find that they are power-suppressed by m_V/m_Z and m_V/m_W. We will ignore these amplitudes in the following and consequently, the indirect amplitudes both for pseudoscalar and vector mesons are identical up to tiny corrections.

The full decay amplitude can be decomposed into form factors again:

$$\begin{aligned} i\mathcal{A}(Z \to M^+W^-) = \pm \frac{g^2 f_M}{4\sqrt{2}\cos\theta_W}\, V_{ij} \left(1 - \frac{m_W^2}{m_Z^2} \right) \\ \times \left(i\epsilon_{\mu\nu\alpha\beta}\, \frac{k^\mu q^\nu \varepsilon_Z^\alpha\, \varepsilon_W^{*\beta}}{k \cdot q}\, F_1^M - \varepsilon_Z \cdot \varepsilon_W^*\, F_2^M + \frac{q \cdot \varepsilon_Z\, k \cdot \varepsilon_W^*}{k \cdot q}\, F_3^M \right). \end{aligned} \tag{4.101}$$

The form factor F_3^M did not exist for the radiative decays. It is associated with the final state W boson being longitudinally polarized and therefore no analog term exists for $Z/W \to M\gamma$.

The direct contributions to these form factors are once again easily evaluated using the leading-twist light cone projectors. We find:

$$\begin{aligned} F_1^M &= \int_0^1 dx\, \phi_M(x,\mu) \left[\frac{Z_d}{x + \bar{x}\, r} + \frac{Z_u}{\bar{x} + x\, r} \right], \\ F_2^M &= \int_0^1 dx\, \phi_M(x,\mu) \left[\frac{Z_d}{x + \bar{x}\, r} - \frac{Z_u}{\bar{x} + x\, r} \right] + 2, \\ F_3^M &= \int_0^1 dx\, \phi_M(x,\mu) \left[\frac{Z_d}{x + \bar{x}\, r} + \frac{Z_u}{\bar{x} + x\, r} \right] (\bar{x} - x), \end{aligned} \tag{4.102}$$

where $Z_q = v_q + a_q$ and $r = m_W^2/m_Z^2$. Observe that with r being close to 1 and $x+\bar{x} = 1$, the expressions in the brackets are almost independent of x. We could now rewrite these convolution integrals into sums over Gegenbauer moments, as we did in the previous sections. However, the presence of r in the denominators gives rise to complicated results for the integrals over the generating function $((1+t)^2-4xt)^{-3/2}$ and we therefore evaluate the integrals numerically for our phenomenological results. We can still demonstrate the weak dependence on the LCDAs by expanding around $r \approx 1$ to first order, which yields:

$$\begin{aligned}
F_1^M &= \frac{3-r}{2}(Z_u + Z_d) + \frac{3(1-r)}{10}(Z_u - Z_d)\, a_1^M(\mu) + \mathrm{O}(r-1)^2\,, \\
F_2^M &= 2 - \frac{3-r}{2}(Z_u - Z_d) - \frac{3(1-r)}{10}(Z_u + Z_d)\, a_1^M(\mu) + \mathrm{O}(r-1)^2\,, \\
F_3^M &= \frac{r-1}{10}(Z_u - Z_d) - \frac{3(r-3)}{10}(Z_u - Z_d)\, a_1^M(\mu) \\
&\qquad + \frac{6(r-1)}{36}(Z_u - Z_d) a_2^M(\mu) + \mathrm{O}(r-1)^2\,.
\end{aligned} \tag{4.103}$$

Gegenbauer moments of higher rank do not contribute at this order in r and enter our predictions with tiny coefficients. From the above set of equations, it might look like the form factor F_3^M contributes a term proportional to the first Gegenbauer moment but when squaring the amplitude, F_3^M enters with an additional factor of $1-r$, further suppressing the term. The scale dependence of this result is mild: In eq. (4.101), the only quantities affected by QCD running at leading order are the Gegenbauer moments. However, as we saw just now, they enter the result with small coefficients. How this picture changes when QCD loop corrections are included is an interesting question that we leave for future projects.

4.6. Phenomenological Analysis

This section is devoted to our phenomenological analysis. In the first part, we derive numerical predictions for the branching ratios $Z \to M\gamma$, $W \to M\gamma$ and $Z \to M^+W^-$, and compare them to existing predictions in the literature. In the second part, we will briefly comment on the possibility to measure Z-couplings to quarks using $Z \to M\gamma$. The final part will discuss the experimental situation. A detailed discussion of the various hadronic input parameters is provided in Appendix C. If not explicitly stated otherwise, numerical parameters like masses of SM particles and SM couplings are taken from ref. [101].

4.6.1. Numerical Predictions

We will start with the radiative Z-boson decays. Squaring the amplitude in eq. (4.48), we find the expression for the decay rates into nonsinglet mesons M:

$$\Gamma(Z \to M\gamma) = \frac{\alpha m_Z}{6v^2}\left(\left|F_1^M\right|^2 + \left|F_2^M\right|^2\right), \tag{4.104}$$

where $\alpha = 1/137.036$ is the fine-structure constant, evaluated at $q^2 = 0$ [101]. The Higgs vacuum expectation value v is evaluated at the scale $\mu = m_Z$, according to

$$v(m_Z) = m_Z \frac{s_W c_W}{\sqrt{\pi\,\alpha(m_Z)}} = 245.36\,\text{GeV}\,, \tag{4.105}$$

where $\alpha(m_Z) = 1/127.940 \pm 0.014$, $s_W^2 = 0.23126 \pm 0.00005$ [102] and $m_Z = (91.1876 \pm 0.0021)$ GeV [101]. For the strong coupling constant we use $\alpha_s(m_Z) = 0.1185$ and scale-evolve it using three-loop running provided by the `RunDec` package [103]. By normalizing the rates to the total Z-boson width $\Gamma_Z = (2.4955 \pm 0.0009)$ GeV [101], we obtain the branching ratios given in Table 4.3. We include error estimates from varying the scale between $m_Z/2$ and $2m_Z$, the error of the decay constants and the Gegenbauer moments (see Appendix C for more details on the error budgets of the last two). The branching ratios are generically small, as one would expect: The Z boson needs to decay into two quarks and a photon, with the two quarks being collinear to each other. This condition selects a tiny amount of the phase space and thus the branching ratios scale roughly with $\sim m_Z^{-1}$. The smallness of the neutral pion mode $Z \to \pi^0\gamma$ owes to the fact that the form factors (4.50) are proportional to $f_\pi(1 - 4s_w^2)$, which enters in quadrature and is coincidentally very small. In the last row of the table, the $\Upsilon(nS)$ is the sum of the branching ratios into the first three states $n = 1, 2, 3$. The largest errors are typically the ones associated with the shape of the meson LCDA, with the exception of the Υ channels, where the relation (4.27) constrains the relevant convolution integral [77].

In the last two columns of Table 4.3, we show how the predictions change under various approximations: The results in the column "asym." are obtained by using the one-loop expressions for the hard-scattering coefficients, but only employing the asymptotic form of the LCDA $\phi(x, \mu \to \infty)$, where all moments $a_n = 0$. The rates in this approximation read:

$$\Gamma(Z^0 \to M^0\gamma)\Big|_{\text{asym}} = \frac{\alpha m_Z}{6v^2}\left(\sum_q f_M^q Q_M^q\right)^2 \left[1 - \frac{10}{3}\frac{\alpha_s(m_Z)}{\pi}\right]. \tag{4.106}$$

In the last column we show results obtained including the Gegenbauer moments but using only tree-level hard scattering coefficients. Generically, the asymptotic result does well in approximating the branching ratios whereas using only leading-order hard-scattering coefficients results in branching ratios typically overshooting

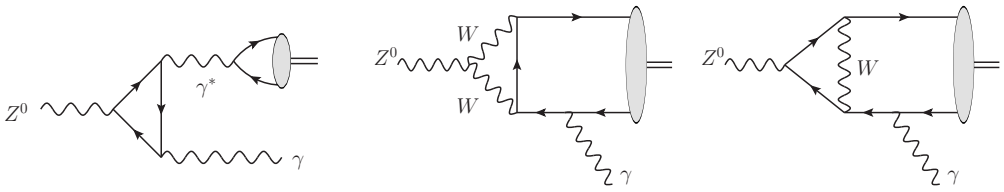

Fig. 4.11.: Examples of QED (left) and electroweak radiative corrections (center and right) to the $Z \to M\gamma$ decay amplitudes. The last two diagrams can give rise to flavor-violating decays in the Standard Model.

the NLO results. This is just a consequence of the high factorization scale, which leads to the weak sensitivity of the rates to the LCDA shape. For mesons with heavy quarks, the LCDA has a more pronounced peak structure because of the new scale the heavy quark introduces. Even at the high factorization scales we are assuming, the LCDAs are relatively far away from their asymptotic form (see Fig. 4.2). As a result, the branching ratios in the asymptotic approximation differ more strongly from the full result. The expression (4.106) is consistent with the corresponding tree-level expressions in ref. [93]. The author of ref. [104] quotes a rate for $Z \to \pi^0\gamma$ that is lower than ours by a factor of 4/9. In this paper, the theoretical framework is set up using a local operator-product expansion for the exclusive decays $Z \to W\pi$, with a power-counting parameter $\omega_0 = 2(m_Z^2 - m_W^2)/(m_Z^2 + m_W^2)$. For the radiative decays, the W is then replaced by the photon, leading to $\omega_0 = 2$, which is not an appropriate expansion parameter. The discrepancy of a factor 4/9 can be traced back to this.

Corrections to our predictions arise at two-loop order in QCD and one-loop order in the electroweak theory. We estimate that the uncertainties from higher order QCD corrections should be covered by the scale variation errors that we include. Electroweak corrections are assumed to be small, with the potentially most dangerous diagram being the first one in Fig 4.11: Here the photon propagator $1/k^2$ could give a large enhancement. However, the $Z\gamma\gamma^*$ is proportional to k^2, canceling the enhancement [105]. The diagram is thus suppressed by a standard loop factor and negligible. A detailed study of these contributions to $Z \to J/\psi\gamma$ has been done by the authors of ref. [106], confirming the insignificance of these corrections. Furthermore, the authors have derived predictions for various other channels of the type $Z \to V\gamma$, finding

$$\begin{aligned} \mathrm{Br}(Z \to \phi\gamma) &= (11.7 \pm 0.8) \cdot 10^{-9}\,, \\ \mathrm{Br}(Z \to J/\psi\,\gamma) &= (9.96 \pm 1.86) \cdot 10^{-8}\,, \\ \mathrm{Br}(Z \to \Upsilon(1S)\,\gamma) &= (4.93 \pm 0.51) \cdot 10^{-8}\,, \end{aligned} \tag{4.107}$$

Decay mode	Branching ratio	asym.	LO
$Z \to \pi^0\gamma$	$(9.80\,^{+0.09}_{-0.14\,\mu} \pm 0.03_f \pm 0.61_{a_2} \pm 0.82_{a_4}) \cdot 10^{-12}$	7.71	14.67
$Z \to \rho^0\gamma$	$(4.19\,^{+0.04}_{-0.06\,\mu} \pm 0.16_f \pm 0.24_{a_2} \pm 0.37_{a_4}) \cdot 10^{-9}$	3.63	5.68
$Z \to \omega\gamma$	$(2.82\,^{+0.03}_{-0.04\,\mu} \pm 0.15_f \pm 0.28_{a_2} \pm 0.25_{a_4}) \cdot 10^{-8}$	2.48	3.76
$Z \to \phi\gamma$	$(1.04\,^{+0.01}_{-0.02\,\mu} \pm 0.05_f \pm 0.07_{a_2} \pm 0.09_{a_4}) \cdot 10^{-8}$	0.86	1.49
$Z \to J/\psi\,\gamma$	$(8.02\,^{+0.14}_{-0.15\,\mu} \pm 0.20_f\,^{+0.39}_{-0.36\,\sigma}) \cdot 10^{-8}$	10.48	6.55
$Z \to \Upsilon(1S)\,\gamma$	$(5.39\,^{+0.10}_{-0.10\,\mu} \pm 0.08_f\,^{+0.11}_{-0.08\,\sigma}) \cdot 10^{-8}$	7.55	4.11
$Z \to \Upsilon(4S)\,\gamma$	$(1.22\,^{+0.02}_{-0.02\,\mu} \pm 0.13_f\,^{+0.02}_{-0.02\,\sigma}) \cdot 10^{-8}$	1.71	0.93
$Z \to \Upsilon(nS)\,\gamma$	$(9.96\,^{+0.18}_{-0.19\,\mu} \pm 0.09_f\,^{+0.20}_{-0.15\,\sigma}) \cdot 10^{-8}$	13.96	7.59

Tab. 4.3.: Predicted branching fractions for various $Z \to M\gamma$ decays, including error estimates due to scale dependence (subscript "μ") and the uncertainties in the meson decay constants ("f"), the Gegenbauer moments of light mesons ("a_n"), and the width parameters of heavy mesons ("σ"). See text for further explanations.

with the last two being in good agreement with our predictions within the quoted uncertainties. The discrepancy in the ϕ channel presumably originates from the authors only including leading logarithmic QCD corrections. We find that the non-logarithmic corrections at $\mathcal{O}(\alpha_s)$ reduce the branching ratio. Furthermore, we find that the LCDA shape uncertainty amounts to a larger uncertainty than quoted by the authors.

The form factor of the $Z \to \eta^{(\prime)}\gamma$ decays exhibits a strong dependence on the parameterization of the mixing between η and η'. The details of the parameterization are discussed in Appendix C. We use two different sets of mixing parameters, given in eqs. (C.13) and (C.14). For the first set of mixing parameters, the form factors entering the $Z \to \eta^{(\prime)}\gamma$ rates are:

$$\begin{aligned}\frac{F_1^{\eta}}{\kappa_{\rm NLO}} &= 16.3\,\text{MeV}\left(1 + 1.41a_2^q - 0.97a_2^s + 0.40b_2 + 0.99a_4^q - 0.68a_4^s + 0.25b_4 + \ldots\right),\\ \frac{F_1^{\eta'}}{\kappa_{\rm NLO}} &= 86.5\,\text{MeV}\left(1 + 0.22a_2^q + 0.22a_2^s + 0.46b_2 + 0.15a_4^q + 0.16a_4^s + 0.29b_4 + \ldots\right).\end{aligned} \tag{4.108}$$

Not displayed are small corrections $\delta_P = 0.36 f_P^c + 0.32 f_P^b$ to these expressions arising from the intrinsic charm and bottom contents of the mesons. The explicit values are $\delta_\eta \approx -0.45$ MeV and $\delta_{\eta'} = -1.2$ MeV, using the decay constants given in eq. (C.24). We also ignore the tiny imaginary parts which do not contribute to the rates at $\mathcal{O}(\alpha_s)$. The hadronic parameters entering the form factors are afflicted by uncer-

tainties not displayed in the above expression. We demonstrate them by showing the uncertainties on the leading term, arising from the FKS mixing parameters:

$$\begin{aligned} F_1^{\eta} &= \kappa_{\text{NLO}} \left(16.3 \pm 1.5_{\varphi} \pm 1.0_{f_q} \pm 1.6_{f_s}\right) \text{MeV} + \dots \,, \\ F_1^{\eta'} &= \kappa_{\text{NLO}} \left(86.5 \pm 0.3_{\varphi} \pm 0.8_{f_q} \pm 2.0_{f_s}\right) \text{MeV} + \dots \,. \end{aligned} \tag{4.109}$$

Using the second set of FKS parameters (C.14), we find:

$$\begin{aligned} \frac{F_1^{\eta}}{\kappa_{\text{NLO}}} &= 6.3\,\text{MeV} \left(1 + 3.64 a_2^q - 3.20 a_2^s + 0.27 b_2 + 2.56 a_4^q - 2.25 a_4^s + 0.17 b_4 + \dots\right), \\ \frac{F_1^{\eta'}}{\kappa_{\text{NLO}}} &= 98.0\,\text{MeV} \left(1 + 0.20 a_2^q + 0.24 a_2^s + 0.46 b_2 + 0.14 a_4^q + 0.17 a_4^s + 0.29 b_4 + \dots\right), \end{aligned} \tag{4.110}$$

with the uncertainties on the leading term as follows:

$$\begin{aligned} F_1^{\eta} &= \kappa_{\text{NLO}} \left(6.3 \pm 2.4_{\varphi} \pm 1.4_{f_q} \pm 1.7_{f_s}\right) \text{MeV} + \dots \,, \\ F_1^{\eta'} &= \kappa_{\text{NLO}} \left(98.0\, {}^{+0.1}_{-0.2}{}_{\varphi} \pm 1.2_{f_q} \pm 1.9_{f_s}\right) \text{MeV} + \dots \,. \end{aligned} \tag{4.111}$$

Comparing the results (4.108) and (4.110) as well as eqs. (4.109) and (4.111) shows just how strongly the form factor F_1^{η} depends on the set of employed mixing parameters. While the form factor $F_1^{\eta'}$ seems more stable, the difference between the results for the different parameter sets is still larger than the uncertainties within each set. The reason for this behavior can be understood from the fact that the dominant contributions to the form factors are proportional to the decay constant f_P^{uds}, defined in eq. (4.36). At mixing angles around $\varphi \sim 40°$, the combination f_η^{uds} is close to zero, making it very sensitive to small changes in φ. As a result, F_1^{η} changes strongly with different mixing parameters and is also smaller by around an order of magnitude compared to $F_1^{\eta'}$.

The contributions from the gluon contribution are important, especially for the η': Here the contributions from the gluon LCDA are much larger than the ones from the quark LCDA at equal order in the Gegenbauer expansion, even though the hard-scattering coefficients for the gluon diagrams start at one loop. In the form factor of the η meson, the quark Gegenbauer moments have larger coefficients but there are strong cancellations between the terms proportional to a_n^q and a_n^s.

Compared with the large uncertainties from the hadronic input parameters, scale variations have generally only tiny effects. We demonstrate this by showing the form factors as functions of the Gegenbauer moments and their coefficients when the scale

Model	(i)	(ii)	(iii)
$\mathrm{Br}(Z \to \eta\gamma)$	0.16 ± 0.05	0.17 ± 0.05	0.16 ± 0.05
$\mathrm{Br}(Z \to \eta'\gamma)$	4.70 ± 0.23	4.77 ± 0.24	4.73 ± 0.24
Model	(iv)	(v)	(vi)
$\mathrm{Br}(Z \to \eta\gamma)$	0.11 ± 0.03	0.10 ± 0.03	$0.010\,^{+0.014}_{-0.010}$
$\mathrm{Br}(Z \to \eta'\gamma)$	3.43 ± 0.17	3.08 ± 0.15	4.84 ± 0.23

Tab. 4.4.: Central values of the $Z \to \eta^{(\prime)}\gamma$ branching ratios in units of 10^{-9}, obtained using six different models of hadronic input parameters, see Table C.5. Models (i)–(v) use the mixing parameters in (C.13), while model (vi) uses those in (C.14). We take $\kappa_{\mathrm{NLO}} = 0.89$ to account for NLO evolution effects.

is varied between the $m_Z/2$ and $2m_Z$. We find:

$$\begin{aligned}
\frac{\mathrm{Re}\, F_1^{\eta}}{\kappa_{\mathrm{NLO}}} &= 16.3\,\mathrm{MeV}\left[(1 \pm 0.01) + \left(1.41^{+0.01}_{-0.02}\right) a_2^q - (0.97 \pm 0.01)\, a_2^s + \left(0.40^{+0.00}_{-0.02}\right) b_2\right], \\
\frac{\mathrm{Re}\, F_1^{\eta'}}{\kappa_{\mathrm{NLO}}} &= 86.5\,\mathrm{MeV}\left[(1 \pm 0.01) + \left(0.22^{+0.00}_{-0.01}\right) a_2^q - (0.22 \pm 0.00)\, a_2^s + \left(0.46^{+0.00}_{-0.02}\right) b_2\right].
\end{aligned} \tag{4.112}$$

Table 4.4 compiles the results for the branching ratios $\mathrm{Br}(Z \to \eta^{(\prime)}\gamma)$, when the different parameter sets compiled in Tab. C.5 are used and $\kappa_{\mathrm{NLO}} = 0.89$. The strong dependence of the branching ratios on the input parameters is apparent from the spread between the numerical predictions. Remarkably, the different LCDA parameters were all obtained from fits to the same low-energy data. We conclude that a measurement of $Z \to \eta^{(\prime)}\gamma$ with high statistics could prove useful towards a better determination of the hadronic parameters. This is especially true since the uncertainties due to power corrections or higher-order perturbative corrections are much smaller than for the low-energy $\gamma\gamma^* \to \eta^{(\prime)}$ experiments.

The decay rates of the radiative W boson decays are given by

$$\Gamma(W^+ \to M^+\gamma) = \frac{\alpha m_W}{48 v^2}\left(\left|F_1^M\right|^2 + \left|F_2^M\right|^2\right), \tag{4.113}$$

with $m_W = (80.385 \pm 0.015)$ GeV. The branching ratios are then obtained by normalizing the rate to the total width of the W boson, given by $\Gamma_W = (2.0897 \pm 0.0008)$ GeV. We also need the relevant entries of the CKM matrix. We use:

$$\begin{aligned}
|V_{ud}| &= 0.97425 \pm 0.00022\,, & |V_{us}| &= 0.2253 \pm 0.0008\,, \\
|V_{cs}| &= 0.986 \pm 0.016\,, & |V_{cd}| &= 0.225 \pm 0.008\,, \\
|V_{cb}| &= (41.1 \pm 1.3) \cdot 10^{-3}\,, & |V_{ub}| &= (4.13 \pm 0.49) \cdot 10^{-3}\,.
\end{aligned} \tag{4.114}$$

$W \to$	Branching ratio	asym.	LO
$\pi^\pm\gamma$	$(4.00\,^{+0.06}_{-0.11}{}_{\mu} \pm 0.01_f \pm 0.49_{a_2} \pm 0.66_{a_4}) \cdot 10^{-9}$	2.45	8.09
$\rho^\pm\gamma$	$(8.74\,^{+0.17}_{-0.26}{}_{\mu} \pm 0.33_f \pm 1.02_{a_2} \pm 1.57_{a_4}) \cdot 10^{-9}$	6.48	15.12
$K^\pm\gamma$	$(3.25\,^{+0.05}_{-0.09}{}_{\mu} \pm 0.03_f \pm 0.24_{a_1} \pm 0.38_{a_2} \pm 0.51_{a_4}) \cdot 10^{-10}$	1.88	6.38
$K^{*\pm}\gamma$	$(4.78\,^{+0.09}_{-0.14}{}_{\mu} \pm 0.28_f \pm 0.39_{a_1} \pm 0.66_{a_2} \pm 0.80_{a_4}) \cdot 10^{-10}$	3.18	8.47
$D_s\gamma$	$(3.66\,^{+0.02}_{-0.07}{}_{\mu} \pm 0.12_{\text{CKM}} \pm 0.13_f\,^{+1.47}_{-0.82}{}_{\sigma}) \cdot 10^{-8}$	0.98	8.59
$D^\pm\gamma$	$(1.38\,^{+0.01}_{-0.02}{}_{\mu} \pm 0.10_{\text{CKM}} \pm 0.07_f\,^{+0.50}_{-0.30}{}_{\sigma}) \cdot 10^{-9}$	0.32	3.42
$B^\pm\gamma$	$(1.55\,^{+0.00}_{-0.03}{}_{\mu} \pm 0.37_{\text{CKM}} \pm 0.15_f\,^{+0.68}_{-0.45}{}_{\sigma}) \cdot 10^{-12}$	0.09	6.44

Tab. 4.5.: Predicted branching fractions for various $W \to M\gamma$ decays, including error estimates due to scale dependence and the uncertainties in the CKM matrix elements, the meson decay constants and the LCDAs. The notation is the same as in Table 4.3. See text for further explanations.

We then obtain the branching ratios listed in Table 4.5. The decays into π, ρ and D_s mesons involve the diagonal CKM matrix elements and are the largest. On the other hand, the modes $W \to K^{(*)}\gamma$ and $W \to B\gamma$ are strongly CKM-suppressed and therefore smaller by a few orders of magnitude.

As we did for the Z decays, we also give predictions in the asymptotic approximation (labeled "asym." in the table) as well as for tree-level hard functions (labeled "LO"). The rates in the asymptotic approximation read:

$$\Gamma(W^\pm \to M^\pm\gamma)\big|_{\text{asym}} = \frac{\alpha m_W f_M^2}{24v^2}\,|V_{ij}|^2\left[1 - \frac{17}{3}\frac{\alpha_s(m_W)}{\pi}\right]. \tag{4.115}$$

The rate corresponding rate $W^\pm \to \pi^\pm\gamma$ was computed in ref. [98] using the approach put forward in ref. [104]. For the same reasons that in ref. [104] the $Z \to \pi\gamma$ rate was too small by a factor of 4/9, the rates for $W^\pm \to \pi^\pm\gamma$ were too small by factor of 2/9 in ref. [98].

The emergent picture is consistent with the Z decays: For light mesons, the asymptotic approximation lies reasonably close to our full result, whereas the tree-level approximation does not. For mesons containing heavy quarks, the asymptotic approximation does not so well since the heavy quark introduces an additional scale and with that a more distinct shape of the LCDA.

For the decay rates of the weak radiative decays $Z \to M^+W^-$ we find:

$$\begin{aligned}\Gamma(Z \to M^+W^-) =& \frac{\alpha(m_Z) m_Z f_M^2}{48 v^2} |V_{ij}|^2 (1-r)^2 \\ & \times \left[\left|F_1^M\right|^2 + \left|F_2^M\right|^2 + \frac{1}{2r} \left| \frac{1+r}{2} F_2^M - \frac{1-r}{2} F_3^M \right|^2 \right] ,\end{aligned} \tag{4.116}$$

where we used $r = m_W^2/m_Z^2 = c_W^2$. As discussed in the previous section, the rates are only mildly sensitive to the shape parameter of the meson LCDA because the hard-scattering functions vary slowly with x. Additionally, the combination

$$\frac{1+r}{2} F_2^M - \frac{1-r}{2} F_3^M = 1 \tag{4.117}$$

is completely independent of the LCDA shape. Evaluating the convolution integrals numerically, we obtain for the expression in the square brackets in eq. (4.116) the result:

$$\left|F_1^M\right|^2 + \left|F_2^M\right|^2 + \frac{1}{2r} = 1.911 + 0.003\, a_1^M(\mu) - 0.011\, a_2^M(\mu) + \dots . \tag{4.118}$$

The appropriate factorization scale in this case is lower than for the decays into a photon. Instead of the mass of the decaying Z boson, two possible choices are either the typical momentum transfer $\mu^2 \sim 2k \cdot q = (m_Z^2 - m_W^2) \approx (43\,\text{GeV})^2$ or twice the energy of the final state meson in the rest frame of the Z boson, leading to $\mu \sim (m_Z^2 - m_W^2)/m_Z \approx 20$ GeV. Due to the insensitivity of the rates on the Gegenbauer moments, the exact scale choice does not noticeably change the final result.

The numerical predictions for the various $Z \to M^\pm W^\mp$ branching ratios are listed in Table 4.6. They are generically smaller than the corresponding $W \to M\gamma$ rates. Note that the branching ratio $Z \to \pi^\pm W^\mp$ is about 15 times larger than $Z \to \pi^0\gamma$, due to the fact of the latter being proportional to $(1 - 4s_W^2)^2$, while $Z \to \pi^\pm W^\mp$ is not. The only significant uncertainties are the ones from the meson decay constants and in some cases the CKM matrix elements. For the reasons we dwelt upon in the last paragraph, scale uncertainties are negligible in all cases. Whether these tiny uncertainties cover perturbative uncertainties from higher order QCD corrections or not is an open question that we leave for future work.

The results we obtained for this class of decays are numerically consistent with those found in ref. [104]. As explained earlier, this work relies on a framework tailored for the $Z \to \pi^\pm W^\mp$ channel. It exploits the fact that the intermediate propagator, which gives rise to our form factors F_i^M, depend only weakly on x. The expansion around the parameter $\omega_0/2 = (m_Z^2 - m_W^2)/(m_Z^2 + m_W^2)$ used in this work is similar to the expansion around $r = 1$ performed in eqs. (4.103).

Decay mode	Branching ratio
$Z^0 \to \pi^\pm W^\mp$	$(1.51 \pm 0.005_f) \cdot 10^{-10}$
$Z^0 \to \rho^\pm W^\mp$	$(4.00 \pm 0.15_f) \cdot 10^{-10}$
$Z^0 \to K^\pm W^\mp$	$(1.16 \pm 0.01_f) \cdot 10^{-11}$
$Z^0 \to K^{*\pm} W^\mp$	$(1.96 \pm 0.12_f) \cdot 10^{-11}$
$Z^0 \to D_s^\pm W^\mp$	$(6.04 \pm 0.20_{\rm CKM} \pm 0.22_f) \cdot 10^{-10}$
$Z^0 \to D^\pm W^\mp$	$(1.99 \pm 0.14_{\rm CKM} \pm 0.10_f) \cdot 10^{-11}$

Tab. 4.6.: Predicted branching fractions for various $Z \to MW$ decays, including error estimates due to the uncertainties in the CKM matrix elements and the meson decay constants. Uncertainties in the shapes of the LCDAs have a negligible impact at tree level. Not shown are perturbative uncertainties due to the neglect of $\mathcal{O}(\alpha_s)$ corrections.

4.6.2. Probing Quark Couplings to Z Bosons

Possible future precision measurements of the exclusive $Z \to M\gamma$ decays can serve as powerful probes of the QCD factorization approach in a theoretically clean environment. Since the decay rates into vector mesons $Z \to V\gamma$ depend on the axial-vector couplings a_q, one could use a precision measurement of these rates to determine these couplings. At LEP, the couplings $|a_b|$ and $|a_c|$ have been measured with an accuracy of around 1% [107]. Using our predictions, a measurement with an accuracy of $\sim 6\%$ could be done for the axial-vector couplings of light quarks.

Our results can also straightforwardly be generalized to include effects from flavor-changing neutral currents (FCNCs), which arise in many new-physics models. If such couplings are present, then they would allow decays $Z \to M\gamma$ into flavor-nondiagonal mesons at the tree level, like K^0, D^0, B^0 and B_s. Parameterizing the flavor-changing couplings through the interaction

$$\mathcal{L}_{\rm FCNC} \supset \frac{g}{c_W} Z_\mu \, \bar{q}_i \left[\gamma^\mu \left(v_{ij} - a_{ij}\gamma^5\right)\right] q_j \,, \tag{4.119}$$

we find the predictions listed in Table 4.7. In the SM, some graphs (like the last two shown in Fig. 4.11) contribute to these modes at the loop-level. We estimate their importance by using naive dimensional analysis and assume that they scale like $(\alpha/\pi)|V_{ik}V_{kj}^*|/s_W^2$. Expressing the CKM matrix elements through the Wolfenstein parameter $\lambda \sim 0.2$, we find the rough estimates given in the last column of the table. These backgrounds pose a limit on how accurately one can probe the FCNC couplings v_{ij} and a_{ij}.

In addition to this, possible FCNC couplings of the Z boson would lead to tree-level neutral meson mixing. Precision flavor physics experiments impose stringent constraints on these $\Delta F = 2$ amplitudes. Matching the tree-level mixing amplitudes

Channel	Branching ratio	SM background
$Z^0 \to K^0\gamma$	$\left[(7.70 \pm 0.83)\,\lvert v_{sd}\rvert^2 + (0.01 \pm 0.01)\,\lvert a_{sd}\rvert^2\right] \cdot 10^{-8}$	$\frac{\lambda}{s_W^2}\,\frac{\alpha}{\pi} \sim 2 \cdot 10^{-3}$
$Z^0 \to D^0\gamma$	$\left[(5.30\,^{+0.67}_{-0.43})\,\lvert v_{cu}\rvert^2 + (0.62\,^{+0.36}_{-0.23})\,\lvert a_{cu}\rvert^2\right] \cdot 10^{-7}$	$\frac{\lambda}{s_W^2}\,\frac{\alpha}{\pi} \sim 2 \cdot 10^{-3}$
$Z^0 \to B^0\gamma$	$\left[(2.08\,^{+0.59}_{-0.41})\,\lvert v_{bd}\rvert^2 + (0.77\,^{+0.38}_{-0.26})\,\lvert a_{bd}\rvert^2\right] \cdot 10^{-7}$	$\frac{\lambda^3}{s_W^2}\,\frac{\alpha}{\pi} \sim 8 \cdot 10^{-5}$
$Z^0 \to B_s\gamma$	$\left[(2.64\,^{+0.82}_{-0.52})\,\lvert v_{bs}\rvert^2 + (0.87\,^{+0.51}_{-0.33})\,\lvert a_{bs}\rvert^2\right] \cdot 10^{-7}$	$\frac{\lambda^2}{s_W^2}\,\frac{\alpha}{\pi} \sim 4 \cdot 10^{-4}$

Tab. 4.7.: Branching fractions for FCNC transitions $Z \to M\gamma$, which could arise from physics beyond the Standard Model. The different theoretical uncertainties have been added in quadrature. The last column shows our estimates for the irreducible Standard Model background up to which one can probe the flavor-changing couplings v_{ij} and a_{ij}. Here $\lambda \approx 0.2$ is the Wolfenstein parameter.

generated by the interaction terms (4.119) onto the effective operator basis defined in ref. [108], the only non-zero coefficients are:

$$C_1 = \frac{4G_F}{\sqrt{2}}(v_{ij} + a_{ij})^2\,, \quad \tilde{C}_1 = \frac{4G_F}{\sqrt{2}}(v_{ij} - a_{ij})^2\,, \quad C_5 = -\frac{4G_F}{\sqrt{2}}(v_{ij}^2 - a_{ij}^2)\,. \quad (4.120)$$

Using the bounds reported in refs. [108–110], we find the upper bounds on various combinations of v_{ij} and a_{ij} listed in Table 4.8. We find particularly strong bounds for the coefficients C_5, corresponding to the right column in the table. In models with exclusively chirality-preserving flavor-changing couplings, these bounds are avoided, since this amounts to $v_{ij} = \pm a_{ij}$. In this particular scenario, the limits on the couplings are $|v_{sd}| < 8.5{\cdot}10^{-5}$, $|v_{cu}| < 7.4{\cdot}10^{-5}$, $|v_{bd}| < 1.0{\cdot}10^{-4}$ and $|v_{bs}| < 3.7{\cdot}10^{-4}$, with identical constraints on the corresponding axial-vector couplings. If we assume these bounds to be maximally saturated, we can give the maximal branching ratios by inserting the couplings into the expressions in Table 4.7. The resulting branching ratios are of order 10^{-15}, with the largest one being the $Z^0 \to B_s\gamma$ rate at $\sim 10^{-14}$. Consequently, these modes are unobservable at the LHC and every future machine currently conceivable. The concept is still interesting for several reasons. First, the bounds on the $\Delta F = 2$ meson mixing processes $(K - \bar{K})$, $(D - \bar{D})$ and $(B_{d,s} - \bar{B}_{d,s})$ are not completely model-independent since the interaction does not have to be mediated by a Z boson: Additional heavy particles with tree-level FCNC couplings could be responsible for generating the mixing amplitudes and could in principle also (at least partially) cancel out the contributions from a possible FCNC coupling of the Z boson. Additionally, in the derivation of bounds on one Wilson coefficient, one assumes the other coefficients to be zero. A method like the one presented here, on the other hand, would allow to prove for flavor-changing Z couplings in a direct and model-independent way. Barring large cancellations between flavor-changing

$\lvert\mathrm{Re}[(v_{sd} \pm a_{sd})^2]\rvert$	$< 2.9 \cdot 10^{-8}$	$\lvert\mathrm{Re}[(v_{sd})^2 - (a_{sd})^2]\rvert$	$< 3.0 \cdot 10^{-10}$
$\lvert\mathrm{Im}[(v_{sd} \pm a_{sd})^2]\rvert$	$< 1.0 \cdot 10^{-10}$	$\lvert\mathrm{Im}[(v_{sd})^2 - (a_{sd})^2]\rvert$	$< 4.3 \cdot 10^{-13}$
$\lvert(v_{cu} \pm a_{cu})^2\rvert$	$< 2.2 \cdot 10^{-8}$	$\lvert(v_{cu})^2 - (a_{cu})^2\rvert$	$< 1.5 \cdot 10^{-8}$
$\lvert(v_{bd} \pm a_{bd})^2\rvert$	$< 4.3 \cdot 10^{-8}$	$\lvert(v_{bd})^2 - (a_{bd})^2\rvert$	$< 8.2 \cdot 10^{-9}$
$\lvert(v_{bs} \pm a_{bs})^2\rvert$	$< 5.5 \cdot 10^{-7}$	$\lvert(v_{bs})^2 - (a_{bs})^2\rvert$	$< 1.4 \cdot 10^{-7}$

Tab. 4.8.: Indirect constraints on the flavor-changing Z-boson couplings v_{ij} and a_{ij} (at 95% confidence level) derived from neutral-meson mixing [108–110].

Z-boson couplings and other new physics effects in $\Delta F = 2$ processes, the $Z \to M\gamma$ decays are unsuitable to look for these couplings. As we will see later however, the method can in principle be used to search for anomalous Higgs boson couplings.

4.6.3. Experimental Accessibility of the Decays

With all the results gathered in the previous section, we can now discuss estimates for event numbers and reconstruction efficiencies to get an understanding of how feasible measurements of the various decays modes are.

After the high-luminosity run of the LHC (assuming an integrated luminosity of 3000 fb^{-1}), the LHC will have produced around 10^{11} Z bosons ans $5 \cdot 10^{11}$ W bosons. Future lepton colliders like FCCee, could produce 10^{12} Z bosons per year running at the Z pole and 10^7 W bosons at the WW threshold [111]. Due to the large branching fraction of $t \to Wb$, many W bosons could also produced above the $t\bar{t}$ threshold.

For the $Z \to M\gamma$ decays, one could trigger on photons, and muons if the final state meson decays to muons. The most promising modes in that regard are $Z \to J/\psi\,\gamma$ and $Z \to \Upsilon(nS)\gamma$, where the vector meson decays leptonically. The rates for these decay chains are small: The branching ratios $Z \to (V \to \mu^+\mu^-)\gamma$ are of order $5 \cdot 10^{-9}$ for $V = J/\psi$ and $1.5 \cdot 10^{-9}$ for $V = \Upsilon(1S)$. Still, several hundred J/ψ events and up to one hundred $\Upsilon(1S)$ events could be observed at the LHC by the end of the high-luminosity phase. The ATLAS collaboration uses exactly this decay chain to identify the modes $Z \to J/\psi\,\gamma$ and $Z \to \Upsilon(nS)\gamma$ [112], and the current upper bounds (at 95% CL) on the branching fractions are $\mathrm{Br}(Z \to J/\psi\,\gamma) < 2.6 \cdot 10^{-6}$, $\mathrm{Br}(Z \to \Upsilon(1S)\,\gamma) < 3.4 \cdot 10^{-6}$, $\mathrm{Br}(Z \to \Upsilon(2S)\,\gamma) < 6.5 \cdot 10^{-6}$, and $\mathrm{Br}(Z \to \Upsilon(3S)\,\gamma) < 5.4 \cdot 10^{-6}$. For decays into ϕ and ρ mesons, one uses their decays to oppositely charged pairs of kaons and pions, respectively [113]. The upper bounds quoted by ATLAS are $\mathrm{Br}(Z \to \phi\,\gamma) < 0.9 \cdot 10^{-6}$ and $\mathrm{Br}(Z \to \rho\,\gamma) < 25 \cdot 10^{-6}$. For light mesons decaying into two photons, like π^0 and η, the reconstruction could

be possible when one of the photons converts into an e^+e^- pair.

For $W \to M\gamma$, the situation seems worse. The charged hadron in the final state is challenging to reconstruct, given the large hadronic background at the LHC. The decay $W \to D_s\gamma$ should yield around 10000 events under the above assumptions and might be the most promising mode, assuming the D_s can be identified. The large $t\bar{t}$ production cross section could be used to identify W boson events: Since both t quarks practically always decay into bW, one has an event with two W bosons and two b quarks. One then requires one W to decay leptonically and identify the b-jets to identify a W boson event [98].

A much more promising possibility of searching for $Z \to M\gamma$ would be a possible future lepton collider. With a dedicated run at the Z pole, the currently envisioned machines could produce 10^{12} Z bosons every year in a very clean environment. This opens up the possibility of dedicated precision studies for many decay channels studied here. Except for $Z \to \pi^0\gamma$, all modes should be accessible, and in the channels with the largest rates, percent-level accuracy should be achievable. Some of the $Z \to WM$ modes might also be observable, depending on the reconstruction efficiencies. Dedicated runs at the WW or $t\bar{t}$ thresholds should allow for a study of the larger $W \to M\gamma$ decay modes.

5. Exclusive Higgs Decays

With the discovery of the Higgs boson at the LHC, the field of high energy physics has advanced into the era of Higgs physics: While the Higgs discovery put an end to the question whether or not the particle exists, many of its properties are still in the dark and many questions still remain for particle physics.

The hierarchy problem, for instance, denotes the question of what stabilizes the Higgs mass against quantum corrections that lead to non-multiplicative renormalization. As a consequence, the renormalization group running of the Higgs mass picks up large contributions when heavy degrees of freedom, that couple to the Higgs, enter the theory at their threshold. This naturalness problem is a challenge to beyond-the-SM (BSM) physics, since every theory involving new heavy particles needs to compensate these corrections or change the fundamental of the Higgs boson.

The Higgs could be involved in the generation of neutrino masses through a see-saw scenario, where the Higgs couples to heavy sterile neutrinos and generates a mass-mixing between them and the light neutrinos after electroweak symmetry breaking (EWSB).

As another major aspect, the flavor structure of the standard model is completely determined by the anatomy of Higgs boson couplings to the fermions. In the standard model, these couplings enter the Lagrangian as completely arbitrary parameters:

$$\mathcal{L}_{\text{yuk}} = -\bar{Q}_L \tilde{\phi}\, Y_u u_R - Q_L \phi\, Y_d d_R - \bar{E}_L \phi Y_e e_R\,, \tag{5.1}$$

where the three Yukawa matrices are non-diagonal 3×3 matrices in flavor-space. After EWSB, the mass basis and the interaction basis are misaligned and charged current gauge interactions become flavor-violating, a phenomenon parameterized by the CKM matrix. Its entries, and with that the flavor structure of the SM, are determined by the Yukawa couplings $\mathbf{Y}_i$ with $i = u, d$. It remains to be seen, if the structure of the Yukawa matrices are really random free parameters or whether they follow a more fundamental mechanism, as is suggested by the hierarchy of the fermion masses and the close-to-symmetric nature of the CKM matrix. For instance, models exist where the couplings of light quarks depend non-trivially on the Higgs field, leading to these hierarchies in a natural way [114, 115]. Measurements of Higgs couplings exist for the heavier end of the SM particle spectrum like W, Z and third-generation fermions [116–118], but not for light quarks. Therefore, models predicting

significantly different Higgs couplings for light particles are still compatible with observation [119].

This (not exhaustive) list clearly shows how the Higgs boson's nature ties into many open questions of our understanding of the universe. It is therefore imperative to measure every accessible property of the Higgs in as many ways as possible. In this section, we will advocate the case for exclusive Higgs decays of the classes $h \to V\gamma$, $h \to ZM$ and $h \to W^{\pm}M^{\mp}$, some of which have been explored in the literature already [120–124]. When the final state meson can be identified, the branching ratio allows for the determination of the Yukawa couplings of the associated valence quarks in a novel way. Furthermore, the intricate interplay between different diagram topologies will allow us to extract more information on a measurement than just the branching ratio of $h \to q\bar{q}$.

With the theoretical framework set up in the previous section, we can swiftly derive predictions for the various branching ratios. While the technicalities of the computation are very similar to the previous section, the phenomenology is richer as the Higgs sector allows more room for modifications to the SM.

5.1. Effective Lagrangian and Bounds

In order to perform a model-independent analysis, we employ the effective Lagrangian

$$\begin{aligned}\mathcal{L}_{\text{eff}} = \kappa_W \frac{2m_W^2}{v} h W_\mu^+ W^{-\mu} + \kappa_Z \frac{m_Z^2}{v} h Z_\mu Z^\mu - \frac{h}{\sqrt{2}} \sum_{f=u,d,e} \left(\bar{f}_L Y_f f_R + \text{h.c.}\right) \\ + \frac{\alpha}{4\pi v}\left(\kappa_{\gamma\gamma} h F_{\mu\nu}F^{\mu\nu} - \tilde{\kappa}_{\gamma\gamma} h F_{\mu\nu}\tilde{F}^{\mu\nu} + \frac{2\kappa_{\gamma Z}}{s_W c_W} h F_{\mu\nu} Z^{\mu\nu} - \frac{2\tilde{\kappa}_{\gamma Z}}{s_W c_W} h F_{\mu\nu}\tilde{Z}^{\mu\nu}\right).\end{aligned} \tag{5.2}$$

The first line of this Lagrangian contains SM operators supplemented with parameters that can depart from their SM value. That means in the SM, we have $\kappa_W = \kappa_Z = 1$ and the 3×3 Yukawa matrices Y are diagonal matrices with the entries proportional to the fermion masses. We normalize the diagonal entries of the Yukawa matrices to their SM couplings and define rescaling parameters κ_f and $\tilde{\kappa}_f$ according to

$$(Y_f)_{ii} = (\kappa_{f_i} + i\tilde{\kappa}_{f_i})\frac{\sqrt{2}m_{f_i}}{v}\,. \tag{5.3}$$

In the SM, $\kappa_{f_i} = 1$ and $\tilde{\kappa}_{f_i} = 0$. In our notation we use the indices f_i and the names of the fermions interchangeably for a more compact notation. For later convenience, we also introduce rescaled parameters

$$\bar{\kappa}_q = \kappa_q \frac{m_q}{m_b}\,, \qquad\qquad \bar{\tilde{\kappa}}_q = \tilde{\kappa}_q \frac{m_q}{m_b}\,, \tag{5.4}$$

normalized to the mass of the b quark. Bounds on these parameters have been derived from a global fit to the measured Higgs rates [122, 125], yielding

$$\begin{aligned} \sqrt{|\kappa_u|^2 + |\tilde{\kappa}_u|^2} &< 3000\,, & \sqrt{|\kappa_d|^2 + |\tilde{\kappa}_d|^2} &< 1500\,, \\ \sqrt{|\kappa_s|^2 + |\tilde{\kappa}_s|^2} &< 75\,, & \sqrt{|\kappa_c|^2 + |\tilde{\kappa}_c|^2} &< 6.2\,. \end{aligned} \tag{5.5}$$

at 95% CL.

The CP-odd couplings of third generation quarks can be constrained by their impact on electric dipole moments (EDMs) [126]. Assuming SM-like couplings of the Higgs to the electron, the strongest constraints come from the the electron EDM, originating from two-loop Barr-Zee graphs such as the one shown on the left in Fig. 5.1. The obtained bounds are $|\tilde{\kappa}_t| < 0.01$, $|\tilde{\kappa}_b| < 1.9$ and $|\tilde{\kappa}_\tau| < 2.4$ at 90% CL. The neutron EDM poses weaker constraints, but they are less model-dependent as they do not rely on $\kappa_e = 1$, $\tilde{\kappa}_e = 0$. From measurements of $h \to b\bar{b}$ and $h \to \tau^+\tau^-$ at the LHC, upper limits on the combinations $|\kappa_{b,\tau}|^2 + |\tilde{\kappa}_{b,\tau}|^2$ can be obtained. At 95% CL the bounds are $|\tilde{\kappa}_b| < 1.44$ and $|\tilde{\kappa}_\tau| < 1.24$ from CMS [116], and $|\tilde{\kappa}_b| < 1.3$ and $|\tilde{\kappa}_\tau| < 1.5$ from ATLAS [117].

For flavor-violating Higgs couplings a global analysis of indirect constraints for q_i, $q_j \neq t$ quotes the bounds [122]

$$|(Y_q)_{ij}| < 10^{-5} \; - \; 10^{-3}\,, \tag{5.6}$$

which makes these couplings irrelevant to our analysis. Flavor-changing Higgs couplings involving the top quark are constrained by LHC measurements of the $t \to qh$ branching ratios for $q = c, u$. The current 95% C.L. bounds are [127]

$$\sqrt{|Y_{tc}|^2 + |Y_{ct}|^2} < 0.18\,, \qquad \sqrt{|Y_{tu}|^2 + |Y_{ut}|^2} < 0.17\,, \tag{5.7}$$

evaluated at the scale $\mu = m_h$. The bounds are expected to tighten to 0.04 after an integrated luminosity of $3000\,\text{fb}^{-1}$ has been collected at the LHC [128].

The effective operators in the second line of the Lagrangian (5.2) are absent in the SM and typically arise from loop-diagrams with heavy NP degrees of freedom. Note that we did not include all possible operators in this Lagrangian. For example, we did not include operators of the form $hW_{\mu\nu}W^{\mu\nu}$ and $hW_{\mu\nu}\tilde{W}^{\mu\nu}$, on which strong bounds exist. They enter our analysis through the one-loop amplitudes $h \to \gamma\gamma^*$, $h \to Z\gamma^*$ and $h \to Z^*\gamma$, and can be absorbed into $\kappa_{\gamma\gamma}$, $\kappa_{\gamma Z}$ and their CP-odd counterparts. Bounds on these operators come from the electron EDM, arising from loop diagrams like the one on the right in Fig. 5.1 [129]. Evaluating this graph, we

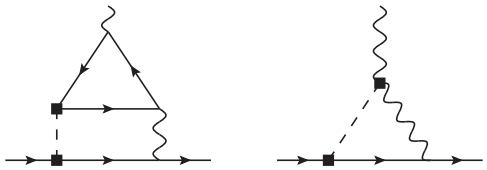

Fig. 5.1.: Two-loop Barr-Zee diagram (left) and effective one-loop contribution (right) to the EDM of the electron arising from the CP-odd couplings $\tilde{\kappa}_f$, $\tilde{\kappa}_{\gamma\gamma}$ and $\tilde{\kappa}_{\gamma Z}$ in the effective Lagrangian (5.2).

find

$$\begin{aligned}\frac{d_e}{e} = -\frac{\alpha}{16\pi^3}\frac{m_e}{v^2}\Bigg[&\left(\log\frac{\mu^2}{m_h^2}+\frac{3}{2}\right)(\tilde{\kappa}_{\gamma\gamma}\kappa_e+\kappa_{\gamma\gamma}+\tilde{\kappa}_e)\\ &+\frac{1-4s_W^2}{4s_W^2c_W^2}\left(\log\frac{\mu^2}{m_h^2}+\frac{3}{2}+\frac{\xi_Z\,\log\xi_Z}{1-\xi_Z}\right)(\tilde{\kappa}_{\gamma Z}\kappa_e+\kappa_{\gamma Z}\tilde{\kappa}_e)\Bigg]\,,\end{aligned} \tag{5.8}$$

with $\xi_Z = m_Z^2/m_h^2$. The expression is logarithmically UV divergent since it involves an effective operator of dimension greater than four. The term proportional to $\tilde{\kappa}_{\gamma\gamma}\kappa_e$ agrees with the analysis in ref. [130]. The renormalization scale μ should be set to the scale at which new physics are integrated out and the inner structure of effective vertex is resolved. Setting this scale to $\Lambda = 1$ TeV for an estimate, choosing $\kappa_e = 1$ and $\tilde{\kappa}_e = 0$, and comparing the result to the present bound $|d_e| < 8.7 \cdot 10^{-29} e$ cm (at 90% CL), the constraint is:

$$|\tilde{\kappa}_{\gamma\gamma} + 0.09\tilde{\kappa}_{\gamma Z}| < 0.006\,. \tag{5.9}$$

Assuming no cancellations between the two terms, this implies $|\tilde{\kappa}_{\gamma\gamma}| < 0.006$ and $|\tilde{\kappa}_{\gamma Z}| < 0.07$.

5.2. Radiative Decays

In this section, we discuss the decays of the type $h \to M\gamma$. At leading power, the meson M can only be a transversely polarized vector meson. Starting from our effective Lagrangian (5.2), we find two different diagram topologies, similar to the radiative W decays $W \to M\gamma$ and the weak radiative Z decays $Z \to MW$, discussed in the previous chapter. We will name them "direct" and "indirect" contributions. We refer to contributions from the first two diagrams in Fig. 5.2 as direct contributions, since the Higgs couples directly to the quarks forming the final state meson V [91, 131]. These contributions are computed using the QCD factorization

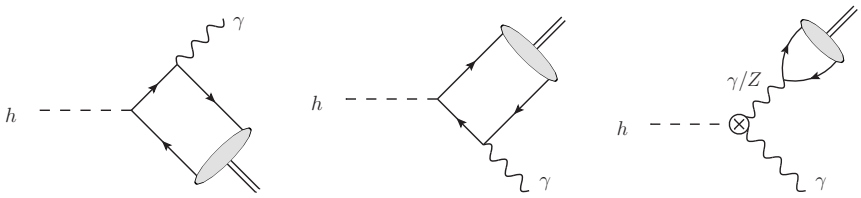

Fig. 5.2.: Direct (left and center) and indirect (right) contributions to the $h \to V\gamma$ decay amplitude. The crossed circle in the third diagram denotes the off-shell $h \to \gamma\gamma^*$ and $h \to \gamma Z^*$ amplitudes, which in the SM arise first at one-loop order.

approach, described in Chapter 4. In the indirect contributions, the Higgs boson decays to a photon and an off-shell vector boson $V^* = \gamma^*, Z^*$, which subsequently converts into the meson [120]. The $h\gamma V^*$ coupling is generated from the effective operators in our effective Lagrangian and from loop diagrams in the SM.

In the SM, the indirect and direct amplitudes interfere destructively. Since the direct amplitudes are proportional to the Yukawa couplings of the quark in the meson, they are most important for heavy mesons. For the $\Upsilon(1S)$, the indirect and direct contributions are of similar size and largely cancel against each other. For light mesons, the indirect contribution will be dominant whereas the direct one will be a small correction.

As in the previous chapter, we present the amplitude in its form factor decomposition:

$$i\mathcal{A}(h \to V\gamma) = -\frac{e f_V}{2}\left[\left(\varepsilon_V^* \cdot \varepsilon_\gamma^* - \frac{(q\cdot\varepsilon_V^*)(k\cdot\varepsilon_\gamma^*)}{k\cdot q}\right) F_1^V - i\epsilon_{\mu\nu\rho\sigma}\frac{k^\mu q^\nu \varepsilon_V^{*\rho}\varepsilon_\gamma^{*\sigma}}{k\cdot q} F_2^V\right]. \tag{5.10}$$

The decay constants f_V are defined as superpositions of the flavor-specific decay constants f_V^q, as we defined them earlier in Chapter 4. For neutral flavor-diagonal mesons, mixing effects lead to complicated relations between them. The combinations we denote by f_V can be related to the electromagnetic decay rate $V \to e^+e^-$ of the meson V. We define

$$Q_V f_V \equiv \sum_q Q_q f_V^q\,, \qquad \text{where} \quad Q_V = \sum_q c_q^V Q_q\,, \tag{5.11}$$

where c_q^V are the flavor coefficients in the naive constituent-quark model. We then have

$$\frac{f_{\rho^0}}{\sqrt{2}} = \sum_q Q_q f_{\rho^0}^q\,, \qquad \frac{f_\omega}{3\sqrt{2}} = \sum_q Q_q f_\omega^q\,, \qquad -\frac{f_\phi}{3} = \sum_q Q_q f_\phi^q\,. \tag{5.12}$$

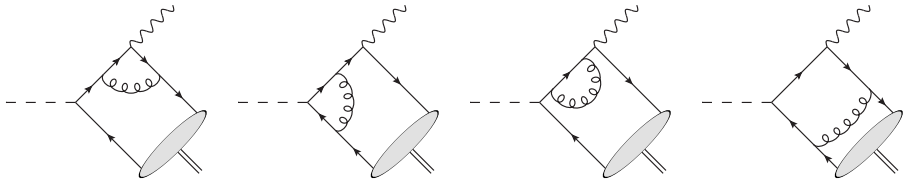

Fig. 5.3.: One-loop QCD corrections to the first diagram in Figure 5.2. Analogous corrections exist for the second diagram.

This leads to the decay rate defined in eq. (C.18), from which the values for f_V are determined, see Appendix C.

5.2.1. Direct Contributions

We start our analysis by computing the direct contributions to the decay amplitude, using the QCD factorization approach described in Chapter 4. The relevant light-cone projector $M_V^\perp$, defined in eq. (4.9), is proportional to the transverse decay constant of the meson $f_V^\perp$. As we did for the decay constants f_V, we relate the flavor-specific transverse decay constants to $f_V^\perp$ through $f_V^\perp = (\sum_q Q_q f_V^{q\perp})/Q_V$. The fact that $f_V^\perp$ is scale-dependent is due to the tensor current not being conserved in QCD, as explained in section 4.1.2. Note that we should in principle also define flavor-specific LCDAs, however since these functions are generically not well-known, we employ SU(3) symmetry and set $\phi_V^{q\perp}(x,\mu) \to \phi_V^\perp(x,\mu)$.

We find the direct contributions to the form factors in eq. (5.10) to be

$$F_{1,\text{direct}}^V = \bar\kappa_V Q_V F_V\,, \qquad\qquad F_{2,\text{direct}}^V = i\bar{\bar\kappa}_V Q_V F_V\,, \tag{5.13}$$

with

$$\bar\kappa_V = \frac{1}{Q_V}\sum_q \bar\kappa_q\, Q_q\, \frac{f_V^{q\perp}}{f_V^\perp}\,, \qquad \bar{\bar\kappa}_V = \frac{1}{Q_V}\sum_q \bar{\bar\kappa}_q\, Q_q\, \frac{f_V^{q\perp}}{f_V^\perp}\,, \tag{5.14}$$

and

$$F_V = \frac{m_b(\mu)}{v}\frac{f_V^\perp(\mu)}{f_V}\int_0^1 dx \frac{\phi_V^\perp(x,\mu)}{x\bar x}\left[1+\frac{C_F\alpha_s(\mu)}{4\pi}h(x,m_h,\mu)+\mathcal{O}(\alpha_s^2)\right]. \tag{5.15}$$

The one-loop hard scattering kernel is given by:

$$h(x,m_h,\mu) = 2\log(x\bar x)\left(\log\frac{m_h^2}{\mu^2}-i\pi\right)+\log^2 x+\log^2\bar x-3\,. \tag{5.16}$$

Up to a typographical error, this result agrees with a computation done in ref. [79]. The function is logarithmically UV-divergent, see Appendix D for details on the

removal of the poles. The Yukawa couplings have been written in terms of the running b-quark mass in the above expressions. They are scale-evolved using the RG equations

$$\mu\frac{d}{d\mu}m_q(\mu) = \gamma^m(\mu)m_q(\mu)\,, \tag{5.17}$$

which, at two-loop order, were obtained in ref. [132]. The solution to the RG equation is:

$$m_q(\mu) = \left(\frac{\alpha_s(\mu)}{\alpha_s(\mu_0)}\right)^{-\frac{\gamma_0^m}{2\beta_0}}\left[1 - \frac{\gamma_1^m\beta_0 - \beta_1\gamma_0^m}{2\beta_0^2}\,\frac{\alpha_s(\mu)-\alpha_s(\mu_0)}{4\pi} + \ldots\right]m_q(\mu_0)\,, \tag{5.18}$$

where the relevant one- and two-loop anomalous dimensions are:

$$\gamma_0^m = -6C_F\,, \qquad \gamma_1^m = -3C_F^2 - \frac{97}{3}\,C_FC_A + \frac{20}{3}\,C_FT_Fn_f\,. \tag{5.19}$$

With the Gegenbauer expansion of the LCDA

$$\phi_V^\perp(x,\mu) = 6x\bar{x}\left[1 + \sum_{n=1}^{\infty} a_n^{V_\perp}(\mu)C_n^{(3/2)}(2x-1)\right]\,, \tag{5.20}$$

and using the method explained in Appendix F, we can rewrite the form factor as:

$$F_V = \frac{6m_b(\mu)}{v}\frac{f_V^\perp(\mu)}{f_V}\left[1 - \frac{C_F\alpha_s(\mu)}{\pi}\log\frac{m_h^2}{\mu^2}\right]I_V(m_h)\,, \tag{5.21}$$

where

$$I_V(m_h) = \sum_{n=0}^{\infty} C_{2n}(m_h,\mu)a_{2n}^{V_\perp}\,. \tag{5.22}$$

The hard scattering coefficients C_n at $\mathcal{O}(\alpha_s)$ are given by:

$$C_n(m_h,\mu) = 1 + \frac{C_F\alpha_s(\mu)}{4\pi}\left[-4(H_{n+1}-1)\left(\log\frac{m_h^2}{\mu^2} - i\pi\right) + 4H_{n+1}^2 - 3 + 4i\pi\right]\,. \tag{5.23}$$

Evaluating the hard scattering function at the factorization scale $\mu = m_h$ and evolving it down to the hadronic reference scale μ_0 resums the large logarithms of the form $\alpha_s\log(\mu_0^2/m_h^2)$ to all orders. The scaling relation for the Gegenbauer moments is (see Section 4.1.2 for details):

$$a_n^{V_\perp}(\mu) = \left(\frac{\alpha_s(\mu)}{\alpha_s(\mu_0)}\right)^{\frac{\gamma_n^\perp}{2\beta_0}}a_n^{V_\perp}(\mu_0)\,, \qquad \text{with} \quad \gamma_n^\perp = 8C_F(H_{n+1}-1)\,. \tag{5.24}$$

Meson	Form factor with errors [%]	Combined [%]
F_{ρ^0}	$4.30\,^{+0.04}_{-0.05\,\mu} \pm 0.03_{m_b} \pm 0.24_f \pm 0.12_{a_2} \pm 0.22_{a_4}$ $+i\big(0.67\,^{+0.14}_{-0.10\,\mu} \pm 0.00_{m_b} \pm 0.04_f \pm 0.03_{a_2} \pm 0.06_{a_4}\big)$	(4.30 ± 0.35) $+i(0.67 \pm 0.14)$
F_{ω}	$4.26\,^{+0.04}_{-0.05\,\mu} \pm 0.03_{m_b} \pm 0.30_f \pm 0.14_{a_2} \pm 0.21_{a_4}$ $+i\big(0.66\,^{+0.14}_{-0.10\,\mu} \pm 0.00_{m_b} \pm 0.05_f \pm 0.03_{a_2} \pm 0.06_{a_4}\big)$	(4.26 ± 0.40) $+i(0.66 \pm 0.14)$
F_{ϕ}	$4.53\,^{+0.04}_{-0.05\,\mu} \pm 0.03_{m_b} \pm 0.24_f \pm 0.15_{a_2} \pm 0.23_{a_4}$ $+i\big(0.70\,^{+0.14}_{-0.10\,\mu} \pm 0.01_{m_b} \pm 0.04_f \pm 0.04_{a_2} \pm 0.06_{a_4}\big)$	(4.53 ± 0.37) $+i(0.70 \pm 0.15)$
$F_{J/\psi}$	$4.54\,^{+0.02}_{-0.04\,\mu} \pm 0.03_{m_b} \pm 0.70_f\,^{+0.13}_{-0.17\,\sigma_V}$ $+i\big(0.63\,^{+0.11}_{-0.08\,\mu} \pm 0.00_{m_b} \pm 0.10_f\,^{+0.03}_{-0.04\,\sigma_V}\big)$	(4.54 ± 0.72) $+i(0.63 \pm 0.14)$
$F_{\Upsilon(1S)}$	$5.04\,^{+0.02}_{-0.03\,\mu} \pm 0.04_{m_b} \pm 0.18_f\,^{+0.09}_{-0.07\,\sigma_V}$ $+i\big(0.66\,^{+0.12}_{-0.08\,\mu} \pm 0.00_{m_b} \pm 0.02_f\,^{+0.02}_{-0.01\,\sigma_V}\big)$	(5.04 ± 0.21) $+i(0.66 \pm 0.10)$
$F_{\Upsilon(2S)}$	$5.09\,^{+0.02}_{-0.04\,\mu} \pm 0.04_{m_b} \pm 0.24_f\,^{+0.13}_{-0.12\,\sigma_V}$ $+i\big(0.68\,^{+0.12}_{-0.09\,\mu} \pm 0.00_{m_b} \pm 0.03_f\,^{+0.03}_{-0.02\,\sigma_V}\big)$	(5.09 ± 0.27) $+i(0.68 \pm 0.11)$
$F_{\Upsilon(3S)}$	$5.11\,^{+0.02}_{-0.04\,\mu} \pm 0.04_{m_b} \pm 0.24_f\,^{+0.15}_{-0.14\,\sigma_V}$ $+i\big(0.69\,^{+0.12}_{-0.09\,\mu} \pm 0.00_{m_b} \pm 0.03_f\,^{+0.04}_{-0.03\,\sigma_V}\big)$	(5.11 ± 0.29) $+i(0.69 \pm 0.12)$

Tab. 5.1.: Theory predictions for the reduced form factors F_V including error estimates.

As we can by now expect from what we have seen in the last chapter, the form factors depend only weakly on the shape parameter after these RG effects have been taken into account. From eq. (5.22) we obtain for the first five terms in the sum:

$$\begin{aligned}\operatorname{Re} I_V(m_h) &= 1.01 + 1.13 a_2^{V_\perp}(m_h) + 1.21 a_4^{V_\perp}(m_h) + 1.29 a_6^{V_\perp}(m_h) + 1.35 a_8^{V_\perp}(m_h) \\ &\approx 1.01 + 0.51 a_2^{V_\perp}(\mu_0) + 0.36 a_4^{V_\perp}(\mu_0) + 0.29 a_6^{V_\perp}(\mu_0) + 0.24 a_8^{V_\perp}(\mu_0)\,,\end{aligned} \tag{5.25}$$

demonstrating this point once again. As in the previous chapter, we have used $\mu_0 = 1$ GeV as the hadronic reference scale.

The effective couplings $\bar\kappa_V$ for the heavy quarkonia J/ψ and $\Upsilon(nS)$ are, to a very good approximation, given by $\bar\kappa_{J/\psi} \approx \bar\kappa_c$ and $\bar\kappa_{\Upsilon(nS)} \approx \bar\kappa_b$, and analogously for the CP-odd parameters $\bar{\tilde\kappa}_V$. For light vector mesons, flavor-mixing effects have in general non-negligible impacts on these relations: Even for the mesons ρ^0 and ω, tiny admixtures of a flavor state $|s\bar s\rangle$ can be important since the s-quark Yukawa coupling is much larger than the one to u and d. For the ρ^0 meson, this flavor-mixing can only happen through electromagnetic or isospin-violating effects in QCD, both of which are estimated to be tiny and we employ the naive relation

$$\bar\kappa_{\rho^0} \approx \frac{2\bar\kappa_u + \bar\kappa_d}{3} \overset{\text{SM}}{\to} 6.1 \cdot 10^{-4}\,. \tag{5.26}$$

For ω and ϕ mesons, the situation is different, and we discuss the details of the parameterization in Appendix C. Assuming $|\bar{\kappa}_s| \gg |\bar{\kappa}_{u,d}|$ and working in the SU(3) limit we obtain to first order in the mixing angle $\theta_{\omega\phi}$:

$$\begin{aligned} \bar{\kappa}_\omega &\approx 2\bar{\kappa}_u - \bar{\kappa}_d + \sqrt{2}\,\bar{\kappa}_s\,\theta_{\omega\phi}(m_\omega^2) \quad &&\overset{\text{SM}}{\to}\ (-0.08 + 26.8\,\theta_{\omega\phi})\cdot 10^{-3}\,, \\ \bar{\kappa}_\phi &\approx \bar{\kappa}_s\left[1 + \frac{\theta_{\omega\phi}(m_\phi^2)}{\sqrt{2}}\right] &&\overset{\text{SM}}{\to}\ 0.019 + 0.013\,\theta_{\omega\phi}\,. \end{aligned} \tag{5.27}$$

We can see that for the ω meson, the contributions of u and d cancel almost precisely, leaving the mixing contribution to be the dominant term. Estimates for the mixing angle $\theta_{\omega\phi}$ derived from mass-independent analyses are $\theta_{\omega\phi} \approx 0.05$ [133] and $\theta_{\omega\phi} \approx 0.06$ [134, 135]. A more recent, mass-dependent analysis yielded $\theta_{\omega\phi}(m_\omega^2) \approx 0.008$ and $\theta_{\omega\phi}(m_\phi^2) \approx 0.081$ [136]. Consequently, we assume $\bar{\kappa}_\phi \approx \bar{\kappa}_s$ to be good approximation, whereas interpreting $\bar{\kappa}_\omega$ in terms of quark Yukawa couplings would require a better description of the relevant flavor-mixing effects.

In Table 5.1, we present our numerical predictions for the direct form factors F_V, defined in eq. (5.21). Along with the central values, we include detailed error estimates: The subscript "μ" denotes the scale uncertainty from varying the factorization scale between $m_h/2$ and $2m_h$, and the subscript "m_b" marks the uncertainty from the b-quark mass. Hadronic uncertainties come from the decay constants f_V, the ratio $f_V^\perp/f_V$ (denoted by "f_V"), and finally from the LCDA shape parameters (denoted by the subscript a_n for light mesons and σ_V for heavy quarkonia). These uncertainties dominate the combined errors, seen in the last column of the table. The uncertainties are between 4% and 9%, with the exception of the J/ψ where the decay constant is afflicted with a larger uncertainty coming from the ratio $f_V^\perp/f_V$ (around 16%). Note that the spread between the numerical values of F_V for different mesons is small.

As we have seen in the previous chapter, power corrections to these results start at $\mathcal{O}(\Lambda_{\text{QCD}}^2/m_H^2)$ for light mesons and $\mathcal{O}(m_V^2/m_H^2)$ for heavy mesons. Due to the smallness of these suppression factors, we ignore them and work with the leading projections. Electroweak loop corrections and two-loop QCD corrections, like the ones shown in Fig. 5.4, can contribute without being proportional to the Yukawa coupling of the valence quark in the meson. The first diagram can be proportional to the top-quark Yukawa and a loop factor $y_t\alpha/\pi \sim 2\cdot 10^{-3}$ whereas the second one consists of purely gauge interactions and comes with $m_W\alpha/(v\pi) \sim 0.7\cdot 10^{-3}$. The corrections are thus of the order of the strange-quark Yukawa and smaller than the charm-quark Yukawa by roughly a factor of 10. Consequently, in order to measure the strange-quark Yukawa in the SM, these corrections need to be taken into account. These levels of sensitivity are however unrealistic for the LHC. The third and fourth diagram of Fig. 5.4 shows neglected QCD corrections. The third diagram is the equivalent of the gluon contribution contributing at leading twist to

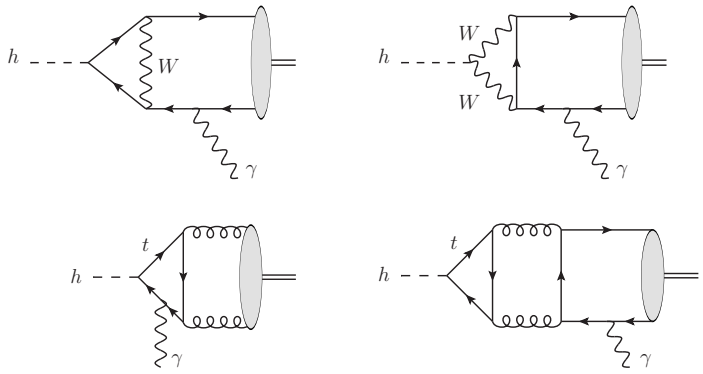

Fig. 5.4.: Examples of electroweak radiative corrections (top row) and higher-order QCD radiative corrections (bottom row) to the $h \to V\gamma$ decay amplitudes.

the decays $Z \to \eta^{(\prime)}\gamma$. For vector mesons, the two-gluon LCDA does not exist at leading twist and thus such a contribution is suppressed. The last diagram shows a higher-order QCD correction in which the Higgs also couples to the top-quark. We estimate these contributions to be negligible.

5.2.2. Indirect Contributions

The indirect contributions arise from diagrams where the Higgs couples to γZ or $\gamma\gamma$ and either the Z or one of the photons convert into the final state meson, see the third diagram in Fig. 5.2. These couplings are generated in the SM beginning at one-loop order by diagrams like the ones shown in Fig. 5.5. Due to the smallness of the Yukawa couplings entering the direct contributions, the indirect amplitudes typically dominate over the direct ones, despite starting at one-loop order. We therefore keep the effect of the meson mass and the off-shellness of the intermediate gauge boson.

The one-loop expressions for the $h \to \gamma\gamma^*$ and $h \to \gamma Z^*$ vertices have been

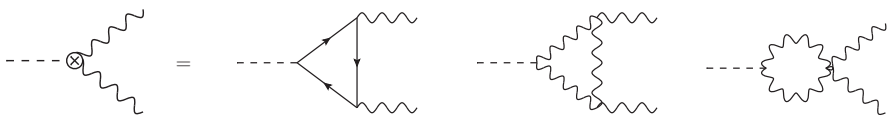

Fig. 5.5.: One-loop SM contributions to the effective $h\gamma\gamma$ and $h\gamma Z$ vertices.

obtained in ref. [137]. We find for the indirect form factors:

$$\begin{aligned} F^V_{1,\text{indirect}} &= \frac{\alpha(m_V)}{\pi}\,\frac{m_h^2-m_V^2}{m_V\,v}\left[Q_V\,C_{\gamma\gamma}(x_V) - \frac{v_V}{(s_W c_W)^2}\,\frac{m_V^2}{m_Z^2-m_V^2}\,C_{\gamma Z}(x_V)\right], \\ F^V_{2,\text{indirect}} &= i\,\frac{\alpha(m_V)}{\pi}\,\frac{m_h^2-m_V^2}{m_V\,v}\left[Q_V\,\tilde{C}_{\gamma\gamma}(x_V) - \frac{v_V}{(s_W c_W)^2}\,\frac{m_V^2}{m_Z^2-m_V^2}\,\tilde{C}_{\gamma Z}(x_V)\right], \end{aligned} \tag{5.28}$$

with $x_V = m_V^2/m_h^2$ and $v_V \equiv \sum_q c_q^V v_q$, analogously to the couplings defined in eq. (5.11). Here v_q are the vector couplings of the Z boson to fermions. We neglect flavor-mixing effects in the $h \to \gamma Z^* \to \gamma V$ amplitude. The loop functions entering the form factors are:

$$\begin{aligned} C_{\gamma\gamma}(x_V) &= \sum_q \kappa_q\,\frac{2N_c Q_q^2}{3}\,A_f(\tau_q,x_V) + \sum_l \kappa_l\,\frac{2Q_l^2}{3}\,A_f(\tau_l,x_V) \\ &\quad - \frac{\kappa_W}{2}\,A_W^{\gamma\gamma}(\tau_W,x_V) + \kappa_{\gamma\gamma}\,, \\ C_{\gamma Z}(x_V) &= \sum_q \kappa_q\,\frac{2N_c Q_q v_q}{3}\,A_f(\tau_q,x_V) + \sum_l \kappa_l\,\frac{2Q_l v_l}{3}\,A_f(\tau_l,x_V) \\ &\quad - \frac{\kappa_W}{2}\,A_W^{\gamma Z}(\tau_W,x_V) + \kappa_{\gamma Z}\,, \end{aligned} \tag{5.29}$$

and

$$\begin{aligned} \tilde{C}_{\gamma\gamma}(x_V) &= \sum_q \tilde{\kappa}_q N_c Q_q^2\,B_f(\tau_q,x_V) + \sum_l \tilde{\kappa}_l\,Q_l^2\,B_f(\tau_l,x_V) + \tilde{\kappa}_{\gamma\gamma}\,, \\ \tilde{C}_{\gamma Z}(x_V) &= \sum_q \tilde{\kappa}_q N_c Q_q v_q\,B_f(\tau_q,x_V) + \sum_l \tilde{\kappa}_l\,Q_l v_l\,B_f(\tau_l,x_V) + \tilde{\kappa}_{\gamma Z}\,. \end{aligned} \tag{5.30}$$

Here the first two terms in each expression represent the quarks and leptons in the loop, the third terms are the gauge-boson loops and the last terms are the tree-level contributions from the Lagrangian (5.2). The loop functions A_f, $A_W^{\gamma V}$ and B_f, given explicitly in Appendix G, depend on the variables $\tau_X = 4m_X^2/m_h^2$ with $X = q, l, W$. When evaluating the variables τ_q, we use the running quark masses at the scale m_h, using eq. (5.18).

The dominant contributions to the form factors are the ones where the intermediate gauge-boson is a photon: Since it is off-shell only by the mass of the meson, the photon propagator enhances the amplitude. The contributions $C_{\gamma Z}$ on the other hand are suppressed by a factor $m_V^2/(m_Z^2-m_V^2)$. The off-shellness, parameterized by the variable x_V is tiny. Evaluating the functions $C_{\gamma\gamma}$ and $C_{\gamma Z}$ at $x_V = 0$ numerically,

we find:

$$\begin{aligned} C_{\gamma\gamma}(0) &= \kappa_{\gamma\gamma} - 4.164\kappa_W + 0.920\kappa_t - (0.012 - 0.011i)\kappa_\tau - (0.007 - 0.008i)\kappa_b \\ &\quad - (0.015 - 0.010i)\bar{\kappa}_c - 0.001\bar{\kappa}_s + \dots , \\ C_{\gamma Z}(0) &= \kappa_{\gamma Z} - 2.173\kappa_W + 0.132\kappa_t - (0.004 - 0.004i)\kappa_b \\ &\quad - (0.002 - 0.001i)\bar{\kappa}_c + \dots , \end{aligned} \tag{5.31}$$

and similar expressions for their CP-odd counterparts. Note that the coupling parameters $\bar{\kappa}_q$ for the quarks are normalized to the b-quark mass. This means that contributions from second-generation fermions would be small even if their Yukawa couplings would be as large as the b-quark Yukawa, meaning $\bar{\kappa}_q = 1$. In the SM, we find $C_{\gamma\gamma}(0) = -3.266 + 0.21i$ and $C_{\gamma Z}(0) = -2.046 + 0.005i$, whereas $\tilde{C}_{\gamma\gamma}$ and $\tilde{C}_{\gamma Z}$ vanish. The leading term in the form factor is proportional to $1/m_V$, leading to an enhancement of the indirect contribution for lighter mesons.

Two-loop corrections to these results exist both from QCD and the electroweak theory. Radiative corrections between the quarks forming the final-state meson are by definition included in the decay constant. Loops between the effective $h\gamma\gamma$ and $h\gamma Z$ vertices and the quarks in the meson lead to amplitudes that do not receive the enhancement from the almost on-shell photon propagator and also need at least two gluons to be exchanged for color conservation. They can therefore be neglected. QCD-corrections to the effective $h\gamma\gamma$ and $h\gamma Z$ vertices arise from gluon exchanges inside the quark loops. They have been calculated numerically in ref. [138] and analytically in ref. [139]. These corrections are only relevant for the top-quark contribution and they enhance the decay amplitude by a few percent. Two-loop electroweak corrections to the $h \to \gamma\gamma$ amplitude in the SM have been computed in refs. [140–142]. They are small and numerically negative. For a Higgs mass of $m_h = 125.09\,\text{GeV}$, the effects of QCD and electroweak corrections almost cancel each other, leaving a total correction of about -0.2% [141]. We therefore ignore these corrections.

5.2.3. Building the Observable

Assuming the electron Yukawa coupling to be close to the SM prediction, the CP-odd form factor F_2^V is tiny compared to F_1^V. We therefore focus our discussion here on the CP-even F_1^V. For the significant terms, we find numerically:

$$\begin{aligned} F_1^{\Upsilon(1S)} &= 0.022\kappa_W - 0.005\kappa_t - 0.005\kappa_{\gamma\gamma} - (0.017 \pm 0.001)\kappa_b + \dots , \\ F_1^{J/\psi} &= -0.137\kappa_W + 0.030\kappa_t + 0.033\kappa_{\gamma\gamma} + (0.030 \pm 0.005)\bar{\kappa}_c + \dots , \\ F_1^{\phi} &= 0.206\kappa_W - 0.045\kappa_t - 0.049\kappa_{\gamma\gamma} - (0.015 \pm 0.001)\bar{\kappa}_\phi + \dots . \end{aligned} \tag{5.32}$$

Recall that we wanted to probe the Yukawa couplings associated with the final state meson, meaning for instance that we wanted to probe κ_b through $F_1^{\Upsilon(1S)}$ and κ_c from $F_1^{J/\psi}$. We observe, however, that the parameters of interest only have a subdominant effect on the form factors F_1^V. Instead, there are larger contributions from other terms, all of which can be altered beyond the SM. Clearly, we need to find a way to remove the dependence on the parameters we are not interested in without making model-dependent assumptions.

The proper observable to consider in this case is thus not simply the branching ratio $h \to V\gamma$. Instead, we normalize it to the branching ratio of $h \to \gamma\gamma$: The parameters κ_W, κ_t, $\kappa_{\gamma\gamma}$ in the above form factors all enter through the loop functions of the effective $h \to \gamma\gamma^*$ and $h \to \gamma Z^*$ vertices. Since the photon in the first case is only off-shell by a small amount $k^2 = m_V^2$ and the $h \to \gamma Z^*$ amplitude is a small effect, the effects of the "unwanted" κ_i largely cancel out. Furthermore, in the ratio of the two branching fractions, the total Higgs width cancels out, removing yet another theoretical uncertainty. We find:

$$\frac{\mathrm{Br}(h \to V\gamma)}{\mathrm{Br}(h \to \gamma\gamma)} = \frac{8\pi\alpha^2(m_V)}{\alpha} \frac{Q_V^2 f_V^2}{m_V^2} \left(1 - \frac{m_V^2}{m_h^2}\right)^2 \frac{\left|1 - \Delta_V\right|^2 + \left|r_{\mathrm{CP}} - \tilde{\Delta}_V\right|^2}{1 + |r_{\mathrm{CP}}|^2}\,, \tag{5.33}$$

where $r_{\mathrm{CP}} = \tilde{C}_{\gamma\gamma}(0)/C_{\gamma\gamma}(0)$. We can also eliminate the sensitivity to the decay constant, by multiplying the above ratio by $m_V/\Gamma(V \to e^+e^-)$, yielding

$$\frac{m_V}{\Gamma(V \to e^+e^-)} \frac{\mathrm{Br}(h \to V\gamma)}{\mathrm{Br}(h \to \gamma\gamma)} = \frac{6}{\alpha} \left(1 - \frac{m_V^2}{m_h^2}\right)^2 \frac{\left|1 - \Delta_V\right|^2 + \left|r_{\mathrm{CP}} - \tilde{\Delta}_V\right|^2}{1 + |r_{\mathrm{CP}}|^2}\,, \tag{5.34}$$

which has the advantage of further reducing hadronic uncertainties.

The quantities we need to explore now are the Δ_V and $\tilde{\Delta}_V$. We will discuss the CP-even quantities Δ_V here at length and relegate the CP-odd ones to Appendix H (along with more explicit expressions for the CP-even quantities). The functions are given by:

$$\begin{aligned}
\Delta_V &= -\bar{\kappa}_V \frac{F_V}{C_{\gamma\gamma}(0)} \frac{\pi m_V v}{\alpha(m_V)\, m_h^2} - \frac{C_{\gamma\gamma}(x_V) - C_{\gamma\gamma}(0)}{C_{\gamma\gamma}(0)} + \frac{m_V^2}{m_Z^2} \frac{v_V}{Q_V s_W^2 c_W^2} \frac{C_{\gamma Z}(0)}{C_{\gamma\gamma}(0)}\,, \\
\tilde{\Delta}_V &= -\bar{\tilde{\kappa}}_V \frac{F_V}{C_{\gamma\gamma}(0)} \frac{\pi m_V v}{\alpha(m_V)\, m_h^2} - \frac{\tilde{C}_{\gamma\gamma}(x_V) - \tilde{C}_{\gamma\gamma}(0)}{C_{\gamma\gamma}(0)} + \frac{m_V^2}{m_Z^2} \frac{v_V}{Q_V (s_W c_W)^2} \frac{\tilde{C}_{\gamma Z}(0)}{C_{\gamma\gamma}(0)}\,,
\end{aligned} \tag{5.35}$$

where we expanded in m_V^2/m_Z^2 and $x_V = m_V^2/m_h^2$. Since every term is normalized to $C_{\gamma\gamma}(0)$, we define an effective parameter $\kappa_{\gamma\gamma}^{\mathrm{eff}}$, given by:

$$\begin{aligned}
\kappa_{\gamma\gamma}^{\mathrm{eff}} = \frac{C_{\gamma\gamma}(0)}{\left[C_{\gamma\gamma}(0)\right]_{\mathrm{SM}}} = \Big[&1.275\kappa_W - 0.282\kappa_t + (0.004 - 0.003i)\kappa_\tau + (0.002 - 0.002i)\kappa_b \\
&+ (0.004 - 0.003i)\bar{\kappa}_c - 0.306\kappa_{\gamma\gamma}\Big]/(1 - 0.006i)\,.
\end{aligned} \tag{5.36}$$

Since the Higgs couplings to W bosons and third-generation fermions agree with the SM predictions within errors, the only considerable departure from the SM value of $\kappa_{\gamma\gamma}^{\text{eff}}$ can originate from $\kappa_{\gamma\gamma}$. The tiny imaginary parts, arising from light fermions in the loops, have no noticeable impact on our analysis. The quantity r_{CP} is zero in the SM and is given exclusively by the CP-odd coupling parameters:

$$\begin{aligned} r_{\text{CP}} = &\frac{-(0.429+0.003i)\tilde{\kappa}_t + (0.004-0.003i)\tilde{\kappa}_\tau + (0.002-0.002i)\tilde{\kappa}_b}{\kappa_{\gamma\gamma}^{\text{eff}}} \\ &+ \frac{(0.005-0.003i)\bar{\tilde{\kappa}}_c - (0.306+0.002i)\tilde{\kappa}_{\gamma\gamma}}{\kappa_{\gamma\gamma}^{\text{eff}}}\,. \end{aligned} \tag{5.37}$$

Clearly, the parameters with the largest impact on this quantity are $\tilde{\kappa}_t$ and $\tilde{\kappa}_{\gamma\gamma}$. The strong bounds discussed in section. 5.1 however imply that, assuming the Higgs couplings to electrons do not greatly depart from the SM values, r_{CP} must be of the order 1% and is thus not important. In principle, the parameter could be directly probed through $h \to \gamma\gamma$, where both photons convert to e^+-e^- pairs in the detector, although this appears to be challenging [143].

We can now discuss the numerical results for the Δ_V and $\tilde{\Delta}_V$. The explicit dependence on all significant κ_i parameters is given in Appendix H. Here, we only display the direct contribution and evaluate the indirect one assuming SM values for all κ_i. We find

$$\begin{aligned} \Delta_{\rho^0} &= \Big[(0.068\pm0.006) + i(0.011\pm0.002)\Big]\,\frac{\bar{\kappa}_{\rho^0}}{\kappa_{\gamma\gamma}^{\text{eff}}} + 0.00002\,, \\ \Delta_{\omega} &= \Big[(0.068\pm0.006) + i(0.011\pm0.002)\Big]\,\frac{\bar{\kappa}_{\omega}}{\kappa_{\gamma\gamma}^{\text{eff}}} - 0.00011\,, \\ \Delta_{\phi} &= \Big[(0.093\pm0.008) + i(0.015\pm0.003)\Big]\,\frac{\bar{\kappa}_{\phi}}{\kappa_{\gamma\gamma}^{\text{eff}}} + 0.00014\,, \\ \Delta_{J/\psi} &= \Big[(0.281\pm0.045) + i(0.040\pm0.009)\Big]\,\frac{\bar{\kappa}_{c}}{\kappa_{\gamma\gamma}^{\text{eff}}} + 0.00005\,, \end{aligned} \tag{5.38}$$

and

$$\begin{aligned} \Delta_{\Upsilon(1S)} &= \Big[(0.948\pm0.040) + i(0.130\pm0.019)\Big]\,\frac{\kappa_b}{\kappa_{\gamma\gamma}^{\text{eff}}} + 0.0184 - 0.0015i\,, \\ \Delta_{\Upsilon(2S)} &= \big[(1.014\pm0.054) + i(0.141\pm0.022)\big]\,\frac{\kappa_b}{\kappa_{\gamma\gamma}^{\text{eff}}} + 0.0207 - 0.0015i\,, \\ \Delta_{\Upsilon(3S)} &= \Big[(1.052\pm0.060) + i(0.148\pm0.025)\Big]\,\frac{\kappa_b}{\kappa_{\gamma\gamma}^{\text{eff}}} + 0.0221 - 0.0015i\,. \end{aligned} \tag{5.39}$$

We see that the power corrections from the indirect amplitudes, represented by the constant terms, are tiny, and only reach the percent level for the $\Upsilon(nS)$ mesons.

For the CP-odd coefficients $\tilde{\Delta}_V$, the direct terms are identical, with the obvious replacement $\kappa_i \to \tilde{\kappa}_i$ and $\bar{\kappa}_i \to \bar{\tilde{\kappa}}_i$. The indirect power corrections come with larger coefficients but are most-likely negligible in view of the strong bounds on the relevant $\tilde{\kappa}_i$, see Appendix H.

The parameters Δ_V can be compared to the literature by converting the respective results to our notation. From ref. [122] we find $\Delta_{\rho^0} = (0.095 \pm 0.020)\,(2\bar{\kappa}_u + \bar{\kappa}_d)/3$, $\Delta_\omega = (0.092 \pm 0.021)\,(2\bar{\kappa}_u + \bar{\kappa}_d)$ and $\Delta_\phi = (0.130 \pm 0.027)\bar{\kappa}_s$, while from [77] we get $\Delta_{J/\psi} = (0.392 \pm 0.053)\bar{\kappa}_c$, $\Delta_{\Upsilon(1S)} = (1.048 \pm 0.046)\kappa_b$, $\Delta_{\Upsilon(2S)} = (1.138 \pm 0.053)\kappa_b$ and $\Delta_{\Upsilon(3S)} = (1.175 \pm 0.056)\kappa_b$. The values found in the literature are consistently higher than ours, owing to the fact that the authors have not completely included QCD corrections and RG effects in the direct contributions. In the case of the $\Upsilon(nS)$ channels, the small imaginary part is crucial because the direct and indirect contributions almost exactly cancel. In ref. [122], the result for Δ_ω misses the important contribution from $\omega - \phi$ mixing and has a sign mistake in front of $\bar{\kappa}_d$. Additionally, we find that our uncertainties are significantly smaller.

5.2.4. Phenomenology

Let us now put together the predictions for the various branching ratios. We will start the discussion by giving the SM predictions and then explore the new physics reach. Using the Higgs mass $m_h = 125.09$ GeV, the SM branching ratio prediction $\mathrm{Br}(h \to \gamma\gamma) = (2.28 \pm 0.11) \cdot 10^{-3}$ [144] and multiplying it with the quantity eq. (5.33) we obtain the SM predictions:

$$\begin{aligned} \mathrm{Br}(h \to \rho^0\gamma) &= (1.68 \pm 0.02_{f_\rho} \pm 0.08_{h\to\gamma\gamma}) \cdot 10^{-5}\,, \\ \mathrm{Br}(h \to \omega\gamma) &= (1.48 \pm 0.03_{f_\omega} \pm 0.07_{h\to\gamma\gamma}) \cdot 10^{-6}\,, \\ \mathrm{Br}(h \to \phi\gamma) &= (2.31 \pm 0.03_{f_\phi} \pm 0.11_{h\to\gamma\gamma}) \cdot 10^{-6}\,. \end{aligned} \tag{5.40}$$

The main uncertainties are the ones from the decay constants f_V and the from the $h \to \gamma\gamma$ branching ratio, with the latter being dominant. The results obtained here are lower and have a smaller uncertainty than the ones presented in ref. [122], where $\mathrm{Br}(h \to \rho^0\gamma) = (1.9 \pm 0.15) \cdot 10^{-5}$, $\mathrm{Br}(h \to \omega\gamma) = (1.6 \pm 0.17) \cdot 10^{-6}$ and $\mathrm{Br}(h \to \phi\gamma) = (3.0 \pm 0.13) \cdot 10^{-6}$. For the heavy mesons, we find:

$$\begin{aligned} \mathrm{Br}(h \to J/\psi\,\gamma) &= (2.95 \pm 0.07_{f_{J/\psi}} \pm 0.06_{\text{direct}} \pm 0.14_{h\to\gamma\gamma}) \cdot 10^{-6}\,, \\ \mathrm{Br}(h \to \Upsilon(1S)\,\gamma) &= (4.61 \pm 0.06_{f_{\Upsilon(1S)}}\, {}^{+1.75}_{-1.21}{}_{\text{ direct}} \pm 0.22_{h\to\gamma\gamma}) \cdot 10^{-9}\,, \\ \mathrm{Br}(h \to \Upsilon(2S)\,\gamma) &= (2.34 \pm 0.04_{f_{\Upsilon(2S)}}\, {}^{+0.75}_{-0.99}{}_{\text{ direct}} \pm 0.11_{h\to\gamma\gamma}) \cdot 10^{-9}\,, \\ \mathrm{Br}(h \to \Upsilon(3S)\,\gamma) &= (2.13 \pm 0.04_{f_{\Upsilon(3S)}}\, {}^{+0.75}_{-1.12}{}_{\text{ direct}} \pm 0.10_{h\to\gamma\gamma}) \cdot 10^{-9}\,. \end{aligned} \tag{5.41}$$

In these channels, the relevant Yukawa couplings are large enough so that the uncertainties from the direct contribution become significant. Note the smallness of

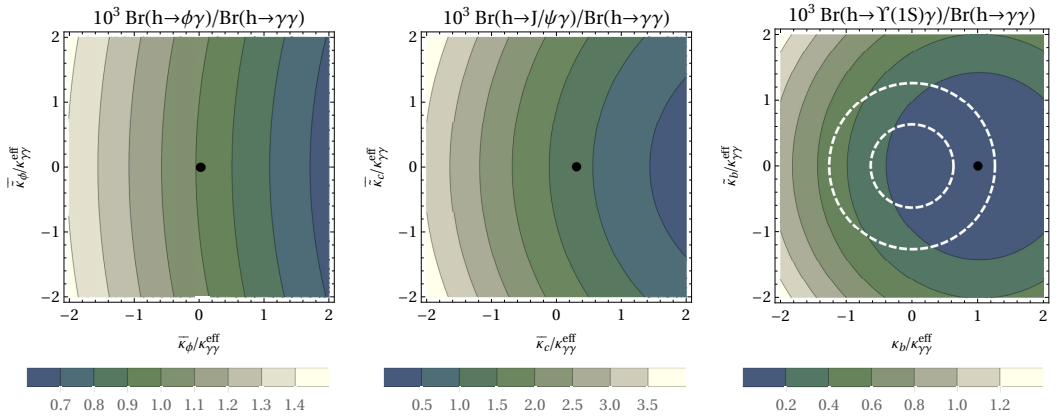

Fig. 5.6.: Predictions (central values) for the ratios of the $h \to V\gamma$ and $h \to \gamma\gamma$ branching fractions with $V = \phi$, J/ψ and $\Upsilon(1S)$ as functions of the rescaled Yukawa couplings normalized to the parameter $\kappa_{\gamma\gamma}^{\text{eff}}$ defined in (5.36). The black dots indicate the SM values. Coupling parameters between the dashed white circles in the third plot are preferred by the current ATLAS result on $h \to b\bar{b}$ [113], assuming a SM-like $h \to \gamma\gamma$ branching ratio [145]. See text for further details.

the branching ratios to Υ mesons due to the larger Yukawa coupling of the b-quark leading to a strong cancellation between direct and indirect contributions. The authors of ref. [77] find $(2.79\,^{+0.16}_{-0.15}) \cdot 10^{-6}$ for J/ψ, $(0.61\,^{+1.74}_{-0.61}) \cdot 10^{-9}$ for $\Upsilon(1S)$, $(2.02\,^{+1.86}_{-1.28}) \cdot 10^{-9}$ for $\Upsilon(2S)$ and $(2.44\,^{+1.75}_{-1.30}) \cdot 10^{-9}$ for $\Upsilon(3S)$. We find good agreement except for the $\Upsilon(1S)$, where the small imaginary part in eq. (5.39), that was neglected by the authors, becomes important.

Despite the small branching fractions, first experimental studies have been performed by the ATLAS Collaboration. For decays into heavy mesons, the reported upper bounds are $\text{Br}(h \to J/\psi\,\gamma) < 1.5 \cdot 10^{-3}$, $\text{Br}(h \to \Upsilon(1S)\,\gamma) < 1.3 \cdot 10^{-3}$, $\text{Br}(h \to \Upsilon(2S)\,\gamma) < 1.9 \cdot 10^{-3}$ and $\text{Br}(h \to \Upsilon(3S)\,\gamma) < 1.3 \cdot 10^{-3}$, all at 95% CL [112]. The expected results are smaller by a factor of 500 for J/ψ, whereas the Υ modes are out of reach for the LHC within the SM. We will see later, that this can change drastically when new physics effects are allowed. With an integrated luminosity of $3\,\text{ab}^{-1}$, the LHC will have produced around $1.7 \cdot 10^8$ Higgs bosons per experiment at the end of the high-luminosity phase [146]. Reconstructing the J/ψ using its leptonic decays into muons, one can expect around 30 events per experiment, with an estimated effective branching ratio $\text{Br}(h \to J/\psi\,\gamma \to \mu^+\mu^-\gamma) = 1.8 \cdot 10^{-7}$. Assuming one can also use the decays into electrons, then the total number of expected events increases to 120. See ref. [120] for more details on reconstruction and background. In a recent conference note, ATLAS also reports upper bounds on the decays into

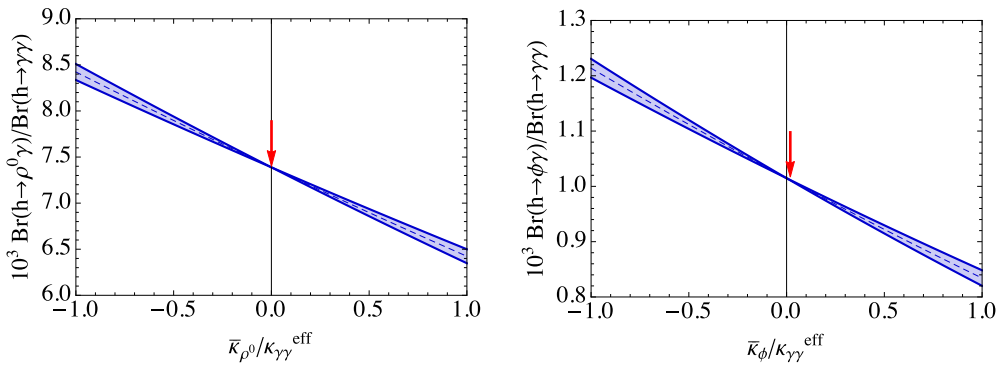

Fig. 5.7.: Predictions for the $h \to \rho\gamma$ and $h \to \phi\gamma$ branching ratios, normalized to the $h \to \gamma\gamma$ branching fraction, as functions of $\bar{\kappa}_{\rho^0} \approx (2\bar{\kappa}_u + \bar{\kappa}_d)/3$ and $\bar{\kappa}_\phi \approx \bar{\kappa}_s$, respectively, normalized to $\kappa_{\gamma\gamma}^{\rm eff}$. The SM values are indicated by the red arrows.

light mesons $h \to \rho^0\gamma$ and $h \to \phi\gamma$ [113]. At 95% CL, they report the upper bounds $\mathrm{Br}(h \to \phi\gamma) < 4.8 \cdot 10^{-4}$ and $\mathrm{Br}(h \to \rho\gamma) < 8.8 \cdot 10^{-4}$, meaning they are larger than our predictions by a factor of 200 and 500, respectively. The authors of ref. [122] assume an efficiency of $\epsilon_{\phi\gamma} = 0.75$, which is significantly higher than the current value reported by ATLAS, $\epsilon_{\phi\gamma} = 0.17$. For the ρ^0 channel, the efficiency reported is even lower, $\epsilon_{\rho^0\gamma} = 0.10$. In the SM one can expect a total number of events of $400\epsilon_{\phi\gamma}$ and $2900\epsilon_{\rho^0\gamma}$ for the two channels, respectively. Assuming that the current efficiencies do not dramatically increase, this corresponds to ~ 80 events in the $h \to \phi\gamma$ channel and ~ 300 events in $h \to \rho^0\gamma$.

We can now discuss implications of new physics effects on our predictions. In Fig. 5.6 we show how the branching ratio varies when the effective couplings $\bar{\kappa}_i$ and $\bar{\tilde{\kappa}}_i$ governing the direct contributions, are varied. The black dots represent the SM prediction. We do not show plots for ρ^0 and ω mesons, as they are qualitatively the same as the one for the ϕ. Similarly, the $\Upsilon(nS)$ with $n > 1$ are not shown since they are similar to the $1S$ case. In the plots, a value of 0.4 corresponds to a branching ratio of $\mathrm{Br}(h \to V\gamma) \sim 10^{-6}$, assuming that the $h \to \gamma\gamma$ is SM-like. If not, the numbers must be rescaled by $\mathrm{Br}(h \to \gamma\gamma)/\mathrm{Br}(h \to \gamma\gamma)_{\rm SM}$. This holds for all numbers given in the following discussion. Furthermore, the relevant quark-Yukawa rescaling parameters κ_i enter the predictions always normalized to the effective parameter $\kappa_{\gamma\gamma}^{\rm eff}$, meaning that new physics effects can enter through each of these parameters. However, the effects entering via $\kappa_{\gamma\gamma}^{\rm eff}$ would uniformly enter all branching ratios.

Let us further study the branching ratios under the assumption that the CP-odd Yukawa couplings vanish. In Fig. 5.7, we show the dependence of the branching

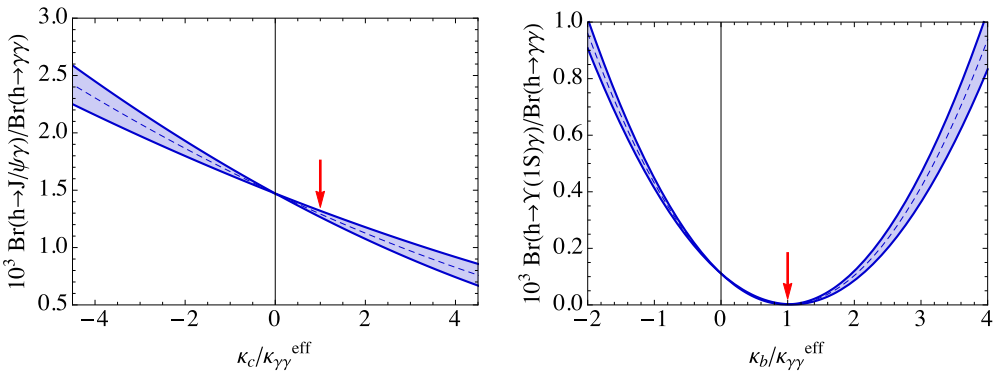

Fig. 5.8.: Predictions for the $h \to J/\psi\,\gamma$ and $h \to \Upsilon(1S)\,\gamma$ branching ratios, normalized to the $h \to \gamma\gamma$ branching fraction, as functions of κ_c and κ_b, respectively, normalized to $\kappa_{\gamma\gamma}^{\rm eff}$. The SM values are indicated by the red arrows.

ratios $h \to \rho^0\gamma$ and $h \to \phi\gamma$ of the CP-even parameters κ_{ρ^0} and κ_ϕ. The uncertainties of our predictions are indicated by the width of the colored band. The plot for $h \to \omega\gamma$ would look identical to the one for the ρ^0 with a different vertical scaling. All three channels exhibit only weak dependences on the Yukawa couplings of interest. A measurement of the $h \to \rho^0\gamma$ branching ratio with an accuracy of 10% would only yield the bound $\bar{\kappa}_{\rho^0}/\kappa_{\gamma\gamma}^{\rm eff} < 0.8$, which means that a combination of u- and d-quark Yukawas could not be larger than 80% of the b-quark Yukawa. Even a 1% measurement would yield an upper bound of only $\bar{\kappa}_{\rho^0}/\kappa_{\gamma\gamma}^{\rm eff} < 0.08$, which is still larger than the SM prediction by a factor of more than 100. For the ϕ meson, the situation is similar: A 10% measurement of $h \to \phi\gamma$ would yield $-0.55 < \bar{\kappa}_\phi/\kappa_{\gamma\gamma}^{\rm eff} < 0.62$. A measurement at 1% accuracy would yield $-0.04 < \bar{\kappa}_\phi/\kappa_{\gamma\gamma}^{\rm eff} < 0.08$, which is closer to the SM value of $\bar{\kappa}_\phi \approx 0.02$, but is completely out of reach at the LHC. The situation is much different for the heavy quarkonia. Fig. 5.8 displays the dependences of the branching ratios $h \to J/\psi\gamma$ and $h \to \Upsilon(1S)\gamma$ of the CP-even quark Yukawa couplings. Measuring the branching ratio in the J/ψ channel at an accuracy of 20% would yield the constraint $-0.51 < \kappa_c/\kappa_{\gamma\gamma}^{\rm eff} < 3.07$. With a 10% measurement, we obtain $0.32 < \kappa_c/\kappa_{\gamma\gamma}^{\rm eff} < 1.53$, and with a 5% measurement one could reach $0.75 < \kappa_c/\kappa_{\gamma\gamma}^{\rm eff} < 1.19$. At a future 100 TeV collider, these measurements could be done and provide important insights on the CP-even c-quark Yukawa coupling. For the $\Upsilon(1S)$, the dependence on the b-quark Yukawa coupling is quite dramatic: The coefficient function $\Delta_{\Upsilon(1S)} \approx 1$ to a good approximation due to the large b-quark Yukawa coupling in the SM. Consequently, the direct and indirect amplitudes cancel almost exactly, as the diagram on the right in Fig. 5.8 shows. A departure from $\kappa_b = 1$ strongly influences the branching fraction. An especially interesting

case is $\kappa_b = -1$, which boosts the prediction by a factor of ~ 220 over the SM value and would still be compatible with a SM-like observation of $h \to b\bar{b}$, which is entirely insensitive to the sign (and in fact the CP-phase, see below).

The dependence of the results on the CP-odd parameters $\tilde{\kappa}_V$ is virtually non-existent for the light mesons and only small for the J/ψ. We conclude that only the $\Upsilon(nS)$ channels can probe CP-odd Yukawa couplings. In the previous paragraph, we already saw the strong dependence of the branching ratio on the CP-even Yukawa coupling. We now generalize the discussion to the case of $\tilde{\kappa}_b \neq 0$. First, note in the right plot of Fig. 5.6, that the SM value lies almost exactly in the center of the colored circles in the κ-$\tilde{\kappa}$ plane. A measurement of the branching ratio $\mathrm{Br}(h \to \Upsilon(1S)\gamma)$ therefore constrains the allowed couplings to a circular band centered around the point $(1, 0)$. On the other hand, a measurement of $h \to b\bar{b}$, normalized to $h \to \gamma\gamma$ is only sensitive to

$$\lambda_{b\gamma} \equiv \sqrt{\left|\frac{\kappa_b}{\kappa_{\gamma\gamma}^{\mathrm{eff}}}\right|^2 + \left|\frac{\tilde{\kappa}_b}{\kappa_{\gamma\gamma}^{\mathrm{eff}}}\right|^2}\,. \tag{5.42}$$

Recent measurements by the ATLAS collaboration are in support of both SM-like rates for $h \to \gamma\gamma$ and $h \to b\bar{b}$ [118, 145]. Combining the reported results $\mu_{h\to b\bar{b}} = 0.90 \pm 0.27$ and $\kappa_{\gamma\gamma}^{\mathrm{eff}} = 0.93^{+0.09}_{-0.08}$, we find:

$$\lambda_{b\gamma} = 1.02\,{}^{+0.19}_{-0.25\,b}\,{}^{+0.10}_{-0.11\,\gamma}\,, \tag{5.43}$$

where uncertainties from $h \to b\bar{b}$ and $h \to \gamma\gamma$ are displayed separately. These values lead to the dashed white circles in Fig. 5.6. Therefore, combining $h \to b\bar{b}$ and $h \to \Upsilon(1S)\gamma$ can have a greater benefit for our knowledge of κ_b and $\tilde{\kappa}_b$ than just shrinking the error bars. To demonstrate this point, we consider two hypothetical future scenarios:

$$\begin{aligned} &\text{(I)} \qquad \lambda_{b\gamma} = 1.0 \pm 0.15\,, \qquad && \frac{\mathrm{Br}(h \to \Upsilon(1S)\gamma)}{\mathrm{Br}(h \to \gamma\gamma)} < 0.2 \cdot 10^{-3}\,, \\ &\text{(II)} \qquad \lambda_{b\gamma} = 0.65 \pm 0.10\,, \qquad && \frac{\mathrm{Br}(h \to \Upsilon(1S)\gamma)}{\mathrm{Br}(h \to \gamma\gamma)} = (0.4 \pm 0.2) \cdot 10^{-3}\,. \end{aligned} \tag{5.44}$$

The corresponding exclusion plots are displayed in Fig. 5.9. In scenario (I), the ratio $\mathrm{Br}(h \to b\bar{b})/\mathrm{Br}(h \to \gamma\gamma)$ is measured to be its SM value and an upper bound $0.5 \cdot 10^{-6}$ is obtained on the $h \to \Upsilon(1S)\gamma$ branching ratio. This scenario produces the left plot. Even without an observation of the exclusive decay, one can now constrain the parameters κ_b and $\tilde{\kappa}_b$ to a non-trivial region, namely the overlap of the regions extracted from the two measurements. This scenario is compatible with the SM expectation. However, the allowed region also includes the case where the b-quark Yukawa coupling is completely CP-odd, with a phase of up to $\pm\pi/2$. The value $\kappa_b/\kappa_{\gamma\gamma}^{\mathrm{eff}} = -1$, which would have been compatible with the measurement of $\lambda_{b\gamma}$

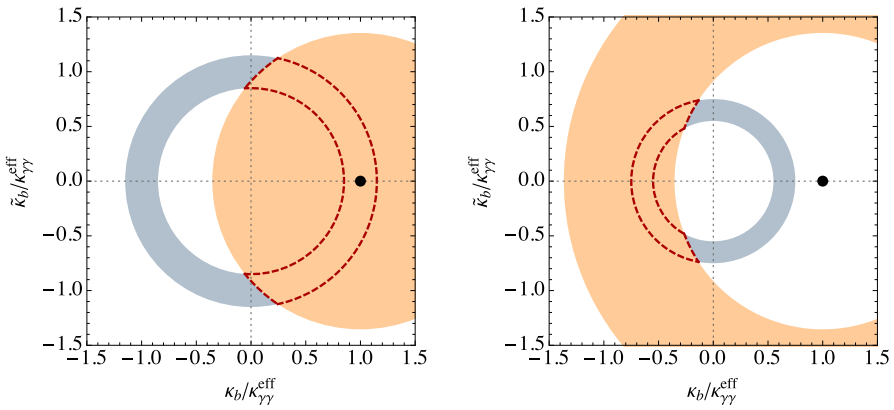

Fig. 5.9.: Constraints on the effective coupling strengths $\kappa_b/\kappa_{\gamma\gamma}^{\rm eff}$ and $\tilde{\kappa}_b/\kappa_{\gamma\gamma}^{\rm eff}$ derived in two possible scenarios for future measurements of the ratios $\mathrm{Br}(h \to b\bar{b})/\mathrm{Br}(h \to \gamma\gamma)$ (light blue) and $\mathrm{Br}(h \to \Upsilon(1S)\,\gamma)/\mathrm{Br}(h \to \gamma\gamma)$ (orange). The allowed parameter space is given by the red-shaded intersection of the two rings. The black dot indicates the SM value.

alone, is then ruled out by the exclusive hadronic decay. The second plot in Fig. 5.9 shows the allowed regions for scenario (II). Here, measurements for both $\lambda_{b\gamma}$ and the exclusive decay exist and their overlap excludes the SM point completely due to the observation of the $h \to \Upsilon(1S)\gamma$ decay. This would be a spectacular sign of new physics. In conclusion, we see that the exclusive hadronic decay combined with the more direct searches can yield interesting results in that they do not only enhance the statistics, but also reveal more information. If one combines the various $\Upsilon(nS)$ channels, one can double the statistics of the exclusive search.

We note in passing, that at a future 100 TeV hadron collider one could measure the $h \to V\gamma \to l^+l^-\gamma$ to such good accuracy, that the possibility of observing even the polarization of the final state photon and meson might open up. This could be done by looking at events where the photon converts into an e^+-e^- pair, as was proposed for $h \to \gamma\gamma$ and $B \to K^*\gamma$ [143, 147]. This way, one could differentiate between the different Lorentz structures in the amplitude and thus obtain information on the sign of the ratio $\tilde{\kappa}_q/\kappa_q$ and discriminate between upper and lower half-planes in Fig. 5.9.

5.3. Weak Radiative Neutral Current Decays

In this section, we discuss the weak radiative decays $h \to MZ$. They are similar to the $h \to V\gamma$ decays, however the Z boson can be longitudinally polarized and therefore, both vector mesons and a pseudoscalar mesons can be produced. This leads to a different helicity structure of the amplitude and could give interesting new information on the couplings entering the prediction. Similar to the $Z \to MW$ decays, the factorization scale is lower than m_h. We use the value $\mu_{hZ} = (m_h^2 - m_Z^2)/m_h \approx 58.6$ GeV in our analysis. To capture NP effects as model-independently as possible we will again use the effective Lagrangian (5.2).

For pseudoscalar mesons in the final state, the amplitude is given by

$$i\mathcal{A}(h \to PZ) = \frac{2g}{c_W v}\, k \cdot \varepsilon_Z^*\, F^{PZ}\,. \tag{5.45}$$

Here, the Z boson must be longitudinally polarized. For vector mesons we can write

$$i\mathcal{A}(h \to VZ) = -\frac{2gm_V}{c_W v}\left[\varepsilon_V^{\parallel *}\cdot\varepsilon_Z^{\parallel *}\, F_\parallel^{VZ} + \varepsilon_V^{\perp *}\cdot\varepsilon_Z^{\perp *}\, F_\perp^{VZ} + \frac{\epsilon_{\mu\nu\alpha\beta}\, k^\mu q^\nu \varepsilon_V^{*\alpha}\varepsilon_Z^{*\beta}}{\sqrt{(k\cdot q)^2 - k^2q^2}}\, \widetilde{F}_\perp^{VZ}\right]. \tag{5.46}$$

The longitudinal and transverse polarization vectors of the meson are given by

$$\varepsilon_V^{\parallel\mu} = \frac{1}{m_V}\,\frac{k\cdot q}{\left[(k\cdot q)^2 - k^2q^2\right]^{1/2}}\left(k^\mu - \frac{k^2}{k\cdot q}\,q^\mu\right), \qquad \varepsilon_V^{\perp\mu} = \varepsilon_V^\mu - \varepsilon_V^{\parallel\mu}\,. \tag{5.47}$$

Replacing $m_V \to m_Z$ and $k \leftrightarrow q$ yields the corresponding expressions for the Z boson polarization vector. Squaring the amplitudes and integrating over phase-space we obtain the rates:

$$\begin{aligned}
\Gamma(h \to PZ) &= \frac{m_h^3}{4\pi v^4}\,\lambda^{3/2}(1, r_Z, r_P)\,\left|F^{PZ}\right|^2, \\
\Gamma(h \to VZ) &= \frac{m_h^3}{4\pi v^4}\,\lambda^{1/2}(1, r_Z, r_V)\,(1 - r_Z - r_V)^2 \\
&\quad\times\left[\left|F_\parallel^{VZ}\right|^2 + \frac{8 r_V r_Z}{(1-r_Z-r_V)^2}\left(\left|F_\perp^{VZ}\right|^2 + \left|\widetilde{F}_\perp^{VZ}\right|^2\right)\right],
\end{aligned} \tag{5.48}$$

with $\lambda(x,y,z) = (x-y-z)^2 - 4yz$ and $r_X = m_X^2/m_h^2$. The decay rates into transverse vector mesons are suppressed, as can be read off from the coefficient of the transverse form factors. The form factors are obtained from the diagrams in Fig. 5.10. We split them up into the direct (graphs like the first two) and indirect contributions (third and fourth graph), just like we did for $h \to V\gamma$.

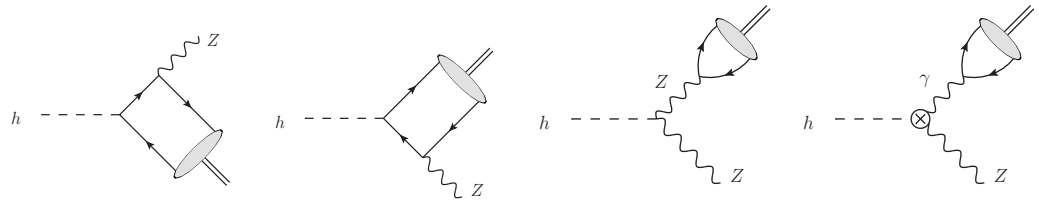

Fig. 5.10.: Leading-order diagrams contributing to the decays $h \to MZ$. The crossed circle in the last graph denotes contributions from one-loop SM diagrams to $h \to Z\gamma^*$ as well as tree-level effective vertices. This last graph only contributes if $M = V_\perp$.

5.3.1. Indirect Contributions

The indirect contributions are again dominant and we will start our discussion here. For the corresponding form factors we find:

$$\begin{aligned}
F^{PZ}_{\text{indirect}} &= \kappa_Z \sum_q f_P^q \, a_q \,, \\
F^{VZ}_{\parallel\,\text{indirect}} &= \frac{\kappa_Z}{1 - r_V/r_Z} \sum_q f_V^q \, v_q + C_{\gamma Z} \, \frac{\alpha(m_V)}{4\pi} \, \frac{4 r_Z}{1 - r_Z - r_V} \sum_q f_V^q \, Q_q \,, \\
F^{VZ}_{\perp\,\text{indirect}} &= \frac{\kappa_Z}{1 - r_V/r_Z} \sum_q f_V^q \, v_q + C_{\gamma Z} \, \frac{\alpha(m_V)}{4\pi} \, \frac{1 - r_Z - r_V}{r_V} \sum_q f_V^q \, Q_q \,, \\
\widetilde{F}^{VZ}_{\perp\,\text{indirect}} &= \widetilde{C}_{\gamma Z} \, \frac{\alpha(m_V)}{4\pi} \, \frac{\lambda^{1/2}(1, r_Z, r_V)}{r_V} \sum_q f_V^q \, Q_q \,.
\end{aligned} \tag{5.49}$$

The functions $C_{\gamma Z}$ and $\tilde{C}_{\gamma Z}$ were defined in eqs. (5.29) and (5.30). The terms proportional to κ_Z originate from the the third diagram in Fig. 5.10 while the terms proportional to $C_{\gamma Z}$ and $\tilde{C}_{\gamma Z}$ come from the fourth diagram. Naively, one would expect the third diagram to be the dominant one, since it is a tree-level graph, whereas the fourth diagram starts at one-loop (or through the effective $h\gamma Z$ vertex). However, the last contribution is enhanced by the photon propagator being almost on-shell. The two effects cancel and thus both contributions are important. For light vector mesons, the photon-pole graph is the leading contribution, whereas for heavy vector mesons it is subdominant. This agrees with the findings of ref. [123]. The importance of the photon-pole graph was overlooked in refs. [121, 148].

To evaluate the loop functions numerically, we use the running quark masses at

the hard scale μ_{hZ} whereas for the top quark, the pole mass is used. We find:

$$\begin{aligned}
C_{\gamma Z} &= \kappa_{\gamma Z} - 2.53\,\kappa_W + 0.135\,\kappa_t - (1.66 - 0.83\,i)\cdot 10^{-3}\,\kappa_b - (1.35 - 0.46\,i)\cdot 10^{-4}\,\kappa_c \\
&\quad - (7.45 - 3.21\,i)\cdot 10^{-5}\,\kappa_\tau - (1.35 - 0.30\,i)\cdot 10^{-6}\,\kappa_s + \ldots \\
&\xrightarrow{\text{SM}} -2.395 + 0.001\,i\,, \\
\widetilde{C}_{\gamma Z} &= \tilde{\kappa}_{\gamma Z} + 0.206\,\tilde{\kappa}_t - (1.90 - 0.83\,i)\cdot 10^{-3}\,\tilde{\kappa}_b - (1.48 - 0.46\,i)\cdot 10^{-4}\,\tilde{\kappa}_c \\
&\quad - (8.36 - 3.21\,i)\cdot 10^{-5}\,\tilde{\kappa}_\tau - (1.43 - 0.30\,i)\cdot 10^{-6}\,\tilde{\kappa}_s + \ldots \\
&\xrightarrow{\text{SM}} 0\,.
\end{aligned} \tag{5.50}$$

Note that the light quarks and leptons contribute weakly to the result, even if we allow for large rescaling of their SM Yukawa couplings. Within the current bounds on these parameters, however, they cannot noticeably influence our result and we will therefore use the values

$$C_{\gamma Z} = -2.395 + \kappa^{\text{eff}}_{\gamma Z}\,, \qquad\qquad \tilde{C}_{\gamma Z} = \tilde{\kappa}^{\text{eff}}_{\gamma Z}\,, \tag{5.51}$$

in our analysis, where $\kappa^{\text{eff}}_{\gamma Z}$ and $\tilde{\kappa}^{\text{eff}}_{\gamma Z}$ parameterize NP effects in the $h\gamma Z$ coupling. They vanish in the SM and are approximately given by $\kappa^{\text{eff}}_{\gamma Z} \approx \kappa_{\gamma Z} - 2.53(\kappa_W - 1) + 0.135(\kappa_t - 1)$ and $\tilde{\kappa}^{\text{eff}}_{\gamma Z} \approx \tilde{\kappa}_{\gamma Z} + 0.206\,\tilde{\kappa}_t$. Current upper bounds on $\kappa_{\gamma Z}$ and $\tilde{\kappa}_{\gamma Z}$ come from the search for $h \to \gamma Z$ decay at the LHC. The upper limit on this branching ratio, reported by ATLAS [149], implies:

$$\sqrt{\left|\kappa^{\text{eff}}_{\gamma Z} - 2.395\right|^2 + \left|\tilde{\kappa}^{\text{eff}}_{\gamma Z}\right|^2} < 5.1\,. \tag{5.52}$$

As discussed in section 5.1, the CP-odd parameter $\tilde{\kappa}^{\text{eff}}_{\gamma Z}$ also receives a strong bound from the electron EDM. This bound can be avoided in models where the Higgs does not couple to electrons. We therefore do not impose these bounds.

5.3.2. Direct Contributions

The direct contributions are once again computed in the QCDF framework. The form factors for $M = V_\parallel,\ P$ arise from subleading-twist projections. We discuss the details of these projections in Appendix A. Neglecting three-particle LCDAs and using the asymptotic form $\phi_P(x) = 6x\bar{x}$, we obtain the form factor:

$$F^{PZ}_{\text{direct}} = \sum_q f^q_P\, a_q\, \kappa_q\, \frac{m_q}{m_h^2}\,(2\mu_P - 3m_q)\,\frac{1 - r_Z^2 + 2r_Z \log r_Z}{(1 - r_Z)^3}\,, \tag{5.53}$$

with $\mu_P = m_P^2/(m_{q_1} + m_{q_2})$. Note that this contribution is suppressed by $\mu_P m_q/m_h^2$ relative to the indirect form factors in eq. (5.49). It is therefore negligible. The same holds for the longitudinal vector meson form factor $F^{VZ}_{\parallel\,\text{direct}}$.

For transversely polarized vector mesons, the direct contributions to the form factors arise from leading-twist projections. We find

$$\begin{aligned} F_{\perp\,\text{direct}}^{VZ} &= \frac{1-r_Z}{4}\sum_q \frac{m_q f_V^{q\perp}}{m_V}\int_0^1 dx\left(\frac{v_q\kappa_q+ia_q\tilde{\kappa}_q}{x+r_Z\bar{x}}+\frac{v_q\kappa_q-ia_q\tilde{\kappa}_q}{\bar{x}+r_Z x}\right)\phi_V^\perp(x)\,, \\ \tilde{F}_{\perp\,\text{direct}}^{VZ} &= \frac{1-r_Z}{4}\sum_q \frac{m_q f_V^{q\perp}}{m_V}\int_0^1 dx\left(\frac{v_q\tilde{\kappa}_q-ia_q\kappa_q}{x+r_Z\bar{x}}+\frac{v_q\tilde{\kappa}_q+ia_q\kappa_q}{\bar{x}+r_Z x}\right)\phi_V^\perp(x)\,, \end{aligned} \tag{5.54}$$

which, when the asymptotic form of the LCDA is used, become:

$$\begin{aligned} F_{\perp\,\text{direct}}^{VZ} &= \sum_q f_V^{q\perp} v_q\,\kappa_q\,\frac{3m_q}{2m_V}\,\frac{1-r_Z^2+2r_Z\log r_Z}{(1-r_Z)^2}\,, \\ \widetilde{F}_{\perp,\text{direct}}^{VZ} &= \sum_q f_V^{q\perp} v_q\,\tilde{\kappa}_q\,\frac{3m_q}{2m_V}\,\frac{1-r_Z^2+2r_Z\log r_Z}{(1-r_Z)^2}\,. \end{aligned} \tag{5.55}$$

While these form factor are parametrically of the same order as the indirect one, they happens to be numerically small.

5.3.3. Numerical Evaluation of the Form Factors

We now present the numerical results for the form factors to demonstrate their dependence on the various coupling parameters in the Lagrangian (5.2). For pseudoscalar mesons we find :

$$\begin{aligned} F^{\pi^0 Z} &\approx 46.1\,\kappa_Z\ \text{MeV}\,, \\ F^{\eta Z} &\approx 27.7\,\kappa_Z\ \text{MeV}\,, \\ F^{\eta' Z} &\approx -33.8\,\kappa_Z\ \text{MeV}\,. \end{aligned} \tag{5.56}$$

Numerically, only the indirect contributions are relevant. The direct contributions are numerically suppressed by roughly seven orders of magnitude and can thus be ignored to excellent precision. For vector mesons, the direct contributions are mostly negligible, as well. However, several of the κ_i parameters enter through the photon-pole graph:

$$\begin{aligned} F_\parallel^{\rho^0 Z} &\approx 41.11\,\kappa_Z - 0.98 + 0.41\,\kappa_{\gamma Z}^{\text{eff}}\,, \\ F_\perp^{\rho^0 Z} &\approx -2640 + 1102\,\kappa_{\gamma Z}^{\text{eff}} + 41.11\,\kappa_Z + 0.018\,\kappa_d + 0.005\,\kappa_u\,, \\ F_\parallel^{\omega Z} &\approx -7.14\,\kappa_Z - 0.29 + 0.12\,\kappa_{\gamma Z}^{\text{eff}}\,, \\ F_\perp^{\omega Z} &\approx -775.4 + 323.7\,\kappa_{\gamma Z}^{\text{eff}} - 7.14\,\kappa_Z + 0.032\,\kappa_s - 0.014\,\kappa_d + 0.004\,\kappa_u\,, \\ F_\parallel^{\phi Z} &\approx -40.41\,\kappa_Z + 0.48 - 0.20\,\kappa_{\gamma Z}^{\text{eff}}\,, \\ F_\perp^{\phi Z} &\approx 744.1 - 310.7\,\kappa_{\gamma Z}^{\text{eff}} - 40.41\,\kappa_Z - 0.43\,\kappa_s - 0.0007\,\kappa_d + 0.0002\,\kappa_u\,, \end{aligned}$$

$$\begin{aligned}
F_{\parallel}^{J/\psi\, Z} &\approx 38.69\,\kappa_Z - 1.75 + 0.73\,\kappa_{\gamma Z}^{\text{eff}}\,, \\
F_{\perp}^{J/\psi\, Z} &\approx -294.8 + 123.1\,\kappa_{\gamma Z}^{\text{eff}} + 38.69\,\kappa_Z + 1.95\,\kappa_c\,, \\
F_{\parallel}^{\Upsilon(1S)\, Z} &\approx -119.63\,\kappa_Z + 1.52 - 0.64\,\kappa_{\gamma Z}^{\text{eff}}\,, \\
F_{\perp}^{\Upsilon(1S)\, Z} &\approx 26.83 - 11.20\,\kappa_{\gamma Z}^{\text{eff}} - 119.62\,\kappa_Z - 10.47\,\kappa_b\,.
\end{aligned} \tag{5.57}$$

The results for the CP-odd form factors $\tilde{F}_{\perp}^{VZ}$ are obtained from $F_{\perp}^{VZ}$ by omitting the constant terms, and setting $\kappa_Z \to 0$ and $\kappa_{\gamma Z}^{\text{eff}} \to \tilde{\kappa}_{\gamma Z}^{\text{eff}}$ and $\kappa_q \to \tilde{\kappa}_q$. In these results, terms proportional to κ_Z come from the third graph in Fig. 5.10, whereas constant terms and terms proportional to $\kappa_{\gamma Z}^{\text{eff}}$ arise from the photon-pole graph. Direct contributions from the quark Yukawa couplings are displayed in cases where they are numerically significant. Even in the $\Upsilon(nS)$ channels, they enter with relatively small coefficients.

5.3.4. Standard Model Results

The branching ratios within the SM are computed by normalizing the expressions in eq. (5.48) to the total Higgs width $\Gamma_h = (4.08 \pm 0.16)$ MeV [144]. The numerical results are presented in Tab. 5.2, with dominant uncertainties stemming from the meson decay constants and the theory estimate for the Higgs width. The branching ratios range from $6 \cdot 10^{-7}$ for the decay $h \to \omega Z$ up to $1.5 \cdot 10^{-5}$ for the decay $h \to \Upsilon(1S)\, Z$.

Since some of the modes have been considered in the literature, it is worthwhile to compare the results. Ref. [121] reported the branching ratios (in units of 10^{-6}) $\text{Br}(\pi^0 Z) = 3.0$, $\text{Br}(\phi Z) = 2.2$, $\text{Br}(\rho^0 Z) = 1.2$ and $\text{Br}(J/\psi\, Z) = 2.2$, while the authors of ref. [148] obtained $\text{Br}(J/\psi\, Z) = 1.7$ and $\text{Br}(\Upsilon(1S)\, Z) = 16$. In these papers the indirect contributions to the $h \to VZ$ modes involving the $h\gamma Z$ vertex have not been taken into account. As a result, the rate for $h \to \rho^0 Z$ decay in particular is much too small. In ref. [123], the branching ratios $\text{Br}(J/\psi\, Z) = 3.2$ and $\text{Br}(\Upsilon(1S)\, Z) = 17$ were presented, whereas the authors of ref. [124] found $\text{Br}(J/\psi\, Z) = 3.6$ and $\text{Br}(\Upsilon(1S)\, Z) = 22$. While we find a negative sign for the interference term between the third and fourth graph in Fig. 5.10, these two studies report a positive sign, explaining their higher branching ratios.

5.3.5. Sensitivity to New Physics

Recall that in the case of $h \to V\gamma$, we found an interesting dependence on the Yukawa couplings of the valence quarks in some cases. The weak decays $h \to MZ$ do not exhibit this property. Instead, the leading terms are proportional to κ_Z, $\kappa_{\gamma Z}^{\text{eff}}$ and $\tilde{\kappa}_{\gamma Z}^{\text{eff}}$. Since κ_Z is tightly constrained to being close to 1 by LHC data [150], the only viable application is a search for NP in the effective $h\gamma Z$ vertex. Note that

Decay mode	Branching ratio $[10^{-6}]$	Decay constant [MeV]
$h \to \pi^0 Z$	$2.30 \pm 0.01_f \pm 0.09_{\Gamma_h}$	130.4 ± 0.2
$h \to \eta Z$	$0.83 \pm 0.08_f \pm 0.03_{\Gamma_h}$	$f_\eta^s = -110.7 \pm 5.5$
$h \to \eta' Z$	$1.24 \pm 0.12_f \pm 0.05_{\Gamma_h}$	$f_{\eta'}^s = 135.2 \pm 6.4$
$h \to \rho^0 Z$	$7.19 \pm 0.09_f \pm 0.28_{\Gamma_h}$	216.3 ± 1.3
$h \to \omega Z$	$0.56 \pm 0.01_f \pm 0.02_{\Gamma_h}$	$f_\omega = 194.2 \pm 2.1\,, \quad f_\omega^s = -13.8 \pm 4.8$
$h \to \phi Z$	$2.42 \pm 0.05_f \pm 0.09_{\Gamma_h}$	$f_\phi = 223.0 \pm 1.4\,, \quad f_\phi^s = 230.4 \pm 2.6$
$h \to J/\psi\, Z$	$2.30 \pm 0.06_f \pm 0.09_{\Gamma_h}$	403.3 ± 5.1
$h \to \Upsilon(1S)\, Z$	$15.38 \pm 0.21_f \pm 0.60_{\Gamma_h}$	684.4 ± 4.6
$h \to \Upsilon(2S)\, Z$	$7.50 \pm 0.14_f \pm 0.29_{\Gamma_h}$	475.8 ± 4.3
$h \to \Upsilon(3S)\, Z$	$5.63 \pm 0.10_f \pm 0.22_{\Gamma_h}$	411.3 ± 3.7

Tab. 5.2.: SM predictions for the branching ratios of the rare exclusive decays $h \to MZ$ for a variety of pseudoscalar and vector mesons. The decay rates are normalized to the SM prediction for the total Higgs width. The quoted errors show the uncertainties related to the decay constants and the total width.

the pseudoscalar modes depend solely on κ_Z and are thus highly model-independent predictions.

The four diagrams in Fig. 5.11 demonstrate the values of the various branching ratios when the parameters $\kappa_{\gamma Z}^{\text{eff}}$ and $\tilde{\kappa}_{\gamma Z}^{\text{eff}}$ are varied. For each value of $\kappa_{\gamma Z}^{\text{eff}}$, the branching ratio can take a range of values depending on the respective value of $\tilde{\kappa}_{\gamma Z}^{\text{eff}}$. The lower edge of the region corresponds to $\tilde{\kappa}_{\gamma Z}^{\text{eff}} = 0$, whereas the upper edge corresponds to the maximum value allowed for $\tilde{\kappa}_{\gamma Z}^{\text{eff}}$ according to the bound in eq. (5.52). The black dots denote the SM parameter point $\kappa_{\gamma Z}^{\text{eff}} = \tilde{\kappa}_{\gamma Z}^{\text{eff}} = 0$. We find that the branching ratios can be significantly enhanced or slightly reduced with respect to their SM expectation, see the numbers compiled in Tab. 5.3. While this seems like the $h \to MZ$ channels have the promising potential to probe NP in the $h\gamma Z$ coupling, it should be noted that by the time they are experimentally accessible they will probably also be measurable directly through $h \to \gamma Z$. However, combining the results for $h \to \gamma Z$ and $h \to MZ$ could help to further constrain the parameter space, since $h \to \gamma Z$ only puts one a circular band in the $(\kappa_{\gamma Z}^{\text{eff}}, \tilde{\kappa}_{\gamma Z}^{\text{eff}})$ plane, centered around $(2.395, 0)$. On the other hand, the decay $h \to \Upsilon(1S)Z$ is almost independent of $\tilde{\kappa}_{\gamma Z}^{\text{eff}}$ and probes $\kappa_{\gamma Z}^{\text{eff}}$ directly, as can be appreciated in the fourth diagram in Fig. 5.11.

Before we proceed to the last class of decays, we quickly discuss the possibility of probing flavor-changing Yukawa couplings. In this case, the indirect contributions

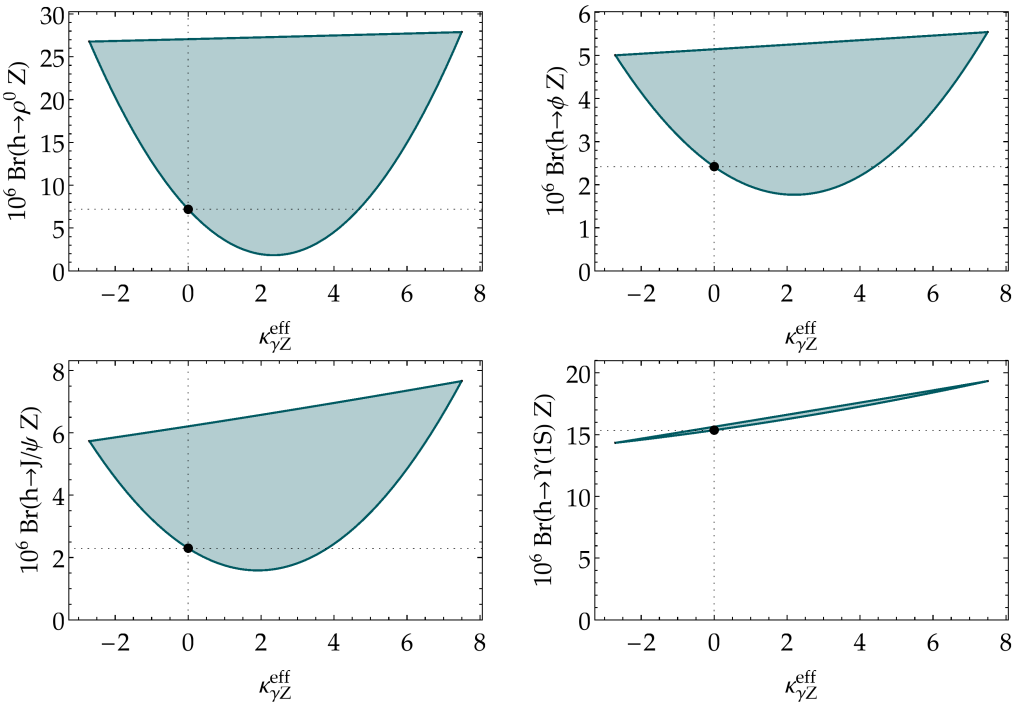

Fig. 5.11.: Allowed regions for four of the $h \to VZ$ branching ratios in the presence of new-physics contributions to the effective $h\gamma Z$ vertices. The parameters $\kappa^{\rm eff}_{\gamma Z}$ and $\tilde\kappa^{\rm eff}_{\gamma Z}$ are varied in the range allowed by the constraint (5.52) derived from the $h \to \gamma Z$ decay rate. The black dots show the SM values.

vanish and the only contribution comes from the generalization of the direct form factors in eq. (5.54). The full expression is for the decay rate is:

$$\Gamma(h \to V_{qq'}Z) = \frac{m_h (f_V^\perp)^2}{64\pi v^2}\, r_Z (1-r_Z)^3 \left\{ \left| \int_0^1 dx \left(H_1^\perp(x) + H_2^\perp(x) \right) \phi_V^\perp(x) \right|^2 + \left| \int_0^1 dx \left(\tilde H_1^\perp(x) + \tilde H_2^\perp(x) \right) \phi_V^\perp(x) \right|^2 \right\}, \tag{5.58}$$

with the various hard scattering kernels:

$$\begin{aligned} H_1^\perp(x) &= \frac{v_q (Y_{qq'} + Y_{q'q}^*) + a_q (Y_{qq'} - Y_{q'q}^*)}{x + r_Z \bar x}, \\ H_2^\perp(x) &= \frac{v_{q'} (Y_{qq'} + Y_{q'q}^*) - a_{q'} (Y_{qq'} - Y_{q'q}^*)}{\bar x + r_Z x}, \end{aligned} \tag{5.59}$$

Decay mode	SM branching ratio $[10^{-6}]$	Range with new physics $[10^{-6}]$
$h \to \rho^0 Z$	7.19 ± 0.29	$1.83 - 53.3$
$h \to \omega Z$	0.56 ± 0.02	$0.06 - 4.56$
$h \to \phi Z$	2.42 ± 0.10	$1.77 - 9.12$
$h \to J/\psi\, Z$	2.30 ± 0.11	$1.59 - 13.1$
$h \to \Upsilon(1S)\, Z$	15.38 ± 0.64	$13.7 - 20.8$

Tab. 5.3.: Allowed ranges for the $h \to VZ$ branching ratios in the presence of new-physics contributions to the effective $h\gamma Z$ vertices. Only central values are shown.

and

$$\begin{aligned} \tilde{H}_1^\perp(x) &= \frac{v_q(Y_{qq'} - Y_{q'q}^*) + a_q(Y_{qq'} + Y_{q'q}^*)}{x + r_Z \bar{x}}\,, \\ \tilde{H}_2^\perp(x) &= \frac{v_{q'}(Y_{qq'} - Y_{q'q}^*) - a_{q'}(Y_{qq'} + Y_{q'q}^*)}{\bar{x} + r_Z x}\,. \end{aligned} \tag{5.60}$$

This result reduces to

$$\Gamma(h \to V_{qq'} Z) = \frac{9 m_h (f_V^\perp)^2}{8\pi v^2}\, v_q^2 \left(|Y_{qq'}|^2 + |Y_{q'q}|^2\right) \frac{r_Z}{(1-r_Z)^3} \left(1 - r_Z^2 + 2 r_Z \ln r_Z\right)^2, \tag{5.61}$$

when the asymptotic form $\phi_V^\perp(x) = 6x(1-x)$ is employed. Flavor-changing Yukawa couplings not involving the top-quark are constrained by neutral meson mixing. The weakest bound is on Y_{bs} and Y_{sb}, extracted from the measurement of $B_s - \bar{B}_s$ mixing. At 95% CL, it is

$$|Y_{bs}|^2 + |Y_{sb}|^2 < 7 \cdot 10^{-6}\,. \tag{5.62}$$

Using a typical estimate for $f_{B_s^*} \approx 0.2$ GeV, we obtain the branching ratio

$$\mathrm{Br}(h \to B_s^* Z) \approx 2.3 \cdot 10^{-11} \times \frac{|Y_{bs}|^2 + |Y_{sb}|^2}{10^{-5}}\,, \tag{5.63}$$

which is too small to observe it at the LHC or any other future machine under consideration. Backgrounds in these channels exist from one-loop electroweak amplitudes. For the specific decay at hand, we estimate the form factors to be of order $F^{B_s^{(*)} Z} \sim \alpha\, |V_{tb} V_{ts}^*| / (4\pi s_W^2)$, which leaves us with branching ratios of order $4 \cdot 10^{-13}$.

5.4. Weak Radiative Charged Current Decays

We now move on to the decays $h \to M^+W^-$. They are interesting by the fact that the final-state meson can be flavor non-diagonal. Just like in the previous cases, we find direct and indirect contributions. In contrast to $h \to MZ$, no photon-pole graph exists and thus the indirect contribution is given exclusively by the tree-level hW^+W^- vertex. The direct contributions once again involve the Yukawa couplings and the charged-current interaction of the W and the quarks. An interesting scenario arises when we allow flavor-changing Yukawa couplings, since the indirect and direct amplitudes can the depend on different CKM matrix elements. Before we explore this possibility, we will discuss the simpler case of flavor-diagonal Yukawa couplings.

5.4.1. Decay Rates for Flavor-Diagonal Higgs Couplings

The decay amplitudes decomposed into form factors are given by

$$i\mathcal{A}(h \to P^+W^-) = \frac{g}{\sqrt{2}v}\, k \cdot \varepsilon_W^*\, F^{MW}\,, \tag{5.64}$$

for pseudoscalar mesons in close analogy to (5.45), and

$$\begin{aligned} i\mathcal{A}(h \to V^+W^-) = -\frac{g m_V}{\sqrt{2}v}\Big[\varepsilon_V^{\parallel *} \cdot \varepsilon_W^{\parallel *}\, F_\parallel^{VW} + \varepsilon_V^{\perp *} \cdot \varepsilon_W^{\perp *}\, F_\perp^{VW} \\ + \frac{\epsilon_{\mu\nu\alpha\beta}\, k^\mu q^\nu \varepsilon_V^{*\alpha} \varepsilon_W^{*\beta}}{\sqrt{(k\cdot q)^2 - k^2 q^2}}\, \widetilde{F}_\perp^{VW}\Big]\,, \end{aligned} \tag{5.65}$$

where we used the longitudinal and transverse polarization vectors, defined in (5.47). With $r_W = m_W^2/m_h^2$ we can write the decay rates as

$$\Gamma(h \to P^+W^-) = \frac{m_h^3}{32\pi v^4}\, \lambda^{3/2}(1, r_W, r_P)\left|F^{MW}\right|^2\,, \tag{5.66}$$

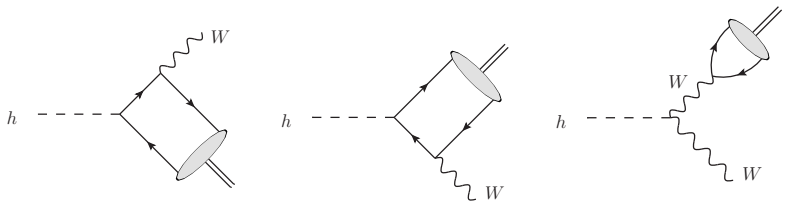

Fig. 5.12.: Leading-order diagrams contributing to the decays $h \to M^+W^-$.

Decay mode	Branching ratio $[10^{-6}]$	Decay constant [MeV]
$h \to \pi^+ W^-$	$4.30 \pm 0.01_f \pm 0.00_{\rm CKM} \pm 0.17_{\Gamma_h}$	130.4 ± 0.2
$h \to \rho^+ W^-$	$10.92 \pm 0.15_f \pm 0.00_{\rm CKM} \pm 0.43_{\Gamma_h}$	207.8 ± 1.4
$h \to K^+ W^-$	$0.33 \pm 0.00_f \pm 0.00_{\rm CKM} \pm 0.01_{\Gamma_h}$	156.2 ± 0.7
$h \to K^{*+} W^-$	$0.56 \pm 0.03_f \pm 0.00_{\rm CKM} \pm 0.02_{\Gamma_h}$	203.2 ± 5.9
$h \to D^+ W^-$	$0.56 \pm 0.03_f \pm 0.04_{\rm CKM} \pm 0.02_{\Gamma_h}$	204.6 ± 5.0
$h \to D^{*+} W^-$	$1.04 \pm 0.12_f \pm 0.07_{\rm CKM} \pm 0.04_{\Gamma_h}$	278 ± 16
$h \to D_s^+ W^-$	$17.12 \pm 0.61_f \pm 0.56_{\rm CKM} \pm 0.67_{\Gamma_h}$	257.5 ± 4.6
$h \to D_s^{*+} W^-$	$25.10 \pm 1.45_f \pm 0.81_{\rm CKM} \pm 0.98_{\Gamma_h}$	311 ± 9
$h \to B^+ W^-$	$(1.54 \pm 0.15_f \pm 0.36_{\rm CKM} \pm 0.06_{\Gamma_h}) \cdot 10^{-4}$	186 ± 9
$h \to B^{*+} W^-$	$(1.41 \pm 0.10_f \pm 0.34_{\rm CKM} \pm 0.06_{\Gamma_h}) \cdot 10^{-4}$	175 ± 6
$h \to B_c^+ W^-$	$(8.21 \pm 0.57_f \pm 0.52_{\rm CKM} \pm 0.32_{\Gamma_h}) \cdot 10^{-2}$	434 ± 15

Tab. 5.4.: SM predictions for the branching ratios of the rare exclusive decays $h \to M^+ W^-$ for a variety of pseudoscalar and vector mesons. The decay rates are normalized to the SM prediction for the total Higgs width. The quoted errors show the uncertainties related to the decay constants, the relevant CKM matrix elements and the total width.

for pseudoscalar mesons and

$$\begin{aligned}\Gamma(h \to V^+ W^-) = \frac{m_h^3}{32\pi v^4}\, \lambda^{1/2}(1, r_W, r_V)\, (1 - r_W - r_V)^2 \\ \times \left[\left| F_\parallel^{VW} \right|^2 + \frac{8 r_V r_W}{(1 - r_W - r_V)^2} \left(\left| F_\perp^{VW} \right|^2 + \left| \widetilde{F}_\perp^{VW} \right|^2 \right) \right] .\end{aligned} \tag{5.67}$$

Similar to the results (5.49), the indirect contributions to the form factors arising from the last diagram in Fig. 5.12 are

$$F_{\rm indirect}^{PW} = \kappa_W f_P V_{ij} \,, \quad F_{\parallel\,\rm indirect}^{VW} = F_{\perp\,\rm indirect}^{VW} = \frac{\kappa_W f_V V_{ij}}{1 - r_V/r_W} \,, \quad \widetilde{F}_{\perp\,\rm indirect}^{VW} = 0 \,, \tag{5.68}$$

where V_{ij} is the relevant CKM matrix element. Just as with the $h \to MZ$ decays, the direct contributions arise from subleading-twist projections and are completely negligible in this case - a fact that will change drastically when we allow flavor-

changing Higgs couplings. The decay rates now take the compact forms:

$$\begin{aligned}\Gamma(h \to P^+W^-) &= \kappa_W^2 \, |V_{ij}|^2 \, \frac{m_h^3 \, f_P^2}{32\pi v^4} \, \lambda^{3/2}(1, r_W, r_P) \,, \\ \Gamma(h \to V^+W^-) &= \kappa_W^2 \, |V_{ij}|^2 \, \frac{m_h^3 \, f_V^2}{32\pi v^4} \, \frac{\lambda^{1/2}(1, r_W, r_V)}{(1 - r_V/r_W)^2} \Big[\lambda(1, r_W, r_V) + 12 r_V r_W\Big] \,.\end{aligned} \tag{5.69}$$

The numerical results for the SM branching ratios are given in Tab. 5.4 along with the relevant uncertainties arising from decay constants, the CKM matrix elements and the Higgs width. Since the only coupling parameter entering our prediction is κ_W, there is no room for NP effects here. Some of the modes have been analyzed in the literature: Ref. [121] obtains the branching ratios (in units of 10^{-6}) $\mathrm{Br}(\pi^+W^-) = 6$, $\mathrm{Br}(\rho^+W^-) = 8$, $\mathrm{Br}(K^+W^-) = 0.4$, $\mathrm{Br}(D^+W^-) = 0.7$, $\mathrm{Br}(D^{*+}W^-) = 1.2$, $\mathrm{Br}(D_s^+W^-) = 21$ and $\mathrm{Br}(D_s^{*+}W^-) = 35$. The results deviate slightly from ours for reasons that we could not trace.

5.4.2. Effects of Flavor-Changing Higgs Couplings

When we allow flavor-changing Higgs couplings, the structure of our results changes due to the possible interplay of the Higgs and W couplings: The intermediate quarks in the direct amplitudes can now be top quarks, lifting the m_q suppression we previously found. In these direct amplitudes with a final-state meson M_{ij}, the relevant CKM matrix will always be $V_{t(i/j)}$. The relevant Yukawa couplings are then $Y_{t(j/i)}$. The indirect amplitude however will simply contain V_{ij}. It is then possible to have cases where the indirect amplitude is heavily CKM-suppressed whereas the direct amplitude is enhanced by the top-quark mass and thus it is possible to probe the corresponding Yukawa coupling.

Ignoring terms not enhanced by m_t, we find the form factors for pseudoscalar and longitudinal vector mesons to be:

$$F^{MW}_{\text{direct}} = \frac{v}{2\sqrt{2}} \, \frac{f_M \, m_t}{m_h^2} \, Y_{it} \, V_{tj} \int_0^1 dx \, \frac{\phi_M(x)}{r_t - \bar{x} - r_W x} \,, \tag{5.70}$$

with $r_t = m_t^2/m_h^2$. For transversely polarized vector mesons, we find

$$\begin{aligned}F^{VW}_{\perp\,\text{direct}} &= -\frac{v}{4\sqrt{2}} \, \frac{f_V^\perp}{m_V} \, (1 - r_W) \int_0^1 dx \, \phi_V^\perp(x) \sum_k \left(\frac{(Y_u)^*_{ki} \, V_{kj}}{r_t \, \delta_{k3} - \bar{x} - r_W x} - \frac{V_{ik} \, (Y_d)_{kj}}{x + r_W \bar{x}} \right) \\ &\approx -\frac{v}{4\sqrt{2}} \, \frac{f_V^\perp}{m_V} \, Y^*_{ti} \, V_{tj} \, (1 - r_W) \int_0^1 dx \, \frac{\phi_V^\perp(x)}{r_t - \bar{x} - r_W x} \,,\end{aligned} \tag{5.71}$$

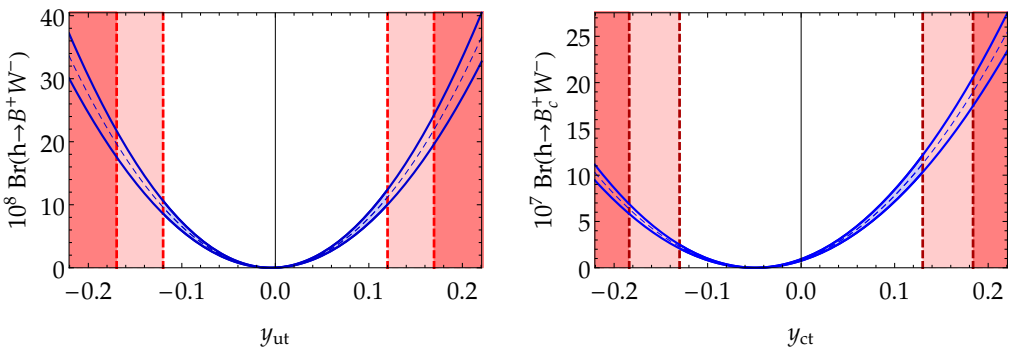

Fig. 5.13.: Predictions for the branching ratios $\mathrm{Br}(h \to B^+W^-)$ (left) and $\mathrm{Br}(h \to B_c^+W^-)$ (right) as functions of $y_{qt} = \mathrm{Re}(Y_{qt})$. The red bands indicate the exclusion bounds from (5.7) when $Y_{tq} = 0$ (dark red) and $|Y_{tq}| = |Y_{qt}|$ (bright red).

and

$$\begin{aligned}\widetilde{F}^{VW}_{\perp\,\mathrm{direct}} &= -i\,\frac{v}{4\sqrt{2}}\,\frac{f_V^\perp}{m_V}\,(1-r_W)\int_0^1 dx\,\phi_V^\perp(x)\sum_k\left(\frac{(Y_u)^*_{ki}\,V_{kj}}{r_t\,\delta_{k3}-\bar{x}-r_W x}+\frac{V_{ik}\,(Y_d)_{kj}}{x+r_W\bar{x}}\right)\\ &\approx -i\,\frac{v}{4\sqrt{2}}\,\frac{f_V^\perp}{m_V}\,Y^*_{ti}\,V_{tj}\,(1-r_W)\int_0^1 dx\,\frac{\phi_V^\perp(x)}{r_t-\bar{x}-r_W x}\,,\end{aligned} \tag{5.72}$$

where in the last step we have only kept the terms involving the top quark. Terms proportional to other quarks are bounded to be small by the constraints reviewed in section 5.1. Although there is no enhancement from m_t in the transverse form factors, there is an enhancement factor of v/m_V, which can potentially boost this form factor into a regime where it becomes numerically relevant.

We find the largest effects to be the channels involving B mesons. Here, the CKM matrix element entering the direct amplitude is $V_{tb} \approx 1$, while the one entering the indirect amplitude is generally small. In a lack of input parameters for the B^* LCDA, we use the LCDA of the B meson as an approximation valid in the heavy-quark limit. Similarly, we use heavy-quark spin symmetry to estimate $f_{B^*}^\perp/f_{B^*} \approx 1$ at the low scale. Setting Yukawa couplings not involving the top quark to zero, we find:

$$\begin{aligned}\mathrm{Br}(h \to B^+W^-) &= 1.54\cdot 10^{-10}\left(\kappa_W^2 + 427\,\kappa_W\,\mathrm{Re}\,Y_{ut} + 45615\,|Y_{ut}|^2\right),\\ \mathrm{Br}(h \to B^{*+}W^-) &= 1.41\cdot 10^{-10}\,(0.98\,\kappa_W^2 + 0.02 + 417\,\kappa_W\,\mathrm{Re}\,Y_{ut} - 27\,\mathrm{Re}\,Y_{tu}\\ &\qquad + 44296\,|Y_{ut}|^2 + 25833\,|Y_{tu}|^2)\,,\\ \mathrm{Br}(h \to B_c^+W^-) &= 8.21\cdot 10^{-8}\left(\kappa_W^2 + 41\,\kappa_W\,\mathrm{Re}\,Y_{ct} + 413\,|Y_{ct}|^2\right).\end{aligned} \tag{5.73}$$

The branching ratio $\mathrm{Br}(h \to B^{*+}W^-)$ has also been computed in ref. [122]. While we agree with their result for the term not involving the off-diagonal Yukawa couplings, we find large deviations in the other terms. Translated into their notation, we find a correction factor $\left[0.98\kappa_W^2 + 0.02 + 7.01\kappa_W \,\mathrm{Re}\,\bar{\kappa}_{ut} - 0.45\,\mathrm{Re}\,\bar{\kappa}_{tu} + 12.53\,|\bar{\kappa}_{ut}|^2 + 5.89\,|\bar{\kappa}_{tu}|^2\right]$ with respect to the SM, where the authors obtain $\left[\kappa_W^2 + 26\,\bar{\kappa}_{ut}^2 + 22\,\bar{\kappa}_{tu}^2\right]$.

Note the dramatic sensitivity of the branching ratios to the Yukawa couplings, leading to potentially strong enhancements. In Fig. 5.13, we demonstrate this dependence under the assumptions that the Yukawa couplings Y_{ij} are real and that all other couplings are SM-like. The bright red band indicates the bound from (5.7) one obtains when $|Y_{tq}| = |Y_{qt}|$, while the dark red band corresponds to the assumption that $Y_{tq} = 0$. In this most extreme scenario, the $h \to B^+W^-$ and $h \to B^{*+}W^-$ branching ratios can be enhanced by up to three orders of magnitude with respect to the SM. The enhancement of the $h \to B_c^+W^-$ branching fraction is less dramatic. Unfortunately, even under the most optimistic assumptions the resulting rates are still predicted to be very small.

We show the full dependence of the ratios $\mathrm{Br}(h \to B_{(c)}^+W^-)$ in the complex plane of Y_{qt} in Fig. 5.14. The results are similar to the purely real case. For $h \to B^+W^-$, the circles representing the bounds on Y_{ut} and the ones representing different values for the branching ratios are almost concentric since the SM piece is strongly suppressed by V_{ub}. For the decay into charmed B mesons, the circles have a very slight offset. We cannot think of a realistic scenario where this could be used as an advantage even if this decay could be observed.

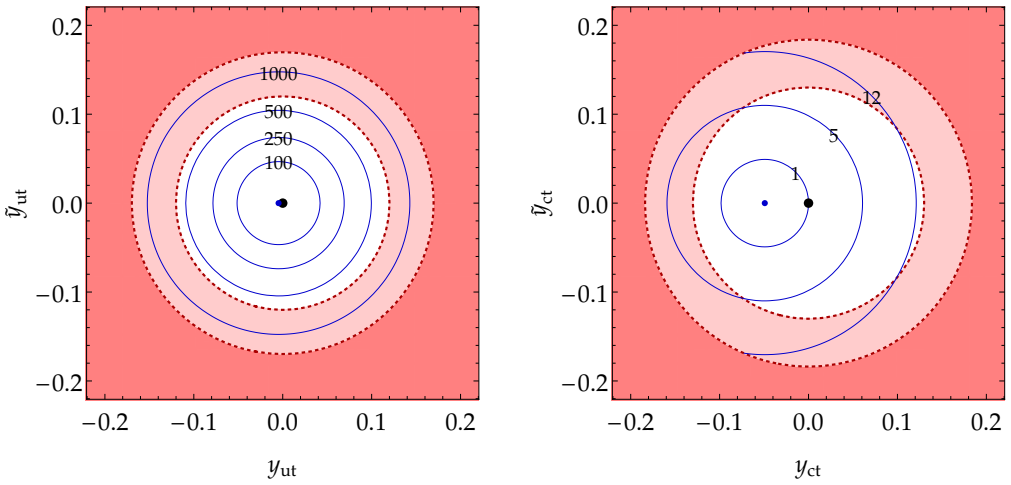

Fig. 5.14.: Enhancement of the branching ratios $\mathrm{Br}(h \to B^+W^-)$ (left) and $\mathrm{Br}(h \to B_c^+W^-)$ (right) over the SM prediction as functions of the couplings $Y_{qt} = y_{qt} + i\tilde{y}_{qt}$. The red shaded regions indicate the exclusion bounds from (5.7) when $Y_{tq} = 0$ (dark red) and $|Y_{tq}| = |Y_{qt}|$ (bright red). The SM value is given by the black dot, while the blue dot denotes the point where the branching ratio vanishes.

6. Renormalization Group Evolution of Neutrino Masses

As a different example of an EFT application, this chapter describes an analysis using renormalization group techniques to evaluate the plausibility of flavor anarchic neutrino mass models. We will first (briefly) review the aspect of neutrino masses and some popular models to generate them beyond the SM. After this, the actual analysis is presented [151].

6.1. Neutrino Oscillations

It is well-established that the elusive neutrinos have non-vanishing, albeit tiny masses. When electron neutrinos are produced in nuclear reactions, their flux can be measured at different distances from the source. When this is done, the measurement shows that neutrinos seem to have "disappeared", as the flux is lower than expected. This was first observed when the neutrino flux produced by the sun was measured [152–154]. These fluctuations can be explained by assigning masses to neutrinos: A neutrino is produced in the flavor eigenstate $|\nu_i\rangle$, which is a superposition of the mass eigenstates. If these mass eigenstates have small masses and small mass differences compared to their kinetic energies, they will propagate with practically identical velocities relative to each other and thus remain in coherence even after traveling long distances, where we can still observe the interference between the different mass eigenstates. As an instructive example, we can go to a two-flavor case with the flavor eigenstates $|\nu_e\rangle$ and $|\nu_\mu\rangle$, related to the mass eigenstates through a basis transformation:

$$\begin{pmatrix} |\nu_e\rangle \\ |\nu_\mu\rangle \end{pmatrix} = \begin{pmatrix} \cos\theta & \sin\theta \\ -\sin\theta & \cos\theta \end{pmatrix} \begin{pmatrix} |\nu_1\rangle \\ |\nu_2\rangle \end{pmatrix}. \tag{6.1}$$

The time-evolution operator in the mass basis is then given by the diagonal matrix

$$[U(t)]_{ii} = \exp\left\{ -\frac{it}{2|\vec{p}|} \left(m_i^2 + 2\vec{p}^{\,2} + \mathcal{O}(m^3/|\vec{p}|^3) \right) \right\}, \tag{6.2}$$

where $\vec{p}$ is the spatial momentum vector of the neutrino mass eigenstate. The oscillation probabilities $P_{a\to b} = |\langle a|b\rangle|^2$ are then given by:

$$\begin{aligned} P_{\nu_e\to\nu_e}(t) &= 1 - \sin^2 2\theta \, \sin^2\left(\frac{L}{4E}(m_2^2 - m_1^2)\right) , \\ P_{\nu_e\to\nu_\mu}(t) &= \sin^2 2\theta \, \sin^2\left(\frac{L}{4E}(m_2^2 - m_1^2)\right) , \end{aligned} \tag{6.3}$$

where L is the distance from the source (or *baseline*) and E is the kinetic energy of the neutrino.

The SM features three generations of leptons and the generalization of the above steps to three flavors of neutrinos is straightforward. The matrix transforming flavor eigenstates into the mass basis is defined in analogy to the CKM matrix with three mixing angles and a CP-phase,

$$\begin{aligned} U_{\text{PMNS}} &= \begin{pmatrix} 1 & 0 & 0 \\ 0 & c_{23} & s_{23} \\ 0 & -s_{23} & c_{23} \end{pmatrix} \begin{pmatrix} c_{13} & 0 & s_{13}e^{-i\delta_{\text{CP}}} \\ 0 & 1 & 0 \\ -s_{13}e^{i\delta_{\text{CP}}} & 0 & c_{13} \end{pmatrix} \begin{pmatrix} c_{12} & s_{12} & 0 \\ -s_{12} & c_{12} & 0 \\ 0 & 0 & 1 \end{pmatrix} \\ &= \begin{pmatrix} c_{12}c_{13} & s_{12}c_{13} & s_{13}e^{-i\delta_{\text{CP}}} \\ -s_{12}c_{23} - c_{12}s_{23}s_{13}e^{i\delta_{\text{CP}}} & c_{12}c_{23} - s_{12}s_{23}s_{13}e^{i\delta_{\text{CP}}} & s_{23}c_{13} \\ s_{12}s_{23} - c_{12}c_{23}s_{13}e^{i\delta_{\text{CP}}} & -c_{12}s_{23} - s_{12}c_{23}s_{13}e^{i\delta_{\text{CP}}} & c_{23}c_{13} \end{pmatrix} , \end{aligned} \tag{6.4}$$

and is called *Pontecorvo-Maki-Nakagawa-Sakata (PMNS) matrix* [155, 156]. We used the standard notation where s_{ij} and c_{ij} are the sine and cosine of the mixing angle θ_{ij} and δ is the CP-phase. In the basis where the charged-lepton mass matrix is diagonal, the PMNS-matrix transitions between the flavor- and mass-bases:

$$\begin{pmatrix} \nu_e \\ \nu_\mu \\ \nu_t \end{pmatrix} = U_{\text{PMNS}} \cdot \begin{pmatrix} \nu_1 \\ \nu_2 \\ \nu_3 \end{pmatrix} . \tag{6.5}$$

It follows that, within the SM, all parameters in the above matrix are unphysical, since the neutrinos are massless and the rotation just leads to a relabeling of the mass-degenerate fields ν_L^i. We can therefore choose $U_{\text{PMNS}} = \mathbf{1}$, which makes lepton-flavor conservation in the SM explicit.

The expressions in eq. (6.3) and the corresponding three-flavor generalization show how to measure the angles θ_{ij}: One uses a neutrino source and measures the flavor composition of the neutrino flux at different baselines L, at obtains the value of $\Delta m_{ij}^2 L/(4E)$ from the oscillation frequency. The amplitude of the oscillation then directly probes the neutrino mixing angle. Of course, this requires that the process of neutrino generation in the source is sufficiently well-understood.

For the values of the oscillation parameters, we will use the results provided in a fit from 2014 [157]. The mass-squared differences $\Delta m_{ij}^2 = \left|m_i^2 - m_j^2\right|$ are

$$\Delta m_{12}^2 = (7.5 \pm 0.2) \cdot 10^{-5}\text{eV}^2\,, \qquad \Delta m_{3l}^2 = (2.5 \pm 0.1) \cdot 10^{-3}\text{eV}^2\,, \tag{6.6}$$

where the index l depends on the mass hierarchy of the neutrinos. In the normal hierarchy (NH), the mass ordering is $m_1 < m_2 \ll m_3$ while in the inverted hierarchy (IH), it is $m_3 \ll m_1 < m_2$. The index l is thus $l = 1$ for normal hierarchy and $l = 2$ for inverted[1]. The mixing angles extracted from the fit are then:

$$\sin^2\theta_{12} = 0.304\,, \qquad \sin^2\theta_{23} = \begin{cases} 0.452 \text{ (NH)} \\ 0.579 \text{ (IH)} \end{cases} \quad \text{and} \qquad \sin^2\theta_{13} = 0.0218\,, \tag{6.7}$$

where the value for θ_{23} also depends on the choice of mass ordering.

6.2. Neutrino Mass Generation

In the SM, neutrinos are massless and no right-handed gauge-singlet fermions exist to form Dirac mass terms. The evidence of neutrinos not being massless is thus a clear indication of physics beyond the SM. An extension to the SM generating neutrino masses must then contain a mechanism to explain the unnaturally small masses. In this work, we focus on the most popular of them, the seesaw mechanism [158, 159], specifically the *type-I seesaw model*. In this model, one supplements the SM with right-handed neutrinos that transform as full singlets under the SM gauge group. They have Majorana masses, which are assumed to be large, since they are not protected by any symmetry. The right-handed neutrinos couple to the SM field content via Yukawa couplings to the left-handed neutrinos. The Lagrangian reads

$$\mathcal{L}_{\text{type-I}} = \mathcal{L}_{SM} - Y_\nu^{ij}\,\bar{N}_R^i\,\tilde{\phi}^\dagger L^j - \frac{1}{2} m_N^{ij}\,\bar{N}^i\left(N^j\right)^c + \text{h.c.}\,, \tag{6.8}$$

where L^i denotes the three left-handed lepton doublets, N_R^i the right-handed neutrinos and $\tilde{\phi} = i\sigma_2\phi^*$ is the conjugate Higgs doublet. At low energies, the heavy neutrinos decouple and can be integrated out. After electroweak symmetry breaking (EWSB) the Lagrangian can be written as

$$\mathcal{L}_{\text{type-I}} \supset -\left(\overline{\nu_L^c},\ \bar{N}_R\right)\begin{pmatrix} 0 & Y_\nu^T v/\sqrt{2} \\ Y_\nu\, v/\sqrt{2} & m_N \end{pmatrix}\begin{pmatrix} \nu_L \\ N_R^c \end{pmatrix}. \tag{6.9}$$

[1] The fit actually yields slightly different values for the mass splittings depending on the hierarchy scenario, see the paper for reference.

When the heavy right-handed neutrinos are integrated out, the left-handed neutrinos obtain effective mass terms:

$$\mathcal{L}^{\text{eff}}_{\text{type-I}} = \mathcal{L}_{\text{SM}} - \frac{1}{2} m_\nu^{ij} \, \overline{(\nu_L^i)^c} \, \nu_L^j + \text{h.c.}\,, \tag{6.10}$$

where the effective mass matrix m_ν is given by the celebrated seesaw formula:

$$m_\nu = -\frac{v^2}{2} \left\{ Y_\nu^T m_N^{-1} Y_\nu + \mathcal{O}\left(\frac{v^2}{m_N^2}\right) \right\}. \tag{6.11}$$

This formula holds at the matching scale where the heavy fields are removed. Since the Majorana mass matrix m_N enters with inverse power, the model naturally accommodates very small neutrino masses. The matrix m_ν is diagonalized by the field transformation $\nu_L^i \to V_\nu^{ij} \nu_L^j$. If we assume the charged-lepton mass matrix to be diagonal, then $V_\nu = U_{\text{PMNS}}$. In a general basis, the charged-lepton mass matrix $m_e = Y_e v/\sqrt{2}$ is diagonalized by $e_L^i \to V_e^{ij} e_L^j$ and the PMNS matrix is given by $U_{\text{PMNS}} = V_e^\dagger V_\nu$. Note that while the mass term for the ν_L fields looks like a dimension-four operator in the broken phase, it is actually of dimension five: In the unbroken phase, it involves two Higgs doublets and is in fact the only dimension-five operator consistent with the gauge symmetries of the SM [160]:

$$\mathcal{L}_{d=5} = \frac{\mathcal{C}_5(\mu)}{\Lambda} \bar{L}^c \tilde{\phi}^* \tilde{\phi}^\dagger L\,. \tag{6.12}$$

The standard seesaw mechanism generates the neutrino masses at tree-level, but there are also models where the neutrino masses are generated radiatively. In these models, the new particles do not need to be as heavy as in the tree-level case, since the masses are naturally loop-suppressed.

In our analysis, we will also consider a variant of the type-I seesaw model, the inverse seesaw model [161, 162] (see also refs. [163–167] for completions giving rise to a model of this kind). In this model, the right-handed neutrinos do not have a Majorana mass matrix but acquire their mass by forming pseudo-Dirac terms together with a second type of singlet fields, called S. The latter have Majorana masses. The Lagrangian is:

$$\mathcal{L}_{\text{ISS}} = \mathcal{L}_{\text{SM}} - (Y_\nu^\dagger)^{ij} \bar{L}^i \tilde{\phi} N_R^j - M_D^{ij} \bar{S}^i (N_R^j)^c - \frac{1}{2} m_S^{ij} \bar{S}^i (S^j)^c + \text{h.c.}\,. \tag{6.13}$$

When n_S generations of S fields and n_N generations of N_R fields are added, the matrices Y_ν, M_D and m_S have the dimensions $n_N \times 3$, $n_S \times n_N$ and $n_S \times n_S$ respectively. After EWSB, the mass Lagrangian is

$$\mathcal{L}_{\text{ISS}} \supset -\begin{pmatrix} \overline{\nu_L^c}, & \bar{N}_R, & \bar{S} \end{pmatrix} \begin{pmatrix} 0 & Y_\nu^T v/\sqrt{2} & 0 \\ Y_\nu v/\sqrt{2} & 0 & M_D^T \\ 0 & M_D & m_S \end{pmatrix} \begin{pmatrix} \nu_L \\ N_R^c \\ S^c \end{pmatrix}. \tag{6.14}$$

The effective Majorana mass matrix for the left-handed neutrinos at the low scale is then:

$$m_\nu = \frac{v^2}{2}\left\{Y_\nu^T M_D^{-1} m_S M_D^{-1} Y_\nu + \mathcal{O}\left(\frac{v^2}{M_D^2}\right)\right\}. \tag{6.15}$$

One finds the correct ranges of masses for the left-handed neutrinos $m_\nu \lesssim \mathcal{O}(\text{eV})$ when $M_D \sim \mathcal{O}(\text{TeV})$ and $m_S \sim \mathcal{O}(\text{keV})$. Comparing this to eq. (6.11) makes apparent that the inverse seesaw model is simply a type-I seesaw model with a specific structure of the mass- and Yukawa-matrices. While the pseudo-Dirac masses m_D are large and the Majorana masses m_S are small, a field redefinition can be performed such that the picture becomes the opposite, with large Majorana masses. Since $n_S \neq n_N$ in general, $(n_S - n_N)$ fields remain light with masses of $\mathcal{O}(m_S \sim \text{keV})$ after this field rotation if there are more generations of S than there are N_R. The residual light fields could act as candidates for keV-mass dark matter.

We will also study one possible completion of the ISS model, where the difference between baryon and lepton number is gauged [164]. The gauge boson of the imposed $U(1)_{B-L}$, which we will call Z', is assumed to have a mass of $\mathcal{O}(100\,\text{TeV})$ after the symmetry is broken. The scalar associated with the breaking of the $U(1)_{B-L}$ will be called χ and its quantum numbers under the extended gauge group $SU(3)_c \times SU(2)_L \times U(1)_Y \times U(1)_{B-L}$ are $(1, 1, 0, -1)$. Like in the previously discussed ISS model, we introduce the fermions S and N_R, where the numbers of generations are n_S and n_N respectively. These new fermions now carry charge under the new gauge group according to Tab. 6.1. In order to ensure anomaly cancellation, we need to add n_S generations of n'_S oppositely charged under the new $U(1)_{B-L}$ with respect to the S fields. We furthermore assume the couplings to the other fields (except the Z') to be forbidden by a discrete symmetry. The details of such a symmetry are not relevant to this analysis and we will ignore S' in the rest of the analysis except for its contribution to the RG evolution of the new gauge coupling. Finally, the Lagrangian is:

$$\begin{aligned}\mathcal{L} \supset -\frac{1}{4} Z'_{\mu\nu} Z'^{\mu\nu} + \sum_\psi i\,\bar{\psi}\not{D}\psi + (D_\mu\chi)(D^\mu\chi)^\dagger \\ - \left[(Y_\nu^\dagger)^{ij}\,\bar{L}_L^i\,\tilde{H}\,N_R^j + \lambda_S^{ij}\,\bar{S}^i\,\chi^\dagger\,(N_R^j)^c + \text{h.c.}\right] \\ + \mu_2\,\chi^\dagger\chi + \lambda_2\,(\chi^\dagger\chi)(H^\dagger H) + \lambda_3\,(\chi^\dagger\chi)^2 + \frac{1}{\Lambda^3}\overline{S^c}\chi^4 S\,,\end{aligned} \tag{6.16}$$

where the sum in the first lines runs over $\psi = N_R, S, S'$ and the covariant derivative acting on the new fields is $D_\mu = \partial_\mu - i g_{B-L} Q_{B-L}\, Z'_\mu$. The dimension-seven term in the last row generates the otherwise forbidden Majorana masses for the S fermions after the scalar χ acquires its vacuum expectation value $\langle\chi\rangle$. After the breaking,

fields	χ	N_R	S	S'	Z'_μ
spin	0	1/2	1/2	1/2	1
Q_{B-L}	-1	-1	+2	-2	0

Tab. 6.1.: The new field content of the inverse seesaw model with gauged $U(1)_{B-L}$. All listed fields are SM singlets. As usual, standard model leptons have $B-L$ charge -1, while quarks have $B-L$ charges of 1/3.

the Z' picks up the mass $m'_Z = \sqrt{2} g_{B-L} \langle\chi\rangle$. Furthermore, the second term in the square brackets becomes a pseudo-Dirac mass term, generating the effective mass mixing between S and N_R.

6.3. Flavor Anarchy

The matrices entering the Lagrangians (6.8), (6.16) and (6.13) determine the flavor structure of the respective model. They are a priori filled with arbitrary complex numbers. One now has the option of either introducing additional flavor symmetries to constrain the structure of these matrices or simply assigning random numbers to them. We pursue the latter option, a scenario called *flavor anarchy* [168, 169]. It is motivated by the idea that the entries could have been chosen similar to a quantum mechanic measurement, at random. It is also a viable assumption for a low-energy theory if the UV completion has a sufficiently complicated structure. The idea of flavor anarchy also exists in the context of other models, not connected to neutrino masses, like sterile neutrinos [170, 171], extra-dimensions [172], grand unified theories [173–175] and string theory [176, 177].

The entries of the matrices are chosen randomly and independently from a statistical distribution. In order not to introduce a preferred basis, the requirement of basis independence is imposed, meaning that the distributions are invariant under unitary field rotations. It has been shown that this requirement implies that the parameters of U_{PMNS} have a flat distribution in the *Haar measure* [169]. For the PMNS-Matrix, it reads:

$$dU_{\text{PMNS}} = d(\sin^2\theta_{12})\, d(\sin^2\theta_{23})\, d(\cos^4\theta_{13})\, d\delta_{\text{CP}}\, d\phi_1\, d\phi_2\, d\delta_e\, d\delta_\mu\, d\delta_\tau\,, \tag{6.17}$$

where we have included the Majorana phases ϕ_1 and ϕ_2 and the unphysical phases δ_l with $l = e, \mu, \tau$ following the convention of [178]. We call a distribution flat in the Haar measure when the parameters $d(\ldots)$ are flat within their physically allowed ranges [179]. To obtain a Haar-flat PMNS matrix, the elements of the neutrino Yukawa coupling matrices need to be drawn from a Gaussian distribution $\propto \exp(-|Y_\nu^{\alpha\beta}|^2)$, while the entries for the Majorana mass matrices of the sterile

neutrinos must be drawn from $\propto \exp(-|M^{\alpha\alpha}|^2/\mathcal{M}^2)$ for the diagonal entries and $\propto \exp(-2|M^{\alpha\beta}|^2/\mathcal{M}^2)$ for the others [180]. The parameter $\mathcal{M}$ sets the absolute mass scale of the right-handed neutrinos.

The knowledge about the Haar measure now allows us to use a statistical test, from which p-values can be assigned to the measured values of the neutrino oscillation parameters [169, 181–183]. In this way, one can quantify the likeliness of a random parameter choice to be close to the ones observed in nature. We employ the multidimensional Kolmogorov-Smirnov (KS) test for this purpose, following refs. [181, 183][2]. The test for a parameter x is defined by:

$$D_{\mathrm{KS}}(x_0) \equiv \sup_{x'} \left|\theta(x' - x_0) - F(x')\right|, \tag{6.18}$$

where x_0 is the observed value, $F(x')$ is the theoretically predicted cumulative distribution function (CDF) and $\theta(x' - x_0)$ is the experimentally observed approximation to the CDF. Since we only have one measurement, it is simply given by a step function. The test statistics function measures maximum the distance between the two CDFs $F(x')$ and $\theta(x' - x_0)$ and provides a measure for the compatibility of the anarchy hypothesis and the measured values. The parameter x in our case is one of the parameters appearing in the Haar measure. Their predicted PDFs are flat, hence $F(x) = x$ and for a single parameter the test statistics function reduces to

$$D_{\mathrm{KS}}(x_0) = \frac{1}{2} + \left|\frac{1}{2} - x_0\right| . \tag{6.19}$$

The p-value, defined by

$$p_{\mathrm{KS}}(x_0) = 2[1 - D_{\mathrm{KS}}(x_0)] = 1 - |1 - 2x_0| , \tag{6.20}$$

then gives the probability to find a randomly drawn value x' for which the test statistics is $D_{\mathrm{KS}}(x') \geq D_{\mathrm{KS}}(x_0)$. Simply put, it measures the likeliness of x_0 being the result of a random draw from the underlying distribution. Small values thus mean that data does not support the hypothesis. Since the anarchy hypothesis makes statements about more than just one parameter, we need to test the likeliness of all mixing parameters to be the result of a random draw. We define the probability as:

$$P_{\mathrm{KS}} \equiv \int_0^1 ds_{12}^2\, ds_{23}^2\, dc_{13}^4\, \theta\left[p_{\mathrm{KS}}(s_{12}^{2,\mathrm{obs}})\, p_{\mathrm{KS}}(s_{23}^{2,\mathrm{obs}})\, p_{\mathrm{KS}}(c_{13}^{4,\mathrm{obs}})\right.$$
$$\left. - p_{\mathrm{KS}}(s_{12}^2)\, p_{\mathrm{KS}}(s_{23}^2)\, p_{\mathrm{KS}}(c_{13}^4)\right] , \tag{6.21}$$

[2] In the publication corresponding to this chapter, we also explore other statistical tests. Since this was work mainly done by my collaborators and does not significantly add to the discussion, it is skipped here [151].

where we do not include unphysical phases for obvious reasons and δ_{CP} because no conclusive measurement has been achieved. Since the parameters are statistically independent, the generalization to the case including it is straightforward. The observed values for the mixing parameters (6.7) depend on the mass ordering, therefore we have to define a hierarchy-weighted probability of the data under the anarchy hypothesis:

$$\tilde{P}_{\mathrm{KS}} = p_{\mathrm{NH}}\, P_{\mathrm{KS,NH}} + p_{\mathrm{IH}}\, P_{\mathrm{KS,IH}}\,, \tag{6.22}$$

where for the weight factors we use the estimates $p_{\mathrm{NH}} \sim 0.95$ and $p_{\mathrm{IH}} \sim 0.0.5$ from numerically sampling a large number of parameter points. We find:

$$\tilde{P}_{\mathrm{KS}} = 0.411\,, \tag{6.23}$$

meaning that in 41.1% of random draws, we obtain a set of parameters that fit the anarchy hypothesis worse than the observed ones. This is of course less than 50%, but given that we only have one real data point to compare to, we can still conclude that anarchy is a viable hypothesis.

6.4. Renormalization Group Evolution and Anarchy

The neutrino oscillation parameters are functions of the Yukawa couplings and mass terms in the Lagrangian of the theory. As such, they are subject to renormalization group running. It is reasonable to assume that the random drawing of the parameters is associated to a very high energy scale. For the statistical test of anarchy this means that we are comparing parameters observed at low energies to a distribution predicted at high energies. Therefore, in order to obtain consistent p-values for the anarchy hypothesis, we need to connect the observed values and the predicted distributions using the renormalization group. In this work we will assume that the parameters are drawn at a scale $M_{\mathrm{GUT}} \sim 10^{16}$ GeV, motivated by grand unification theories, although the choice is ad-hoc.

In the following, we will be looking at the RG running of oscillation parameters in three different variants of type-I seesaw models, discussed in Sec. 6.2. Our general procedure is as follows: For a given model, we generate a large number of randomly drawn parameter points. Each parameter point is then RG evolved down to the electroweak scale using the appropriate RG equations. At the low scale, we then extract the distributions of the parameters from a polynomial fit and perform the KS test with the RG-improved distributions. In a sense, the final goal is to compute the RG running of the test parameter $\tilde{P}_{\mathrm{KS}}$.

6.4.1. The Technical Aspect

While conceptionally easy enough, the analysis is technically involved, because the different entries of the mass and Yukawa matrices all mix under renormalization. An exact analytical solution of the RG equations is not feasible. We thus carry out the analysis purely using numerical methods. Although for some models, programs exist and are discussed in the literature, we found that they have several technical shortcomings forcing us to develop our own implementation[3].

In our numerical implementation, the quantities that are evolved to the low scale are the entries of the mass and coupling matrices in the models. In order to correctly remove heavy particles from the effective theory, we need to keep track of the mass eigenvalues to obtain the correct matching scales. To find these matching scales, we look for the scale μ_i, at which the highest mass eigenvalue in the mass matrix M_i is equal to the renormalization scale $\mu_i = M_i$. At this scale, the theory is transformed into the mass basis. By definition no mass-mixing terms are present in this basis and thus we can simply drop the row and column associated with the heaviest field. Therefore, at each matching scale, the number of running parameters decreases. After removing the last heavy neutrino from the theory, the neutrino mass matrix will be a 3×3 complex symmetric matrix, that we evolve to the weak scale $m_Z = 91.19$ GeV and extract the oscillation parameters for the statistical analysis.

In order to numerically find the thresholds, one could simply scan across the scales covered by the RG running and look for the scales that satisfy the requirement $\mu_i = M_i$. In practice this turns out to be rather slow since the mass matrix needs to be diagonalized at every point. To approximate the procedure, we first estimate the thresholds from the input parameters at the high scale and apply a correction factor κ_M to them. We typically use $\kappa_M = 0.9$ as a first guess and then refine the parameter each time we find the correct scale. We then use the numerical solutions to the RG equations to sample the mass eigenvalues at $\mathcal{O}(10)$ chosen values for the scales around the guessed value and fit it to a function of the form

$$M_{\text{fit}}(\mu) = a_0 + a_{1/2}\sqrt{\mu} + a_1\mu + a_l \log(\mu)\,. \tag{6.24}$$

After this is done, the matching scale is extracted from equating $M_{\text{fit}}(\mu) = \mu$. We find excellent agreement between this methods and the scanning one, with the important difference of the fit method being computationally much cheaper, making the numerical analysis a lot faster.

After each parameter point is evolved to the low scale, we obtain distributions of the mixing parameters, that we fit using cubic polynomials $p(x)$. In order to apply the KS test, it is important that the parameters are statistically independent. This

[3] One example of an existing implementation is the `REAP` package [184]. While it was not feasible to use the package for the actual analysis, it still provided numerous cross-checks for our implementation.

check is performed numerically by extracting the Pearson correlation coefficients for the different parameter pairs, defined for two parameters x and y as:

$$\rho_{x,y} = \left| \frac{\langle x \cdot y \rangle}{\langle x \rangle \langle y \rangle} \right| . \tag{6.25}$$

One could imagine the RG evolution to generate correlations between the parameters, as they effectively all mix under renormalization. Fortunately, we find values $\rho_{x,y} \leq 0.02$ for all combinations of parameters and conclude that the parameters are still uncorrelated, as they were at the high scale. In order to reuse the test statistic function in eq. (6.21), we rescale the parameters to obtain flat distributions by rescaling the fit-polynomials such that the integrals over the physical range of each x are $\int_{x_0}^{x_1} dx f(x) = 1$. After this, we define new variables $x' = \int_0^x d\tilde{x} f(\tilde{x})$, in which the distributions are flat by construction. Using these new variables x', we can simply reuse formula (6.21) to obtain the RG-improved test-statistics.

6.4.2. Results for the Type-I Seesaw Model

We can now quote our results for the type-I seesaw models. The Lagrangian is given by 6.8. The renormalization group equations for the type-I seesaw model have been studied in great detail in refs. [184–188]. They are given in Appendix I for reference. To investigate the effect of RG evolution on neutrino anarchy in this model, we have randomly generated 10^5 sets of parameters, defined by the Yukawa matrices Y_ν and the right-handed neutrino mass matrices M. We assume these randomly generated matrices to enter the Lagrangian at the high scale $M_{\rm GUT} = 10^{16}$ GeV. As explained earlier, to ensure basis invariance of the probability distributions and statistical independence of different mass matrix elements, the elements of $Y_\nu^{\alpha\beta}$ must follow a Gaussian distribution $\propto \exp[-|Y_\nu^{\alpha\beta}|^2/\mathcal{Y}]$. The diagonal elements $M^{\alpha\alpha}$ of the right-handed Majorana mass matrix follow a similar distribution $\propto \exp[-|M^{\alpha\alpha}|^2/\mathcal{M}]$, while the distribution of the off-diagonal elements $M^{\alpha\beta}$ is $\propto \exp[-2|M^{\alpha\beta}|^2/\mathcal{M}]$. Here $\mathcal{Y}$ is a dimensionless parameter which we choose to be one, while $\mathcal{M}$ is dimensionful, and we choose $\mathcal{M} = 10^{14}$ GeV to reproduce the correct order of magnitude for the light neutrino masses. We will shortly discuss the effects of varying $\mathcal{M}$ after presenting the results.

For the parameters of the standard model at the high scale we have chosen a set of values used by the `REAP` package [184]:

$$Y_u(M_{\rm GUT}) = \begin{pmatrix} 5.4039 \cdot 10^{-6} & 0 & 0 \\ 0 & 1.5637 \cdot 10^{-3} & 0 \\ 0 & 0 & 0.4829 \end{pmatrix} ,$$

$$Y_d(M_{\rm GUT}) = 10^{-5} \times \begin{pmatrix} 2.1176 & 4.5697 + 0.0112i & 2.1367 + 0.2581i \\ 4.5697 - 0.0112i & 22.3698 & 25.7097 - 0.0019i \\ 2.1367 - 0.2571i & 25.7097 + 0.0019i & 614.0010 \end{pmatrix} ,$$

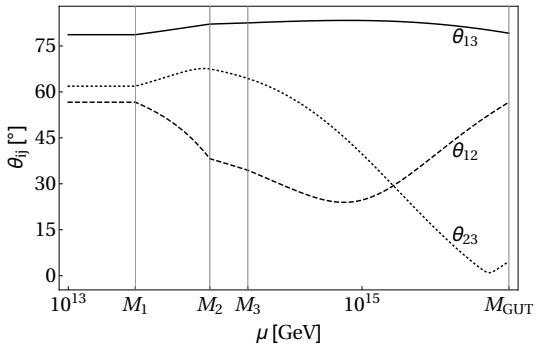

Fig. 6.1.: A parameter point of the type-I seesaw model with large running effects in the neutrino mixing angles. The vertical dotted lines show the decoupling thresholds of the heavy singlet neutrinos, $M_1 = 2.9 \cdot 10^{13}$ GeV, $M_2 = 9.2 \cdot 10^{13}$ GeV and $M_3 = 1.67 \cdot 10^{14}$ GeV . Note how RG running ceases after the last heavy neutrino is integrated out. The masses of the active neutrinos at the low scale are $m_1 = 0.02$ eV, $m_2 = 0.32$ eV and $m_3 = 0.36$ eV.

$$Y_e(M_{\rm GUT}) = \begin{pmatrix} 2.8370 \cdot 10^{-6} & 0 & 0 \\ 0 & 0.5988 \cdot 10^{-3} & 0 \\ 0 & 0 & 10.1789 \cdot 10^{-3} \end{pmatrix} . \tag{6.26}$$

Of course the exact low-scale values of the quark and charged lepton Yukawa matrices depend on the additional field content beyond the SM and on the values of the new parameters introduced. Therefore, we typically cannot reproduce the SM Yukawa couplings exactly, with deviations being of order 10%. Nevertheless, since our interest here is in the running of the neutrino masses and mixing parameters, these small deviations are negligible for our purposes.

We evolve each parameter point down to the electroweak scale, which we represent by $m_Z = 91.19$ GeV. In principle, we should evolve the mixing parameters down to an even lower scale, integrating out SM particles at their respective thresholds. However, as we will see, the running of the mixing parameters dominantly happens at scales $\gg m_Z$ and thus it is justified to stop the RG evolution at m_Z. Both at $M_{\rm GUT}$ and at m_Z, we extract the values of the physical mixing parameters by diagonalizing the mass matrices and using the prescriptions given in Appendix A of ref. [178]. When diagonalizing m_ν, we have to specify a convention for the ordering of the mass eigenvalues. We choose them to be in ascending order (corresponding to scenario called A3 in section II.B of ref. [179]). Note that we should in principle decouple the Higgs boson and the top quark below their threshold scale, which has non-negligible effects on the running of the neutrino mass eigenvalues [189]. It does however not affect the mixing parameters and phases, so we neglect these effects (see

e.g. Fig. 6.1).

We show the distributions of the mixing parameters θ_{ij}, δ_{CP} and the Majorana phases ϕ_1 and ϕ_2 in Fig. 6.2. By construction, the distributions are flat at the high scale up to statistical fluctuations. At the low scale, we find a slight bias for smaller mixing angles. This can also be seen in the distributions of the RG-induced shifts $\Delta x = x(m_Z) - x(M_{\mathrm{GUT}})$, shown in Fig. 6.3. Included in the graphics are also plots of Gaussian fits

$$f(x) = \frac{1}{\sqrt{2\pi}\sigma(x)} \exp\left[-\frac{(x-\overline{x})^2}{2[\sigma(x)]^2} \right], \tag{6.27}$$

to the distributions, along with their central values $\overline{x}$ and the widths $\sigma(x)$. We find a slight preference for the mixing angles to decrease by 1 - 2° after running them to m_Z. The distributions of $\Delta\theta_{ij}$ are all peaked at small negative values. The Dirac CP phases δ_{CP} in Fig. 6.2 (d) show a slight preference to be close to zero after running, while the distributions of the Majorana phases ϕ_1 and ϕ_2 in Fig. 6.2 (e), (f) stay flat both after running them from M_{GUT} to m_Z. Note that these distributions can only make statements about the average behavior of large samples of parameter points. Individual points can exhibit much stronger running effects. It is known that points with at least two neutrino masses being close to each other can potentially have very pronounced RG running for he mixing angles [184].

The parameter point on which the graphs in Fig. 6.1 are based is an example of such a point. We observe that even points showing significant RG running, only do so at scales above the masses of the heavy singlet neutrinos. Whenever a heavy neutrino is removed from the theory, we find the running of angles and phases to grow weaker, stopping completely after the last heavy neutrino has been integrated out. From this we can deduce how the choice of the heavy neutrino mass scale $\mathcal{M}$ affects the RG evolution of the mixing parameters: For larger values of $\mathcal{M}$ heavy neutrinos are removed from the theory at a higher scale, stopping the running of the mixing parameters sooner. Consequently, for larger values of $\mathcal{M}$, the running is less pronounced and vice versa. We have confirmed this behavior in a numerical study.

While it seems peculiar that the angles have a preferred direction of running, a simple explanation exists. The leptonic mixing matrix depends on the matrix V_ν that diagonalizes m_ν as well as on the matrix V_e that diagonalizes $Y_e^\dagger Y_e$ according to $V_e Y_e^\dagger Y_e V_e^\dagger = D$, where D is diagonal. The flavor non-trivial terms in the beta functions for the mass and Yukawa matrices (see App. I) are dominated by the $\mathcal{O}(1)$ terms containing Y_ν, subdominant terms involving Y_e are negligible. Recall that Y_ν is randomly chosen and hence cannot lead to a preference for the direction of the running. The only possible source of such a preference can come from the lepton Yukawa matrices Y_e, for which the beta function is dominated by

$$16\pi^2 \beta_{Y_e} = -\frac{3}{2} Y_e (Y_\nu^\dagger Y_\nu) + \dots . \tag{6.28}$$

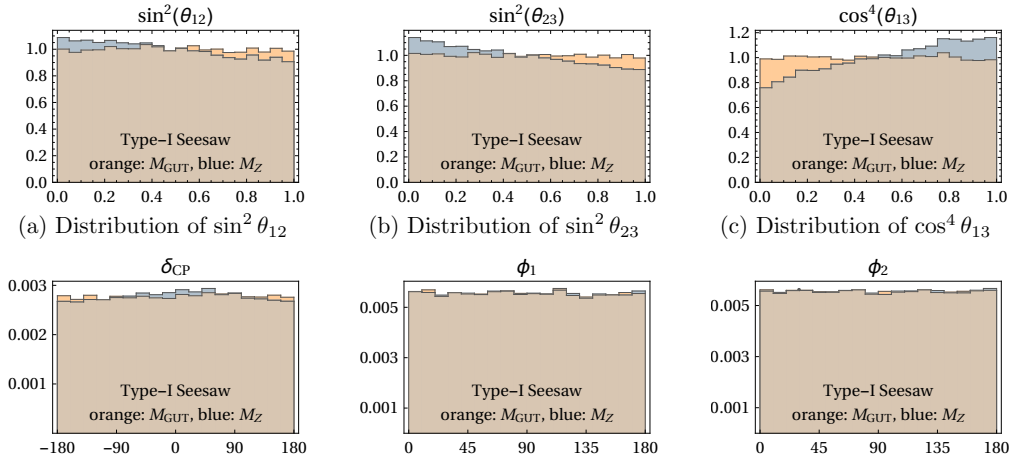

(a) Distribution of $\sin^2\theta_{12}$ (b) Distribution of $\sin^2\theta_{23}$ (c) Distribution of $\cos^4\theta_{13}$

(d) Distribution of $\delta_{\rm CP}$ [°] (e) Distribution of ϕ_1 [°] (f) Distribution of ϕ_2 [°]

Fig. 6.2.: Distributions of the three mixing angles, the Dirac CP phase $\delta_{\rm CP}$ and the two Majorana CP phases ϕ_1 and ϕ_2 before and after renormalization group running in the type-I seesaw model. Orange regions correspond to parameters at $M_{\rm GUT}$, blue regions to parameters at m_Z. Note that the physical range for $\delta_{\rm CP}$ is $[-180°, 180°)$, while the physical ranges for ϕ_1 and ϕ_2 are only $[0, 180°)$ [179].

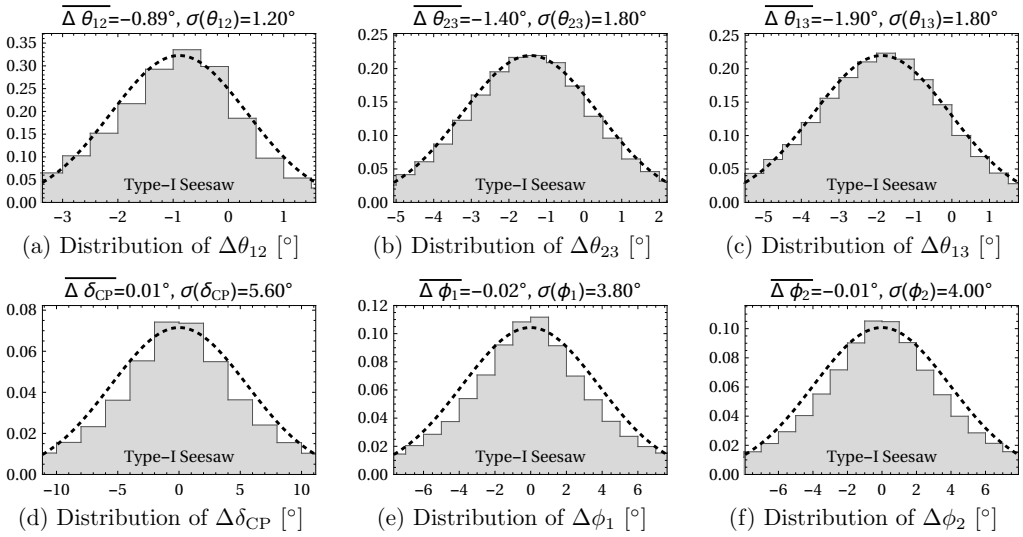

(a) Distribution of $\Delta\theta_{12}$ [°] (b) Distribution of $\Delta\theta_{23}$ [°] (c) Distribution of $\Delta\theta_{13}$ [°]

(d) Distribution of $\Delta\delta_{\rm CP}$ [°] (e) Distribution of $\Delta\phi_1$ [°] (f) Distribution of $\Delta\phi_2$ [°]

Fig. 6.3.: Distributions of the RG-induced shifts in the mixing parameters, $\Delta x \equiv x(m_Z) - x(M_{\rm GUT})$ in the type-I seesaw model. Also shown are the central values $\overline{\Delta x}$ and the widths $\sigma(x)$ of Gaussian fits to the distributions.

The dots indicate the subdominant and flavor-trivial terms, which we can ignore for the purpose of this argument. The high-scale value of $Y_e(M_{\rm GUT})$ is a diagonal matrix (see eq. (6.26)), with its strongly hierarchical eigenvalues sorted in ascending order. The structure of eq. (6.28) shows that after RG running, the elements in the k-th row of Y_e will change by an amount proportional to the element $Y_e^{kk}(M_{\rm GUT})$. If we consider a two-flavor scenario for simplicity, it can easily be shown that the mixing angle parameterizing V_e is positive. Since V_e enters the PMNS matrix as its hermitian conjugate, $U_{\rm PMNS} = V_e^\dagger V_\nu$ and V_ν cannot introduce any preference, the mixing angle describing $U_{\rm PMNS}$ prefers a negative value. This whole argument only holds for the model in consideration here, since the sign in front of the dominant term in eq. (6.28) can be different. The type-II seesaw model is an example of such a case [190].

Using the test procedure explained in the previous section, we find the RG-improved statistics $\tilde{P}_{\rm KS}^{\rm RG}$ to be:

$$\tilde{P}_{\rm KS}^{\rm RG} = 0.477\,. \tag{6.29}$$

This is a slight improvement over the value obtained without RG effects, which was $\tilde{P}_{\rm KS} = 0.411$. In the next section, we will explore whether the inverse seesaw model exhibits stronger RG effects.

Before we proceed however, we comment on the running of the absolute neutrino masses. We can approximate their RG evolution by $dm/d\log\mu = \gamma m$. Averaging over the generated events, we find a mean value of $\gamma \simeq 0.027$. This implies that the neutrino masses decrease by 60% when evolved from $M_{\rm GUT}$ to m_Z.

6.4.3. Results for the Inverse Seesaw Model

We now demonstrate the results for the inverse seesaw model, discussed in section 6.2. The corresponding RG equations are found in App. I, they agree with the ones given in [191].

The analysis is done in complete analogy to the one for the type-I seesaw model: A sample of 10^5 parameter points is generated and evolved from $M_{\rm GUT} = 10^{16}$ GeV to $m_Z = 91.19$ GeV. The distributions of the oscillation parameters are shown in Fig. 6.4. Qualitatively, our findings are very similar to the type-I seesaw model: Mixing angles preferentially decrease whereas $\delta_{\rm CP}$ slightly peaks around zero. The distributions of Majorana phases are unaffected by the running. In contrast to the type-I model, we find the shifts of the mixing parameters to be larger, with average shifts between -4° and -5.5°. Note also that the widths are significantly larger than in the type-I seesaw model, meaning a larger spread in the magnitude of the running between individual parameter points. We also find a more pronounced running of the neutrino mass eigenvalues, where the approximate anomalous dimension is

0.037, corresponding to an average of 70% decrease when evolved from $M_{\rm GUT}$ to m_Z. Finally, the test-statistics with and without RG evolution yields:

$$\tilde{P}_{\rm KS} = 0.411 \quad \xrightarrow{\rm RGE} \quad \tilde{P}_{\rm KS} = 0.593\,, \tag{6.30}$$

meaning that RG effects significantly improve the support of the anarchy hypothesis.

6.4.4. Results for the Gauged Baryon-Lepton Model

We now proceed with the analysis of the $U(1)_{B-L}$ model to see whether the different structure above the breaking scale, compared to the ISS model, changes the RG evolution of the model. In this model additional parameter choices need to be made other than the random choice of the mass matrix. Furthermore, to make the analysis more feasible, a number of simplifying assumptions are made.

In order to avoid having to deal with the multitude of different effective theories that can arise depending on where $B-L$ is broken relative to the masses of the heavy $\mathcal{O}$(TeV) neutrinos, we always fix the $U(1)_{B-L}$ breaking scale at $f_{B-L} = 100$ TeV, well above the heavy neutrino masses. Moreover, we assume for simplicity that the $B-L$ breaking scale f_{B-L}, the vev $\langle\chi\rangle$, and the mass m_χ of χ are identical, so that we do not need to consider running between these scales. We choose the numerical value of g_{B-L} such that it unifies to the extent possible at the GUT scale with the SM gauge couplings, see 6.6. We find that a reasonable choice is $g_{B-L} = 0.58$ at the GUT scale. By demanding that the running Z' mass parameter $M_{Z'}(\mu) \equiv \sqrt{2} g_{B-L}(\mu)\,\langle\chi\rangle$ equals the scale μ, we find the threshold mass $M_{Z'} \approx 39$ TeV. Since this is sufficiently close to $f_{B-L} = 100$ TeV on a logarithmic scale, we integrate out χ and Z' simultaneously. As a further simplification, we ignore renormalization group effects on the quadratic terms in the scalar potential, and consequently the scale dependence of the scalar vevs. Since the scalar quartic couplings do not affect the flavor structure, their only influence on the neutrino mixing parameter can be indirect, by changing the various mass scales of the theory. Finally, we neglect kinetic mixing between the Z' and the standard model hypercharge gauge boson B, which would be allowed by the symmetries. Kinetic mixing is in general absent at the grand unification scale, where we assume that $U(1)_{B-L}$ emerges from a larger, non-Abelian gauge group. Even though kinetic mixing does get induced in the renormalization group evolution to lower scales at one loop level, its effect on other running parameters is suppressed by two loop factors and therefore negligible compared to other parameters appearing in the RG equations. In the same spirit we will also assume the Higgs portal coupling λ_2 to be strongly suppressed.

With these simplifications, the effective theory valid at scales $\mu < f_{B-L}$ is simply the ISS model. We thus only need to evolve the parameters of the full model from $M_{\rm GUT}$ to f_{B-L} and then feed them into the previously discussed evolution equations

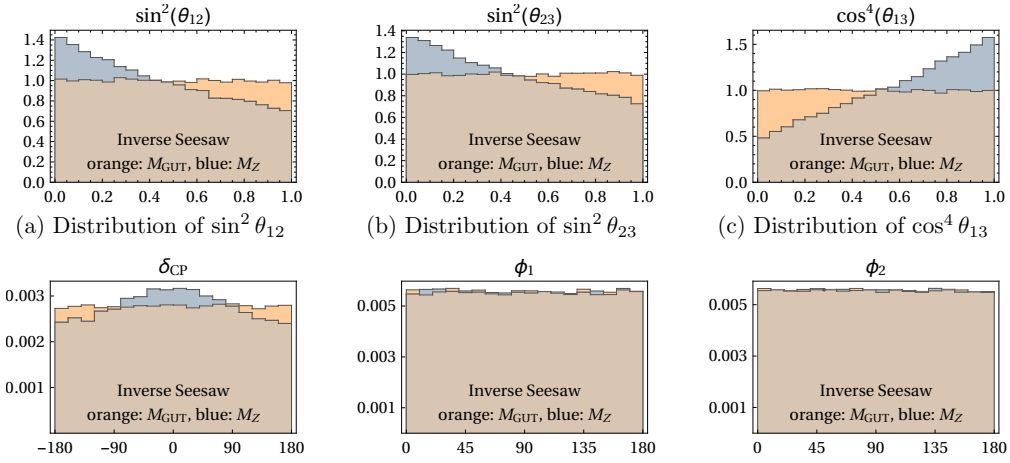

(a) Distribution of $\sin^2\theta_{12}$ (b) Distribution of $\sin^2\theta_{23}$ (c) Distribution of $\cos^4\theta_{13}$

(d) Distribution of δ_{CP} [°] (e) Distribution of ϕ_1 [°] (f) Distribution of ϕ_2 [°]

Fig. 6.4.: Distributions of the mixing angles and physical CP phases before and after renormalization group running in the inverse seesaw model. The orange regions correspond to the parameters at M_{GUT}, the blue regions to the parameters at m_Z. For the mixing angles and the Dirac CP phase, the running is much stronger than in the type-I seesaw case.

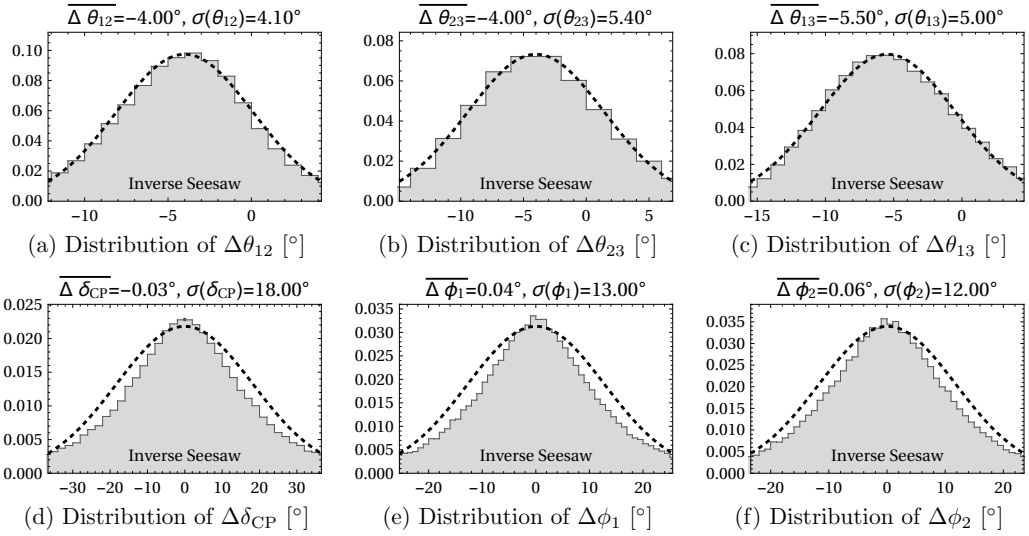

(a) Distribution of $\Delta\theta_{12}$ [°] (b) Distribution of $\Delta\theta_{23}$ [°] (c) Distribution of $\Delta\theta_{13}$ [°]

(d) Distribution of $\Delta\delta_{\mathrm{CP}}$ [°] (e) Distribution of $\Delta\phi_1$ [°] (f) Distribution of $\Delta\phi_2$ [°]

Fig. 6.5.: Shift in the mixing angles and the CP phases during RG evolution form M_{GUT} to m_Z in the inverse seesaw model, obtained from 10^5 randomly generated mass matrices. We use the notation $\Delta x \equiv x(m_Z) - x(M_{\mathrm{GUT}})$, where x stands for any of the mixing angles or complex phases. Also shown are Gaussian fits with central values $\overline{\Delta x}$ and widths $\sigma(\Delta x)$.

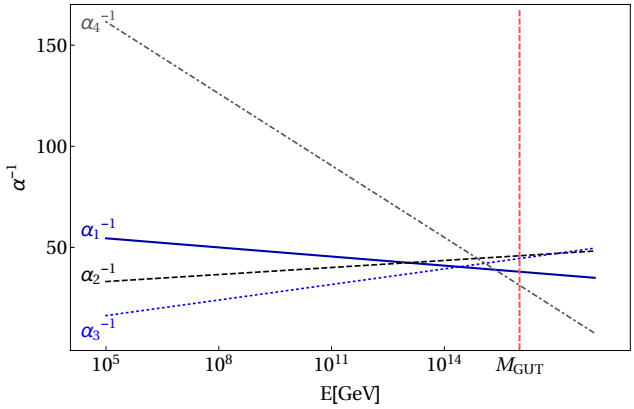

Fig. 6.6.: Running of the fine structure constant α_1 for $U(1)_Y$ (dark blue solid), α_2 for $SU(2)_L$ (black dashed), α_3 for $SU(3)_c$ (blue dotted), and $\alpha_4 \equiv g_{B-L}^2/(4\pi)$ for $U(1)_{B-L}$ (dark gray dot-dashed) in the inverse seesaw model with gauged $U(1)_{B-L}$.

for the phenomenological inverse seesaw model. The renormalization group equations for the inverse seesaw model with gauged $B - L$ are given in App. I.2. While their form is independent of the number of generations of singlet fields introduced, we implement three N_R fields and four S fields, yielding one $\mathcal{O}$(keV) mass-eigenstate as a possible DM candidate.

The distributions of the mixing parameters at different scales are shown in Fig. 6.7, the distributions of the shifts in Fig. 6.8. We find that the distributions look practically identical to the ones from the phenomenological ISS model discussed in the previous section. The RG-improved statistics $\tilde{P}_{\rm KS}^{\rm RG}$ is now

$$\tilde{P}_{\rm KS}^{\rm RG} = 0.604\,, \tag{6.31}$$

which is also an improvement over $\tilde{P}_{\rm KS} = 0.411$, but almost the same value as for the ISS model.

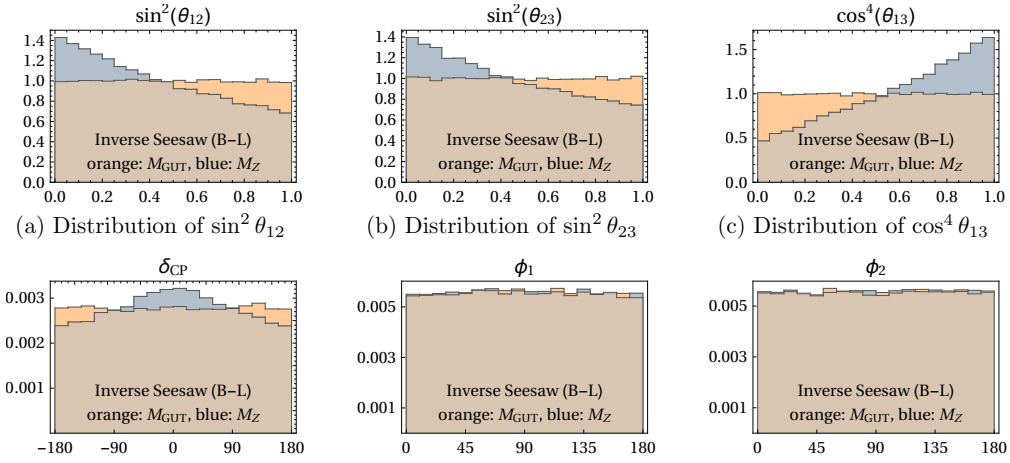

(a) Distribution of $\sin^2\theta_{12}$ (b) Distribution of $\sin^2\theta_{23}$ (c) Distribution of $\cos^4\theta_{13}$

(d) Distribution of δ_{CP} [°] (e) Distribution of ϕ_1 [°] (f) Distribution of ϕ_2 [°]

Fig. 6.7.: Distributions of the mixing angles and physical CP phases before and after renormalization group running in the inverse seesaw model with gauged $B-L$. The orange regions correspond to the parameters at M_{GUT}, the blue regions to the parameters at m_Z. The distributions are practically identical to those in the phenomenological ISS model, see Fig. 6.4.

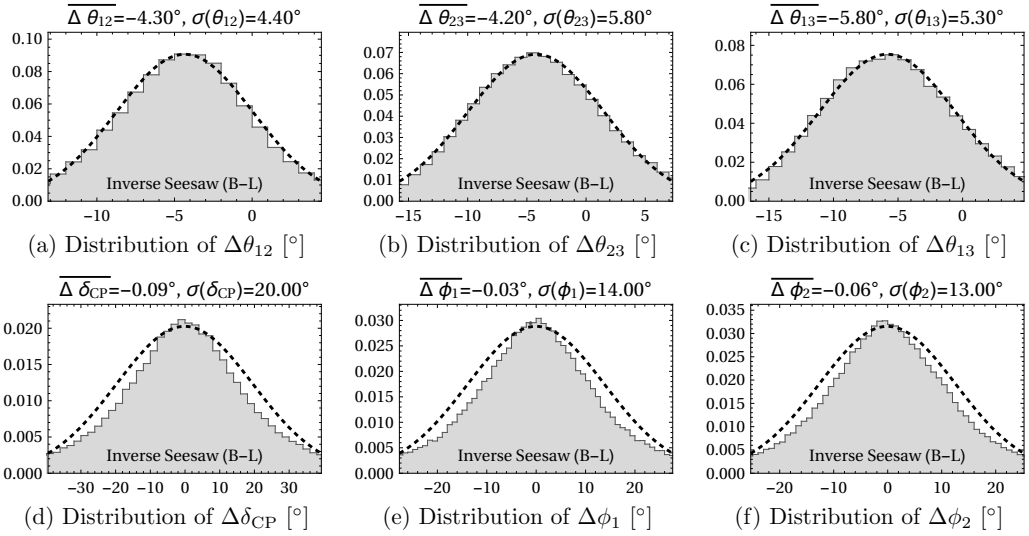

(a) Distribution of $\Delta\theta_{12}$ [°] (b) Distribution of $\Delta\theta_{23}$ [°] (c) Distribution of $\Delta\theta_{13}$ [°]

(d) Distribution of $\Delta\delta_{\mathrm{CP}}$ [°] (e) Distribution of $\Delta\phi_1$ [°] (f) Distribution of $\Delta\phi_2$ [°]

Fig. 6.8.: RG-Shifts $\Delta x \equiv x(M_Z) - x(M_{\mathrm{GUT}})$ in mixing angles and phases in the inverse seesaw model with gauged $B-L$, obtained from 10^5 randomly generated mass matrices. Also shown are Gaussian fits with central values $\overline{\Delta x}$ and widths $\sigma(\Delta x)$. The distributions are practically identical to those in the phenomenological ISS model, see Fig. 6.5.

7. Summary and Conclusions

In this work we have demonstrated several applications of effective field theories. The QCD factorization formula for exclusive hadronic decays was derived using Soft-Collinear Effective Theory. In this framework, the decay amplitude is given as an expansion in the ratio of the two scales in the process, given by the mass of the decaying boson and the scale associated with the non-perturbative effects of hadronization. We have shown that it suffices to keep only the leading term in this expansion and that power corrections are tiny and mostly negligible. The factorization formula separates the amplitudes into hard scattering kernels, that can be computed using perturbation theory, and process-universal non-local hadronic matrix elements called light-cone distribution amplitudes. Using the renormalization group evolution of these quantities, we were able to resum the large QCD logarithms of the scale ratio $\alpha_s \log(\Lambda_{\text{QCD}}/m_B)$, where m_B is the mass of the decaying boson. We have seen that the presence of the huge scale hierarchy greatly suppresses the dependence on the exact shape of the LCDAs, decreasing the hadronic uncertainties entering our predictions for the decay rates. We have included next-to-leading order QCD corrections and carefully accounted for the effects of flavor-singlet admixtures in the final state meson. In this way, the decays $Z \to M\gamma$ and $W \to M\gamma$ are theoretically clean probes of the QCD factorization approach, with the major drawback being the very small rates making experimental observations rather challenging.

We have also presented an exploratory study of the channels $Z \to WM$, where the factorization scale is no longer given by the mass of the Z boson but still higher than in previous applications of the QCDF approach. In this case we found the impact of the LCDA shape to be tiny for the additional reason that the hard-scattering kernel varied slowly with the relevant convolution variable leading to the rates being mostly governed by the normalization of the LCDAs.

Following this analysis, we generalized the framework to exclusive hadronic Higgs decays. The study was performed with a phenomenological Lagrangian allowing for deviations of the Higgs couplings from their respective SM values. We have seen that an observation of some channels of the class $h \to M\gamma$ can be used as an interesting probe of anomalous quark Yukawa couplings due to a non-trivial interference structure of different diagram topologies. Predictions were also derived for the weak decays $h \to MZ$ and $h \to MW$. The $h \to MZ$ decays are largely governed by the coupling of the Higgs boson to two Z bosons or a Z boson and a photon, the latter being generated at the loop level within the SM or by effective

operators of higher mass dimension. For the final state meson being a vector meson, we find the decays to be potentially useful in probing this effective $h\gamma Z$-coupling, whereas the pseudoscalar channel only involves the gauge coupling of the Higgs boson and is not expected to show any new physics effects. In the case of $h \to WM$, we find potentially large enhancements in some channels when allowing flavor-changing Yukawa couplings. In all channels however, the rates are small and only some of them become accessible at the LHC in its high-luminosity run. Current upper bounds from the ATLAS and CMS collaborations are several orders of magnitudes above our predicted rates. More channels are believed to be accessible at a possible future hadron collider serving as a Higgs factory.

Finally, we have performed a study of neutrino oscillation parameters in the context of a selection of flavor-anarchic seesaw models and tested the stability of the anarchy hypothesis under renormalization group evolution. We found that the probability of a random draw yielding the observed parameters increases when RG effects are taken into account, at least in the models considered. This can be understood from the fact that the neutrino mixing angles have a tendency to decrease when scale-evolved from a high scale down to the electroweak scale due to the charged lepton masses. We noted that this most-likely does not hold for other models of neutrino mass generation (like type-II seesaw models, for example), where the beta functions of the neutrino masses have a different flavor structure.

In conclusion, we have seen several examples of how effective field theories can be used to treat problems in which multiple distinct scales are present. The list of possible applications is virtually endless and the examples covered here do not come close to covering the vast variety of usages. A search on `inspirehep.net` for "effective field theory" currently yields over 55,000 search results. With or without the discovery of physics beyond the Standard Model, the framework will clearly continue to be an indispensable tool for a wide range of analyses of multi-scale problems.

A. Subleading Twist Projections

The light-cone projector for pseudoscalar mesons at next-to-leading power is given by [63, 64]

$$M_P(k,x,\mu) = \frac{if_P}{4}\left\{\not{k}\gamma_5\,\phi_P(x,\mu) - \mu_P(\mu)\,\gamma_5\Big[\phi_p(x,\mu) - i\sigma_{\mu\nu}\,\frac{k^\mu\,\bar n^\nu}{k\cdot\bar n}\,\frac{\phi_\sigma'(x,\mu)}{6} + i\sigma_{\mu\nu}k^\mu\,\frac{\phi_\sigma(x,\mu)}{6}\,\frac{\partial}{\partial k_{\perp\nu}}\Big] + \text{3-particle LCDAs}\right\}. \tag{A.1}$$

The functions ϕ_p and ϕ_σ are two-particle LCDAs at twist-3 order[1]. We did not explicitly write down terms involving the three-particle LCDAs, where the meson can be formed from two quarks and a gluon. We will neglect three-particle contributions, which is referred to as the Wandzura-Wilczek approximation (WWA) [192], in which the QCD equations of motion fix the twist-3 LCDAs to [193]

$$\begin{aligned}\phi_p(x,\mu)|_{\text{WWA}} &= 1\,,\\ \phi_\sigma(x,\mu)|_{\text{WWA}} &= 6x\bar x\,.\end{aligned} \tag{A.2}$$

The light-cone projector at leading and subleading power for a longitudinally polarized vector meson is given by [64, 74–76]

$$M_{V_\parallel}(k,x,\mu) = -\frac{if_V}{4}\not{k}\,\phi_V(x,\mu) - \frac{if_V^\perp(\mu)\,m_V}{4}\left\{\frac{h_\parallel^{\prime(s)}(x,\mu)}{2} - i\sigma_{\mu\nu}\,\frac{k^\mu\,\bar n^\nu}{k\cdot\bar n}\,h_\parallel^{(t)}(x,\mu) - i\sigma_{\mu\nu}k^\mu\int_0^x dy\,\Big[\phi_V^\perp(y,\mu) - h_\parallel^{(t)}(y,\mu)\Big]\,\frac{\partial}{\partial k_{\perp\nu}} + \text{3-particle LCDAs}\right\}. \tag{A.3}$$

In the WWA, the QCD equations of motion imply the relations [64, 76]

$$\begin{aligned} h_\parallel^{(t)}(x,\mu)\big|_{\text{WWA}} &= (2x-1)\,\Phi_v(x,\mu)\,, \qquad h_\parallel^{\prime(s)}(x,\mu)\big|_{\text{WWA}} = -2\Phi_v(x,\mu)\,,\\ \int_0^x dy\,\Big[\phi_V^\perp(y,\mu) - h_\parallel^{(t)}(y,\mu)\Big]_{\text{WWA}} &= x(1-x)\,\Phi_v(x,\mu)\,,\end{aligned} \tag{A.4}$$

with

$$\Phi_v(x,\mu) = \int_0^x dy\,\frac{\phi_V^\perp(y,\mu)}{1-y} - \int_x^1 dy\,\frac{\phi_V^\perp(y,\mu)}{y}\,. \tag{A.5}$$

[1] The quantity twist is defined by the dimension of an operator minus the spin.

In this approximation, the twist-3 two-particle amplitudes can be expressed in terms of the twist-2 LCDA $\phi_V^\perp$.

For a transversely polarized vector meson the projector is [64]:

$$\begin{aligned} M_{V_\perp}(k,x,\mu) = \frac{if_V^\perp(\mu)}{4}\not{k}\not{\varepsilon}_V^{\perp *}\,\phi_V^\perp(x,\mu) - \frac{if_V m_V}{4}\Bigg\{ & \not{\varepsilon}_V^{\perp *}\, g_\perp^{(v)}(x,\mu) \\ & - \frac{i}{4}\,\epsilon_{\mu\nu\alpha\beta}\,\gamma^\mu\gamma_5\,\varepsilon_V^{\perp *\nu}k^\alpha\left(\frac{\bar n^\beta}{k\cdot\bar n}\,g_\perp^{\prime(a)}(x,\mu) - g_\perp^{(a)}(x,\mu)\,\frac{\partial}{\partial k_{\perp\beta}}\right) \\ & - \not{k}\,\varepsilon_{V\mu}^{\perp *}\int_0^x dy\left[\phi_V(y,\mu) - g_\perp^{(v)}(y,\mu)\right]\frac{\partial}{\partial k_{\perp\mu}} + \text{3-particle LCDAs}\Bigg\}. \end{aligned} \tag{A.6}$$

Again using the WWA, one obtains from the QCD equations of motion [64, 75, 76]

$$\begin{aligned} g_\perp^{(v)}(x,\mu)\big|_{\text{WWA}} &= \frac{1}{2}\left[\int_0^x dy\,\frac{\phi_V(y,\mu)}{1-y} + \int_x^1 dy\,\frac{\phi_V(y,\mu)}{y}\right], \\ g_\perp^{(a)}(x,\mu)\big|_{\text{WWA}} &= 2\left[(1-x)\int_0^x dy\,\frac{\phi_V(y,\mu)}{1-y} + x\int_x^1 dy\,\frac{\phi_V(y,\mu)}{y}\right], \\ g_\perp^{\prime(a)}(x,\mu)\big|_{\text{WWA}} &= -2\left[\int_0^x dy\,\frac{\phi_V(y,\mu)}{1-y} - \int_x^1 dy\,\frac{\phi_V(y,\mu)}{y}\right], \\ \int_0^x dy\left[\phi_V(y,\mu) - g_\perp^{(v)}(y,\mu)\right] &= \frac{1}{2}\left[(1-x)\int_0^x dy\,\frac{\phi_V(y,\mu)}{1-y} - x\int_x^1 dy\,\frac{\phi_V(y,\mu)}{y}\right]. \end{aligned} \tag{A.7}$$

The form factors governing the decay amplitudes $Z \to V_\perp\gamma$ and $W \to V_\perp\gamma$ are then

$$\begin{aligned} F_1^\perp = \frac{\mathcal{Q}_V}{6}\Bigg\{ & \int_0^1 dx\left(\frac{1+x}{x} + \frac{1+\bar x}{\bar x}\right) g_\perp^{(v)}(x) - \int_0^1 dx\left(\frac{1-x}{x} - \frac{1-\bar x}{\bar x}\right)\frac{g_\perp^{\prime(a)}(x)}{4} \\ & + \int_0^1 dx\left(\frac{1}{x} + \frac{1}{\bar x}\right)\frac{g_\perp^{(a)}(x)}{4} + \int_0^1 dx\left(\frac{1}{x} - \frac{1}{\bar x}\right)\int_0^x dy\left[\phi_V(y) - g_\perp^{(v)}(y)\right]\Bigg\}, \end{aligned} \tag{A.8}$$

and

$$\begin{aligned} F_2^\perp = \frac{\mathcal{Q}_V'}{6}\Bigg\{ & \int_0^1 dx\left(\frac{1-x}{x} - \frac{1-\bar x}{\bar x}\right) g_\perp^{(v)}(x) - \int_0^1 dx\left(\frac{1+x}{x} + \frac{1+\bar x}{\bar x}\right)\frac{g_\perp^{\prime(a)}(x)}{4} \\ & + \int_0^1 dx\left(\frac{1}{x} - \frac{1}{\bar x}\right)\frac{g_\perp^{(a)}(x)}{4} + \int_0^1 dx\left(\frac{1}{x} + \frac{1}{\bar x}\right)\int_0^x dy\left[\phi_V(y) - g_\perp^{(v)}(y)\right]\Bigg\}. \end{aligned} \tag{A.9}$$

For $h \to MZ$, the leading projections arise at subleading twist. For pseudoscalar mesons we find:

$$\begin{aligned} F_{\text{direct}}^{PZ} = -\sum_q f_P^q \frac{m_q}{2m_h^2} \int_0^1 dx \Bigg\{ & \frac{1}{x + r_Z \bar{x}} \Big[(a_q \kappa_q - i v_q \tilde{\kappa}_q)\, m_q\, \phi_P(x) \\ & - (a_q \kappa_q + i v_q \tilde{\kappa}_q)\, \mu_P \left(x\, \phi_p(x) + \frac{\phi_\sigma(x)}{3} - \left[x + \frac{2 r_Z}{1 - r_Z} \right] \frac{\phi_\sigma'(x)}{6} \right) \Big] \\ & + \frac{1}{\bar{x} + r_Z x} \Big[(a_q \kappa_q + i v_q \tilde{\kappa}_q)\, m_q\, \phi_P(x) \\ & - (a_q \kappa_q - i v_q \tilde{\kappa}_q)\, \mu_P \left(\bar{x}\, \phi_p(x) + \frac{\phi_\sigma(x)}{3} + \left[\bar{x} + \frac{2 r_Z}{1 - r_Z} \right] \frac{\phi_\sigma'(x)}{6} \right) \Big] \\ & + \text{terms involving 3-particle LCDAs} \Bigg\}, \end{aligned} \tag{A.10}$$

which can be simplified by the means of eq. (A.2). For flavor-diagonal mesons, the LCDAs $\phi_P(x)$, $\phi_p(x)$ and $\phi_\sigma(x)$ are symmetric under $x \leftrightarrow (1-x)$, and only the terms proportional to $a_q \kappa_q$ survive. The simplified result is then the one given in eq. (5.53).

The direct contributions to the form factors $F_{\parallel\,\text{direct}}^{VZ}$ for a longitudinal vector meson are obtained from (A.10) by replacing $f_P^q \to f_V^q$, $v_q \leftrightarrow a_q$, $\phi_P(x) \to \phi_V(x)$, $\mu_P \to m_V f_V^{q\perp}/f_V^q$, and

$$\begin{aligned} & \phi_p(x) \to \mp \frac{1}{2}\, h_\parallel'^{(s)}(x)\,, \quad \frac{\phi_\sigma(x)}{3} \to \pm 2 \int_0^x dy \left[\phi_V^\perp(y) - h_\parallel^{(t)}(y) \right], \\ & \frac{\phi_\sigma'(x)}{6} \to \mp h_\parallel^{(t)}(x)\,. \end{aligned} \tag{A.11}$$

Here the upper (lower) signs refer to the contributions from the first (second) diagram in Figure 5.10, which can be identified by the different denominator structures in (A.10). For flavor-diagonal final-state mesons, the LCDAs $\phi_V(x)$ and $h_\parallel^{(t)}(x)$ are symmetric under the exchange $x \leftrightarrow (1-x)$, while $h_\parallel'^{(s)}(x)$ and $\int_0^x dy[\phi_V^\perp(y) - h_\parallel^{(t)}(y)]$ is anti-symmetric. In this case only the terms proportional to $v_q \kappa_q$ survive.

B. The Fifth Gamma Matrix

When evaluating loop amplitudes in $d = 4 - 2\epsilon$ dimensional regularization, an important issue is the fact that γ^5 is ill-defined in this framework. The definitions

$$\gamma^5 = \frac{i}{4!}\epsilon^{\mu\nu\rho\sigma}\gamma_\mu\gamma_\nu\gamma_\rho\gamma_\sigma \qquad \text{and} \qquad \{\gamma^\mu, \gamma^5\} = 0 \tag{B.1}$$

are algebraically inconsistent, since the Levi-Civita symbol, and with that γ^5, is an intrinsically four-dimensional object, whereas the Lorentz indices run from 1 to d. Several possible solutions have been proposed, the simplest one being *naive dimensional regularization* (NDR), where we simply assume a vanishing anti-commutator between γ^5 and the other Dirac matrices. However, it is known that this prescription does not always reproduce correct results [194].

In this work we will use the scheme proposed by 't Hooft and Veltman [195]. In the HV scheme, one splits the Dirac matrices γ^μ into a four-dimensional piece $\hat{\gamma}^\mu$ that anticommutes with γ^5, and a $(d-4)$-dimensional piece $\gamma_\perp^\mu$ that commutes with γ^5. These two pieces can be combined to form the $d = (4 - 2\epsilon)$-dimensional Dirac matrix γ^μ as well as a $\bar{d} = (4 + 2\epsilon)$-dimensional Dirac matrix[1]:

$$\gamma^\mu = \hat{\gamma}^\mu + \gamma_\perp^\mu\,, \qquad\qquad \bar{\gamma}^\mu = \hat{\gamma}^\mu - \gamma_\perp^\mu\,. \tag{B.2}$$

Moving a γ^5 past one of these Dirac matrices changes it from γ to $\bar{\gamma}$ and vice versa:

$$\gamma^5\gamma^\mu = -\bar{\gamma}^\mu\gamma^5 \qquad \text{and} \qquad \gamma^5\bar{\gamma}^\mu = -\gamma^\mu\gamma^5\,. \tag{B.3}$$

When evaluating expressions with these $\bar{\gamma}$, we simply convert them to regular Dirac matrices by splitting up four-vectors and metric tensors in the same way as in eq. (B.2) and employing the identities:

$$\begin{aligned} &\bar{\gamma}_\mu = \bar{g}_{\mu\nu}\gamma^\nu\,, \qquad \bar{p}_\mu = g_{\mu\nu}p^\nu\,, \qquad \bar{p}^\mu = p^\mu \text{ (for external momenta } p)\,, \\ &\bar{g}^\mu{}_\mu = \bar{d}\,, \qquad \bar{g}^{\mu\nu}g_{\nu\rho} = \bar{g}^\mu{}_\rho\,, \qquad \bar{g}^{\mu\nu}\bar{g}_{\nu\rho} = g^\mu{}_\rho\,. \end{aligned} \tag{B.4}$$

Traces involving γ^5 will now receive corrections at $\mathcal{O}(\epsilon)$ and higher. Combined with the divergent pieces of loop integrals, these corrections can give rise to finite shifts in loop amplitudes. Problematically, the shifts can generate so-called *spurious*

[1] This differs from the usual convention found in the literature but has the benefit of not generating extra terms whenever an expression containing a γ^5 is manipulated.

anomalies [196, 197], spoiling gauge invariance. For example, when renormalizing $(V-A)$ currents

$$j^{\mu}_{V-A} = j^{\mu} - j^{\mu 5} = \bar{\psi}\gamma^{\mu}\psi - \bar{\psi}\gamma^{\mu}\gamma^{5}\psi\,, \tag{B.5}$$

at one-loop order in QCD, we do not only obtain a radiative correction proportional to j^{μ}_{V-A} but an additional (finite) piece proportional only to j^{μ}_{A}. Thus, the renormalization of the $(V-A)$-current has to be done according to

$$j^{\mu}_{V-A} = Z_{V-A}\left(j^{\mu}_{(0)} - Z_{HV}\, j^{\mu 5}_{(0)}\right)\,, \tag{B.6}$$

where Z_{HV} is the finite counterterm arising from the γ^5 in the loop. It is obtained most easily by computing the one-loop correction first in the NDR scheme, then in the HV scheme, and subtracting the results. This isolates the finite shift that we need to remove to multiplicatively renormalize j^{μ}_{V-A}. We find for the shift in the vertex function:

$$\begin{aligned} \Gamma^{\mu 5}_{\mathrm{HV-NDR}} &= \bar{u}(p)\gamma^{\mu}\gamma^{5}\, v(k)\left\{1 + \frac{\alpha_s C_F}{\pi}\, K\left(\mu, (p+k)^2\right)\right\} \\ K(\mu, q^2) &= \frac{\sqrt{\pi}}{4}(16\pi)^{\epsilon}\left(-\frac{\mu_{\overline{MS}}}{q^2}\right)^{\epsilon}\frac{\epsilon(2-\epsilon)}{(1-\epsilon)}\frac{\Gamma(1-\epsilon)\Gamma(\epsilon)}{\Gamma\left(\frac{3}{2}-\epsilon\right)} = 1 + \mathcal{O}(\epsilon)\,. \end{aligned} \tag{B.7}$$

From this we can easily determine $Z_{HV} = 1 - \alpha_s C_F/\pi$.

Finally, it should be noted that other solutions to the γ^5-problem exist. Especially in multi-loop computations involving electroweak corrections, disentangling the spurious anomalies generated by schemes like the HV scheme, is difficult. To this end, one can employ non-cyclic regularization procedures, where one gives up the cyclicity of the trace in order to allow for an algebraically consistent treatment of the fifth Dirac matrix [198, 199].

C. Hadronic Input Parameters

In this section, we discuss the relevant hadronic input parameters. We start by parameterizing neutral meson mixing and discuss decay constants and LCDA shape parameters later on.

Parameterizing Meson Mixing

In our phenomenological analyses of the exclusive hadronic decays we frequently deal with neutral mesons whose physical state differs from the naive flavor eigenstates. This state mixing can have sizable effects on our predictions and needs to be taken into account. The mixing between flavor eigenstates and physical eigenstates arises from non-perturbative effects that cannot be accessed from first principles in an analytic way. Rather we will make simplifying assumptions and parameterize the mixing through phenomenological quantities that can be extracted from data.

Mixing between ω and ϕ

The flavor eigenstates of ω and ϕ are defined as $|\omega_I\rangle = \left(|u\bar{u}\rangle + |d\bar{d}\rangle\right)/\sqrt{2}$ and $|\phi_I\rangle = |s\bar{s}\rangle$ and we relate them to the physical states according to

$$\begin{pmatrix} |\omega\rangle \\ |\phi\rangle \end{pmatrix} = \begin{pmatrix} \cos\theta_{\omega\phi} & -\sin\theta_{\omega\phi} \\ \sin\theta_{\omega\phi} & \cos\theta_{\omega\phi} \end{pmatrix} \begin{pmatrix} |\omega_I\rangle \\ |\phi_I\rangle \end{pmatrix} . \tag{C.1}$$

For the radiative Higgs decays, we need the corrections from mixing effects on the transverse decay constants, that we defined as flavor-specific matrix elements:

$$\langle V(k,\varepsilon)|\, \bar{q}\, i\sigma^{\mu\nu} q\, |0\rangle = i f_V^{q\perp}(\mu)\, (k^\mu \varepsilon^{*\nu} - k^\nu \varepsilon^{*\mu}) \, . \tag{C.2}$$

We neglect contributions to the mixing violating the OZI-rule[1], allowing us to relate the flavor specific decay constant to matrix elements

$$\begin{aligned} \langle \omega_I(k,\varepsilon)|\, \frac{\bar{u} i\sigma^{\mu\nu} u + \bar{d} i\sigma^{\mu\nu} d}{\sqrt{2}}\, |0\rangle &= i f_{\omega_I}^{\perp} (k^\mu \varepsilon^{*\nu} - k^\nu \varepsilon^{*\mu}) \, , \\ \langle \phi_I(k,\varepsilon)|\, \bar{s} i\sigma^{\mu\nu} s\, |0\rangle &= i f_{\phi_I}^{\perp} (k^\mu \varepsilon^{*\nu} - k^\nu \varepsilon^{*\mu}) \, . \end{aligned} \tag{C.3}$$

[1] The OZI-rule states that contributions mediated purely by gluons are suppressed because the gluons are off-shell by the meson mass and thus hard.

Under the assumption of isospin symmetry, the decay constants for the u-quark and d-quark currents are equal, yielding:

$$f_\omega^{u\perp} = f_\omega^{d\perp} = \frac{\cos\theta_{\omega\phi}}{\sqrt{2}} f_{\omega_I}^\perp\,, \qquad f_\omega^{s\perp} = -\sin\theta_{\omega\phi} f_{\phi_I}^\perp\,, \tag{C.4}$$

$$f_\phi^{s\perp} = \cos\theta_{\omega\phi} f_{\phi_I}^\perp \qquad f_\phi^{u\perp} = f_\phi^{d\perp} = \frac{\sin\theta_{\omega\phi}}{\sqrt{2}} f_{\omega_I}^\perp \tag{C.5}$$

The relevant decay constants are combinations of these flavor-specific decay constants, weighted by charge factors:

$$f_V^\perp = \frac{\sum_q Q_q f_V^{q\perp}}{\sum_q c_q^V Q_q}\,, \tag{C.6}$$

where c_q^V are the flavor coefficients of the vector meson V and Q_q are the electric charges of the quarks q. It follows now that the relevant decay constants for ω and ϕ are:

$$\begin{aligned} f_\omega^\perp &= \cos\theta_{\omega\phi} f_{\omega_I}^\perp + \sqrt{2}\sin\theta_{\omega\phi} f_{\phi_I}^\perp\,, \\ f_\phi^\perp &= \cos\theta_{\omega\phi} f_{\phi_I}^\perp - \frac{\sin\theta_{\omega\phi}}{\sqrt{2}} f_{\omega_I}^\perp\,. \end{aligned} \tag{C.7}$$

The quantities $\bar\kappa_\omega$ and $\bar\kappa_\phi$, as defined in eq. (5.14), are then

$$\bar\kappa_\omega = 2\bar\kappa_u - \bar\kappa_d + \frac{\sqrt{2}\delta_\omega}{1+\sqrt{2}\delta_\omega}(\bar\kappa_s + \bar\kappa_d - 2\bar\kappa_u)\,, \quad \bar\kappa_\phi = \bar\kappa_s + \frac{\delta_\phi}{\sqrt{2}-\delta_\phi}(\bar\kappa_s + \bar\kappa_d - 2\bar\kappa_u)\,, \tag{C.8}$$

with

$$\delta_\omega = \frac{f_{\phi_I}^\perp}{f_{\omega_I}^\perp}\tan\theta_{\omega\phi}\,, \qquad \delta_\phi = \frac{f_{\omega_I}^\perp}{f_{\phi_I}^\perp}\tan\theta_{\omega\phi}\,, \tag{C.9}$$

where all parameters must be evaluated at $k^2 = m_V^2$. The ratio of decay constants is 1 in the limit of $SU(3)$ flavor symmetry.

Mixing between η and η'

We proceed similarly for the mixing of the η-η' system. We will assume isospin symmetry of all hadronic matrix elements [85] but differentiate between s quarks and the quarks u and d. When an $SU(3)$ flavor-symmetry is assumed, the η and η' would be flavor singlets and octets respectively. From phenomenological data it is known that this is not a good assumption. We will therefore use the FKS scheme [200, 201], where one assumes that the flavor states $|\eta_q\rangle = (|u\bar u\rangle + |d\bar d\rangle)/\sqrt{2}$

and $|\eta_s\rangle = |s\bar{s}\rangle$ mix only through the axial $U(1)$ anomaly. The FKS scheme allows to relate the physical states to the flavor states with a single mixing parameter:

$$\begin{pmatrix} |\eta\rangle \\ |\eta\rangle' \end{pmatrix} = \begin{pmatrix} \cos\varphi & -\sin\varphi \\ \sin\varphi & \cos\varphi \end{pmatrix} \begin{pmatrix} |\eta_q\rangle \\ |\eta_s\rangle \end{pmatrix} . \tag{C.10}$$

One now introduces decay constants and LCDAs for these flavor states f_q, f_s, $\phi_q(x,\mu)$ and $\phi_s(x,\mu)$ [85]. The flavor-specific decay constants under these assumptions are then

$$\begin{aligned} f_\eta^u = f_\eta^d = \frac{f_q}{\sqrt{2}}\cos\varphi\,, \quad f_\eta^s = -f_s\sin\varphi\,, \\ f_{\eta'}^u = f_{\eta'}^d = \frac{f_q}{\sqrt{2}}\sin\varphi\,, \quad f_{\eta'}^s = f_s\cos\varphi\,, \end{aligned} \tag{C.11}$$

and similarly

$$\begin{aligned} f_\eta^u\phi_\eta^u = f_\eta^d\phi_\eta^d = \frac{f_q\phi_q}{\sqrt{2}}\cos\varphi\,, \qquad f_\eta^s\phi_\eta^s = -f_s\phi_s\,\sin\varphi\,, \\ f_{\eta'}^u\phi_{\eta'}^u = f_{\eta'}^d\phi_{\eta'}^d = \frac{f_q\phi_q}{\sqrt{2}}\sin\varphi\,, \quad f_{\eta'}^s\phi_{\eta'}^s = f_s\phi_s\,\cos\varphi\,. \end{aligned} \tag{C.12}$$

The gluon LCDAs are assumed to be equal for η and η', meaning $\phi_\eta^g = \phi_{\eta'}^g \equiv \phi_g$ [85, 86, 88]. The three FKS parameters f_q, f_s and φ have been determined from experimental data, with two fits available. Ref. [200] quotes

$$f_q = (1.07 \pm 0.02) f_\pi\,, \qquad f_s = (1.34 \pm 0.06) f_\pi\,, \qquad \varphi = 39.3^\circ \pm 1.0^\circ\,, \tag{C.13}$$

whereas a more recent analysis finds [202]

$$f_q = (1.09 \pm 0.03) f_\pi\,, \qquad f_s = (1.66 \pm 0.06) f_\pi\,, \qquad \varphi = 40.7^\circ \pm 1.4^\circ\,. \tag{C.14}$$

This second set uses more recent data but only a subset of the processes considered in ref. [200]. The flavor-singlet decay constants $f_{\eta'}^{uds}$ as defined in eq. (4.36) are then $f_\eta^{uds} = 42.0$ MeV and $f_{\eta'}^{uds} = 260.2$ MeV in the first set of mixing parameters and $f_\eta^{uds} = 11.2$ MeV and $f_{\eta'}^{uds} = 295.2$ MeV in the second.

C.1. Meson Decay Constants

The meson decay constants can be extracted from experimental data [205]. For charged pseudoscalar mesons, the semileptonic decays $P^- \to l^-\bar{\nu}_l(\gamma)$ can be used, leading to the values for f_π, f_K, f_D and f_{D_s} shown in the tables below [101].

For light charged mesons, the decay constants can also be extracted from hadronic decays of the τ, with the rates given by

$$\Gamma(\tau^- \to M^- \nu_\tau) = S_{\rm EW} \frac{G_F^2 m_\tau^3}{16\pi} |V_{ij}|^2 f_M^2 \left(1 - \frac{m_M^2}{m_\tau^2}\right)^2 \left(1 + b_M \frac{m_M^2}{m_\tau^2}\right) , \tag{C.15}$$

with $b_P = 0$ and $b_V = 2$ for pseudoscalar mesons P and vector mesons V. The factor $S_{\rm EW}$ is a correction factor including leading-logarithmic [206, 207] and non-logarithmic electroweak corrections [208]. The measured branching ratios are [101]:

$$\begin{aligned} {\rm Br}(\pi^-) &= (10.83 \pm 0.06)\% , \quad {\rm Br}(K^-) = (0.70 \pm 0.01)\% , \\ {\rm Br}(\rho^-) &= (25.22 \pm 0.33)\% , \quad {\rm Br}(K^{*-}) = (1.20 \pm 0.07)\% , \end{aligned} \tag{C.16}$$

with the lifetime of the τ being $\tau_\tau = (290.3 \pm 0.5) \cdot 10^{-15} s$. For the decay constants we then find

$$\begin{aligned} f_\pi &= (130.3 \pm 0.4)\ {\rm MeV} , \quad f_K = (154.3 \pm 1.1)\ {\rm MeV} , \\ f_\rho &= (207.8 \pm 1.4)\ {\rm MeV} , \quad f_{K^*} = (203.2 \pm 5.9)\ {\rm MeV} . \end{aligned} \tag{C.17}$$

Since f_π and f_K can be more reliably extracted from semileptonic decays, we use these values in our analyses.

The decay constants of neutral vector mesons are obtained from electromagnetic decays $V \to l^+ l^-$, where $l = e, \mu$. The rates are given by

$$\Gamma(V \to l^+ l^-) = \frac{4\pi}{3 m_V} f_V^2 \alpha_{\rm EM}^2(m_V) c_V . \tag{C.18}$$

Here $c_V = (\sum_q c_q^V Q_q)^2$ are the relevant electromagnetic charges of the quarks in the meson V, as defined in ref. [205], with $c_\rho = 1/2$, $c_\omega = 1/18$, $c_\phi = 1/9$, $c_{J/\psi} = 4/9$ and $c_\Upsilon = 1/9$. Leading logarithmic corrections are included by evaluating $\alpha_{\rm EM}$ at the scale of the meson mass, using $\alpha_{\rm EM}(m_Z) = 127.94^{-1}$ [101] and the running described in ref. [102]. We average over the modes $V \to e^+ e^-$ and $V \to \mu^+ \mu^-$. The branching ratios obtained this way along with the total decay widths are [101]:

$$\begin{aligned} {\rm Br}(\rho^0) &= (4.715 \pm 0.049) \cdot 10^{-5} , \quad \Gamma(\rho^0) = (147.8 \pm 0.9)\ {\rm MeV} , \\ {\rm Br}(\omega) &= (7.284 \pm 0.140) \cdot 10^{-5} , \quad \Gamma(\omega) = (8.49 \pm 0.08)\ {\rm MeV} , \\ {\rm Br}(\phi) &= (2.952 \pm 0.030) \cdot 10^{-4} , \quad \Gamma(\phi) = (4.266 \pm 0.031)\ {\rm MeV} . \end{aligned} \tag{C.19}$$

This leaves us with

$$f_\rho = (216.3 \pm 1.3)\ {\rm MeV} , \quad f_\omega = (194.2 \pm 2.1)\ {\rm MeV} , \quad f_\phi = (223.0 \pm 1.4)\ {\rm MeV} . \tag{C.20}$$

The effects of $\rho-\omega$ and $\omega-\phi$ mixing raise f_ω by 9.5 MeV and f_ϕ by 7.6 MeV [81].

We extract the heavy quarkonium decay constants directly form their electromagnetic decays $M \to e^+e^-$. The widths are [101]

$$\begin{aligned} \Gamma_{ee}(J/\psi) &= (5.55 \pm 0.14)\ \text{keV}\,, \\ \Gamma_{ee}(\Upsilon(1S)) &= (1.340 \pm 0.018)\ \text{keV}\,, \quad \Gamma_{ee}(\Upsilon(2S)) = (0.612 \pm 0.011)\ \text{keV}\,, \\ \Gamma_{ee}(\Upsilon(3S)) &= (0.443 \pm 0.008)\ \text{keV}\,, \quad \Gamma_{ee}(\Upsilon(4S)) = (0.272 \pm 0.029)\ \text{keV}\,, \end{aligned} \tag{C.21}$$

from which we extract

$$\begin{aligned} f_{J/\psi} &= (403.3 \pm 5.1)\ \text{MeV}\,, \\ f_{\Upsilon(1S)} &= (684.4 \pm 4.6)\ \text{MeV}\,, \quad f_{\Upsilon(2S)} = (475.8 \pm 4.3)\ \text{MeV}\,, \\ f_{\Upsilon(3S)} &= (411.3 \pm 3.7)\ \text{MeV}\,, \quad f_{\Upsilon(4S)} = (325.7 \pm 17.4)\ \text{MeV}\,. \end{aligned} \tag{C.22}$$

For η and η' mesons, the values are obtained from the FKS-scheme, as discussed in the previous section. The intrinsic charm and bottom contents of η and η' can be estimated using relations between FKS parameters mediated by the $U(1)$ axial anomaly, giving [85]

$$f_P^c(\mu_c) \approx -\frac{m_P^2}{12 m_c^2} f_P^u\,, \qquad\qquad f_P^b(\mu_b) \approx -\frac{m_P^2}{12 m_b^2} f_P^u\,, \tag{C.23}$$

which numerically becomes

$$\begin{aligned} f_\eta^c &= -1.2\ \text{MeV}\,, \quad f_\eta^b = -0.1\ \text{MeV}\,, \\ f_{\eta'}^c &= -2.9\ \text{MeV}\,, \quad f_{\eta'}^b = -0.3\ \text{MeV}\,. \end{aligned} \tag{C.24}$$

Similar values are found in refs. [111, 200, 209–211].

For $h \to MW$, we need the decay constants of the heavy mesons $D^*_{(s)}$, B^* and B_c, for which we adopt the values obtained from lattice calculations [203, 204]:

$$\begin{aligned} f_{D^*} &= (278 \pm 16)\ \text{MeV}\,, \quad f_{D_s^*} = (311 \pm 9)\ \text{MeV}\,, \\ f_{B^*} &= (175 \pm 6)\ \text{MeV}\,, \quad f_{B_c} = (434 \pm 15)\ \text{MeV}\,. \end{aligned} \tag{C.25}$$

The analyses discussed in this work where done using different combinations of the decay constants. In the summary tables below, where we compile decay constants and LCDA shape parameters, we indicate which analysis they enter.

Transverse vector-meson decay constants

For the exclusive Higgs decays, we need the ratios $f_V^\perp/f_V$. Rather than computing the decay constants individually and taking the ratio, the ratio can directly be

Meson V	$f_V^\perp(2\,\text{GeV})/f_V$	Method	Reference
ρ	0.76 ± 0.04	lattice (unquenched)	[212]
	0.687 ± 0.027	lattice (unquenched)	[213]
	0.742 ± 0.014	lattice (quenched)	[214]
	$0.72 \pm 0.02\,^{+0.02}_{-0.00}$	lattice (quenched)	[215]
	0.70 ± 0.04	light-cone sum rules	[81]
	$\mathbf{0.72 \pm 0.04}$	our combination	
ω	0.707 ± 0.046	light-cone sum rules†	[81]
	$\mathbf{0.71 \pm 0.05}$	our combination	
ϕ	0.750 ± 0.008	lattice (unquenched)	[213]
	0.780 ± 0.008	lattice (quenched)	[214]
	0.76 ± 0.01	lattice (quenched)	[215]
	0.763 ± 0.041	light-cone sum rules†	[81]
	$\mathbf{0.76 \pm 0.04}$	our combination	

Tab. C.1.: Compilation of theoretical predictions for the ratio $f_V^\perp(\mu)/f_V$ at $\mu = 2\,\text{GeV}$ for light vector mesons. Values marked with a dagger are obtained by taking ratios of individual results for the two decay constants. In our combinations we adopt more conservative error estimates than in some of the original references.

obtained from lattice QCD and light-cone sum rules [81, 212–215] for light mesons. The values obtained in various studies along with our combinations are compiled in Tab. C.1.

For heavy quarkonia, the ratio has been computed in NRQCD, including both leading relativistic [77] and one-loop QCD corrections [79], yielding:

$$\frac{f_V^\perp(\mu)}{f_V} = \frac{m_V}{2m_Q}\left\{1 - \frac{2}{3}\langle v^2\rangle_V + \frac{\alpha_s(\mu)C_F}{4\pi}\log\frac{m_Q^2}{\mu^2}\right\}, \tag{C.26}$$

with m_Q being the pole mass of the heavy quark. The NRQCD matrix elements $\langle v^2\rangle_V$ have been extracted from electromagnetic decays $V \to e^+e^-$ including both corrections from $\mathcal{O}(\alpha_s)$ in QCD as well as relativistic effects [216, 217], they are compiled in Tab. C.2. Since the concept of a pole mass is ill-defined beyond perturbation theory [218, 219] and the rates $\Gamma(V \to e^+e^-)$ in NRQCD receive large corrections at two-loop and three-loop [220], we increase the errors on m_Q and $\langle v^2\rangle_V$ for $\Upsilon(nS)$ in our analysis.

C.2. Gegenbauer Moments

As mentioned in the main text, the LCDA shape parameters are in general poorly known. Estimates for the first few Gegenbauer moments exist for light mesons from

Meson V	m_Q [GeV]	$\langle v^2\rangle_V$	$f_V^\perp(2\,\text{GeV})/f_V$
J/ψ	1.4 ± 0.2	$0.225^{+0.106}_{-0.088}$ [216]	0.91 ± 0.14
$\Upsilon(1S)$	4.6 ± 0.1	-0.009 ± 0.003 [217]	1.09 ± 0.02
$\Upsilon(2S)$	4.6 ± 0.1	0.090 ± 0.011 [217]	1.08 ± 0.02
$\Upsilon(3S)$	4.6 ± 0.1	0.155 ± 0.018 [217]	1.07 ± 0.03

Tab. C.2.: NRQCD parameters for heavy quarkonia extracted from their electronic decay widths $\Gamma(V \to e^+e^-)$, and resulting values for the ratio of decay constants.

Meson M	f_M [MeV]	$a_1^M(\mu_0)$	$a_2^M(\mu_0)$
π	130.4 ± 0.2	0	0.29 ± 0.08
K	156.2 ± 0.7	-0.07 ± 0.04	0.24 ± 0.08
ρ	212 ± 4	0	0.17 ± 0.07
ω	187 ± 5	0	0.15 ± 0.12
K^*	203 ± 6	-0.06 ± 0.04	0.16 ± 0.09
ϕ	210 ± 5	0	0.23 ± 0.08

Tab. C.3.: Hadronic input parameters for light pseudoscalar and vector mesons, with scale-dependent quantities defined at $\mu_0 = 1\,\text{GeV}$. We assume isospin symmetry and use the same values for charged and neutral mesons. The values for f_π and f_K are taken from [101]. The other decay constants are extracted from $\tau^- \to M^-\nu_\tau$ and $V^0 \to l^+l^-$ decays [205], as discussed above. For all other parameters we adopt the values compiled in [231] from a combination of results obtained using lattice QCD [221] and light-cone QCD sum rules (see e.g. [75, 222–225]), including conservative error estimates. These values were used in the analyses $Z \to M\gamma$, $W \to M\gamma$ and $Z \to MW$ [49].

the lattice [221] and light-cone QCD sum rules [75, 222–225]. Higher moments of the pion have been estimated from sum rules in refs. [226, 227] and extracted from the $\pi^0\gamma^*\gamma$ form factor, measured by BaBar and Belle [228, 229], in ref. [230]. In Tab. C.3, we gather the hadronic input parameters for light pseudoscalar and vector mesons, used for the hadronic Z and W decays, excluding the η and η'. The decay constants and shape parameter used in the methods explained in the main text (see section 4.1.3) are gathered in Tab. C.4.

The LCDA shape parameters for the $\eta^{(\prime)}$ have been extracted from fits to $\gamma\gamma^*\eta^{(\prime)}$ transition form factor, measured at CLEO [234] and BaBar [235]. The authors of ref. [88] have estimated the LCDAs of the flavor states η_q and η_s according to QCD sum-rule calculations for the pion and fitted the first gluon Gegenbauer moment to the data. In ref. [86], the Gegenbauer moments of quark and gluon LCDAs have

Meson M	f_M [MeV]	λ_M [MeV]	$\langle v^2 \rangle$	σ
D	204.6 ± 5.0	460 ± 110	–	0.246 ± 0.059
D_s	257.5 ± 4.6	550 ± 150	–	0.279 ± 0.076
B	186 ± 9	460 ± 110	–	0.087 ± 0.021
B_s	224 ± 10	550 ± 150	–	0.102 ± 0.028
B_c	434 ± 15	–	–	0.305 ± 0.150
J/ψ	403 ± 5	–	0.30 ± 0.15	0.158 ± 0.040
$\Upsilon(1S)$	684 ± 5	–	0.10 ± 0.05	0.091 ± 0.023
$\Upsilon(4S)$	326 ± 17	–	0.10 ± 0.05	0.091 ± 0.023

Tab. C.4.: Hadronic input parameters for pseudoscalar and vector mesons containing heavy quarks, used in the analysis of $Z \to M\gamma$, $W \to M\gamma$ and $Z \to WM$ [49]. Scale-dependent quantities are defined at $\mu_0 = 1\,\text{GeV}$. The values for f_D and f_{D_s} are taken from [101]. The values for f_B and f_B are taken from two recent, unquenched lattice calculations [232, 233], which obtain identical central values but quote very different error estimates. We quote the averages of the uncertainties given by the two groups. The values of the J/ψ and $\Upsilon(nS)$ decay constants have been derived from data, as explained above.

Model	a_2^q	a_4^q	a_2^s	a_4^s	b_2	FKS pars.
(i)	0.10	0.10	0.10	0.10	−0.06	(C.13)
(ii)	0.20	0.00	0.20	0.00	−0.07	(C.13)
(iii)	0.25	−0.10	0.25	−0.10	−0.06	(C.13)
(iv)	−0.10		−0.07		−0.14	(C.13)
(v)	−0.10		−0.07		−0.24	(C.13)
(vi)	−0.09		−0.02		−0.08	(C.14)

Tab. C.5.: Gegenbauer moments of quark and gluon LCDAs at the scale $\mu_0 = 1$ GeV in different benchmark models obtained from analyses of the $\gamma^*\gamma \to \eta^{(\prime)}$ transition form factors. Models (i)–(iii) correspond to the models in Table 2 of [88], while models (iv)–(vi) refer to the first, third and sixth model in Table 2 of [86].

Meson V	f_V [MeV]	$f_V^\perp(2\,\text{GeV})/f_V$	$a_2^{V_\perp}(\mu_0)$	Q_V	v_V
ρ^0	216.3 ± 1.3	0.72 ± 0.04	0.14 ± 0.06	$\frac{1}{\sqrt{2}}$	$\frac{1}{\sqrt{2}}\left(\frac{1}{2} - s_W^2\right)$
ω	194.2 ± 2.1	0.71 ± 0.05	0.15 ± 0.07	$\frac{1}{3\sqrt{2}}$	$-\frac{s_W^2}{3\sqrt{2}}$
ϕ	223.0 ± 1.4	0.76 ± 0.04	0.14 ± 0.07	$-\frac{1}{3}$	$-\frac{1}{4} + \frac{s_W^2}{3}$

Tab. C.6.: Hadronic input parameters for light vector mesons, used in the analysis of $h \to V\gamma$ [50]. The decay constants f_V are extracted from data on the decays $V \to l^+l^-$ [49], while the ratios $f_V^\perp/f_V$ are derived from a compilation of theoretical predictions. The Gegenbauer moments at the scale $\mu_0 = 1\,\text{GeV}$ are taken from [81, 222]. The last two columns show the effective charges Q_V and v_V defined in (5.11) and below (5.28).

Meson V	f_V [MeV]	$f_V^\perp(2\,\text{GeV})/f_V$	$\sigma_V(\mu_0)$	Q_V	v_V
J/ψ	403.3 ± 5.1	0.91 ± 0.14	$0.228 \pm 0.005 \pm 0.057$	$\frac{2}{3}$	$\frac{1}{4} - \frac{2s_W^2}{3}$
$\Upsilon(1S)$	684.4 ± 4.6	1.09 ± 0.04	$0.112 \pm 0.004 \pm 0.028$	$-\frac{1}{3}$	$-\frac{1}{4} + \frac{s_W^2}{3}$
$\Upsilon(2S)$	475.8 ± 4.3	1.08 ± 0.05	$0.144 \pm 0.007 \pm 0.036$	$-\frac{1}{3}$	$-\frac{1}{4} + \frac{s_W^2}{3}$
$\Upsilon(3S)$	411.3 ± 3.7	1.07 ± 0.05	$0.162 \pm 0.010 \pm 0.041$	$-\frac{1}{3}$	$-\frac{1}{4} + \frac{s_W^2}{3}$

Tab. C.7.: Hadronic input parameters for heavy quarkonium states, used in the analysis $h \to V\gamma$ [50]. The decay constants f_V are extracted from the decays $V \to l^+l^-$, while the $f_V^\perp/f_V$ are derived from NRQCD scaling relations. The widths σ_V are obtained from (4.29), with errors from parametric origin and higher-order corrections. The last two columns show the effective charges Q_V and v_V.

been extracted from a fit. Both studies provide several different sets of parameters and we will use a selection of them, compiled in Tab. C.5.

For the radiative Higgs decays $h \to V\gamma$, the final state vector meson is transversely polarized and the relevant input parameters are the ratios $f_V^\perp/f_V$ and the transverse Gegenbauer moments $a_n^{V_\perp}$. For light vector mesons, the relevant parameters are compiled in Tab. C.6. We list the decay constants, the transverse decay constants and the Gegenbauer moment $a_2^{V_\perp}$. Higher moments are unknown and we encode shape uncertainties in $a_4^{V_\perp} = \pm 0.15$. For heavy quarkonia, the input parameters are listed in Tab. C.7. The shape parameters σ_V can be translated into Gegenbauer moments using the model LCDA (4.28) and the inverted Gegenbauer expansion (4.31). For our numerical analysis, we use the first 20 Gegenbauer moments obtained in this way.

D. Cancellation of Poles in the Hard Scattering Kernels

The one-loop corrections to the hard-scattering kernels of the exclusive decays $Z \to M\gamma$, $W \to M\gamma$ and $h \to M\gamma$ are divergent in the limit of $\epsilon \to 0$. These poles are removed by the renormalization of the LCDA, as explained in section 4.1.2. In this appendix we briefly demonstrate how this cancellation occurs explicitly.

For $Z \to M\gamma$, the nonsinglet hard-scattering kernel is

$$H(x) = \frac{1}{x}\left[1 - \frac{\alpha_s C_F}{4\pi}\left(\frac{2\log x + 3}{\epsilon} + \text{finite}\right)\right] . \tag{D.1}$$

From eq. (4.10) we can derive the counterterm for the Wilson coefficient:

$$\int_0^1 dx\, \mathcal{C}_{\text{bare}}(x)\, \langle \mathcal{O}_{\text{bare}}(x)\rangle = \int_0^1 dx \int_0^1 dy\, \mathcal{C}_{\text{bare}}(x) Z^{-1}(x,y,\mu)\, \langle \mathcal{O}_{\text{ren}}(x,\mu)\rangle \tag{D.2}$$

$$= \int_0^1 dx\, \mathcal{C}_{\text{ren}}(x,\mu)\, \langle \mathcal{O}_{\text{ren}}(x,\mu)\rangle \ , \tag{D.3}$$

from which it follows that the renormalized Wilson coefficient is

$$\mathcal{C}_{\text{ren}}(x,\mu) = \int_0^1 dy\, \mathcal{C}_{\text{bare}}(y)\, Z^{-1}(y,x,\mu)\, . \tag{D.4}$$

The tree-level Wilson coefficient for $Z/W \to M\gamma$ is the leading term in eq. (4.53), given by $\mathcal{C}_{\text{bare}} = 1/y$. We then evaluate the integral over the Brodsky-Lepage kernel:

$$\begin{aligned}\mathcal{C}_{\text{ren}}(x,\mu) = \int_0^1 dy\, \frac{1}{y}\Bigg\{\delta(x-y) - \frac{\alpha_s(\mu) C_F}{4\pi\epsilon}\Bigg(&\delta(x-y) \\ &-2c_\Gamma\left[\frac{y}{x}\theta(x-y-\eta) + \frac{\bar y}{\bar x}\theta(y-x-\eta)\right] \\ &-\frac{2}{x\bar x}\left[\frac{y\bar x}{x-y}\theta(x-y-\eta) + \frac{x\bar y}{y-x}\theta(y-x-\eta)\right]_+\Bigg)\Bigg\} .\end{aligned} \tag{D.5}$$

Here η is introduced to regulate the divergences of the integrals when $x = y$ and can be set to zero after summing the terms. Evaluating the integrals we find:

$$\mathcal{C}_{\text{ren}}(x,\mu) = \frac{1}{x}\left[1 + \frac{C_F\alpha_s}{4\pi\epsilon}\left\{\begin{array}{ll} 2\log x + 3\,; & c_\Gamma = 1 \\ \frac{2\log x}{\bar x} + 3\,; & c_\Gamma = 0 \end{array}\right\}\right] . \tag{D.6}$$

Since for $Z \to M\gamma$, the meson M can either be a pseudoscalar or a longitudinal vector meson, $c_\Gamma = 1$. We see that the corresponding counterterm is precisely what we need to cancel the pole in eq. (D.1).

In the flavor-singlet case, there is an additional divergent contribution coming from the partonic $Z \to gg\gamma$ graphs. Since these graphs start at $\mathcal{O}(\alpha_s)$, their counterterm must be of a different origin. The two-gluon hard function is

$$H_g(x,\mu) = \frac{2\alpha_s(\mu)\, n_f T_F}{\pi\epsilon}\left(\frac{\log x}{\bar{x}^2} - \frac{\log \bar{x}}{x^2}\right) + \text{finite} \tag{D.7}$$

If we allow for flavor-singlet mesons, the relation (D.4) changes into a matrix equation with a vector $\vec{\mathcal{C}} = (\mathcal{C}_{qq},\ \mathcal{C}_{gg})^T$:

$$\begin{pmatrix} \mathcal{C}^{(qq)}_{\text{ren}}(x,\mu) \\ \mathcal{C}^{(gg)}_{\text{ren}}(x,\mu) \end{pmatrix} = \int_0^1 dy\, (Z^{-1})^T(y,x) \begin{pmatrix} \mathcal{C}^{(qq)}_{\text{bare}}(y,\mu) \\ \mathcal{C}^{(gg)}_{\text{bare}}(y,\mu) \end{pmatrix} \tag{D.8}$$

with

$$Z(x,y,\mu) = \mathbf{1}\delta(x-y) + \frac{\alpha_s}{4\pi\epsilon}\begin{pmatrix} V_{qq}(x,y) & V_{qg}(x,y) \\ V_{gq}(x,y) & V_{gg}(x,y) \end{pmatrix}, \tag{D.9}$$

and the kernel functions defined in eqs. (E.1). When expanded, we see that the combination of the tree-level coefficient $C^{(qq)}_{\text{bare}}$ with the off-diagonal kernel $V_{qg}(x,y)$ generates a counterterm for the two-gluon contribution. It is given by the integral

$$\delta\mathcal{C}^{(gg)}(x,\mu) = -\frac{2\alpha_s(\mu)\, n_f T_F}{\pi\epsilon}\int_0^1 dy\, \mathcal{C}^{(qq)}_{\text{bare}}(y)\left[\frac{y}{x^2}\theta(x-y) - \frac{\bar{y}}{\bar{x}^2}\theta(y-x)\right]. \tag{D.10}$$

Inserting the bare Wilson coefficients from the quark contribution and the reversed diagram $\mathcal{C}^{(qq)}_{\text{bare}} = 1/y + 1/\bar{y}$, we obtain:

$$\mathcal{C}^{(gg)}_{\text{ren}}(x,\mu) = \mathcal{C}^{(gg)}_{\text{bare}}(x) + \frac{2\alpha_s(\mu)\, n_f T_F}{\pi\epsilon}\left(\frac{\log \bar{x}}{x^2} - \frac{\log x}{\bar{x}^2}\right), \tag{D.11}$$

which cancels the pole in the hard function (D.7).

For the decays $h \to V\gamma$, the hard scattering kernel was:

$$H(x) = \frac{1}{x\bar{x}}\left[1 - \frac{\alpha_s C_F}{4\pi}\left(\frac{2\log(x\bar{x})}{\epsilon} + \text{finite}\right)\right] \tag{D.12}$$

The renormalization is then performed by integrating the leading term $1/(x\bar{x}) = 1/x + 1/\bar{x}$ over the Brodsky-Lepage kernel with $c_\Gamma = 0$. The result for the part

$1/x$ is given in the second line of eq. (D.6), and the one for $1/\bar{x}$ is obtained by the obvious replacement, yielding the renormalized tree-level function:

$$H_{\rm ren}^{\rm tree}(x) = \frac{1}{x}\left[1 + \frac{\alpha_s C_F}{4\pi\epsilon}\left(\frac{2\log x}{\bar{x}} + 3\right)\right] + \frac{1}{\bar{x}}\left[1 + \frac{\alpha_s C_F}{4\pi\epsilon}\left(\frac{2\log \bar{x}}{x} + 3\right)\right] . \quad \text{(D.13)}$$

Supplementing the tree-level terms in eq. (D.12) with the counterterms, we find that the poles cancel up to a remainder

$$H_{\rm ren}(x) = \frac{1}{x\bar{x}}\left[1 + \frac{\alpha_s C_F}{4\pi}\left(\frac{3}{\epsilon} + \text{finite}\right)\right] , \quad \text{(D.14)}$$

which is canceled by the counterterm for the Yukawa coupling,

$$Z_y = 1 - \frac{3\alpha_s C_F}{4\pi\epsilon} . \quad \text{(D.15)}$$

E. RG Evolution for Flavor-Singlets

The renormalization kernels defined in eq. (4.42) are [89–92]

$$\begin{aligned}
V_{qq}(x,y) &= -2C_F\left[\frac{x}{y}\left(1+\frac{1}{y-x}\right)\theta(y-x)+\left(\begin{array}{c} x\to\bar{x}\\ y\to\bar{y}\end{array}\right)\right]_+,\\
V_{qg}(x,y) &= 8T_F n_f\left[\frac{x}{y^2}\,\theta(y-x)-\left(\begin{array}{c} x\to\bar{x}\\ y\to\bar{y}\end{array}\right)\right],\\
V_{gq}(x,y) &= -C_F\left[\frac{x^2}{y}\,\theta(y-x)-\left(\begin{array}{c} x\to\bar{x}\\ y\to\bar{y}\end{array}\right)\right],\\
V_{gg}(x,y) &= -\beta_0\,\delta(x-y)\\
&\quad -2C_A\left\{\frac{x}{y}\left[\left(\frac{\theta(y-x)}{y-x}\right)_+ +\frac{2x-1}{y}\,\theta(y-x)\right]+\left(\begin{array}{c} x\to\bar{x}\\ y\to\bar{y}\end{array}\right)\right\}.
\end{aligned}\tag{E.1}$$

After inserting the Gegenbauer expansion for the LCDAs, we obtain anomalous dimensions for the individual Gegenbauer moments a_n^P and b_n^P, defined in eq. (4.46). The explicit expression for the γ_n^{ij} are [89–92]

$$\begin{aligned}
\gamma_n^{qq} &= 2C_F\left[4H_{n+1}-3-\frac{2}{(n+1)(n+2)}\right],\\
\gamma_n^{qg} &= -T_F n_f\,\frac{40n(n+3)}{3(n+1)(n+2)}, \qquad\qquad \gamma_n^{gq} = -C_F\,\frac{12}{5(n+1)(n+2)},\\
\gamma_n^{gg} &= 2C_A\left[4H_{n+1}-\frac{8}{(n+1)(n+2)}\right]-2\beta_0\,.
\end{aligned}\tag{E.2}$$

At leading order in RG-improved perturbation theory, the explicit solution for the evolution matrix $\boldsymbol{U}_n^S(\mu_1,\mu_2)$ in (4.74) is given by [89–92]

$$\begin{aligned}
\boldsymbol{U}_n^S(\mu_1,\mu_2) &= \exp\left[-\frac{1}{2\beta_0}\,\log\frac{\alpha_s(\mu_1)}{\alpha_s(\mu_2)}\begin{pmatrix}\gamma_n^{qq} & \gamma_n^{qg}\\ \gamma_n^{gq} & \gamma_n^{gg}\end{pmatrix}^T\right]\\
&= \begin{pmatrix}
\frac{1+r_n}{2}\left(\frac{\alpha_s(\mu_2)}{\alpha_s(\mu_1)}\right)^{\frac{\gamma_n^+}{2\beta_0}}+\frac{1-r_n}{2}\left(\frac{\alpha_s(\mu_2)}{\alpha_s(\mu_1)}\right)^{\frac{\gamma_n^-}{2\beta_0}} & \frac{\gamma_n^{gq}}{\gamma_n^+-\gamma_n^-}\left[\left(\frac{\alpha_s(\mu_2)}{\alpha_s(\mu_1)}\right)^{\frac{\gamma_n^+}{2\beta_0}}-\left(\frac{\alpha_s(\mu_2)}{\alpha_s(\mu_1)}\right)^{\frac{\gamma_n^-}{2\beta_0}}\right]\\
\frac{\gamma_n^{qg}}{\gamma_n^+-\gamma_n^-}\left[\left(\frac{\alpha_s(\mu_2)}{\alpha_s(\mu_1)}\right)^{\frac{\gamma_n^+}{2\beta_0}}-\left(\frac{\alpha_s(\mu_2)}{\alpha_s(\mu_1)}\right)^{\frac{\gamma_n^-}{2\beta_0}}\right] & \frac{1-r_n}{2}\left(\frac{\alpha_s(\mu_2)}{\alpha_s(\mu_1)}\right)^{\frac{\gamma_n^+}{2\beta_0}}+\frac{1+r_n}{2}\left(\frac{\alpha_s(\mu_2)}{\alpha_s(\mu_1)}\right)^{\frac{\gamma_n^-}{2\beta_0}}
\end{pmatrix},
\end{aligned}\tag{E.3}$$

where

$$r_n = \frac{\gamma_n^{qq} - \gamma_n^{gg}}{\gamma_n^+ - \gamma_n^-}\,, \qquad \gamma_n^\pm = \frac{1}{2}\left(\gamma_n^{qq} + \gamma_n^{gg} \pm \sqrt{\left(\gamma_n^{qq} - \gamma_n^{gg}\right)^2 + 4\gamma_n^{qg}\gamma_n^{gq}}\right). \tag{E.4}$$

Here $\gamma_n^\pm$ are the eigenvalues of the one-loop anomalous-dimension matrix. The corresponding solution of the evolution function $U_n(\mu_1, \mu_2)$ is much simpler and reads

$$U_n(\mu_1, \mu_2) = \exp\left[-\frac{\gamma_n^{qq}}{2\beta_0}\,\log\frac{\alpha_s(\mu_1)}{\alpha_s(\mu_2)}\right] = \left(\frac{\alpha_s(\mu_2)}{\alpha_s(\mu_1)}\right)^{\frac{\gamma_n^{qq}}{2\beta_0}}. \tag{E.5}$$

F. Convolution Integrals over Gegenbauer Polynomials

The Gegenbauer polynomials can be defined through their generating function

$$\frac{1}{(1-2\omega t+t^2)^\alpha} = \sum_{n=0}^{\infty} C_n^{(\alpha)}(\omega) t^n \,. \tag{F.1}$$

The convolution integrals of a function $f(x)$ with a Gegenbauer polynomial can then be extracted by multiplying both sides of eq. (F.1) with $f(x)$ and integrating over x:

$$\int_a^b dx\, \frac{f(x)}{(1-2\omega(x)t+t^2)^\alpha} = \sum_{n=0}^{\infty} \left[\int_a^b dx\, C_n^{(\alpha)}\left(\omega(x)\right)\, f(x) \right] t^n \,. \tag{F.2}$$

From this equation we can directly read off, that the convolution of $f(x)$ with the n-th Gegenbauer polynomial is given by the t^n series coefficient of the integral on the left-hand side.

In the example of our hard functions, the function $\omega(x) = 2x-1$ and the integration boundaries are $a=0$, $b=1$. We can then evaluate the convolutions in eq. (4.52) by inserting them in the above equation, yielding:

$$\begin{aligned} \int_0^1 dx \frac{6x\bar{x}\, H_\pm(x, m_V, \mu)}{((1+t)^2-4xt)^{3/2}} &= \frac{3}{1+t} + \frac{3\alpha_s C_F}{4\pi} h_\pm(t) \,, \\ \int_0^1 dx \frac{6x\bar{x}\, H_\pm(\bar{x}, m_V, \mu)}{((1+t)^2-4xt)^{3/2}} &= \frac{3}{1-t} + \frac{3\alpha_s C_F}{4\pi} h_\pm(-t) \,, \end{aligned} \tag{F.3}$$

with

$$\begin{aligned} h_\pm(t) = &\left[\frac{3}{1+t} - \frac{2}{t} + \frac{2(1+t^2)}{t^2(1+t)} \log(1+t) \right] (\log \frac{m_V^2}{\mu^2} - i\pi) \\ &+ \frac{2}{t} - \frac{9}{1+t} \pm \left[\frac{1}{t} - \frac{(1+t)}{t^2} \log(1+t) \right] \\ &+ \frac{2(1+t^2)}{t^2(1+t)} \left[\log^2(1+t) + \mathrm{Li}_2\left(-t\right) \right] . \end{aligned} \tag{F.4}$$

From this, the hard scattering coefficients $C_n^{(\pm)}$ in (4.57) can be extracted.

For the two-gluon contributions the relevant integrals are

$$\int_0^1 dx \frac{30x^2\bar{x}^2 H_g(x)}{((1+t)^2-4xt)^{5/2}} = \frac{5\alpha_s T_F}{\pi} g(t)\,, \tag{F.5}$$

with

$$\begin{aligned} g(t) =& \frac{3+t}{t^2(t^2-1)} - \frac{6}{t^2} - \frac{2(1+t)}{t^3}\left[\log^2(1+t) + \mathrm{Li}_2\left(-t\right)\right] \\ &+ \left[\frac{1+t^2}{t^3(1+t)} + 6\,\frac{(1+t)}{t^3}\right]\log(1+t) \\ &+ \left[\frac{2-t}{(1-t)t^2} - \frac{2(1+t)}{t^3}\log(1+t)\right](\log\frac{m_Z^2}{\mu^2} - i\pi) \end{aligned} \tag{F.6}$$

Extracting the t^n coefficient in the expansion around $t = 0$ gives us the hard scattering coefficients D_n in (4.63).

G. Loop functions for Higgs Decays

The loop functions describing the off-shell $h \to \gamma V^*$ decay amplitudes with $V = \gamma, Z$ have been derived first in [137]. In our notation, they read[1]

$$\begin{aligned}
A_f(\tau,x) &= \frac{3\tau}{2(1-x)}\left\{1 - \frac{2x}{1-x}\left[g(\tau) - g\left(\frac{\tau}{x}\right)\right] + \left(1 - \frac{\tau}{1-x}\right)\left[f(\tau) - f\left(\frac{\tau}{x}\right)\right]\right\}, \\
B_f(\tau,x) &= \frac{\tau}{1-x}\left[f(\tau) - f\left(\frac{\tau}{x}\right)\right], \\
A_W^{\gamma\gamma}(\tau,x) &= \frac{2+3\tau}{1-x}\left\{1 - \frac{2x}{1-x}\left[g(\tau) - g\left(\frac{\tau}{x}\right)\right]\right\} \\
&\quad + \frac{3\tau}{(1-x)^2}\left(2 - \tau - \frac{8x}{3}\right)\left[f(\tau) - f\left(\frac{\tau}{x}\right)\right], \\
A_W^{\gamma Z}(\tau,x) &= \frac{1}{1-x}\left[1 - 2s_W^2 + \left(\frac{5}{2} - 3s_W^2\right)\tau\right]\left\{1 - \frac{2x}{1-x}\left[g(\tau) - g\left(\frac{\tau}{x}\right)\right]\right\} \\
&\quad + \frac{\tau}{(1-x)^2}\left[\left(\frac{5}{2} - 3s_W^2\right)(2-\tau) - 2x\big(3 - 4s_W^2\big)\right]\left[f(\tau) - f\left(\frac{\tau}{x}\right)\right],
\end{aligned} \tag{G.1}$$

where

$$f(\tau) = \begin{cases} \arcsin^2 \dfrac{1}{\sqrt{\tau}} & ; \quad \tau \geq 1\,, \\ -\dfrac{1}{4}\left(\ln \dfrac{1+\sqrt{1-\tau}}{1-\sqrt{1-\tau}} - i\pi\right)^2 & ; \quad \tau < 1\,, \end{cases} \tag{G.2}$$

and $g(\tau) = \tau(1-\tau)\, f'(\tau)$. In the limit $\tau \to \infty$ they simplify to $A_f(\tau,x) \to 1$, $B_f(\tau,x) \to 1$, $A_W^{\gamma\gamma}(\tau,x) \to 7$ and $A_W^{\gamma Z}(\tau,x) \to \frac{31}{6} - 7s_W^2$.

[1] The function $A_f(\tau,x)$ in eq. (4) of ref. [137] contains a typographical error, that we corrected.

H. Coefficient functions of Higgs Decays

In this Appendix, we tabulate the complete expressions for the CP-even coefficients Δ_V and the CP-odd coefficients $\tilde{\Delta}_V$ defined in eq. (5.35). We find for the CP-even quantities:

$$\begin{aligned}
\Delta_{\rho^0} &= \frac{\big[(0.068 \pm 0.006) + i(0.011 \pm 0.002)\big]\bar{\kappa}_{\rho^0} + 0.0001\kappa_W - 0.0001\bar{\kappa}_c}{\kappa_{\gamma\gamma}^{\text{eff}}}\,, \\
\Delta_{\omega} &= \frac{\big[(0.068 \pm 0.006) + i(0.011 \pm 0.002)\big]\bar{\kappa}_{\omega} - 0.0001\kappa_W - 0.0001\bar{\kappa}_c}{\kappa_{\gamma\gamma}^{\text{eff}}}\,, \\
\Delta_{\phi} &= \frac{\big[(0.093 \pm 0.008) + i(0.015 \pm 0.003)\big]\bar{\kappa}_{\phi}}{\kappa_{\gamma\gamma}^{\text{eff}}} \\
&\quad + \frac{0.0002\kappa_W - 0.0002\bar{\kappa}_c - 0.0001\kappa_{\gamma Z}}{\kappa_{\gamma\gamma}^{\text{eff}}}\,, \\
\Delta_{J/\psi} &= \frac{\big[(0.281 \pm 0.045) + i(0.040 \pm 0.009)\big]\bar{\kappa}_c}{\kappa_{\gamma\gamma}^{\text{eff}}} \\
&\quad + \frac{0.0004\kappa_W - 0.0003\kappa_\tau - 0.0001\kappa_b + 0.0001\bar{\kappa}_s - 0.0003\kappa_{\gamma Z}}{\kappa_{\gamma\gamma}^{\text{eff}}}\,, \\
\Delta_{\Upsilon(1S)} &= \frac{\big[(0.948 \pm 0.040) + i(0.130 \pm 0.019)\big]\kappa_b}{\kappa_{\gamma\gamma}^{\text{eff}}} \\
&\quad + \frac{0.019\kappa_W - 0.001\kappa_t - 0.001i\kappa_\tau + (0.001 - 0.002i)\bar{\kappa}_c - 0.010\kappa_{\gamma Z}}{\kappa_{\gamma\gamma}^{\text{eff}}}\,,
\end{aligned} \tag{H.1}$$

where the parameters $\bar{\kappa}_V$ for light mesons are defined in eq. (5.14). We omit the results for the other $\Upsilon(nS)$ states, since they are very similar to the $1S$-state result, see eq. (5.38). The first term in each expression shows the direct contribution, whereas the remaining terms arise from the power-suppressed $h \to \gamma Z^* \to \gamma V$ amplitude and the off-shellness of the photon in the $h \to \gamma\gamma^* \to \gamma V$ amplitude. Both of these effects are generically smaller than the uncertainties in the leading terms.

The CP-odd coefficients $\tilde{\Delta}_V$ are:

$$\begin{aligned}
\tilde{\Delta}_{\rho^0} - r_{\mathrm{CP}} &= \frac{\big[(0.068 \pm 0.006) + i(0.011 \pm 0.002)\big]\bar{\tilde{\kappa}}_{\rho^0}}{\kappa_{\gamma\gamma}^{\mathrm{eff}}} \\
&\quad + \frac{(0.429 + 0.003i)\tilde{\kappa}_t + (0.306 + 0.002i)\tilde{\kappa}_{\gamma\gamma}}{\kappa_{\gamma\gamma}^{\mathrm{eff}}} \\
&\quad - \frac{(0.004 - 0.003i)\tilde{\kappa}_\tau + (0.002 - 0.002i)\tilde{\kappa}_b + (0.005 - 0.003i)\bar{\tilde{\kappa}}_c}{\kappa_{\gamma\gamma}^{\mathrm{eff}}}\,, \\
\tilde{\Delta}_{\omega} - r_{\mathrm{CP}} &= \frac{\big[(0.068 \pm 0.006) + i(0.011 \pm 0.002)\big]\bar{\tilde{\kappa}}_{\omega}}{\kappa_{\gamma\gamma}^{\mathrm{eff}}} \\
&\quad + \frac{(0.429 + 0.003i)\tilde{\kappa}_t + (0.306 + 0.002i)\tilde{\kappa}_{\gamma\gamma}}{\kappa_{\gamma\gamma}^{\mathrm{eff}}} \\
&\quad - \frac{(0.004 - 0.003i)\tilde{\kappa}_\tau + (0.002 - 0.002i)\tilde{\kappa}_b + (0.005 - 0.003i)\bar{\tilde{\kappa}}_c}{\kappa_{\gamma\gamma}^{\mathrm{eff}}}\,, \\
\tilde{\Delta}_{\phi} - r_{\mathrm{CP}} &= \frac{\big[(0.093 \pm 0.008) + i(0.015 \pm 0.003)\big]\bar{\tilde{\kappa}}_{\phi}}{\kappa_{\gamma\gamma}^{\mathrm{eff}}} \\
&\quad + \frac{(0.429 + 0.003i)\tilde{\kappa}_t + (0.306 + 0.002i)\tilde{\kappa}_{\gamma\gamma}}{\kappa_{\gamma\gamma}^{\mathrm{eff}}} \\
&\quad - \frac{(0.004 - 0.003i)\tilde{\kappa}_\tau + (0.002 - 0.002i)\tilde{\kappa}_b + (0.005 - 0.003i)\bar{\tilde{\kappa}}_c}{\kappa_{\gamma\gamma}^{\mathrm{eff}}}\,, \\
\tilde{\Delta}_{J/\psi} - r_{\mathrm{CP}} &= \frac{\big[(0.277 \pm 0.045) + i(0.043 \pm 0.009)\big]\bar{\tilde{\kappa}}_{c}}{\kappa_{\gamma\gamma}^{\mathrm{eff}}} \\
&\quad + \frac{(0.429 + 0.003i)\tilde{\kappa}_t + (0.306 + 0.002i)\tilde{\kappa}_{\gamma\gamma}}{\kappa_{\gamma\gamma}^{\mathrm{eff}}} \\
&\quad - \frac{(0.004 - 0.003i)\tilde{\kappa}_\tau + (0.003 - 0.002i)\tilde{\kappa}_b}{\kappa_{\gamma\gamma}^{\mathrm{eff}}}\,, \\
\tilde{\Delta}_{\Upsilon(1S)} - r_{\mathrm{CP}} &= \frac{\big[(0.945 \pm 0.040) + i(0.132 \pm 0.019)\big]\tilde{\kappa}_{b}}{\kappa_{\gamma\gamma}^{\mathrm{eff}}} \\
&\quad + \frac{(0.427 + 0.003i)\tilde{\kappa}_t + (0.306 + 0.002i)\tilde{\kappa}_{\gamma\gamma}}{\kappa_{\gamma\gamma}^{\mathrm{eff}}} \\
&\quad - \frac{(0.004 - 0.002i)\tilde{\kappa}_\tau + (0.004 - 0.001i)\bar{\tilde{\kappa}}_c + 0.010\tilde{\kappa}_{\gamma Z}}{\kappa_{\gamma\gamma}^{\mathrm{eff}}}\,.
\end{aligned} \tag{H.2}$$

While we find large contributions proportional to $\tilde{\kappa}_t$ and $\tilde{\kappa}_{\gamma\gamma}$, the bounds on these parameters still imply that the direct contribution should give the leading effect.

I. Beta Functions for Neutrino Mass Models

Here we list the relevant one-loop beta functions for the various neutrino mass models, discussed in Chapter 6. We will first discuss the inverse seesaw model. The beta functions for the type-I seesaw model can readily be retrieved from simple replacements.

I.1. Inverse Seesaw Model

I.1.1. Structure of the Mass Matrix

We start from the mass matrix of the inverse seesaw model, eq. (6.14), which we repeat here:

$$M_\nu \equiv \begin{pmatrix} 0 & Y_\nu^T v/\sqrt{2} & 0 \\ Y_\nu v/\sqrt{2} & 0 & M_D^T \\ 0 & M_D & m_s \end{pmatrix} . \tag{I.1}$$

For 3 generations of active neutrinos, n_N generations of heavy N_R fields, and n_S generations of S fields, Y_ν is an $n_N \times 3$ matrix, M_D is an $n_S \times n_N$ matrix, and m_s is an $n_S \times n_S$ matrix. We assume $\|Y_\nu\| \sim \mathcal{O}(1)$, $\|M_D\| \sim$ TeV and $\|m_s\| \sim$ keV. We moreover assume $n_S > n_N$ so that M_ν has at least one $\mathcal{O}$(keV) eigenvalue, providing a dark matter candidate.

For the RG analysis, it is more convenient to work with a matrix which has diagonal elements much larger than the off-diagonal ones. Moreover, it is convenient to group the elements of this matrix by their typical scale. We therefore apply a unitary transformation V to M_ν to bring it to the form

$$\tilde{M}_\nu \equiv V^T M_\nu V = \begin{pmatrix} 0 & \hat{Y}_\nu^T v/\sqrt{2} & \tilde{Y}_\nu^T v/\sqrt{2} \\ \hat{Y}_\nu v/\sqrt{2} & M_N & m_D^T \\ \tilde{Y}_\nu v/\sqrt{2} & m_D & \hat{m}_s \end{pmatrix} . \tag{I.2}$$

V is chosen such that $\|M_N\| \gg \|m_D\|$, $\|\hat{m}_s \sim \text{keV}\|$ and $\|\hat{Y}_\nu\| \sim \|Y_\nu\| \gg \|\tilde{Y}_\nu\|$. Thus, M_N is a $2n_N \times 2n_N$ matrix with eigenvalues of order TeV and $\hat{m}_s$ is an $(n_S - n_N) \times (n_S - n_N)$ matrix.

To construct V explicitly, we first consider the unitary $n_S \times n_S$ matrix u_L and the unitary $n_N \times n_N$ matrix u_R which diagonalize M_D according to

$$M_D^{\text{diag}} = u_L^\dagger M_D u_R \,. \tag{I.3}$$

Here M_D^{diag} means the diagonal matrix of eigenvalues, *ordered in descending order*. From u_L and u_R, we construct

$$U_L = \begin{pmatrix} \mathbf{1}_{3+n_N} & 0 \\ 0 & u_L \end{pmatrix} \qquad U_R = \begin{pmatrix} \mathbf{1}_3 & 0 & 0 \\ 0 & u_R & 0 \\ 0 & 0 & \mathbf{1}_{n_S} \end{pmatrix} \qquad W = U_R U_L^* \,. \tag{I.4}$$

Then, the transformation

$$W^T M_\nu W \tag{I.5}$$

will diagonalize the M_D blocks in m_ν, putting the largest mass eigenvalues on top. After this, we perform a rotation by $\pi/4$ in the singlet block, given by:

$$X = \begin{pmatrix} \mathbf{1}_3 & 0 & 0 \\ 0 & r_{n_N \times n_N} & r_{n_N \times n_S} \\ 0 & -r_{n_S \times n_N} & r_{n_S \times n_S} \end{pmatrix} , \tag{I.6}$$

where

$$r_{n\times m} \equiv \frac{1}{\sqrt{2}} \begin{pmatrix} 1 & \cdots & 0 & 0 & \cdots & 0 \\ \vdots & \ddots & \vdots & \vdots & \ddots & \vdots \\ 0 & \cdots & 1 & 0 & \cdots & 0 \end{pmatrix} \tag{I.7}$$

is the $n \times n$ identity matrix (multiplied by $1/\sqrt{2}$), padded with zeros to turn it into an $n \times m$ matrix. After applying the full rotation

$$V \equiv U_R U_L^* X \tag{I.8}$$

to M_ν, we obtain $\tilde{M}_\nu$ in the form given in eq. (I.2). We summarize the dimensions and the mass scales for the different blocks of M_ν and $\tilde{M}_\nu$ in I.1. The $2n_N \times 2n_N$ matrix M_N has n_N pairs of eigenvalues that differ only by $\Delta M \sim \mathcal{O}(\text{keV})$, much less than the absolute scale of the eigenvalues of order TeV. The eigenstates in each pair couple to the active neutrinos via Yukawa couplings that are equal (up to a factor of i). Their contributions to the light neutrino masses therefore cancel up to terms of order $\Delta M / \|M_N\|$. This explains the smallness of the active neutrino masses despite the fact that $\hat{Y}_\nu$ is $\mathcal{O}(1)$ and M_N is $\mathcal{O}(\text{TeV})$. Another small contribution to the active neutrino masses comes from the $\mathcal{O}(\text{keV})$ mass eigenstate mixing with the active fields through the strongly suppressed $\tilde{Y}_\nu$. We can also understand why M_ν has $n_S - n_N$ eigenvalues of order keV: the off-diagonal elements in the last $n_S - n_N$ rows and columns of X are zero and thus we get $n_S - n_N$ keV states that do not mix with the N_R or ν_L fields.

Original basis		Rotated basis		
matrix	dimensions	matrix	dimensions	scale
Y_ν	$n_N \times 3$	$\hat{Y}_\nu$	$2n_N \times 3$	$\mathcal{O}(Y_\nu)$
M_D	$n_S \times n_N$	$\tilde{Y}_\nu$	$(n_S - n_N) \times 3$	$\mathcal{O}(Y_\nu m_s/M_D)$
m_s	$n_S \times n_S$	M_N	$2n_N \times 2n_N$	$\mathcal{O}(M_D)$
		m_D	$(n_S - n_N) \times 2n_N$	$\mathcal{O}(m_s)$
		$\hat{m}_s$	$(n_S - n_N) \times (n_S - n_N)$	$\mathcal{O}(m_s)$

Tab. I.1.: Dimensions of the submatrices forming the mass matrices M_ν and $\tilde{M}_\nu$ in the inverse seesaw model (see eqs. (I.1) and (I.2)). In the last column, we indicate the typical mass scale of the matrices in the rotated basis, (I.2).

I.1.2. Beta Functions for the Inverse Seesaw Model

We derive the RG equation for the mass matrix $\tilde{M}_\nu$ given in I.2 by using the fact that $\tilde{M}_\nu$ has exactly the same structure as the mass matrix of a type-I seesaw model.

Whenever the renormalization scale μ crosses the mass scale of one of the heavy sterile neutrinos as it is evolved from $M_{\rm GUT}$ to m_Z, the corresponding row and column is removed from the mass matrix $\tilde{M}_\nu$. Moreover the remaining rows and columns are modified to include the effect of integrating out one neutrino state. This in particular implies that the upper 3×3 block of $\tilde{M}_\nu$, which is zero initially, becomes a nonzero matrix κ. (We follow the notation of ref. [184] here.) If we did run down to sub-keV scales and integrated out all sterile states, κ would eventually coincide with $m_\nu = \frac{v^2}{2} Y_\nu^T M_D^{-1} m_s M_D^{-1} Y_\nu$.

For the beta functions of a parameter x, we use the convention

$$\beta_x = \mu \frac{d}{d\mu} x \,. \tag{I.9}$$

The evolution equations read

$$\begin{aligned}
16\pi^2 \beta_{M_N} &= (\hat{Y}_\nu \hat{Y}_\nu^\dagger) M_N + M_N (\hat{Y}_\nu \hat{Y}_\nu^\dagger)^T + (\hat{Y}_\nu \tilde{Y}_\nu^\dagger) m_D + m_D^T (\hat{Y}_\nu \tilde{Y}_\nu^\dagger)^T \\
16\pi^2 \beta_{\hat{m}_s} &= (\tilde{Y}_\nu \tilde{Y}_\nu^\dagger) \hat{m}_s + \hat{m}_s (\tilde{Y}_\nu \tilde{Y}_\nu^\dagger)^T + (\tilde{Y}_\nu \hat{Y}_\nu^\dagger) m_D^T + m_D (\tilde{Y}_\nu \hat{Y}_\nu^\dagger)^T \\
16\pi^2 \beta_{m_D} &= (\tilde{Y}_\nu \tilde{Y}_\nu^\dagger) m_D + m_D (\hat{Y}_\nu \hat{Y}_\nu^\dagger)^T + (\tilde{Y}_\nu \hat{Y}_\nu^\dagger) M + \hat{m}_s (\hat{Y}_\nu \tilde{Y}_\nu^\dagger)^T \\
16\pi^2 \beta_\kappa &= -\frac{3}{2} (Y_e^\dagger Y_e)^T \kappa - \frac{3}{2} \kappa (Y_e^\dagger Y_e) + \frac{1}{2} (\hat{Y}_\nu^\dagger \hat{Y}_\nu)^T \kappa + \frac{1}{2} \kappa (\hat{Y}_\nu^\dagger \hat{Y}_\nu) \\
&\quad + 2\,\mathrm{tr}(Y_e^\dagger Y_e) \kappa + 2\,\mathrm{tr}(Y_\nu^\dagger Y_\nu) \kappa + 6\,\mathrm{tr}(Y_u^\dagger Y_u) \kappa \\
&\quad + 6\,\mathrm{tr}(Y_d^\dagger Y_d) \kappa - 3 g_2^2 \kappa + \lambda \kappa
\end{aligned}$$

$$
\begin{aligned}
16\pi^2\beta_{\hat{Y}_\nu} &= \hat{Y}_\nu\Big[\frac{3}{2}(\tilde{Y}_\nu^\dagger\tilde{Y}_\nu+\hat{Y}_\nu^\dagger\hat{Y}_\nu)-\frac{3}{2}(Y_e^\dagger Y_e)+\mathrm{tr}(\hat{Y}_\nu^\dagger\hat{Y}_\nu+\tilde{Y}_\nu^\dagger\tilde{Y}_\nu)\\
&\qquad+\mathrm{tr}(Y_e^\dagger Y_e)+3\,\mathrm{tr}(Y_u^\dagger Y_u)+3\,\mathrm{tr}(Y_d^\dagger Y_d)-\frac{9}{20}g_1^2-\frac{9}{4}g_2^2\Big]\\
16\pi^2\beta_{\tilde{Y}_\nu} &= \tilde{Y}_\nu\Big[\frac{3}{2}(\tilde{Y}_\nu^\dagger\tilde{Y}_\nu+\hat{Y}_\nu^\dagger\hat{Y}_\nu)-\frac{3}{2}(Y_e^\dagger Y_e)+\mathrm{tr}(\hat{Y}_\nu^\dagger\hat{Y}_\nu+\tilde{Y}_\nu^\dagger\tilde{Y}_\nu)\\
&\qquad+\mathrm{tr}(Y_e^\dagger Y_e)+3\,\mathrm{tr}(Y_u^\dagger Y_u)+3\,\mathrm{tr}(Y_d^\dagger Y_d)-\frac{9}{20}g_1^2-\frac{9}{4}g_2^2\Big]\\
16\pi^2\beta_{Y_e} &= Y_e\Big[\frac{3}{2}Y_e^\dagger Y_e-\frac{3}{2}(\hat{Y}_\nu^\dagger\hat{Y}_\nu+\tilde{Y}_\nu^\dagger\tilde{Y}_\nu)-\frac{9}{4}g_1^2-\frac{9}{4}g_2^2\\
&\qquad+\mathrm{tr}\big[Y_e^\dagger Y_e+\hat{Y}_\nu^\dagger\hat{Y}_\nu+\tilde{Y}_\nu^\dagger\tilde{Y}_\nu+3Y_d^\dagger Y_d+3Y_u^\dagger Y_u\big]\Big]\\
16\pi^2\beta_{Y_d} &= Y_d\Big[\frac{3}{2}Y_d^\dagger Y_d-\frac{3}{2}Y_u^\dagger Y_u-\frac{1}{4}g_1^2-\frac{9}{4}g_2^2-8g_3^2\\
&\qquad+\mathrm{tr}\big[Y_e^\dagger Y_e+\hat{Y}_\nu^\dagger\hat{Y}_\nu+\tilde{Y}_\nu^\dagger\tilde{Y}_\nu+3Y_d^\dagger Y_d+3Y_u^\dagger Y_u\big]\Big]\\
16\pi^2\beta_{Y_u} &= Y_u\Big[\frac{3}{2}Y_u^\dagger Y_u-\frac{3}{2}Y_d^\dagger Y_d-\frac{17}{20}g_1^2-\frac{9}{4}g_2^2-8g_3^2\\
&\qquad+\mathrm{tr}\big[Y_e^\dagger Y_e+\hat{Y}_\nu^\dagger\hat{Y}_\nu+\tilde{Y}_\nu^\dagger\tilde{Y}_\nu+3Y_d^\dagger Y_d+3Y_u^\dagger Y_u\big]\Big]\\
16\pi^2\beta_\lambda &= 6\lambda^2-3\lambda\Big(3g_2^2+\frac{3}{5}g_1^2\Big)+3g_2^4+\frac{3}{2}\Big(\frac{3}{5}g_1^2+g_2^2\Big)^2\\
&\quad+4\lambda\,\mathrm{tr}\big[Y_e^\dagger Y_e+\hat{Y}_\nu^\dagger\hat{Y}_\nu+\tilde{Y}_\nu^\dagger\tilde{Y}_\nu+3Y_d^\dagger Y_d+3Y_u^\dagger Y_u\big]\\
&\quad-8\,\mathrm{tr}\big[Y_e^\dagger Y_e Y_e^\dagger Y_e+(\hat{Y}_\nu^\dagger\hat{Y}_\nu+\tilde{Y}_\nu^\dagger\tilde{Y}_\nu)(\hat{Y}_\nu^\dagger\hat{Y}_\nu+\tilde{Y}_\nu^\dagger\tilde{Y}_\nu)\\
&\qquad+3Y_d^\dagger Y_d Y_d^\dagger Y_d+3Y_u^\dagger Y_u Y_u^\dagger Y_u\big]
\end{aligned}
\tag{I.10}
$$

Note that the new fields introduced in the inverse seesaw model are all singlets under the SM gauge group. Therefore, the one-loop running of the $SU(3)_c\times SU(2)_L\times U(1)_Y$ gauge couplings is described by the SM expressions

$$
\begin{aligned}
g_1^{-2}(\mu) &= g_1^{-2}(m_Z)-\frac{41}{80\pi^2}\log\left(\frac{\mu}{m_Z}\right),\\
g_2^{-2}(\mu) &= g_2^{-2}(m_Z)+\frac{19}{48\pi^2}\log\left(\frac{\mu}{m_Z}\right),\\
g_3^{-2}(\mu) &= g_3^{-2}(m_Z)+\frac{7}{8\pi^2}\log\left(\frac{\mu}{m_Z}\right).
\end{aligned}
\tag{I.11}
$$

I.1.3. Beta Functions for the Type-I Seesaw Model

By comparing the mass matrix of the inverse seesaw model in eq. (I.2), to the mass matrix of the type-I seesaw model

$$M_{\nu,\text{type-I}} \equiv \begin{pmatrix} 0 & Y_\nu^T v/\sqrt{2} \\ Y_\nu v/\sqrt{2} & M \end{pmatrix}, \tag{I.12}$$

we can immediately read off that the RGEs for the type-I seesaw model are obtained from eqs. (I.10) by setting $\hat{Y}_\nu = Y_\nu$, $M_N = M$, $\tilde{Y}_\nu = 0$, $m_D = 0$, and $\hat{m}_s = 0$. The resulting equations agree with the ones found in the literature [184–188].

I.2. Inverse Seesaw Model with Gauged Baryon-Lepton Number

For the model with the gauged $U(1)_{B-L}$ symmetry, described in section 6.2, we find the following evolution equations:

$$\begin{aligned}
16\pi^2\beta_{Y_\nu} &= Y_\nu\left[\frac{1}{2}\lambda_S^T\lambda_S^*\right] + Y_\nu\left[\frac{3}{2}Y_\nu^\dagger Y_\nu - \frac{3}{2}Y_e^\dagger Y_e + \mathrm{tr}(Y_e^\dagger Y_e) + \mathrm{tr}(Y_\nu^\dagger Y_\nu)\right. \\
&\qquad \left. + 3\,\mathrm{tr}(Y_d^\dagger Y_d) + 3\,\mathrm{tr}(Y_u^\dagger Y_u) - \frac{9}{20}g_1^2 - \frac{9}{4}g_2^2 - 6g'^2\right] \\
16\pi^2\beta_{Y_e} &= Y_e\left[\frac{3}{2}Y_e^\dagger Y_e - \frac{3}{2}Y_\nu^\dagger Y_\nu + \mathrm{tr}(Y_e^\dagger Y_e) + \mathrm{tr}(Y_\nu^\dagger Y_\nu) + 3\,\mathrm{tr}(Y_d^\dagger Y_d)\right. \\
&\qquad \left. + 3\,\mathrm{tr}(Y_u^\dagger Y_u) - \frac{9}{4}g_1^2 - \frac{9}{4}g_2^2 - 6g'^2\right] \\
16\pi^2\beta_{\lambda_S} &= \lambda_S\left[\mathrm{tr}(\lambda_S^\dagger\lambda_S) + Y_\nu^* Y_\nu^T + \lambda_S^\dagger\lambda_S - 15g'^2\right] \\
16\pi^2\beta_{Y_u} &= Y_u\left[\frac{3}{2}Y_u^\dagger Y_u - \frac{3}{2}Y_d^\dagger Y_d - \frac{17}{20}g_1^2 - \frac{9}{4}g_2^2 - 8g_3^2 - \frac{2}{3}g'^2\right. \\
&\qquad \left. + \mathrm{tr}(Y_e^\dagger Y_e) + \mathrm{tr}(Y_\nu^\dagger Y_\nu) + 3\,\mathrm{tr}(Y_d^\dagger Y_d) + 3\,\mathrm{tr}(Y_u^\dagger Y_u)\right] \\
16\pi^2\beta_{Y_d} &= Y_d\left[\frac{3}{2}Y_d^\dagger Y_d - \frac{3}{2}Y_u^\dagger Y_u - \frac{1}{4}g_1^2 - \frac{9}{4}g_2^2 - 8g_3^2 - \frac{2}{3}g'^2\right. \\
&\qquad \left. + \mathrm{tr}(Y_e^\dagger Y_e) + \mathrm{tr}(Y_\nu^\dagger Y_\nu) + 3\,\mathrm{tr}(Y_d^\dagger Y_d) + 3\,\mathrm{tr}(Y_u^\dagger Y_u)\right] \\
16\pi^2\beta_{g'} &= Cg'^3
\end{aligned} \tag{I.13}$$

The numerical coefficient C in the beta function for the $U(1)_{B-L}$ coupling constant g' in the last line of (I.13) depends on the number of fields in the model and is given by

$$C = \frac{2}{3} \sum_{\text{fermions}} Q_{B-L}^2 + \frac{1}{3} \sum_{\text{scalars}} Q_{B-L}^2 \,. \tag{I.14}$$

In our specific model, including four generations of S and S' each, we find $C = \frac{97}{3}$. For only three generations of S and S' fields, we would have found $C = 27$ instead. The running of the quartic Higgs coupling λ and of the SM gauge couplings is the same as in the phenomenological inverse seesaw model at one-loop level, see the previous section. Note that we neglect the running of all parameters in the scalar sector other than the quartic Higgs coupling. The running of these couplings influences the evolution of the mixing parameters only indirectly by modifying the $U(1)_{B-L}$ breaking scale.

Where possible, we have checked that we reproduce the applicable terms in the renormalization group equations presented in ref. [236] for a $U(1)_{B-L}$ extension of the SM with three right-handed neutrinos, but without an inverse seesaw mechanism.

Bibliography

[1] G. Aad *et al.* [ATLAS Collaboration],
Observation of a new particle in the search for the Standard Model Higgs boson with the ATLAS detector at the LHC
Phys. Lett. B **716** (2012) 1-29, [arXiv:1207.7214]

[2] S. Chatrchyan *et al.* [CMS Collaboration],
Observation of a new boson at a mass of 125 GeV with the CMS experiment at the LHC
Phys. Lett. B **716** (2012) 30-61, [arXiv:1207.7235]

[3] J. Polchinski,
Effective field theory and the Fermi surface
[arXiv:hep-th/9210046]

[4] H. Georgi,
Effective field theory
Ann. Rev. Nucl. Part. Sci. **43** (1993) 209-252,

[5] A. J. Buras,
Weak Hamiltonian, CP violation and rare decays
[arXiv:hep-ph/9806471]

[6] A. Pich,
Effective field theory: Course
[arXiv:hep-ph/9806303]

[7] M. Neubert,
Effective field theory and heavy quark physics
[arXiv:hep-ph/0512222]

[8] G. Buchalla, A. J. Buras and M. E. Lautenbacher,
Weak decays beyond leading logarithms
Rev. Mod. Phys. **68** (1996) 1125-1144, [arXiv:hep-ph/9512380]

[9] J. Gasser and H. Leutwyler,
On the Low-energy Structure of QCD
Phys. Lett. **125** B (1983) 321-324,

[10] G. Ecker,
Chiral perturbation theory
Prog. Part. Nucl. Phys. **35** (1995) 1-80, [arXiv:hep-ph/9501357]

[11] S. Scherer,
Introduction to chiral perturbation theory
Adv. Nucl. Phys. **27** (2003) 277, [arXiv:hep-ph/0210398]

[12] W. Caswell and G. Lepage,
Effective Lagrangians for Bound State Problems in QED, QCD, and Other Field Theories
Phys. Lett. **167** B (1986) 437-442,

[13] G. T. Bodwin, E. Braaten and G. P. Lepage,
Rigorous QCD analysis of inclusive annihilation and production of heavy quarkonium
Phys. Rev. D **51** (1995) 1125-1171, [arXiv:hep-ph/9407339]

[14] H. Georgi,
An Effective Field Theory for Heavy Quarks at Low-energies
Phys. Lett. B **240** (1990) 447-450,

[15] M. Neubert,
Heavy quark symmetry
Phys. Rept. **245** (1994) 259-396, [arXiv:hep-ph/9306320]

[16] B. Grzadkowski *et al.*,
Dimension-Six Terms in the Standard Model Lagrangian
JHEP **10** (2010) 085, [arXiv:1008.4884]

[17] M. Aaboud *et al.* [ATLAS Collaboration],
Search for new phenomena in dijet events using 37 fb^{-1} of pp collision data collected at $\sqrt{s}$ =13 TeV with the ATLAS detector
[arXiv:1703.09127]

[18] A. M. Sirunyan *et al.* [CMS Collaboration],
Search for new physics with dijet angular distributions in proton-proton collisions at $\sqrt{s} = 13$ TeV
JHEP **07** (2017) 013, [arXiv:1703.09986]

[19] S. Alte, M. König and W. Shepherd,
Searching honestly for contact operators in non-resonant dijet events (in preparation)

[20] S. Alte, M. König and M. Neubert,
Effective Field Theory after a New Physics Discovery (in preparation)

[21] T. Becher, A. Broggio and A. Ferroglia,
Introduction to Soft-Collinear Effective Theory
[arXiv:1410.1892]

[22] M. Beneke and V. A. Smirnov,
Asymptotic expansion of Feynman integrals near threshold
Nucl. Phys. B **522** (1998) 321-344, [arXiv:hep-ph/9711391]

[23] T. Becher and G. Bell,
Analytic Regularization in Soft-Collinear Effective Theory
Phys. Lett. B **713** (2012) 41-46, [arXiv:1112.3907]

[24] T. Becher *et al.*,
Effective Field Theory for Jet Processes
Phys. Rev. Lett. **116** (2016) 192001, [arXiv:1508.06645]

[25] V. A. Smirnov,
Problems of the strategy of regions
Phys. Lett. B **465** (1999) 226-234, [arXiv:hep-ph/9907471]

[26] M. Beneke and T. Feldmann,
Multipole expanded soft collinear effective theory with nonAbelian gauge symmetry
Phys. Lett. B **553** (2003) 267-276, [arXiv:hep-ph/0211358]

[27] C. W. Bauer and A. V. Manohar,
Shape function effects in $B \to X_s\gamma$ and $B \to X_u l\bar{\nu}$ decays
Phys. Rev. D **70** (2004) 034024, [arXiv:hep-ph/0312109]

[28] M. Beneke *et al.*,
Power corrections to $\bar{B} \to X_u l\bar{\nu}(X_s\gamma)$ decay spectra in the 'shape-function' region
JHEP **06** (2005) 071, [arXiv:hep-ph/0411395]

[29] S. W. Bosch *et al.*,
Factorization and shape function effects in inclusive B meson decays
Nucl. Phys. B **699** (2004) 335-386, [arXiv:hep-ph/0402094]

[30] K. S. M. Lee and I. W. Stewart,
Factorization for power corrections to $B \to X_s\gamma$ and $B \to X_u l\bar{\nu}$
Nucl. Phys. B **721** (2005) 325-406, [arXiv:hep-ph/0409045]

[31] S. J. Lee, M. Neubert and G. Paz,
Enhanced Non-local Power Corrections to the $\bar{B} \to X_s\gamma$ Decay Rate
Phys. Rev. D **75** (2007) 114005, [arXiv:hep-ph/0609224]

[32] M. Benzke *et al.*,
Factorization at Subleading Power and Irreducible Uncertainties in $\bar{B} \to X_s\gamma$ Decay
JHEP **08** (2010) 099, [arXiv:1003.5012]

[33] C. W. Bauer, S. Fleming and M. Luke,
Summing Sudakov logarithms in $B \to X_s\gamma$ in effective field theory
Phys. Rev. D **63** (2000) 014006, [arXiv:hep-ph/0005275]

[34] R. Bonciani and A. Ferroglia,
Two-Loop QCD Corrections to the Heavy-to-Light Quark Decay
JHEP **11** (2008) 065, [arXiv:0809.4687]

[35] H. M. Asatrian, C. Greub and B. D. Pecjak,
NNLO corrections to $\bar{B} \to X_u l\bar{\nu}$ in the shape-function region
Phys. Rev. D **78** (2008) 114028, [arXiv:0810.0987]

[36] M. Beneke, T. Huber and X. Li,
Two-loop QCD correction to differential semi-leptonic $b \to u$ decays in the shape-function region
Nucl. Phys. B **811** (2009) 77-97, [arXiv:0810.1230]

[37] G. Bell,
NNLO corrections to inclusive semileptonic B decays in the shape-function region
Nucl. Phys. B **812** (2009) 264-289, [arXiv:0810.5695]

[38] C. Greub, M. Neubert and B. D. Pecjak,
NNLO corrections to $\bar{B} \to X_u l\bar{\nu}(l)$ and the determination of $|V_{ub}|$
Eur. Phys. J. C **65** (2010) 501-515, [arXiv:0909.1609]

[39] T. Becher and M. Neubert,
Toward a NNLO calculation of the $\bar{B} \to X_s\gamma$ decay rate with a cut on photon energy: I. Two-loop result for the soft function
Phys. Lett. B **633** (2006) 739-747, [arXiv:hep-ph/0512208]

[40] T. Becher and M. Neubert,
Toward a NNLO calculation of the $\bar{B} \to X_s\gamma$ decay rate with a cut on photon energy. II. Two-loop result for the jet function
Phys. Lett. B **637** (2006) 251-259, [arXiv:hep-ph/0603140]

[41] M. Neubert,
Renormalization-group improved calculation of the $B \to X_s\gamma$ branching ratio
Eur. Phys. J. C **40** (2005) 165-186, [arXiv:hep-ph/0408179]

[42] T. Becher and M. Neubert,
Analysis of $\mathrm{Br}(\bar{B} \to X_s\gamma)$ at NNLO with a cut on photon energy
Phys. Rev. Lett. **98** (2007) 022003, [arXiv:hep-ph/0610067]

[43] B. O. Lange, M. Neubert and G. Paz,
Theory of charmless inclusive B decays and the extraction of V_{ub}
Phys. Rev. D **72** (2005) 073006, [arXiv:hep-ph/0504071]

[44] C. W. Bauer, D. Pirjol and I. W. Stewart,
A Proof of factorization for $B \to D\pi$
Phys. Rev. Lett. **87** (2001) 201806, [arXiv:hep-ph/0107002]

[45] S. Mantry, D. Pirjol and I. W. Stewart,
Strong phases and factorization for color suppressed decays
Phys. Rev. D **68** (2003) 114009, [arXiv:hep-ph/0306254]

[46] C. W. Bauer *et al.*,
$B \to M_1 M_2$: Factorization, charming penguins, strong phases, and polarization
Phys. Rev. D **70** (2004) 054015, [arXiv:hep-ph/0401188]

[47] C. W. Bauer, I. Z. Rothstein and I. W. Stewart,
SCET analysis of $B \to K\pi$, $B \to K\bar{K}$, and $B \to \pi\pi$ decays
Phys. Rev. D **74** (2006) 034010, [arXiv:hep-ph/0510241]

[48] A. R. Williamson and J. Zupan,
Two body B decays with isosinglet final states in SCET
Phys. Rev. D **74** (2006) 014003, [arXiv:hep-ph/0601214]

[49] Y. Grossman, M. König and M. Neubert,
Exclusive Radiative Decays of W and Z Bosons in QCD Factorization
JHEP **04** (2015) 101, [arXiv:1501.06569]

[50] M. König and M. Neubert,
Exclusive Radiative Higgs Decays as Probes of Light-Quark Yukawa Couplings
JHEP **08** (2015) 012, [arXiv:1505.03870]

[51] S. Alte, M. König and M. Neubert,
Exclusive Radiative Z-Boson Decays to Mesons with Flavor-Singlet Components
JHEP **02** (2016) 162, [arXiv:1512.09135]

[52] S. Alte, M. König and M. Neubert,
Exclusive Weak Radiative Higgs Decays in the Standard Model and Beyond
JHEP **12** (2016) 037, [arXiv:1609.06310]

[53] M. König,
Very rare, exclusive, hadronic decays in QCD factorization
EPJ Web Conf. **129** (2016) 00014,

[54] S. Alte *et al.*,
Exclusive Radiative Decays of Z Bosons in QCD Factorization
PoS ICHEP **2016** (2016) 618, [arXiv:1703.07242]

[55] G. Lepage and S. J. Brodsky,
Exclusive Processes in Quantum Chromodynamics: Evolution Equations for Hadronic Wave Functions and the Form-Factors of Mesons
Phys. Lett. B **87** (1979) 359-365,

[56] G. Lepage and S. J. Brodsky,
Exclusive Processes in Perturbative Quantum Chromodynamics
Phys. Rev. D **22** (1980) 2157,

[57] A. Efremov and A. Radyushkin,
Asymptotical Behavior of Pion Electromagnetic Form-Factor in QCD
Theor. Math. Phys. **42** (1980) 97-110,

[58] A. Efremov and A. Radyushkin,
Factorization and Asymptotical Behavior of Pion Form-Factor in QCD
Phys. Lett. **94** B (1980) 245-250,

[59] V. Chernyak and A. Zhitnitsky,
Asymptotic Behavior of Exclusive Processes in QCD
Phys. Rept. **112** (1984) 173,

[60] M. Beneke and M. Neubert,
QCD factorization for $B \to PP$ and $B \to PV$ decays
Nucl. Phys. B **675** (2003) 333-415, [arXiv:hep-ph/0308039]

[61] M. Beneke *et al.*,
QCD factorization for $B \to \pi\pi$ decays: Strong phases and CP violation in the heavy quark limit
Phys. Rev. Lett. **83** (1999) 1914-1917, [arXiv:hep-ph/9905312]

[62] M. Beneke *et al.*,
QCD factorization for exclusive, nonleptonic B meson decays: General argu-

ments and the case of heavy light final states
Nucl. Phys. B **591** (2000) 313-418, [arXiv:hep-ph/0006124]

[63] M. Beneke *et al.*,
QCD factorization in $B \to \pi K$, $\pi\pi$ decays and extraction of Wolfenstein parameters
Nucl. Phys. B **606** (2001) 245-321, [arXiv:hep-ph/0104110]

[64] M. Beneke and T. Feldmann,
Symmetry breaking corrections to heavy to light B meson form-factors at large recoil
Nucl. Phys. B **592** (2001) 3-34, [arXiv:hep-ph/0008255]

[65] F. Dittes and A. Radyushkin,
Two Loop Contribution to the Evolution of the Pion Wave Function
Phys. Lett. B **134** (1984) 359-362,

[66] S. Mikhailov and A. Radyushkin,
Evolution Kernels in QCD: Two Loop Calculation in Feynman Gauge
Nucl. Phys. B **254** (1985) 89-126,

[67] D. Mueller,
Conformal constraints and the evolution of the nonsinglet meson distribution amplitude
Phys. Rev. D **49** (1994) 2525-2535,

[68] D. Müller,
The Evolution of the pion distribution amplitude in next-to-leading-order
Phys. Rev. D **51** (1995) 3855-3864, [arXiv:hep-ph/9411338]

[69] S. J. Brodsky *et al.*,
Conformal Symmetry: Exclusive Processes Beyond Leading Order
Phys. Rev. D **33** (1986) 1881,

[70] S. S. Agaev *et al.*,
Light Cone Sum Rules for the $\pi^0\gamma^*\gamma$Form Factor Revisited
Phys. Rev. D **83** (2011) 054020, [arXiv:1012.4671]

[71] S. A. Larin,
The Renormalization of the axial anomaly in dimensional regularization
Phys. Lett. B **303** (1993) 113-118, [arXiv:hep-ph/9302240]

[72] B. Melic, B. Nizic and K. Passek,
BLM scale setting for the pion transition form-factor
Phys. Rev. D **65** (2002) 053020, [arXiv:hep-ph/0107295]

[73] D. J. Broadhurst and A. G. Grozin,
Matching QCD and HQET heavy - light currents at two loops and beyond
Phys. Rev. D **52** (1995) 4082-4098, [arXiv:hep-ph/9410240]

[74] A. Ali, V. M. Braun and H. Simma,
Exclusive radiative B decays in the light cone QCD sum rule approach
Z. Phys. C **63** (1994) 437-454, [arXiv:hep-ph/9401277]

[75] P. Ball and V. M. Braun,
The ρ meson light cone distribution amplitudes of leading twist revisited
Phys. Rev. D **54** (1996) 2182-2193, [arXiv:hep-ph/9602323]

[76] P. Ball *et al.*,
Higher twist distribution amplitudes of vector mesons in QCD: Formalism and twist - three distributions
Nucl. Phys. B **529** (1998) 323-382, [arXiv:hep-ph/9802299]

[77] G. T. Bodwin *et al.*,
Relativistic corrections to Higgs boson decays to quarkonia
Phys. Rev. D **90** (2014) 113010, [arXiv:1407.6695]

[78] V. V. Braguta, A. K. Likhoded and A. V. Luchinsky,
The Study of leading twist light cone wave function of η_c meson
Phys. Lett. B **646** (2007) 80-90, [arXiv:hep-ph/0611021]

[79] X. Wang and D. Yang,
The leading twist light-cone distribution amplitudes for the S-wave and P-wave quarkonia and their applications in single quarkonium exclusive productions
JHEP **06** (2014) 121, [arXiv:1401.0122]

[80] V. M. Braun, D. Y. Ivanov and G. P. Korchemsky,
The B meson distribution amplitude in QCD
Phys. Rev. D **69** (2004) 034014, [arXiv:hep-ph/0309330]

[81] P. Ball, G. W. Jones and R. Zwicky,
$B \to V\gamma$ beyond QCD factorisation
Phys. Rev. D **75** (2007) 054004, [arXiv:hep-ph/0612081]

[82] A. G. Grozin and M. Neubert,
Asymptotics of heavy meson form-factors
Phys. Rev. D **55** (1997) 272-290, [arXiv:hep-ph/9607366]

[83] J. Kodaira,
QCD Higher Order Effects in Polarized Electroproduction: Flavor Singlet Co-

efficient Functions
Nucl. Phys. B **165** (1980) 129,

[84] R. J. Hill and M. Neubert,
Spectator interactions in soft collinear effective theory
Nucl. Phys. B **657** (2003) 229-256, [arXiv:hep-ph/0211018]

[85] M. Beneke and M. Neubert,
Flavor singlet B decay amplitudes in QCD factorization
Nucl. Phys. B **651** (2003) 225-248, [arXiv:hep-ph/0210085]

[86] P. Kroll and K. Passek-Kumericki,
The $\eta(\eta')\gamma$ transition form factor and the gluon–gluon distribution amplitude
J. Phys. G **40** (2013) 075005, [arXiv:1206.4870]

[87] P. Kroll and K. Passek-Kumericki,
The Two gluon components of the η and η' mesons to leading twist accuracy
Phys. Rev. D **67** (2003) 054017, [arXiv:hep-ph/0210045]

[88] S. S. Agaev *et al.*,
Transition form factors $\gamma^*\gamma \to \eta$ and $\gamma^*\gamma \to \eta'$ in QCD
Phys. Rev. D **90** (2014) 074019, [arXiv:1409.4311]

[89] M. Terentev,
Factorization in exclusive processes. Form-factor of singlet mesons in quantum chromodynamics
Sov. J. Nucl. Phys. **33** (1981) 911,

[90] T. Ohrndorf,
The Q^2 Dependence of the Flavor Singlet Pseudoscalar Meson Wave Function in QCD
Nucl. Phys. B **186** (1981) 153-164,

[91] M. A. Shifman and M. I. Vysotsky,
Form-Factors of Heavy Mesons in QCD
Nucl. Phys. B **186** (1981) 475,

[92] V. Baier and A. Grozin,
Meson Wave Functions With Two Gluon States
Nucl. Phys. B **192** (1981) 476-488,

[93] L. Arnellos, W. J. Marciano and Z. Parsa,
Radiative Decays $W^\pm \to \rho^\pm\gamma$ and $Z^0 \to \rho^0\gamma$
Nucl. Phys. B **196** (1982) 378,

[94] R. Mertig and W. L. v. Neerven,
The Calculation of the two loop spin splitting functions $P_{ij}^{(1)}(x)$
Z. Phys. C **70** (1996) 637-654, [arXiv:hep-ph/9506451]

[95] A. V. Belitsky *et al.*,
Evolution of nonforward parton distributions in next-to-leading order: Singlet sector
Nucl. Phys. B **546** (1999) 279-298, [arXiv:hep-ph/9810275]

[96] M. Jacob and T. T. Wu,
The Decay $Z \to \pi^0\gamma$
Phys. Lett. B **232** (1989) 529-532,

[97] Y. Y. Keum and X. Y. Pham,
Possible huge enhancement in the radiative decay of the weak W boson into the charmed D_s meson
Mod. Phys. Lett. A **9** (1994) 1545-1556, [arXiv:hep-ph/9303300]

[98] M. Mangano and T. Melia,
Rare exclusive hadronic W decays in a $t\bar{t}$ environment
Eur. Phys. J. C **75** (2015) 258, [arXiv:1410.7475]

[99] S. L. Adler,
Axial vector vertex in spinor electrodynamics
Phys. Rev. **177** (1969) 2426-2438,

[100] J. Bell and R. Jackiw,
A PCAC puzzle: $\pi^0 \to \gamma\gamma$ in the sigma model
Nuovo Cim. A **60** (1969) 47-61,

[101] K. A. Olive *et al.* [Particle Data Group Collaboration],
Review of Particle Physics
Chin. Phys. C **38** (2014) 090001,

[102] J. Erler,
Calculation of the QED coupling $\hat{\alpha}(M_Z)$ in the modified minimal subtraction scheme
Phys. Rev. D **59** (1999) 054008, [arXiv:hep-ph/9803453]

[103] K. G. Chetyrkin, J. H. Kuehn and M. Steinhauser,
RunDec: A Mathematica package for running and decoupling of the strong coupling and quark masses
Comput. Phys. Commun. **133** (2000) 43-65, [arXiv:hep-ph/0004189]

[104] A. V. Manohar,
The Decays $Z \to W\pi$ and $Z \to \gamma\pi$
Phys. Lett. B **244** (1990) 101-106,

[105] K. Hagiwara, Y. Yamada and T. Kuruma,
Three jet distributions from the one loop Zgg vertex at e^+e^- colliders
Nucl. Phys. B **358** (1991) 80-96,

[106] T. Huang and F. Petriello,
Rare exclusive decays of the Z-boson revisited
Phys. Rev. D **92** (2015) 014007, [arXiv:1411.5924]

[107] S. Schael *et al.* [SLD Electroweak Group, DELPHI, ALEPH, SLD, SLD Heavy Flavour Group, OPAL, LEP Electroweak Working Group, L3 Collaboration],
Precision electroweak measurements on the Z resonance
Phys. Rept. **427** (2006) 257-454, [arXiv:hep-ex/0509008]

[108] M. Bona *et al.* [UTfit Collaboration],
Model-independent constraints on $\Delta F = 2$ operators and the scale of new physics
JHEP **03** (2008) 049, [arXiv:0707.0636]

[109] V. Bertone *et al.* [ETM Collaboration],
Kaon Mixing Beyond the SM from N_f=2 tmQCD and model independent constraints from the UTA
JHEP **03** (2013) 089, [arXiv:1207.1287]

[110] N. Carrasco *et al.* [ETM Collaboration],
B-physics from $N_f = 2$ tmQCD: the Standard Model and beyond
JHEP **03** (2014) 016, [arXiv:1308.1851]

[111] A. Blondel *et al.*,
Report of the ICFA Beam Dynamics Workshop 'Accelerators for a Higgs Factory: Linear vs. Circular' (HF2012)
[arXiv:1302.3318]

[112] G. Aad *et al.* [ATLAS Collaboration],
Search for Higgs and Z Boson Decays to $J/\psi\gamma$ and $\Upsilon(nS)\gamma$ with the ATLAS Detector
Phys. Rev. Lett. **114** (2015) 121801, [arXiv:1501.03276]

[113] ATLAS Collaboration,
Search for exclusive Higgs and Z boson decays to $\phi\,\gamma$ and $\rho\,\gamma$ with the ATLAS Detector

[114] G. F. Giudice and O. Lebedev,
Higgs-dependent Yukawa couplings
Phys. Lett. B **665** (2008) 79-85, [arXiv:0804.1753]

[115] M. Bauer, M. Carena and K. Gemmler,
Flavor from the Electroweak Scale
JHEP **11** (2015) 016, [arXiv:1506.01719]

[116] V. Khachatryan *et al.* [CMS Collaboration],
Precise determination of the mass of the Higgs boson and tests of compatibility of its couplings with the standard model predictions using proton collisions at 7 and 8 TeV
Eur. Phys. J. C **75** (2015) 212, [arXiv:1412.8662]

[117] G. Aad *et al.* [ATLAS Collaboration],
Measurements of the Higgs boson production and decay rates and coupling strengths using pp collision data at $\sqrt{s} = 7$ and 8 TeV in the ATLAS experiment
Eur. Phys. J. C **76** (2016) 6, [arXiv:1507.04548]

[118] ATLAS Collaboration,
Evidence for the $h \to b\bar{b}$ decay with the ATLAS detector

[119] R. Harnik, J. Kopp and J. Zupan,
Flavor Violating Higgs Decays
JHEP **03** (2013) 026, [arXiv:1209.1397]

[120] G. T. Bodwin *et al.*,
Higgs boson decays to quarkonia and the $H\bar{c}c$ coupling
Phys. Rev. D **88** (2013) 053003, [arXiv:1306.5770]

[121] G. Isidori, A. V. Manohar and M. Trott,
Probing the nature of the Higgs-like Boson via $h \to V\mathcal{F}$ decays
Phys. Lett. B **728** (2014) 131-135, [arXiv:1305.0663]

[122] A. L. Kagan *et al.*,
Exclusive Window onto Higgs Yukawa Couplings
Phys. Rev. Lett. **114** (2015) 101802, [arXiv:1406.1722]

[123] D. Gao,
A note on Higgs decays into Z boson and $J/\psi(\Upsilon)$
Phys. Lett. B **737** (2014) 366-368, [arXiv:1406.7102]

[124] T. Modak and R. Srivastava,
Probing anomalous Higgs couplings in $H \to ZV$ decays
Mod. Phys. Lett. A **32** (2017) 1750004, [arXiv:1411.2210]

[125] G. Perez *et al.*,
Constraining the charm Yukawa and Higgs-quark coupling universality
Phys. Rev. D **92** (2015) 033016, [arXiv:1503.00290]

[126] J. Brod, U. Haisch and J. Zupan,
Constraints on CP-violating Higgs couplings to the third generation
JHEP **11** (2013) 180, [arXiv:1310.1385]

[127] M. Buschmann *et al.*,
New Signatures of Flavor Violating Higgs Couplings
JHEP **06** (2016) 149, [arXiv:1601.02616]

[128] M. Gorbahn and U. Haisch,
Searching for $t \to c(u)h$ with dipole moments
JHEP **06** (2014) 033, [arXiv:1404.4873]

[129] W. Dekens and J. d. Vries,
Renormalization Group Running of Dimension-Six Sources of Parity and Time-Reversal Violation
JHEP **05** (2013) 149, [arXiv:1303.3156]

[130] D. McKeen, M. Pospelov and A. Ritz,
Modified Higgs branching ratios versus CP and lepton flavor violation
Phys. Rev. D **86** (2012) 113004, [arXiv:1208.4597]

[131] W. Keung,
The Decay of the Higgs Boson Into Heavy Quarkonium States
Phys. Rev. D **27** (1983) 2762,

[132] R. Tarrach,
The Pole Mass in Perturbative QCD
Nucl. Phys. B **183** (1981) 384-396,

[133] M. A. Shifman, A. Vainshtein and V. I. Zakharov,
QCD and Resonance Physics: Applications
Nucl. Phys. B **147** (1979) 448-518,

[134] M. Benayoun *et al.*,
Radiative decays, nonet symmetry and SU(3) breaking
Phys. Rev. D **59** (1999) 114027, [arXiv:hep-ph/9902326]

[135] A. Kucurkarslan and U. Meißner,
$\omega - \phi$ mixing in chiral perturbation theory
Mod. Phys. Lett. A **21** (2006) 1423-1430, [arXiv:hep-ph/0603061]

[136] M. Benayoun *et al.*,
The Dipion Mass Spectrum In e^+e^- Annihilation and τ Decay: A Dynamical (ρ, ω, ϕ) Mixing Approach
Eur. Phys. J. C **55** (2008) 199-236, [arXiv:0711.4482]

[137] L. Bergstrom and G. Hulth,
Induced Higgs Couplings to Neutral Bosons in e^+e^- Collisions
Nucl. Phys. B **259** (1985) 137-155,

[138] A. Djouadi *et al.*,
QCD corrections to gamma gamma decays of Higgs particles in the intermediate mass range
Phys. Lett. B **257** (1991) 187-190,

[139] M. Spira *et al.*,
Higgs boson production at the LHC
Nucl. Phys. B **453** (1995) 17-82, [arXiv:hep-ph/9504378]

[140] U. Aglietti *et al.*,
Two loop light fermion contribution to Higgs production and decays
Phys. Lett. B **595** (2004) 432-441, [arXiv:hep-ph/0404071]

[141] G. Degrassi and F. Maltoni,
Two-loop electroweak corrections to the Higgs-boson decay $H \to \gamma\gamma$
Nucl. Phys. B **724** (2005) 183-196, [arXiv:hep-ph/0504137]

[142] S. Actis *et al.*,
NNLO Computational Techniques: The Cases $H \to \gamma\gamma$ and $H \to gg$
Nucl. Phys. B **811** (2009) 182-273, [arXiv:0809.3667]

[143] F. Bishara *et al.*,
Probing CP Violation in $h \to \gamma\gamma$ with Converted Photons
JHEP **04** (2014) 084, [arXiv:1312.2955]

[144] J. R. Andersen *et al.* [LHC Higgs Cross Section Working Group Collaboration],
Handbook of LHC Higgs Cross Sections: 3. Higgs Properties
[arXiv:1307.1347]

[145] ATLAS Collaboration,
Combined measurements of Higgs boson production and decay in the

$H \to ZZ^* \to 4\ell$ and $H \to \gamma\gamma$ channels using $\sqrt{s} = 13$ TeV pp collision data collected with the ATLAS experiment

[146] S. Dawson *et al.*,
Working Group Report: Higgs Boson
[arXiv:1310.8361]

[147] Y. Grossman and D. Pirjol,
Extracting and using photon polarization information in radiative B decays
JHEP **06** (2000) 029, [arXiv:hep-ph/0005069]

[148] M. Gonzalez-Alonso and G. Isidori,
The $h \to 4l$ spectrum at low m_{34}: Standard Model vs. light New Physics
Phys. Lett. B **733** (2014) 359-365, [arXiv:1403.2648]

[149] M. Aaboud *et al.* [ATLAS Collaboration],
Searches for the $Z\gamma$ decay mode of the Higgs boson and for new high-mass resonances in pp collisions at $\sqrt{s} = 13$ TeV with the ATLAS detector
[arXiv:1708.00212]

[150] G. Aad *et al.* [ATLAS, CMS Collaboration],
Measurements of the Higgs boson production and decay rates and constraints on its couplings from a combined ATLAS and CMS analysis of the LHC pp collision data at $\sqrt{s} = 7$ and 8 TeV
JHEP **08** (2016) 045, [arXiv:1606.02266]

[151] V. Brdar, M. König and J. Kopp,
Neutrino Anarchy and Renormalization Group Evolution
Phys. Rev. D **93** (2016) 093010, [arXiv:1511.06371]

[152] B. Cleveland *et al.*,
Measurement of the solar electron neutrino flux with the Homestake chlorine detector
Astrophys. J. **496** (1998) 505-526,

[153] Y. Fukuda *et al.* [Super-Kamiokande Collaboration],
Measurements of the solar neutrino flux from Super-Kamiokande's first 300 days
Phys. Rev. Lett. **81** (1998) 1158-1162, [arXiv:hep-ex/9805021]

[154] Q. R. Ahmad *et al.* [SNO Collaboration],
Measurement of the rate of $\nu_e + d \to p + p + e^-$ interactions produced by ^8B solar neutrinos at the Sudbury Neutrino Observatory
Phys. Rev. Lett. **87** (2001) 071301, [arXiv:nucl-ex/0106015]

[155] B. Pontecorvo,
Inverse beta processes and nonconservation of lepton charge
Sov. Phys. JETP **7** (1958) 172-173,

[156] Z. Maki, S. Sakata and M. Nakagawa,
Remarks on the unified model of elementary particles
Prog. Theor. Phys. **28** (1962) 870-880,

[157] M. C. Gonzalez-Garcia, M. Maltoni and T. Schwetz,
Updated fit to three neutrino mixing: status of leptonic CP violation
JHEP **11** (2014) 052, [arXiv:1409.5439]

[158] P. Minkowski,
$\mu \to e\gamma$ *at a Rate of One Out of* 10^9 *Muon Decays?*
Phys. Lett. **67** B (1977) 421-428,

[159] R. N. Mohapatra and G. Senjanovic,
Neutrino Mass and Spontaneous Parity Violation
Phys. Rev. Lett. **44** (1980) 912,

[160] S. Weinberg,
Baryon and Lepton Nonconserving Processes
Phys. Rev. Lett. **43** (1979) 1566-1570,

[161] R. Mohapatra and J. Valle,
Neutrino Mass and Baryon Number Nonconservation in Superstring Models
Phys. Rev. D **34** (1986) 1642,

[162] R. Mohapatra,
Mechanism for Understanding Small Neutrino Mass in Superstring Theories
Phys. Rev. Lett. **56** (1986) 561-563,

[163] P. S. B. Dev and R. N. Mohapatra,
TeV Scale Inverse Seesaw in SO(10) and Leptonic Non-Unitarity Effects
Phys. Rev. D **81** (2010) 013001, [arXiv:0910.3924]

[164] S. Khalil,
TeV-scale gauged B-L symmetry with inverse seesaw mechanism
Phys. Rev. D **82** (2010) 077702, [arXiv:1004.0013]

[165] A. G. Dias, C. A. d. S. Pires and P. S. R. d. Silva,
How the Inverse See-Saw Mechanism Can Reveal Itself Natural, Canonical and Independent of the Right-Handed Neutrino Mass
Phys. Rev. D **84** (2011) 053011, [arXiv:1107.0739]

[166] A. G. Dias *et al.*,
A Simple Realization of the Inverse Seesaw Mechanism
Phys. Rev. D **86** (2012) 035007, [arXiv:1206.2590]

[167] C. D. R. Carvajal *et al.*,
Axion Like Particles and the Inverse Seesaw Mechanism
JHEP **05** (2015) 069, [arXiv:1503.03502]

[168] L. Hall, H. Murayama and N. Weiner,
Neutrino mass anarchy
Phys. Rev. Lett. **84** (2000) 2572-2575, [arXiv:hep-ph/9911341]

[169] N. Haba and H. Murayama,
Anarchy and hierarchy
Phys. Rev. D **63** (2001) 053010, [arXiv:hep-ph/0009174]

[170] J. Heeck and W. Rodejohann,
Sterile neutrino anarchy
Phys. Rev. D **87** (2013) 037301, [arXiv:1211.5295]

[171] J. Gluza and R. Szafron,
Real and complex random neutrino mass matrices and theta13
Phys. Rev. D **85** (2012) 047701, [arXiv:1111.7278]

[172] K. Agashe, T. Okui and R. Sundrum,
A Common Origin for Neutrino Anarchy and Charged Hierarchies
Phys. Rev. Lett. **102** (2009) 101801, [arXiv:0810.1277]

[173] G. Altarelli *et al.*,
Repressing Anarchy in Neutrino Mass Textures
JHEP **11** (2012) 139, [arXiv:1207.0587]

[174] G. Altarelli, F. Feruglio and I. Masina,
Models of neutrino masses: Anarchy versus hierarchy
JHEP **01** (2003) 035, [arXiv:hep-ph/0210342]

[175] D. Bennett, H. B. Nielsen and I. Picek,
Understanding Fine Structure Constants and Three Generations
Phys. Lett. B **208** (1988) 275-280,

[176] J. F. Donoghue, K. Dutta and A. Ross,
Quark and lepton masses and mixing in the landscape
Phys. Rev. D **73** (2006) 113002, [arXiv:hep-ph/0511219]

[177] J. F. Donoghue *et al.*,
Likely values of the Higgs vev
Phys. Rev. D **81** (2010) 073003, [arXiv:0903.1024]

[178] S. Antusch *et al.*,
Running neutrino masses, mixings and CP phases: Analytical results and phenomenological consequences
Nucl. Phys. B **674** (2003) 401-433, [arXiv:hep-ph/0305273]

[179] A. d. Gouvêa and J. Jenkins,
The Physical Range of Majorana Neutrino Mixing Parameters
Phys. Rev. D **78** (2008) 053003, [arXiv:0804.3627]

[180] X. Lu and H. Murayama,
Neutrino Mass Anarchy and the Universe
JHEP **08** (2014) 101, [arXiv:1405.0547]

[181] A. d. Gouvea and H. Murayama,
Statistical test of anarchy
Phys. Lett. B **573** (2003) 94-100, [arXiv:hep-ph/0301050]

[182] J. R. Espinosa,
Anarchy in the neutrino sector?
[arXiv:hep-ph/0306019]

[183] A. d. Gouvea and H. Murayama,
Neutrino Mixing Anarchy: Alive and Kicking
Phys. Lett. B **747** (2015) 479-483, [arXiv:1204.1249]

[184] S. Antusch *et al.*,
Running neutrino mass parameters in see-saw scenarios
JHEP **03** (2005) 024, [arXiv:hep-ph/0501272]

[185] J. Mei,
Running neutrino masses, leptonic mixing angles and CP-violating phases: From M_Z to $\Lambda_{\rm GUT}$
Phys. Rev. D **71** (2005) 073012, [arXiv:hep-ph/0502015]

[186] J. A. Casas *et al.*,
General RG equations for physical neutrino parameters and their phenomenological implications
Nucl. Phys. B **573** (2000) 652-684, [arXiv:hep-ph/9910420]

[187] P. H. Chankowski and Z. Pluciennik,
Renormalization group equations for seesaw neutrino masses
Phys. Lett. B **316** (1993) 312-317, [arXiv:hep-ph/9306333]

[188] T. Ohlsson and S. Zhou,
Renormalization group running of neutrino parameters
Nature Commun. **5** (2014) 5153, [arXiv:1311.3846]

[189] N. Haba *et al.*,
Accurate renormalization group analyses in neutrino sector
Nucl. Phys. B **885** (2014) 180-195, [arXiv:1402.4126]

[190] M. A. Schmidt,
Renormalization group evolution in the type I+ II seesaw model
Phys. Rev. D **76** (2007) 073010, [arXiv:0705.3841]

[191] J. Bergstrom *et al.*,
Renormalization group running of neutrino parameters in the inverse seesaw model
Phys. Rev. D **81** (2010) 116006, [arXiv:1004.4628]

[192] S. Wandzura and F. Wilczek,
Sum Rules for Spin Dependent Electroproduction: Test of Relativistic Constituent Quarks
Phys. Lett. **72** B (1977) 195-198,

[193] V. M. Braun and I. Filyanov,
Conformal Invariance and Pion Wave Functions of Nonleading Twist
Z. Phys. C **48** (1990) 239-248,

[194] F. Jegerlehner,
Facts of life with γ_5
Eur. Phys. J. C **18** (2001) 673-679, [arXiv:hep-th/0005255]

[195] G. '. Hooft and M. Veltman,
Regularization and Renormalization of Gauge Fields
Nucl. Phys. B **44** (1972) 189-213,

[196] T. Trueman,
Chiral Symmetry in Perturbative QCD
Phys. Lett. B **88** (1979) 331-334,

[197] G. Bonneau,
Preserving Canonical Ward Identities in Dimensional Regularization With a

Nonanticommuting γ_5
Nucl. Phys. B **177** (1981) 523,

[198] D. Kreimer,
The γ_5 Problem and Anomalies: A Clifford Algebra Approach
Phys. Lett. B **237** (1990) 59-62,

[199] J. Koerner, D. Kreimer and K. Schilcher,
A Practicable γ_5 scheme in dimensional regularization
Z. Phys. C **54** (1992) 503-512,

[200] T. Feldmann, P. Kroll and B. Stech,
Mixing and decay constants of pseudoscalar mesons
Phys. Rev. D **58** (1998) 114006, [arXiv:hep-ph/9802409]

[201] T. Feldmann,
Quark structure of pseudoscalar mesons
Int. J. Mod. Phys. A **15** (2000) 159-207, [arXiv:hep-ph/9907491]

[202] R. Escribano and J. -. Frere,
Study of the $\eta - \eta'$ system in the two mixing angle scheme
JHEP **06** (2005) 029, [arXiv:hep-ph/0501072]

[203] D. Becirevic *et al.*,
D-meson decay constants and a check of factorization in non-leptonic B-decays
JHEP **02** (2012) 042, [arXiv:1201.4039]

[204] B. Colquhoun *et al.* [HPQCD Collaboration],
B-meson decay constants: a more complete picture from full lattice QCD
Phys. Rev. D **91** (2015) 114509, [arXiv:1503.05762]

[205] M. Neubert and B. Stech,
Nonleptonic weak decays of B mesons
Adv. Ser. Direct. High Energy Phys. **15** (1998) 294-344, [arXiv:hep-ph/9705292]

[206] A. Sirlin,
Current Algebra Formulation of Radiative Corrections in Gauge Theories and the Universality of the Weak Interactions
Rev. Mod. Phys. **50** (1978) 573,

[207] W. Marciano and A. Sirlin,
Electroweak Radiative Corrections to tau Decay
Phys. Rev. Lett. **61** (1988) 1815-1818,

[208] E. Braaten and C. Li,
Electroweak radiative corrections to the semihadronic decay rate of the τ lepton
Phys. Rev. D **42** (1990) 3888-3891,

[209] F. Yuan and K. Chao,
The Color octet intrinsic charm in η' and $b \to \eta' X$ decays
Phys. Rev. D **56** (1997) R2495-R2498, [arXiv:hep-ph/9706294]

[210] A. Ali *et al.*,
Contribution of $b \to sgg$ through the QCD anomaly in exclusive decays $B^{\pm} \to (\eta', \eta)(K^{\pm}, K^{*\pm})$ and $B^0 \to (\eta', \eta)(K^0, K^{*0})$
Phys. Lett. B **424** (1998) 161-174, [arXiv:hep-ph/9712372]

[211] A. A. Petrov,
Intrinsic charm of light mesons and CP violation in heavy quark decay
Phys. Rev. D **58** (1998) 054004, [arXiv:hep-ph/9712497]

[212] K. Jansen *et al.* [ETM Collaboration],
Meson masses and decay constants from unquenched lattice QCD
Phys. Rev. D **80** (2009) 054510, [arXiv:0906.4720]

[213] C. Allton *et al.* [RBC-UKQCD Collaboration],
Physical Results from 2+1 Flavor Domain Wall QCD and SU(2) Chiral Perturbation Theory
Phys. Rev. D **78** (2008) 114509, [arXiv:0804.0473]

[214] V. M. Braun *et al.*,
A Lattice calculation of vector meson couplings to the vector and tensor currents using chirally improved fermions
Phys. Rev. D **68** (2003) 054501, [arXiv:hep-lat/0306006]

[215] D. Becirevic *et al.*,
Coupling of the light vector meson to the vector and to the tensor current
JHEP **05** (2003) 007, [arXiv:hep-lat/0301020]

[216] G. T. Bodwin *et al.*,
Improved determination of color-singlet nonrelativistic QCD matrix elements for S-wave charmonium
Phys. Rev. D **77** (2008) 094017, [arXiv:0710.0994]

[217] H. S. Chung, J. Lee and C. Yu,
NRQCD matrix elements for S-wave bottomonia and $\Gamma[\eta_b(nS) \to \gamma\gamma]$ with relativistic corrections
Phys. Lett. B **697** (2011) 48-51, [arXiv:1011.1554]

[218] I. I. Bigi *et al.*,
The Pole mass of the heavy quark. Perturbation theory and beyond
Phys. Rev. D **50** (1994) 2234-2246, [arXiv:hep-ph/9402360]

[219] M. Beneke and V. M. Braun,
Heavy quark effective theory beyond perturbation theory: Renormalons, the pole mass and the residual mass term
Nucl. Phys. B **426** (1994) 301-343, [arXiv:hep-ph/9402364]

[220] M. Beneke *et al.*,
Leptonic decay of the $\Upsilon(1S)$ meson at third order in QCD
Phys. Rev. Lett. **112** (2014) 151801, [arXiv:1401.3005]

[221] R. Arthur *et al.*,
Lattice Results for Low Moments of Light Meson Distribution Amplitudes
Phys. Rev. D **83** (2011) 074505, [arXiv:1011.5906]

[222] P. Ball and G. W. Jones,
Twist-3 distribution amplitudes of K and phi mesons*
JHEP **03** (2007) 069, [arXiv:hep-ph/0702100]

[223] P. Ball and R. Zwicky,
SU(3) breaking of leading-twist K and K distribution amplitudes: A Reprise*
Phys. Lett. B **633** (2006) 289-297, [arXiv:hep-ph/0510338]

[224] P. Ball, V. M. Braun and A. Lenz,
Higher-twist distribution amplitudes of the K meson in QCD
JHEP **05** (2006) 004, [arXiv:hep-ph/0603063]

[225] P. Ball and R. Zwicky,
Operator relations for SU(3) breaking contributions to K and K distribution amplitudes*
JHEP **02** (2006) 034, [arXiv:hep-ph/0601086]

[226] A. P. Bakulev *et al.*,
Pion form-factor in QCD: From nonlocal condensates to NLO analytic perturbation theory
Phys. Rev. D **70** (2004) 033014, [arXiv:hep-ph/0405062]

[227] A. P. Bakulev, S. V. Mikhailov and N. G. Stefanis,
QCD based pion distribution amplitudes confronting experimental data
Phys. Lett. B **508** (2001) 279-289, [arXiv:hep-ph/0103119]

[228] B. Aubert *et al.* [BaBar Collaboration],
Measurement of the $\gamma\gamma^* \to \pi^0$ transition form factor
Phys. Rev. D **80** (2009) 052002, [arXiv:0905.4778]

[229] S. Uehara *et al.* [Belle Collaboration],
Measurement of $\gamma\gamma^* \to \pi^0$ transition form factor at Belle
Phys. Rev. D **86** (2012) 092007, [arXiv:1205.3249]

[230] S. S. Agaev *et al.*,
BELLE Data on the $\pi^0\gamma * \gamma$ Form Factor: A Game Changer?
Phys. Rev. D **86** (2012) 077504, [arXiv:1206.3968]

[231] M. Dimou, J. Lyon and R. Zwicky,
Exclusive Chromomagnetism in heavy-to-light FCNCs
Phys. Rev. D **87** (2013) 074008, [arXiv:1212.2242]

[232] R. J. Dowdall *et al.* [HPQCD Collaboration],
B-Meson Decay Constants from Improved Lattice Nonrelativistic QCD with Physical u, d, s, and c Quarks
Phys. Rev. Lett. **110** (2013) 222003, [arXiv:1302.2644]

[233] F. Bernardoni *et al.* [ALPHA Collaboration],
Decay constants of B-mesons from non-perturbative HQET with two light dynamical quarks
Phys. Lett. B **735** (2014) 349-356, [arXiv:1404.3590]

[234] J. Gronberg *et al.* [CLEO Collaboration],
Measurements of the meson - photon transition form-factors of light pseudoscalar mesons at large momentum transfer
Phys. Rev. D **57** (1998) 33-54, [arXiv:hep-ex/9707031]

[235] P. d. A. Sanchez *et al.* [BaBar Collaboration],
Measurement of the $\gamma\gamma^* \to \eta$ and $\gamma\gamma^* \to \eta'$ transition form factors
Phys. Rev. D **84** (2011) 052001, [arXiv:1101.1142]

[236] L. Basso, S. Moretti and G. M. Pruna,
A Renormalisation Group Equation Study of the Scalar Sector of the Minimal B-L Extension of the Standard Model
Phys. Rev. D **82** (2010) 055018, [arXiv:1004.3039]

[237] C. W. Bauer, D. Pirjol and I. W. Stewart,
Soft collinear factorization in effective field theory
Phys. Rev. D **65** (2002) 054022, [arXiv:hep-ph/0109045]

[238] S. W. Bosch *et al.*,
Factorization and Sudakov resummation in leptonic radiative B decay
Phys. Rev. D **67** (2003) 094014, [arXiv:hep-ph/0301123]

[239] T. Becher, R. J. Hill and M. Neubert,
Factorization in B —> V gamma decays
Phys. Rev. D **72** (2005) 094017, [arXiv:hep-ph/0503263]

[240] T. Becher and M. Neubert,
Drell-Yan Production at Small q_T, Transverse Parton Distributions and the Collinear Anomaly
Eur. Phys. J. C **71** (2011) 1665, [arXiv:1007.4005]